VALIDATION OF FINITE-ELEMENT MODEL OF THOR-NT LOWER ABDOMEN

Romain Desbats
Sabine Compigne
Ernesto Mottola
Toyota Motor Europe NV/SA
Belgium
Mitsutoshi Masuda
Toyota Motor Corporation
Japan
Paper Number 13-0339

ABSTRACT

THOR is expected to be the next regulatory frontal impact crash test dummy. It brings substantial biofidelity improvements and additional measurement capabilities compared to the current Hybrid III dummy. However, THOR-NT lower abdomen biofidelity was reported as limited. To improve it, numerical modelling would allow the evaluation of several design solutions but would need a validated THOR Finite Element (FE) model. Under NHTSA initiative, a THOR FE model was developed and made publically available. The current study aimed at validating the lower abdomen of the THOR-NT version 1.0 FE model issued in 2011. Impactor and seatbelt tests performed on THOR-NT according to published Post Mortem Human Subject test set-ups were simulated using LS-DYNA FE code. Limitations of the current material model used for the abdomen foam block were highlighted and additional material characterisation was performed to take into account foam compression rate sensitivity. Abdomen model response was improved for rigid-bar load type, whereas validation under seat belt tests suggested that additional investigations should be carried out including the validation of the pelvis flesh model.

INTRODUCTION

THOR abdomen biofidelity specifications were defined from Cavanaugh et al. (1986) Post Mortem Human Subject (PMHS) tests. A Biofidelity corridor was defined from them by Hardy et al. (2001) that THOR response only fulfills until 80 mm of penetration as shown by Hanen et al. (2011). This test configuration aimed at simulating the impact between a car occupant and the lower rim of the steering wheel. However, it did not consider the dummy biofidelity under seat belt loading for restrained drivers and other occupants in the car. In addition, Elhagediab et al. (1998) found that the seat belt was reported as the most common source of AIS3+ injuries to the digestive system.

Hanen et al. (2011) evaluated THOR-NT lower abdomen mechanical response under seat belt load and found that the dummy abdomen did not match the PMHS corridors defined by Foster et al. (2006). Proposals for modifications to the THOR lower abdomen were presented by Masuda and Compigne (2012). The prototype response was more biofidelic but could be further improved by tuning its abdomen block characteristics and looking at the interaction with other body parts (upper abdomen, pelvis flesh). This can be efficiently done using the THOR FE model. As a first requirement to this approach, the current abdomen FE model was validated comparing its lower abdomen response to Hanen et al. (2011) experiments on THOR-NT crash test dummy. The comparison of the original model response with the test results is presented in this paper together with improvements of the abdomen foam material properties. Finally, the modified model was evaluated against the same test data.

METHODS

Tests performed by Hanen et al. (2011) on THOR-NT were simulated with THOR FE model under LS-DYNA® software.

Test set-ups

THOR-NT lower abdomen mechanical response was assessed by Hanen et al. (2011) under two kinds of dynamic loading conditions:

- Impactor tests according to Cavanaugh et al. (1986) test set-up were performed with a 25 mm diameter rigid bar of length 300 mm and mass 32 kg. Initial speed was set at 3 and 6.1 m/s. Measured speeds during tests are presented in Table 1. The back of the dummy was unrestrained (Figure 1.a),
- Seatbelt tests according to Foster et al. (2006) test set-up were reproduced with either one or two pretensioners retracting the seatbelt. In that case the back of the dummy was fixed (See Figure 1.b). The retraction velocity profiles for the two conditions are

shown on Figure 1 and peak velocity values are reported in Table 2.

(a) (b)

Figure 1. (a) Impactor test from Hanen et al. (2011), (b) Seatbelt test from Hanen et al. (2011).

Table 1.
Rigid-bar tests

Theoretical speed (m/s)	Impactor mass	Measured velocity (m/s)
Low speed (3 m/s)	TME-1	3.03
	TME-3	2.75
High speed (6.1 m/s)	TME-4	6.16
	TME-5	6.15

Table 2.
Peak retraction velocities for seatbelt tests

Pretensioner	Test Id	Peak velocity (m/s)
A (high speed)	TAP-02	11.4
	TAP-03	10.8
B (low speed)	TAP-04	4.9
	TAP-05	5.1

In rigid-bar simulation set-up, a mass of 32kg was assigned to a cylindrical rigid bar modeled with solid elements having steel material properties, subjected to a 3 m/s or 6.1 m/s initial velocity (average speed of each impactor test configuration was considered). The dummy was positioned on a plane surface with outstretched legs. His lumbar spine joint was in slouched position (9° between lumbar bracket and pelvis bracket). The gravity was applied alone during 500 ms before the impact in order to reproduce the interaction between the dummy pelvis flesh and the ground using an AUTOMATIC_SURFACE_TO_SURFACE contact. An AUTOMATIC_SURFACE_TO_SURFACE contact was also defined between the impactor and dummy components - jacket, front foam block and pelvis flesh. A 0.185 friction coefficient was defined in this contact.
Impact forces were extracted from the contact between the rigid-bar and the dummy. The deflection was calculated by subtracting the longitudinal displacement of THOR abdomen rigid back plate node to the one of an impactor node. Low speed impact simulation was compared to TME-1 and TME-3 tests. High speed impact simulation was compared to TME-4 and TME-5 tests.

In seat belt simulation set-up, the dummy was positioned on a plane surface, its back tangent to a vertical plane surface. No gravity was applied since the dummy / ground interaction was believed to be less important than in the impactor tests due to the limited dummy displacement. The seatbelt is modelled with shell elements with membrane formulation. The material model is FABRIC defined as locally orthotropic with Young's modulus of 4.201GPa in longitudinal and normal directions (0 in transverse direction) and Poisson's ratio of 0.4 in all the directions.
An AUTOMATIC_SURFACE_TO_SURFACE contact was defined between the seatbelt shell elements and a set of dummy parts including the pelvis, the lower jacket and the front foam block of the dummy. This contact included a 0.2875 friction coefficient. The seatbelt velocity profiles specific to each test (Figure 2) was applied as imposed motion to a rigid bar pulling the seatbelt backwards.
The seatbelt force was computed by adding the output forces of two CROSS_SECTIONs. They consisted of shell elements taken on both sides of the seat belt at similar levels than the two seat belt load cells used in tests. The penetration was calculated by subtracting the longitudinal displacement of a node placed on the pelvis flesh side to the one of a seat belt node positioned at the dummy umbilicus.

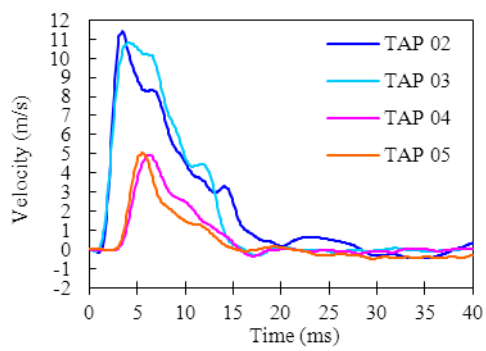

Figure 2. Seatbelt retraction speeds for pretensioner "A" (TAP-02 & TAP-03) and pretensioner "B" (TAP-04 & TAP-05).

Figure 3 and Figure 4 show simulation set-ups for impactor and seatbelt loading respectively. Models were run using the LS-DYNA explicit Finite Element code Version 971sR4 under 8 CPUs with SMP processing.

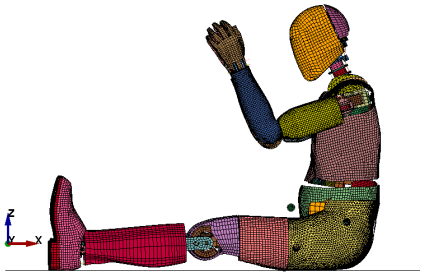

Figure 3. Simulation set-up for rigid-bar tests.

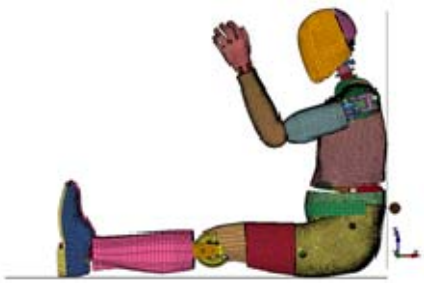

Figure 4. Simulation set-up for seatbelt tests.

Lower abdomen front foam block modelling

The dummy lower abdomen is made of two types of foam. The outer layer is a very soft open cell foam known as charcoal polyester while the inner layer is a stiffer sponge rubber (GESAC, 1998; Figure 5).

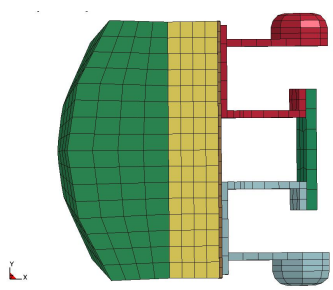

Figure 5. THOR-NT lower abdomen (Top view: outer layer in green, inner layer in yellow).

The material model MAT_LOW_DENSITY_FOAM (057) was used in the THOR model of the front foam block (outer layer). A viscoelastic formulation is included in this material card to account for strain rate effect. However, the material card does not allow the user to define actual stress factor versus strain rate but only some viscoelastic parameters which are difficult to tune. The stress-strain curve implemented in the model corresponded to a strain rate of 35 s^{-1}. This curve was obtained from a compression test at 1.8 m/s on a 50.8 mm side cube. The unloading phase is also computed from this curve.

However, strain rate peaks between 50 s^{-1} and 200 s^{-1} were observed in rigid-bar loading and between 70 s^{-1} and 420 s^{-1} in seat belt loading. Therefore, it was thought useful to use MAT_FU_CHANG_FOAM (083) model (Serifi et al., 2003; Croop et al., 2009) instead of MAT_057 to model the foam strain rate effect. It can also be noticed that the upper abdomen front foam block which is made of same foam as the lower abdomen front block used already MAT_083 formulation for quasi-static loading, 24 and 36 s-1 strain rates. For the lower abdomen front foam block, nine stress-strain curves were input in this model based on dynamic compression test data performed on THOR dummy abdomen foam samples (see APPENDIX 3).
Five curves (83s^{-1} to 304 s^{-1}) were defined from the experiments and four (10 s^{-1} to 60 s^{-1}) were computed from the experimental ones using Croop et al. (2009) linear relationship between Yield stress and strain rate logarithm.
Figure 6 shows the curves entered in the new model compared to the one in the initial model.

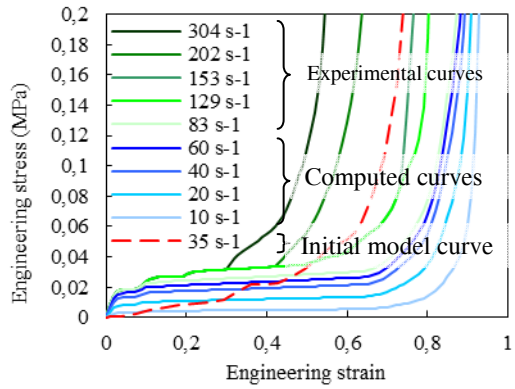

Figure 6. Stress-strain curves implemented in MAT_083 for front abdominal foam block.

Other model improvements

The jacket strap passing in between the dummy legs was added to the model as shown in Figure 7. It was connected to the rest of the jacket by merging their nodes at the extremities of the strap. Material properties of the jacket were applied to the strap.

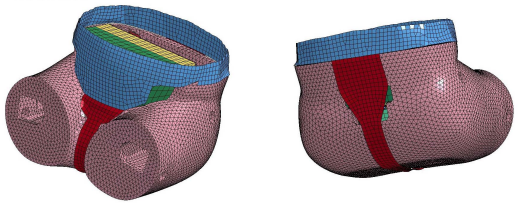

Figure 7. Jacket strap model (in red).

Due to unrealistic penetration between the abdomen back plate and the front foam block, the front foam was covered by NULL shell elements to prevent this phenomenon as shown in Figure 8.

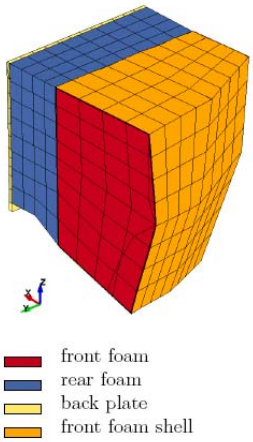

Figure 8. Section view of the lower abdomen with front foam block coated with NULL elements.

RESULTS

In total, 6 simulations were conducted on the initial and the modified THOR models: 2 conditions for rigid bar tests and 4 conditions for seat belt tests. APPENDIX 1 and APPENDIX 2 show pictures of simulation animations and corresponding test videos.

Rigid-bar impact simulations

With the initial model, the rigid-bar simulation results showed a too high abdominal force peak of the lower abdomen when comparing the tests and the simulations (Figure 9 and Figure 10). At low speed impact, the simulated peak force was from 30% to 38% higher than TME-1 and TME-3 results respectively. High speed impact simulations showed a 51% to 80% higher peak force than tests TME-4 and TME-5 respectively. It was found that it was the consequence of the contact between the pelvis flesh and the rigid-bar. Contact between the impactor and the pelvis flesh was observed at 33 ms in the 3 m/s tests and simulation. In the simulation this contact led to a sharpest force peak of 1000 N higher than in the tests. At 6.1 m/s impact, the contact was observed at 14 ms for both the tests and the simulation. In the simulation, the contact force with the pelvis flesh contributes by 70% to the force peak.

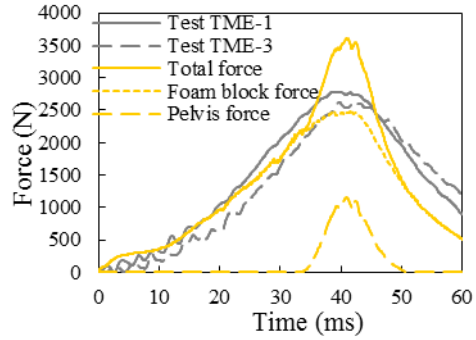

Figure 9. Force-time response curves of the initial model versus the tests for 3 m/s rigid-bar impacts (Total force= Foam block force + Pelvis force).

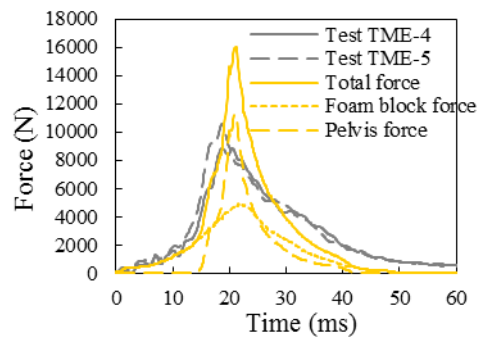

Figure 10. Force-time response curves of the initial model versus the tests for 6.1 m/s rigid-bar impacts (Total force= Foam block force + Pelvis force).

With the implementation of new material model, the impact peak force for the 3 m/s impact was decreased and the deflection peak slightly increased (Table 3). A higher force was obtained during the first 20 ms (Figure 11a). In addition, a change in force-time slope was observed at the time the rigid bar impacted the pelvis flesh which was not observed in tests. This effect could also be seen on the force-deflection curve (Figure 11c). The deflection curve matched well the test data and its peak was just slightly above the initial model one (Figure 11b).

Table 3.
Low speed impactor test and simulation peaks

Test/Simulation Id	Force peak (N)	Deflection peak (mm)
TME-1	2758	98
TME-3	2625	102
Initial model	3614	92
New model	2984	94

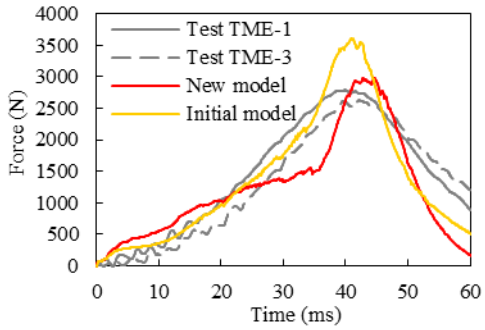

(a) Force-time responses

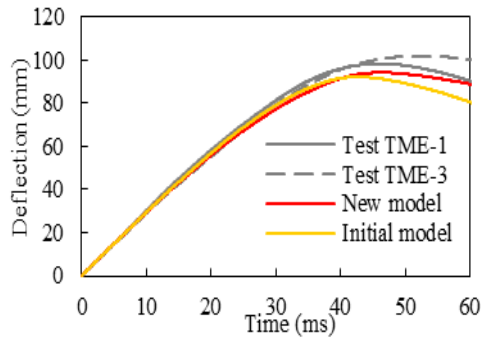

(b) Deflection-time responses

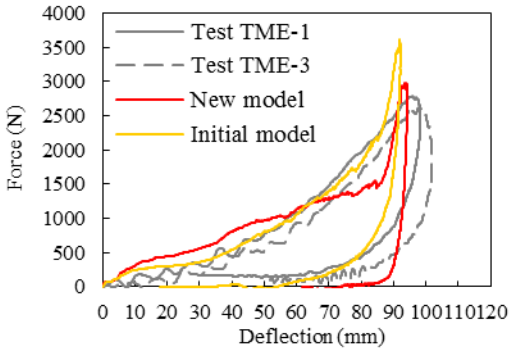

(c) Force-deflection responses

Figure 11. 3 m/s rigid-bar simulation versus test results.

At 6.1 m/s, the new model decreased the peak force by 21%, more in line with test results (Table 4, Figure 12a). Regarding deflection peak values and profiles, the new simulation was closer to the test data (Table 4, Figure 12b). The force-deflection responses are overlaid in Figure 12c. In the simulations, the maximum deflection was obtained at almost the maximum force whereas in the tests, the deflection peaks occurred 10 ms later.

Table 4.
High speed impactor test and simulation peaks

Test/Simulation Id.	Force peak (N)	Deflection peak mm)
TME-4	8875	136
TME-5	10565	119
Initial model	15985	114
New model	12582	115

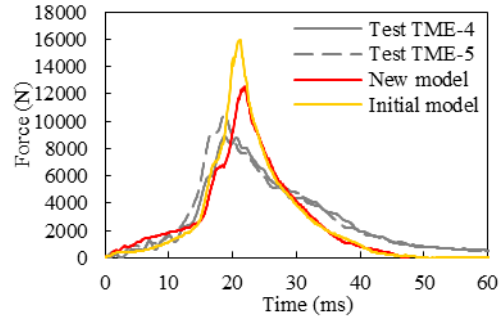

(a) Force-time responses

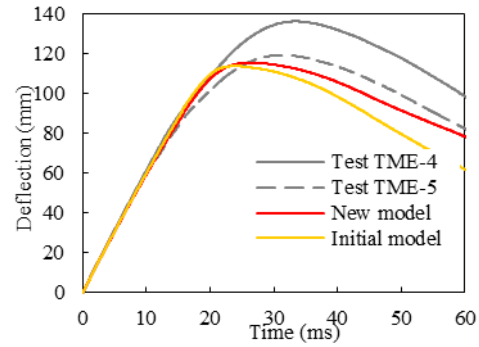

(b) Deflection-time responses

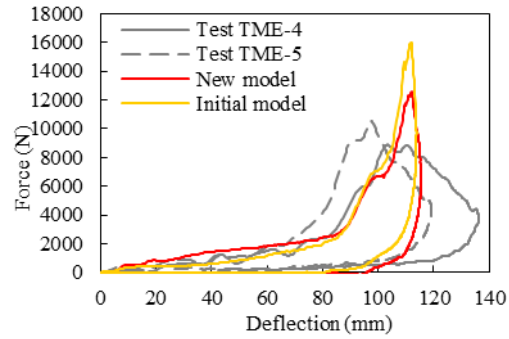

(c) Force-deflection responses

Figure 12. 6.1 m/s rigid-bar simulation versus test results.

Seatbelt simulations

<u>Low speed results</u> for the initial and the new model results are overlaid with test results in Figure 13. The peak values are compared in Table 5. The initial model force result was closer to test data

even though the force magnitude was too high. The beginning of the loading phase showed that the old and new simulation profiles were similar (Figure 13a). The deflection profiles were similar in shape between the old and new simulations, but overall the new simulation showed less deflection, in contradiction with test data (Figure 13b). The force-deflection response had a worse correlation with test data (Figure 13c).

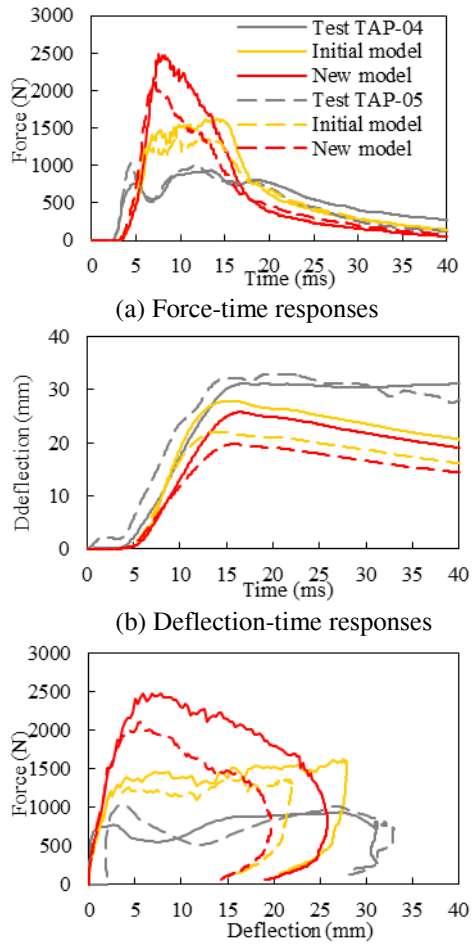

(a) Force-time responses

(b) Deflection-time responses

(c) Force-deflection responses

Figure 13. Low speed seat belt simulation versus test results.

Table 5.
Low speed seatbelt test and simulation peaks

Test/Simulation Id.	Force peak (N)	Deflection peak (mm)
TAP-04	938	31
Initial model	1623	28
New model	2483	26
TAP-05	1038	33
Initial model	1365	22
New model	2104	20

High speed simulations are overlaid with test results in Figure 14 and peak values are compared in Table 6. At the beginning of the loading phase the force profile of old and new simulations matched test data. The force peak was higher for the new simulation and appeared earlier. In the unloading phase, the new simulation matched better TAP-02 curve whereas the old simulation results were closer to TAP-03 ones (Figure 14a). Regarding the deflection profile (Figure 14b), the new simulation showed higher deflection values in line with test data. Comparing the force-deflection curve (Figure 14c), the old simulation curve shape correlated better with the test data due to a force response closer to the tests.

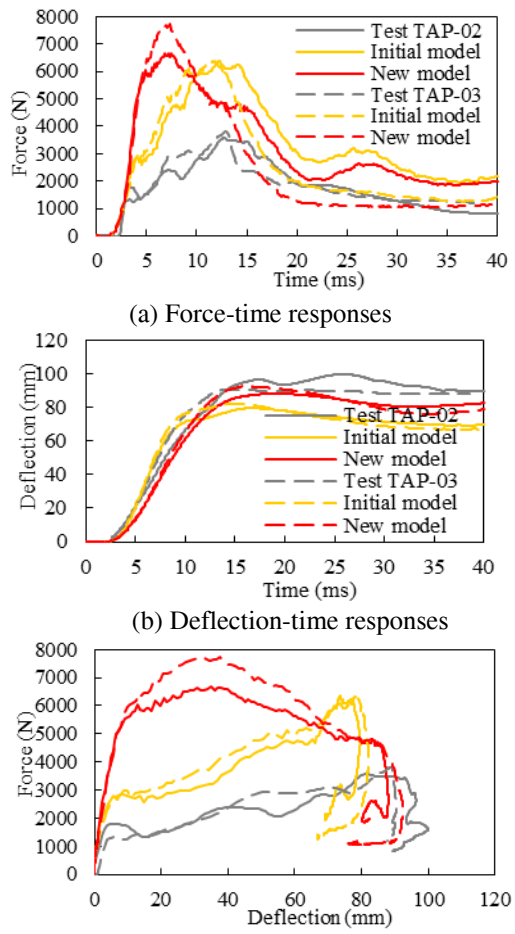

(a) Force-time responses

(b) Deflection-time responses

(c) Force-deflection responses

Figure 14. High speed seat belt simulation versus test results.

Table 6.
High speed seatbelt test and simulation peaks

Test/Simulation Id.	Force peak (N)	Deflection peak (mm)
TAP-02	3573	100
Initial model	6381	80
New model	6663	88
TAP-03	3811	91
Initial model	6405	82
New model	7748	92

The comparison of the force distribution between the abdomen and the pelvis shows that for lowest retraction speed (5 m/s), the force due to the abdomen was higher than the one due to the pelvis in both models (Figure 15). This was not the case for higher retraction speed (10 m/s) for which the pelvis force was twice as high as the abdomen force in the initial model and of similar magnitude than the abdomen force in the new model (Figure 16).

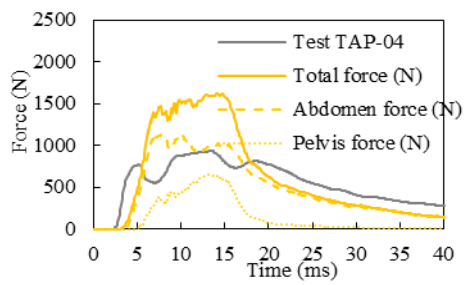

(a) Initial model

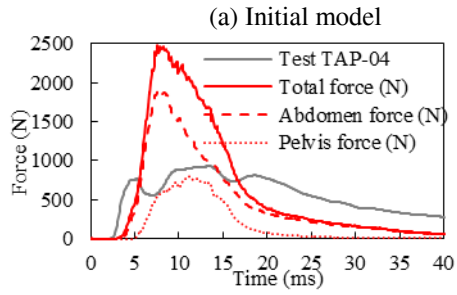

(b) New model

Figure 15. Force distribution between abdomen and pelvis for low speed seat belt simulations.

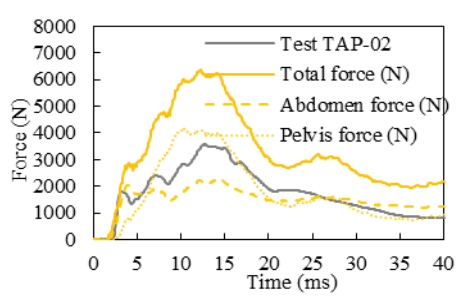

(a) Initial model

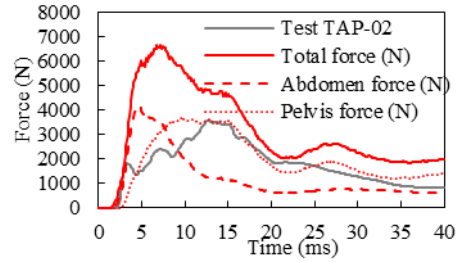

(b) New model

Figure 16. Force distribution between abdomen and pelvis for high speed seat belt simulations, (Total force= Foam block force + Pelvis force).

DISCUSSION

Foam material characterization

The material characterization of the front foam block of the dummy had some limitations in terms of the range of strain rates tested. Strain rates below 83 s^{-1} could not be tested due to the test equipment used and the size of the foam samples. Therefore the abdomen behaviour for low strain rates could only be calculated from the higher strain rate curves. This was based on defining new yield stress values for missing strain rate under the observation that foam yield stress varied linearly with the logarithm of the strain rate (Croop et al., 2009). The lowest strain rate curve (83 s^{-1}) obtained in test was multiplied by a factor chosen to make the new curve passing through the calculated yield stress value for the considered strain rate. The fact that experimental GESAC's curve at 35 s^{-1} did not lie in between the 20 and the 40 s^{-1} curves was not explained but may show an issue with the method used to calculate the stress-strain curves at lower strain rates. However, this might have also been caused by test data obtained from small sample sizes tested at quite high strain rates (83 s^{-1} and above).

THOR abdomen model validation

In future, it appears necessary to carry out additional impact tests on the dummy abdomen without any interference with the pelvis flesh. Interferences with pelvis were seen in all the tests performed so far which did not allow to identify the contribution of the abdomen and the pelvis in the total force and deflection.

Impactor test validation limitations

From actual test videos it seems that the impactor was higher than its theoretical position. This caused the impactor to slip above the pelvis flesh. This

phenomenon happened in one of the two high speed rigid-bar tests (TME-04) but not in the simulation for which a higher peak force was recorded due to the contact with the pelvis flesh.

Seat belt test validation limitations

The simulation validation was not improved by the new abdomen foam properties despite the high strain rates encountered by the abdomen elements (between 50 s^{-1} to 200 s^{-1} for the rigid-bar impacts and 70 s^{-1} to 420 s^{-1} for the seat belt loading) which initially led us to hypothesize that additional strain rate curves should have improved the abdomen response. However, it seems that the interaction between the seat belt and the pelvis flesh played a more predominant role in the dummy lower torso response. The comparison between the test videos and the simulations showed that the deformed shape of the pelvis was not well mimicked by the model. Figure 17 shows that the pelvis side was quite deformed by the seatbelt during the test whereas no major deformation was suggested by the simulation. Additional validation of pelvis material might be recommended in future.

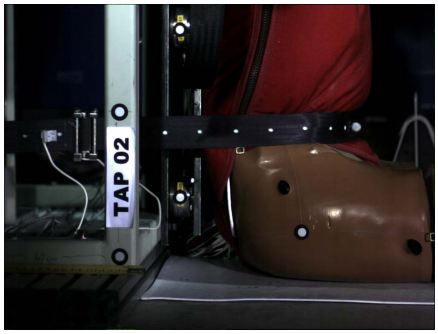

(a) Test at 22 ms

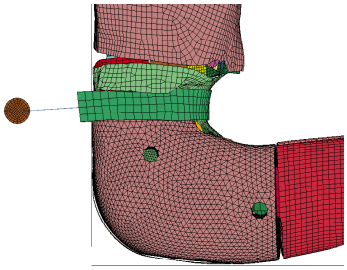

(b) Simulation at 22 ms

Figure 17. Pelvis flesh deformation under high speed seat belt retraction.

CONCLUSION

The last released version of THOR FE model at the time this work was performed was improved by enhancing the front foam block material definition considering various strain rates. Although the response was improved for rigid bar impactor tests, the new model degraded the correlation with test data for seatbelt loading tests. This showed that the seatbelt test condition was harder to replicate in numerical simulation than the impactor test due to the higher number of influential factors such as dummy back / plate contact, pelvis / seatbelt interaction, seatbelt positioning. A well validated THOR abdomen model requires the validation of the other impacted parts, especially pelvis parts, in the targeted impact conditions.

REFERENCES

Cavanaugh J., Nyquist G., Goldberg S., and King A. (1986). Lower abdominal tolerance and response. Stapp Car Crash Conference Proceedings, 30:41–63 .

Croop B. and Lobo H. (2009). Selecting Material Models for the Simulation of Foams in LS-DYNA. In 7th European LS-DYNA Users Conference, 2009.

Elhagediab A. M., Rouhana S. W. (1998). Patterns of abdominal injury frontal automotive crashes, Paper #98-S1-W-26, Proc. of 16th ESV Conference, Windsor, Ontario, Canada, May 31-June4, 1998.

Foster D., Hardy W., Yang K., King A., and Hashimoto S. (2006). High-speed seatbelt pretensioner loading of the abdomen. Stapp Car Crash Journal, 50:27–51, 2006.

GESAC, Inc. Test support for finite element modeling of THOR crash test dummy, Contract/Order No: DTRS57-98-P-80521.

Hanen G. et al. (2011). Contribution to the improvement of crash test dummies in order to decrease abdominal injuries in road accidents, Paper #11-0218, Proc. of 22nd ESV Conference, Washington D.C., June 13-16, 2011.

Hardy W. N., Schneider L. W., Rouhana S. W. (2001). Abdominal impact response to rigid-bar, seat belt and airbag loading. Stapp Car crash Journal, Vol. 45, p.1.

Masuda M., Compigne S. (2012), Dynamic Response of the THOR-NT: Thorax and Abdomen, 2012 SAE-GIM, Washington D.C.

Serifi H., Hirth A., Matthaei S. and Müllershön H.(2003). Modelling of Foams using MAT83 – Preparation and Evaluation of Experimental Data. In 4th European LS-DYNA Users Conference, 2003.

APPENDIX 1: RIGID-BAR IMPACT SIMULATION VERSUS TEST

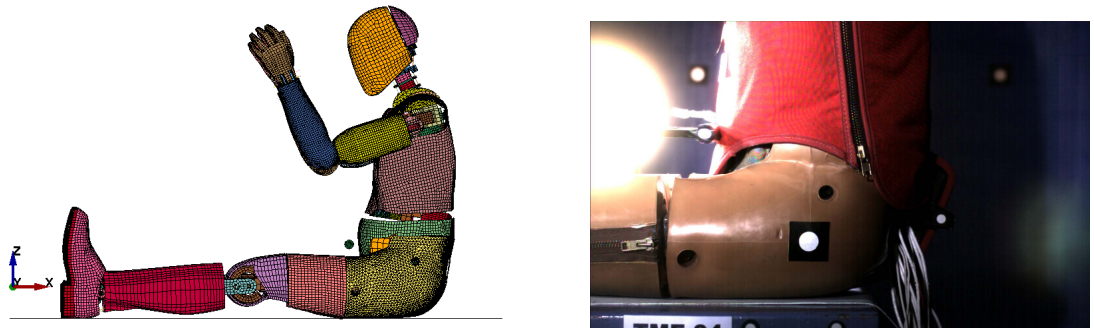

Just before impact

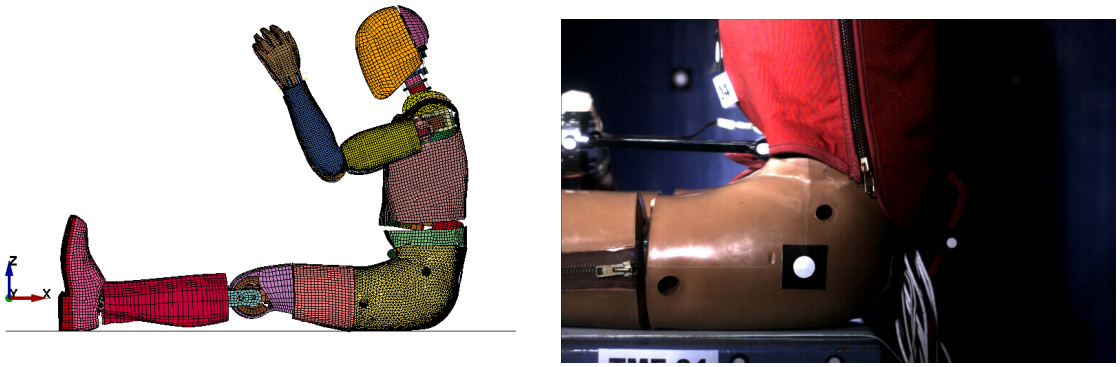

14 ms after impact

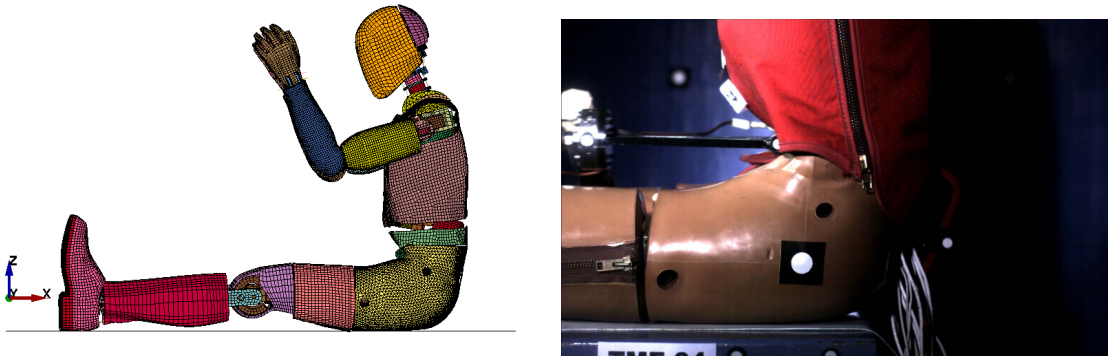

18 ms after impact

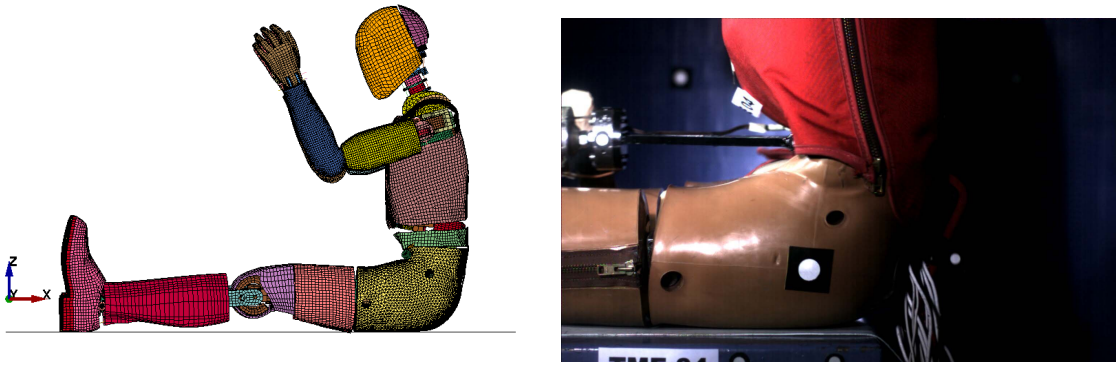

22 ms after impact

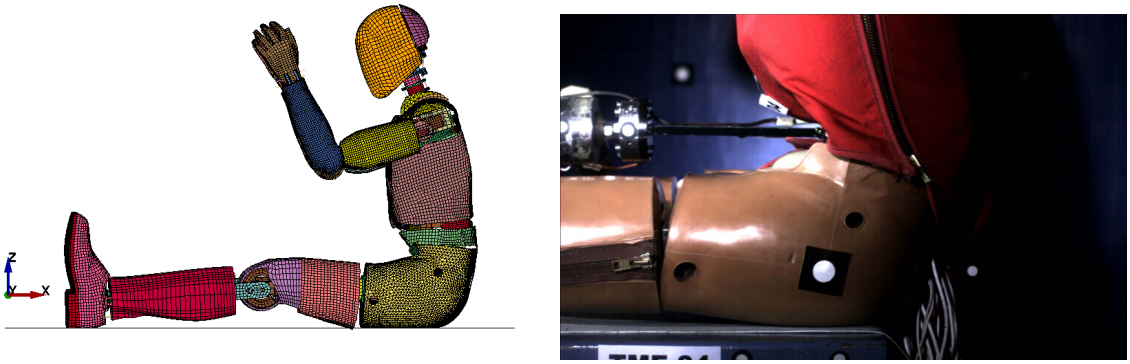

32 ms after impact

Figure 18. 6.1 m/s rigid-bar impact simulation and test (TME-04).

APPENDIX 2: SEAT BELT SIMULATION VERSUS TEST

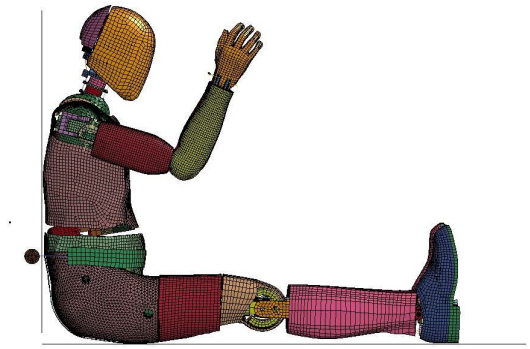

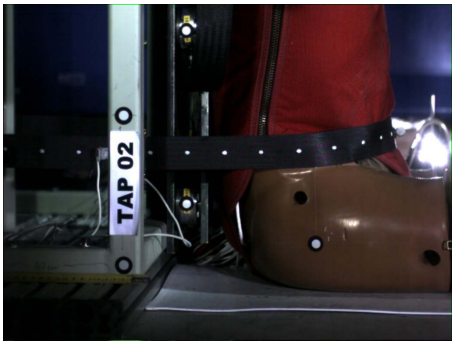

Before seatbelt retraction

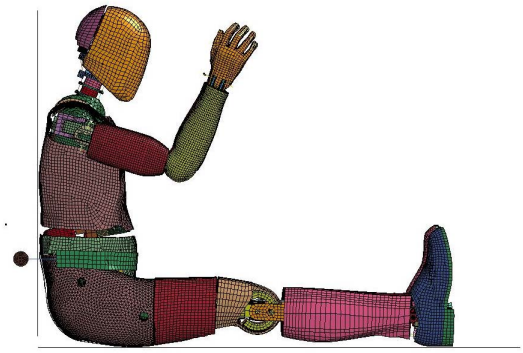

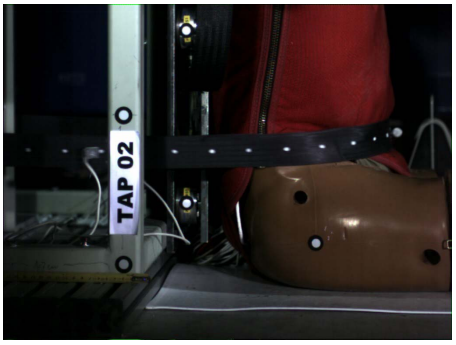

At 4 ms

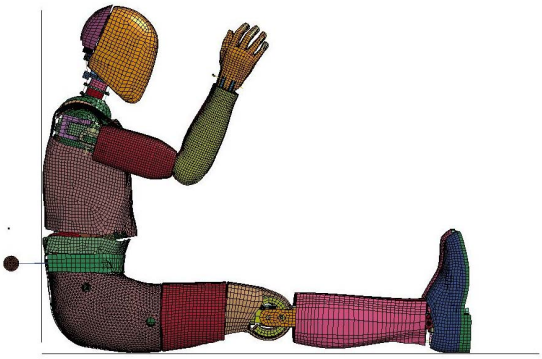

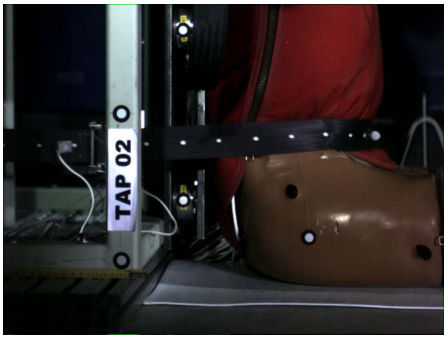

At 8 ms

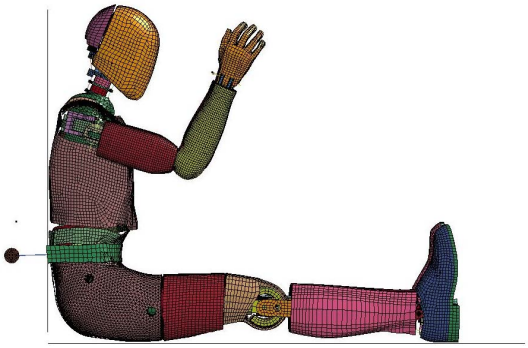

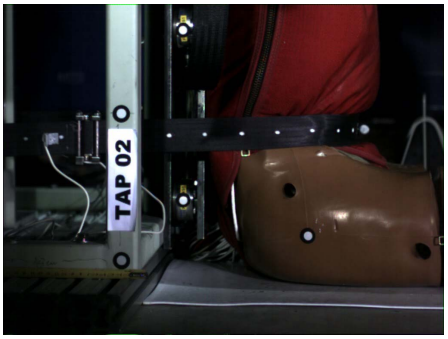

At 12 ms

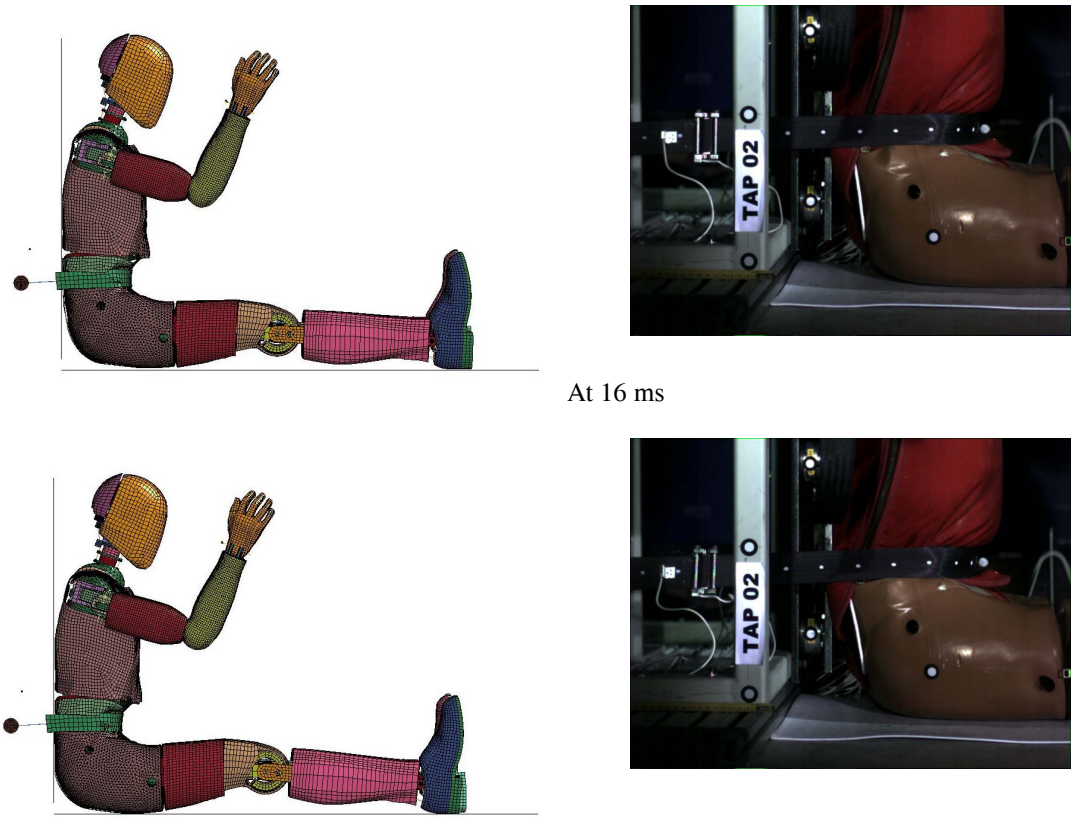

At 16 ms

At 20 ms

Figure 19. High speed seat belt simulation and test (TAP-02).

APPENDIX 3: FOAM TESTING SET-UP

Samples

Five cylindrical samples from THOR-NT lower abdomen front foam block were tested. Their geometry is described in Table 7.

Table 7.
Dimensions of tested samples

samples	Diameter (mm)	Height (mm)
A	36.89	13.07
G1	37.52	23.68
G2	37.76	18.59
G5	45.90	19.87
D5	45.96	16.24

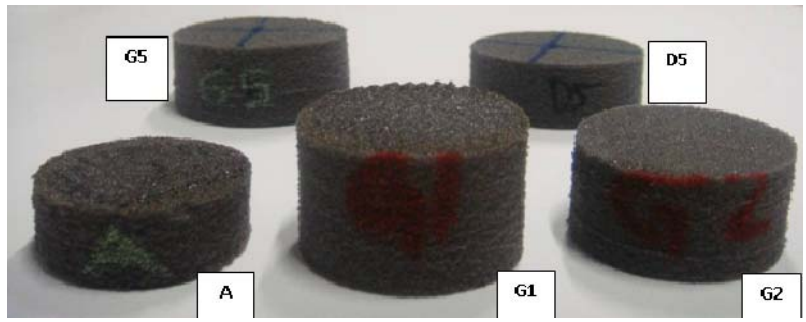

Figure 20. Photo of samples.

Test device

A cylinder impactor was used to perform compression tests on the samples according to the test matrix provided in Table 8.

Table 8.
Test matrix for compression tests on foam samples

Test Id.	Sample Id.	Impact velocity (m/s)	Impactor mass (kg)	Comments
Test 10	A	2	6	first test on sample A
Test 15	A	2	6	second test on sample A
Test 20	G1	2	6	first test on sample G1
Test 25	G1	2	6	second test on sample G1
Test 30	G2	2.5	6	first test on sample G2
Test 35	G2	2.5	6	second test on sample G2
Test 40	G5	4	6	first test on sample G5
Test 45	G5	4	6	second test on sample G5
Test 50	D5	5	6	first test on sample D5
Test 55	D5	5	6	second test on sample D5

Response Comparison for the Hybrid III, THOR Mod Kit with SD-3 Shoulder, and PMHS in a Simulated Frontal Crash

Greg Shaw

David Lessley

Joe Ash

Jeff Crandall

University of Virginia

Center for Applied Biomechanics

United States

Dan Parent

Human Injury Research Division

NHTSA

Paper Number 13-0130

ABSTRACT

This study evaluated the kinematic and chest deflection responses of a THOR Mod Kit dummy with the Chalmers/Humanetics SD-3 shoulder and the 50th percentile Hybrid III (H3) in the frontal impact 40 km/h 14 g Gold Standard 1 (GS1) test condition. THOR and H3 biofidelity were evaluated by comparing dummy response to the response of 8 post mortem human surrogates (PMHS) in prior GS1 tests. The subject was restrained by a three-point lap and shoulder belt in a right-front passenger configuration. Pelvis and lower extremity movements were restricted using a rigid knee bolster and footrest which were adjusted to be in contact with the knees and feet of each subject at the time of impact.

The THOR SD-3 shoulder sustained no damage during the course of the nine test series. In general, THOR peak x-axis chest deflection values for the anterior measurement sites were closer to those of the PMHS than the H3. However, the deflection response of neither dummy approached that of the PMHS relative to the motion of the anterior ribcage away from the spine. The THOR SD-3 exhibited a PMHS-like deflection sensitivity to belt position, a characteristic reported for the H3 (Horsch et al 1991).

The PMHS rearward motion of the loaded shoulder may result in increased chest deflection, while the forward motion of the THOR SD-3 may limit chest deflection. The H3 loaded shoulder motion was likely limited by the stiff H3 shoulder design and lack of range of motion. Because the shoulder interaction with the belt is a determinant of chest deflection, further study of the THOR SD-3 shoulder belt interaction is suggested. Similarly a comprehensive study of spinal kinematics with focus on spinal rotations that may substantially influence interaction between the ribcage and the shoulder belt is also warranted.

INTRODUCTION

While increased seat belt usage and advances in restraint design have, on average, substantially improved the injury outcome for restrained occupants, numerous fatalities and debilitating injuries are still occurring nonetheless (Viano and Ridella 1996, Elvik and Vaa 2004, NHTSA 2008, NHTSA 2009). For restrained vehicle occupants, injuries to the head and thorax are primary sources of mortality occurring from motor vehicle accidents (Huelke et al 1979, Backaitis and Dalmotas 1985, Viano et al 1986, Foret-Bruno et al 1994, Allsop and Kennett 2002, Morris et al 2002, Morris et al 2003, Kent et al 2007). This is especially true for older

occupants who are more susceptible to injury resulting from the restraining forces applied to the torso during a crash (Morris et al 2002, Morris et al 2003, Kent et al 2007). The combination of societal aging and the associated vulnerability of older persons to restraint loading injuries is a principal motivation for continued passenger safety research (Rouhana et al 2003, Bostrom and Haland 2003, Forman et al 2006). Further mitigating injuries to restrained occupants requires a more complete understanding of how the human skeletal system moves during a crash event. Occupant kinematics not only dictate the potential for contact between the vulnerable head and the interior structures of the vehicle, but also determines the interaction between the restraint system and the thorax.

Effectively evaluating the performance of current restraint systems, as well as optimizing future restraint designs, requires the use of biofidelic evaluation tools to emulate human occupant motion and to predict injury during an impact event. Anthropomorphic testing devices (ATDs) and computational models are the most commonly utilized human surrogates for this purpose.

Improved biofidelity of ATD motion and the response of the chest subjected to restraint loading remains a priority for improving frontal impact dummies. A simulated impact (sled test) provides the most realistic conditions for defining human response, as approximated by post mortem human surrogates (PMHS) and subsequently for assessing dummy biofidelity. A frontal sled test involves restraint loading of both the chest and the shoulder complex, a structure that can affect the amount of normal shoulder belt loading applied to the anterior chest.

In support of the National Highway Traffic Safety Administration (NHTSA) effort to enhance the biofidelity of the Test Device for Human Occupant Restraint (THOR) (Ridella and Parent 2011), this study evaluated the kinematic and chest deflection responses of a THOR Mod Kit dummy (SN 16) with the Chalmers/Humanetics SD-3 shoulder (THOR SD-3, for short) (Figure 1) and the 50th percentile Hybrid III (H3) in the frontal impact 40 km/h 14 g Gold Standard 1 (GS1) test condition, described in detail by Shaw et al 2009 (Figure 2). The THOR SD-3 was fitted with a shoulder designed to be more humanlike in both geometry and motion in comparison to that of the original THOR shoulder (Lemmen et al 2013). THOR SD-3 and H3 biofidelity was evaluated by comparing dummy response to the response of 8 PMHS in prior GS1 tests (Table 1) (Shaw et al 2009).

Table 1: Test Matrix

Test Condition		# of tests		
		H3	THOR SD-3	PMHS
GS1	**Gold Standard Condition 1** **40km/h, Standard Belt**	3	3	8

METHODOLOGY

The subject was forward-facing and restrained in a right-front passenger configuration. Subject and restraint positioning were tightly controlled to reduce test-to-test variability. The test fixture (Figure 3) and test methodology, described by Shaw et al 2009, was designed to provide a reasonable approximation of a real-world frontal crash with a restrained occupant while providing repeatable and reproducible test conditions that would allow whole-body kinematic response to be comprehensively measured and analyzed. The restraint consisted of a 3-point lap and shoulder belt with anchor positions approximating those found in a typical mid-size U.S. sedan. The belt did not include a retractor and did not allow for pass-through at the representation of the buckle. The webbing material, which was replaced for each test, was manufactured by Narricut (International twill pattern 13195, 6-8% elongation). Pelvis and lower extremity movements were restricted

using a rigid knee bolster and footrest which were adjusted to be in contact with the knees and feet of each subject at the time of impact. The combination of lap belt, knee bolster, and footrest was designed to minimize pelvic and lower extremity movements during the impact event while allowing the characteristic forward torso motion associated with an actual automotive restraint system.

SD-3 Shoulder Durability Monitoring

In previous testing with the Chalmers SD1 shoulder (Shaw et al 2010), mechanical failure occurred in the joint connecting the upper arm to the shoulder after three tests were carried out. Similar issues were discovered in testing with the SD-2 shoulder, though the number of tests that were carried out before mechanical failure occurred is not clear. Thus, the durability of the SD-3 shoulder was carefully monitored during this test series that included the three tests reported in this paper and an additional six tests with a force-limited shoulder belt. With the jacket removed, the shoulder was examined and manipulated before the test series and after each of the tests with special attention to the distal clavicle ball joint, polymer bumper stops, and fastener security.

Subject Kinematics

A 16-camera, 1000 Hz optoelectronic stereophotogrammetric system (Vicon, MX series, Oxford, UK) was used to obtain trajectories of retroreflective target clusters (Figure 4) attached to the head, spine, shoulders, and pelvis of each subject. The recorded trajectories of the attached target clusters were used to calculate the trajectories of selected underlying anatomical structures using a coordinate transformation and the assumption of rigid body motion described in detail by (Lessley et al. 2011). Using the methodology described by Parent et al, 2012, kinematics were calculated at consistent anatomical landmarks for both the ATDs and the PMHS. While an abundance of kinematic data was obtained for each subject, this paper specifically focuses on the displacements of the 1st thoracic vertebra (T1) and bilateral acromia (Figure 4) relative to the vehicle buck coordinate system (Figure 3), which conformed to the recommendations set forth by SAE (2003). Since the PMHS subjects closely approximated the 50th percentile male, no scaling of the displacement data was performed.

Chest Deflection

Chest deflection was measured by sensors mounted in the ATD thorax. The THOR SD-3 uses double-gimbaled Infrared Telescoping Rods for Assessment of Chest Compression (IR-TRACCs) to measure 3D deflection of the four quadrants of the anterior ribcage relative to the spine (Figure 2b) (Shaw et al 2012). The H3 chest included a rotary potentiometer that recorded X-axis motion of the sternum relative to the spine (chest slider) as well as string potentiometers that recorded data processed to yield X-axis and Y-axis deflection of four points on the upper and lower ribs (Butcher et al 2001) (Figure 2a). PMHS chest deflection was measured at five locations using the same motion capture system used for the kinematic measurements employing a methodology detailed in Shaw et al (2009).

Data Analysis and Presentation

Comparing chest deflection involved calculating the maximum and minimum values recorded in each test and determining the mean and standard deviation for each group (PMHS, THOR SD-3, and H3). PMHS deflection data used for comparison with the dummies excluded one of the 8 subjects who had sustained 29 rib and sternal fractures. Peak deflection was calculated in two ways. The first method involved calculating an average and SD for each quadrant and, for the H3 and PMHS, the sternum. The second method involved identifying the peak X-axis motion toward the spine for each subject no matter where the deflection occurred. Because the calculation was not restricted to a specific region, the resulting average could be greater than that calculated for an individual region. For example, the location of peak deflection occurred at both the sternum and upper quadrants for the PMHS. Therefore, averaging the subjects' peak deflection at any site, either at the sternum,

upper left, or upper right, resulted in a greater "overall" peak than averaging only peak values at any one of these sites.

RESULTS

No problems were encountered recording subject kinematics or chest deflection. The SD-3 shoulder exhibited no evidence of damage or wear in the course of the testing, and all fasteners remained snug.

Kinematics

An overhead view of the subject kinematics in the X-Y plane of the vehicle buck is provided in Figure 5. The positions of the left acromion, right acromion, and T1 are provided for each subject at 20 ms intervals during the impact event up to the time of peak chest deflection which occurred at approximately 120 ms. Figure 5 also provides an overlay of PMHS, THOR, and H3 mean T1 and acromia positions at the time of peak chest deformation. Mean X-axis excursions for T1 and RAc are provided relative to the vehicle buck in Figure 6. Mean peak X-axis displacement values ± 1 standard deviation (SD) are provided in Figure 7.

Chest Deflection

Figure 8 shows the average X-axis deflection time-histories for the THOR SD-3, H3, and PMHS groups. The average PMHS response is shown in thick gray lines, while the individual responses are shown as thin gray lines to illustrate subject-to-subject variability. Belt loads are also plotted in Figure 8 using the same time scale. Table 2 summarizes the peak deflection values along the positive and negative X, Y, and Z axes. For example, a negative X-axis peak indicates the closest a measurement site has moved along a perpendicular path toward the spine, while a positive X-axis peak indicates maximum motion away from the spine. Note that the H3 instruments do not record Z-axis ribcage motion. Figure 9 plots the X-axis peak values. One SD values are provided in Table 2 and indicated with error bars in Figure 9.

DISCUSSION

Chest Deflection

The magnitude of overall chest deflection, since it acts as a proxy for local strains in the rib cage, has been associated with thoracic injuries such as rib and sternal fractures. Specifically, a reduction in the distance between the anterior rib cage and the spine has been used as a measure of rib fracture risk (Shaw et al 2009). In frontal loading, this change in distance is approximated by the change of the X-axis component of the anterior ribcage-to-spine distance. Lateral (Y-axis) and vertical (Z-axis) motion of the anterior ribcage further characterize ribcage deformation.

Peak chest deflection, as defined by the motion of any anterior ribcage site towards the spine (negative X-axis) was found to be greatest for the PMHS. Of the dummies, the THOR SD-3 recorded a higher peak than the H3 (Figure 10).

The location of the peak X-axis deflection was different for the dummies and the PMHS. The location of the peak X-axis deflection for the dummies was always recorded at the lower left site. However, the peaks occurred for the individual PMHS at either the upper left (3/7), sternum (3/7), or the upper right measurement site (1/7). Therefore, the overall peak PMHS deflection was calculated by using peak values that occurred at three sites. Figure 11 illustrates the effect on the overall peak deflection value if the sternum is not included ("Overall Peak w/out Sternum"), a decrease of 11 percent (-66 to -59mm). Alternatively, if only the peak sternal values are used to calculate the overall average deflection, the peak is reduced by only 2 mm (-66 to -64mm). Using the H3 sternal (slider) peak value rather than the lower left reduces the overall average by only 3mm (-36 to -33mm) (Table 2).

Belt Path Effect on Deflection

With one exception, the THOR SD-3 peak deflections were closer than the H3 to the average PMHS, consistent with the findings of the prior quasistatic study discussed above (Shaw et al 2005). However, both the THOR SD-3 upper right X-axis peak and the upper left/right peak ratio were less PMHS-like than the H3 (Figure 9).

The pattern of peak deflection values for the upper ribcage was related to shoulder belt position relative to the upper measurement sites. When the belt paths in the PMHS tests were examined individually, we found a robust relationship between proximity of the belt and the site of peak upper rib cage deflection (Shaw et al 2009) (Figure 12). In general, the shoulder belt path across the upper thorax in the PMHS tests generally fell between the upper left and upper right measurement sites, though there were some exceptions where the belt was lateral to the upper left measurement site. Accordingly, the PMHS upper peak values were mostly symmetrical average deflections of -48mm and -53 mm for the upper left and right, respectively. For the H3, the shoulder belt was between the upper left and right measurement sites on the ribcage, but the chest deflections were less symmetrical than the PMHS ((upper right -20 mm, upper left -31 mm). For the THOR SD-3, the shoulder belt path was lateral of the upper left measurement site, and the resulting chest deflections were noticeably asymmetrical (upper right -5mm, upper left -42 mm). This asymmetry was also present in at least one individual PMHS test in which the belt path was lateral to the upper left measurement site (Figure 13). In this case the peak deflections measured at the upper chest measurement locations were almost identical between THOR SD-3 and PMHS.

In the frontal crash simulated in the reported tests, chest deflection is a function of how the inertially propelled torso loads the shoulder belt. The effects of inertial loading and the motion of the shoulder loaded by the belt were factors examined in this study.

Inertial Loading Effects on Deflection

In a comparison of X-axis peak chest deflections recorded at the different measurement sites, the PMHS values generally were greater than those of the dummies (Table 2), consistent with the results for overall peak deflection and consistent with prior bench top test results for earlier versions of THOR (Shaw et al 2005). For example, a study conducted by Shaw et al (2005) compared quasistatic indentor loading of the anterior ribcage of the H3 and THOR Alpha with PMHS. For the same 25mm deflection applied to the lower quadrant, the recorded reaction force recorded by the indentor load cell was lowest for the PMHS. The reaction force for THOR Alpha was three times higher and that for the H3 thirteen times higher.

However, in this study, the lower left site for both the H3 and the THOR SD-3 moved closer to the spine (negative X-axis) than did the PMHS (Table 2, Figures 8 and 9). Assuming comparable normal belt loading, the quasistatic test results would suggest far greater PMHS deflection than either of the dummies.

The reason for this apparent incongruity may be related to differences in the loading conditions in the bench top and sled test environments. We propose that inertial loading, present in only the sled test condition, may be the most likely and dominant factor.

The possible effects of inertial loading are evident in the X-axis time history deflection plots of the lower two measurement sites (Figure 8). At approximately 50 ms the THOR SD-3 and, more prominently, the PMHS, record motion of both sites away from the spine. This motion occurs even at the lower left measurement site near the belt path. Figure 14 shows the total normal shoulder belt force relative to X-axis deflection using the method described in Salzar et al 2011. This analysis indicates that the sum of normal belt force along the belt must exceed almost 4kN before the PMHS lower left measurement site moves toward the spine (Figure 14, bottom). For the lower right measurement site farthest from the belt path, the motion away from the spine persists for both the PMHS and THOR SD-3. Neither of the H3 lower measurement sites move away from the spine, as expected since the H3 ribcage is known to be more highly coupled than that of the THOR (Shaw et al 2005).

Inertial loading acting on the anterior rib cage, as illustrated in Figure 15, is proposed as the cause for its movement away from the spine. Differential motion of the spine relative to the anterior ribcage requires a restraining force acting on the spine to resist the inertial forces pulling both the spine and anterior ribcage forward. This spine restraining force is provided by the pelvis, well restrained by the lap belt and femurs against the knee bolster, via the pelvic/spine interface. The amount of compliance in this interface and torso angle determines the amount of restraining force acting perpendicular to the upper spine.

The upper segment or segments of the dummy spine are restrained by the rubber lumbar spine. The bending stiffness of this element restrains the spine relative to the anterior ribcage during the early phase of the crash event allowing the ribcage to move away from the spine a few millimeters. This motion is limited by the low inertial forces acting on the low mass of the anterior ribcage relative to the spine box.

The PMHS thoracic spine is restrained by the lumbar spine in the same manner. However, the inertial forces acting on the anterior ribcage are not limited by the mass of the ribcage alone. The forward motion of the internal organs, not replicated in dummy thorax construction, also act to move the ribcage away from the spine. This “bulge out” is most prominent for the PMHS lower right measurement site (Figure 16). That the dummies do not replicate PMHS “bulge out” is not unexpected given a longstanding focus to replicate PMHS thoracic response to compressive loading.

Shoulder Motion

The motion of the loaded shoulder and clavicle is both a response and determinant of shoulder belt interaction with the torso. The normal belt load born by the torso is shared by the clavicle/shoulder complex and the anterior rib cage (Horsch et al 1991). The farther forward the shoulder moves, the more the belt is loaded by the shoulder and the less it is loaded by the anterior ribcage resulting in lower chest deflection.

Figure 5 illustrates differences in the kinematic behavior between PMHS and the ATDs. When viewed from above, the PMHS exhibit a greater clockwise rotation of the shoulders about the vertical Z-axis of the vehicle buck than either of the ATDs. This is most apparent when looking at the overlay of all subjects at 120 ms (Figure 5), which is also the approximate time of peak chest deflection. Relative to the H3, the PMHS are considerably more rotated, however, the comparison with THOR is more complex. The line segment connecting the left acromion (LAc) and T1 are very similarly angled for THOR and the PMHS; however this trend is not repeated for the loaded right shoulder. The line connecting the right acromion (RAc) and T1 is angled much more forward for THOR than for the PMHS, or even the H3.

The PMHS exhibit the largest forward excursion of T1 and also the largest difference between the RAc and T1 excursions relative to the vehicle buck (Figures 6 and 7). THOR exhibits nearly equal excursions of both RAc and T1.

Although this analysis found substantial differences among the test subjects, a more sophisticated analysis is required to fully characterize shoulder and torso motion and to quantify upper spine rotation and its potential effect on chest deflection.

Limitations

This study was not intended to be a definitive evaluation of dummy performance in terms of its ability to approximate the response of PMHS in a frontal crash. The scope of the study was limited to one of at least three test conditions proposed by UVA for the Gold Standard simulated frontal impacts, an effort to produce PMHS-derived performance targets. Findings such as the bulge out may not be as prominent in conditions that do not block the knees at the start of the event. The proposed reason for the bulge out, inertial loading, while consistent with the study findings, was not quantified.

The locations of anterior ribcage measurement sites for the three subjects are in the same quadrant but not necessarily the same location within the quadrant (Figure 2). Although the ribcage deflection measurements

sites on the PMHS targeted similar locations on THOR, constraints in instrument mounting compromised the final location for some subjects. The H3 sites, especially the upper sites, are in different locations relative to THOR and the PMHS.

Study limitations prevent definitive conclusions regarding shoulder motion and its effect on chest deflection. Clavicle motion was estimated by the motion of a segment connecting the T1 and the acromion. However, the motion of the clavicle itself, likely the shoulder component most loaded by the belt, was not measured directly. While the distal end of the clavicle moves with the acromion, the medial end joins the top of the sternum which moves with the (deforming) ribcage. Another parameter not adequately quantified was the position of the belt relative to the clavicle throughout the event. A belt that loaded the clavicle near the sternum would be less affected by forward motion of the distal clavicle/acromion.

The tested THOR SD-3 was a pre-production prototype constructed from a combination of used and new components.

CONCLUSIONS AND RECOMMENDATIONS FOR FURTHER STUDY

The THOR SD-3 sustained no damage or sensor failures during the course of the nine-test series. While not a comprehensive assessment of durability, this result is encouraging.

In general, THOR SD-3 peak X-axis chest deflection values for the anterior measurement sites were closer to those of the PMHS than the H3 (Figure 9). However, the deflection response of neither dummy approached that of the PMHS relative to motion of the anterior ribcage away from the spine (positive X-axis). Further investigation is needed to define the effects of inertial loading, motion of the anterior ribcage away from the spine, and, most importantly, its effect on fracture risk.

The THOR SD-3 also exhibited a PMHS-like deflection sensitivity to belt position, a characteristic reported for the H3. Fully characterizing sensitivity to belt position may produce a valuable dummy response performance target. Additional work would be needed to relate this parameter to fracture risk.

The PMHS rearward motion of the loaded shoulder may result in increased chest deflection, while the forward motion of the THOR SD-3 may limit chest deflection. The H3 loaded shoulder motion was likely limited by the stiff H3 shoulder design and limited range of motion. Because the shoulder interaction with the belt is a determinant of chest deflection, further study of the THOR SD-3 shoulder belt interaction is suggested. Similarly a comprehensive study of spinal kinematics with focus on spinal rotations that may substantially influence interaction between the ribcage and the shoulder belt is also warranted.

ACKNOWLEDGMENTS

The authors acknowledge the support and guidance of the National Highway Traffic Safety Administration (NHTSA), U S Department of Transportation. This study was supported by DOT NHTSA Grant DTNH22-09-H-00247. All findings and views reported in this manuscript are based on the opinions of the authors and do not necessarily represent the consensus or views of the funding organization.

REFERENCES

Allsop, D, Kennett, K. Skull and Facial Bone Trauma. in Accidental Injury: Biomechanics and Prevention- 2nd Edition, editors, Nahum AM;Melvin J. 2002; New York: Springer.

Backaitis, S, Dalmotas, D. Injury Patterns and Injury Sources of Unrestrained and Three Point Belt Restrained Car Occupants in Injury Producing Frontal Collisions. Proceedings of the Association for the Advancement of Automotive Medicine (AAAM). 1985;29.

Bostrom, O, Haland, Y. Benefits of a 3+2 point belt system and an inboard torso side support in frontal, far-side and rollover crashes. Paper 451, International Technical Conference on the Enhanced Safety of Vehicles (ESV). 2003; 18. Nagoya,Japan.

Butcher, J, Shaw, CG, Bass, CR, Kent, RW, Crandall, JR. Displacement Measurements in the Hybrid III Chest. SAE Transactions: Journal of Passenger Cars. 2001;110(6): 26-31. Based on SAE Paper 2001-01-0118.

Elvik R, Vaa, T. The handbook of road safety measures. 2004;Amsterdam, Elsevier Science.

Foret-Bruno, J, Le Cox, J, Thomas, C, Brutel, G. In Depth Analysis of Frontal Collisions As Regards the Influence of Overlap and Intrusion On Occupant Severe and Fatal Injuries. International Technical Conference on the Enhanced Safety of Vehicles (ESV). 1994;14.

Forman, JL, Lessley, DJ, Kent, RW, Bostrom, O, Pipkorn, B. Whole-body Kinematic and Dynamic Response of Restrained PMHS in Frontal Sled Tests. Stapp Car Crash Journal. 2006;50: 299-336.

Horsch, J, Melvin, J, Viano, DC, Mertz, H. Thoracic injury assessment of belt restraint systems based on Hybrid III chest compression. Paper 912895, Society of Automotive Engineers. 1991.

Huelke, DF, Sherman, HW, Murphy, MJ, Kaplan, RJ. Effectiveness of Current and Future Restraint Systems in Fatal and Serious Injury Automobile Crashes. Data From On-Scene Field Accident Investigations. Paper 790323, Society of Automotive Engineers (SAE). 1979.

Kent, RW, Balandin, D, Bolotnik, N, Pilkey, WD, Purtsezov, S. Optimal control of restraint forces in an automobile impact. Journal of Dynamic Systems, Measurement, and Control. 2007;129: 415-424.

Lemmen, P, Bernard Been Jolyon Carroll, David Hynd Johan Davidsson Jeff Crandall, Greg Shaw Cecilia Sunnevang Autoliv Research Erwan Lecuyer, Eric Song Andre Eggers Luis Martinez Philippe Vezin. (2013) An Advanced Thorax-Shoulder Design for the THOR Dummy. Submitted to 2013 ESV.

Lessley, DJ, Shaw, CG, Riley PO, Forman, JL, Crandall, JR. Assessment and Validation of a Methodology for Measuring Anatomical Kinematics of Restrained Occupants During Motor Vehicle Collisions. Journal of Biosensors and Bioelectronics. 2011;S1.

Morris, A, Welsh, R, Frampton, R, Charlton, J, Fildes, B. An Overview of Requirements for the Crash Protection of Older Drivers. Annual Proceedings/Association for the Advancement of Automotive Medicine (AAAM). 2002;46:141-156.

Morris, A, Welsh, R, Hassan, A. Requirements for the Crash Protection of Older Vehicle Passengers. Annual Proceedings/Association for the Advancement of Automotive Medicine (AAAM). 2003;47:165-180.

NHTSA. Motor vehicle occupant protection facts 2006. 2008;Washington, DC, National Highway Traffic Safety Administration.

NHTSA. Fatalities in Frontal Crashes Despite Seat Belts and Air Bags. Review of All CDS Cases Model and Calendar Years 2000-2007 122 Fatalities. 2009;HS 811 202, September, NHTSA US DOT, Washington, DC.

Parent, DP, Lessley, DJ, Shaw, CG, Crandall, JR. Identification of anatomical landmarks for whole-body kinematic measurement in the THOR Mod Kit frontal impact ATD. Paper 20125177, JSAE Annual Congress. 2012.

Ridella, SA, Parent, DP. Modifications to Improve the Durability, Usability and Biofidelity of the THOR-NT Dummy. Paper Number 11-0312. Proceedings of the 22nd International Conference on the Enhanced Safety of Vehicles (ESV). 2011

Rouhana SW; Bedewi PG; Kankanala SV; Prasad P; Zwolinski JJ; Meduvsky AG; Rupp JD; Jeffreys TA; Schneider LW. Biomechanics of 4-Point Seat Belt Systems in Frontal Impacts. Stapp Car Crash Journal. 2003;47: 367-399.

Salzar, RS, Lessley, DJ, Sochor, MR, Shaw, CG, Kent, RW, Crandall, JR. Thoracic Response to Shoulder-Belt Loading: Comparison of Table-Top and Frontal Sled Tests with PMHS. IRCOBI Conference on the Biomechanics of Impact. 2011.

Shaw, CG, Lessley, DJ, Ash, JH, Crandall, JR. Development of an Alternative Frontal Impact Condition to Assess Thoracic Response Using the THOR Mod Kit Dummy. 2012;Paper 20125216, JSAE Annual Congress.

Shaw, CG, Lessley, DJ, Kent, RW, Crandall, JR. Dummy Torso Response to Anterior Quasi-Static Loading. Paper 05-0371, Proceedings of the 19th International Technical Conference on the Enhanced Safety of Vehicles (ESV). 2005.

Shaw, CG, Parent, D, Purtsezov, S, Lessley, D, Crandall, JR, Kent, RW, Guillemot, H, Ridella, SA, Takhounts, E, Martin, P. Impact response of restrained PMHS in frontal sled tests: skeletal deformation patterns under seat belt loading. Stapp Car Crash Journal. 2009;53:1-48.

Shaw, CG, Parent, DP, Purtsezov, S, Lessley, DJ, Crandall, JR, Tornvall, F. (2010) Torso deformation in frontal sled tests: comparisons between THOR NT, THOR NT with Chalmers SD-1 shoulder, and PMHS. IRCOBI Conference on the Biomechanics of Impact.

Society of Automotive Engineers. Surface Vehicle Recommended Practice J211-1 –Instrumentation for Impact Test – Part 1 –Electronic Instrumentation, Warrendale, PA. 2003

Viano DC; Melvin JW; Mccleary JD; Madeira RG; Shee TR; Horsch JD. Measurement of Head Dynamics and Facial Contact Forces in the Hybrid III Dummy. Paper 861891. Stapp Car Crash Conference Proceedings. 1986.

Viano, D, Ridella, S. Crash Causation: a Case Study of Fatal Accident Circumstances and Configurations. Paper 960458, Society of Automotive Engineers (SAE). 1996.

Figures

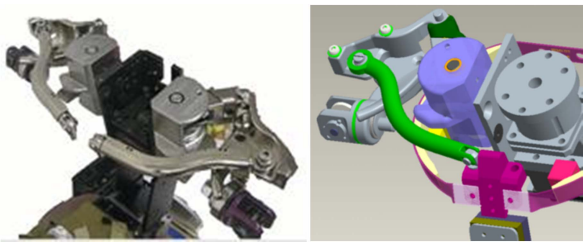

Figure 1. SD-3 shoulder.

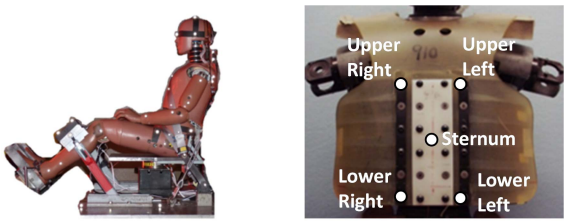

a Hybrid III

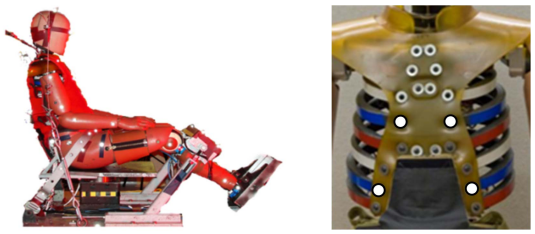

b THOR SD-3

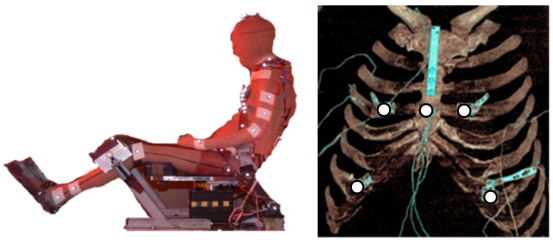

c PMHS

Figure 2. Study subjects and location of deflection measurement sites on the anterior ribcage.

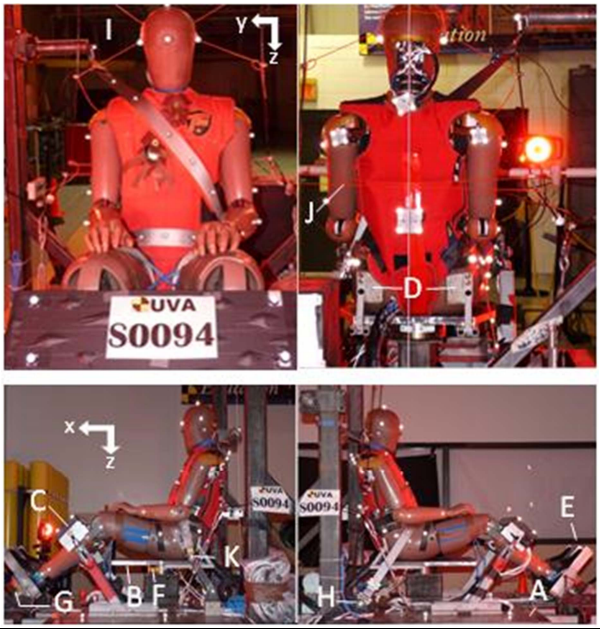

A	Buck	Restraint geometry similar to 1998 Ford Taurus front passenger position.
B	Seat	Rigid horizontal aluminum plate.
C	Knee bolster	Adjustable bilateral non-padded knee channels atop 5-axis load cells.
D	Pelvic block	Adjustable bilateral blocks to prevent pelvic posterior migration pre-test.
E	Footrest	Adjustable bilateral channels with ankle straps to immobilize feet and lower legs.
F	Seat load cell	6-axis load cell supporting seat.
G	Footrest load cell	6-axis load cell supporting seat.
H	Right lap belt anchor	Center of bolt head securing the right belt to the anchor mount defines the buck coordinate system for 3D movement data. Lap belt length adjuster tongue mounts here.
I	Upper shoulder belt anchor	Center of bolt head securing upper shoulder belt segment. Adjustable in Z and Y.
J	Back	Adjustable back and head support provided by horizontal wires attached to vertical cables.
K	Left lap and shoulder belt anchor	Anchor point is position at an OEM location by a "stalk" surrogate. Shoulder belt length adjuster tongue and the left lap belt anchor mount here.

Figure 3. Test hardware. Thor SD-3 shown.

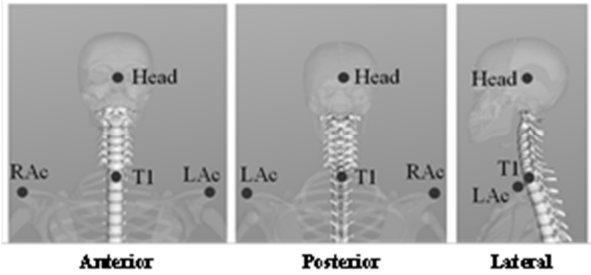

Figure 4. Calculated anatomical kinematic measurement locations.

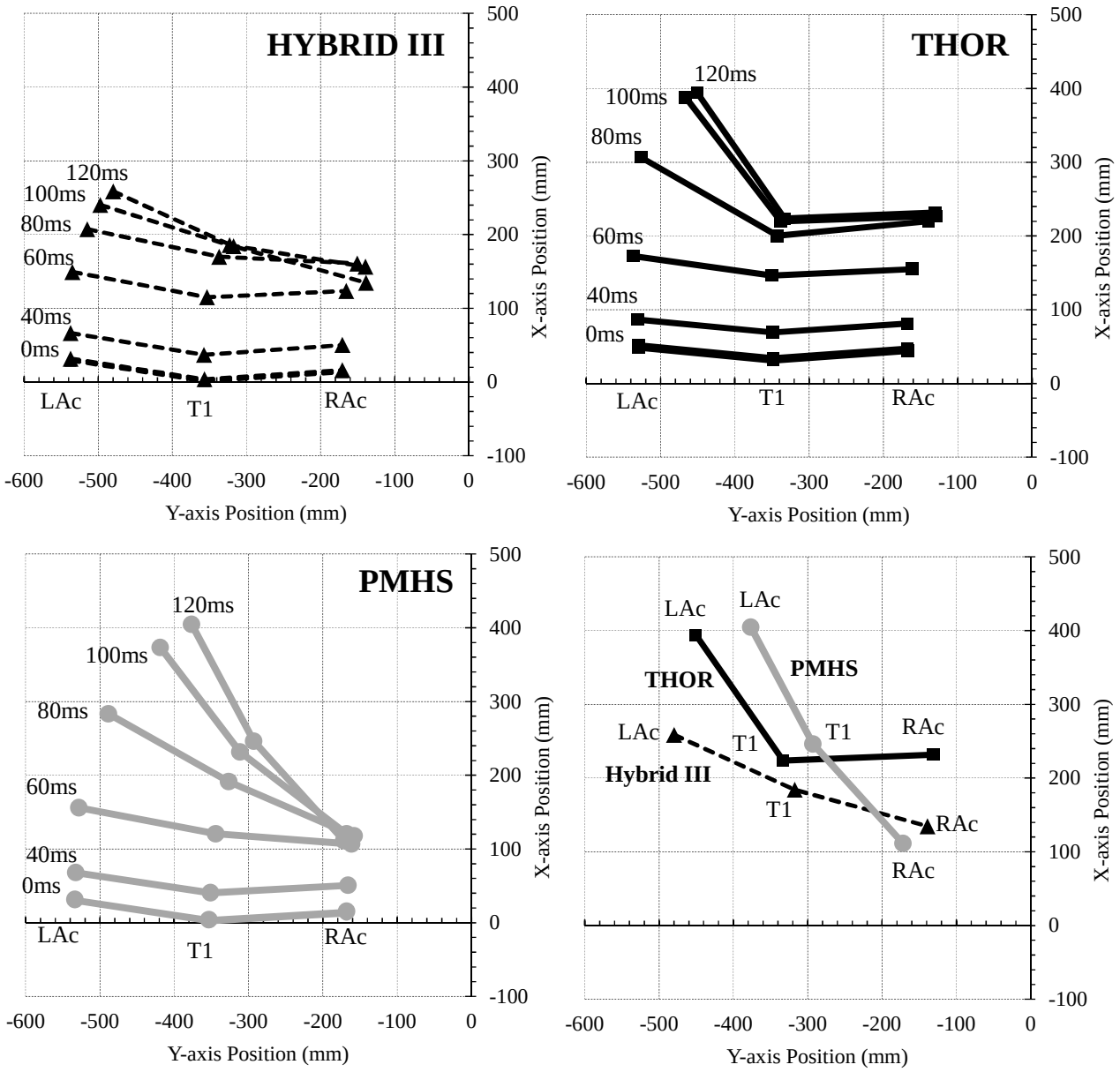

Figure 5. Overhead view of subject kinematics. Position of T1 and bilateral acromia at 20 ms intervals for each subject. Overlay of all subjects at 120 ms (lower right plot).

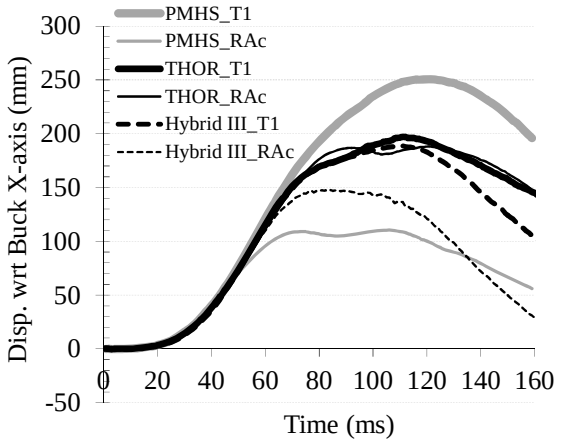

Figure 6. Right Acromion (RAc) and T1 displacement with respect to the vehicle buck. Plots represent the mean from all available tests for each subject.

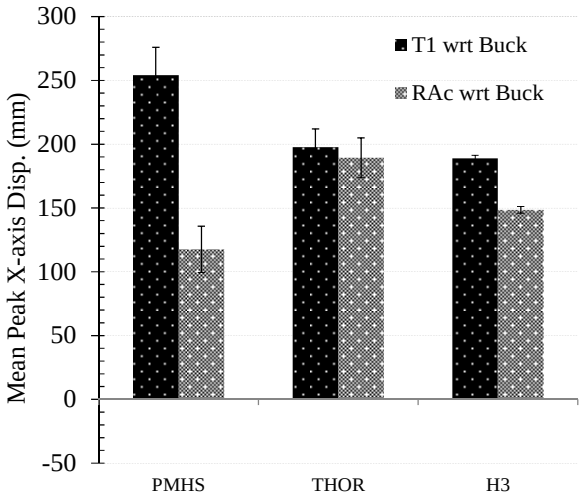

Figure 7. Mean Peak X-axis displacements ± 1 S.D. for each subject.

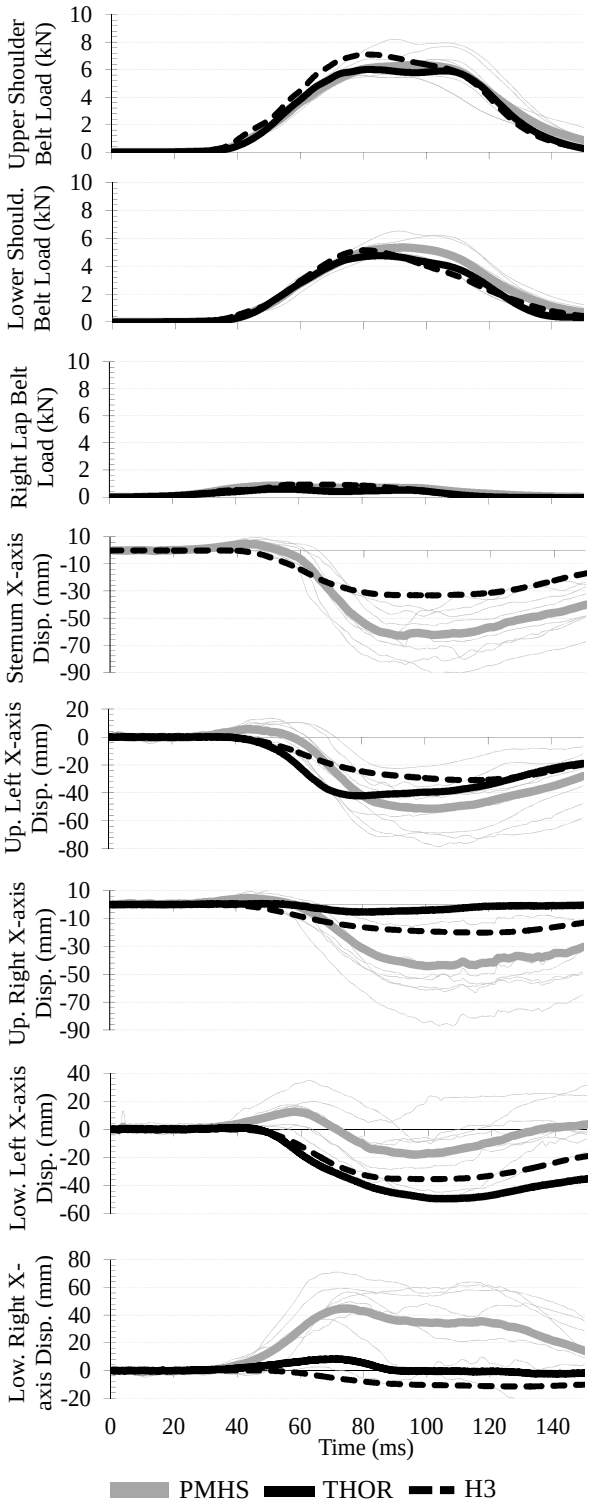

Figure 8. X-axis chest deflection, sled pulse, and belt loads.

Table 2. GS1 Chest Deflection.

		Upper Right							Sternum							Upper Left					
		+X	-X	+Y	-Y	+Z	-Z		+X	-X	+Y	-Y	+Z	-Z		+X	-X	+Y	-Y	+Z	-Z
H3	mm	0	**-20**	7	-1				0	-33						0	-31	4	-1		
	SD	0	0	1	0				0	0						0	0	1	0		
THOR SD-3	mm	**1**	-5	**11**	**-8**	6	-14									**1**	**-42**	**10**	**-5**	17	-7
	SD	0	1	1	1	1	1									0	1	2	1	1	1
PMHS	mm	11	-48	32	-6	16	-20		9	-67	27	-14	21	-10		9	-53	34	-5	15	-11
	SD	10	27	3	7	8	17		5	18	7	11	7	9		6	20	6	6	9	9
		Lower Right														Lower Left					
		+X	-X	+Y	-Y	+Z	-Z									+X	-X	+Y	-Y	+Z	-Z
H3	mm	0	**-12**	6	-1											0	**-36**	3	-4		
	SD	0	0	1	1											0	1	1	1		
THOR SD-3	mm	**9**	-3	**11**	**-6**	10	-6									**4**	-50	**19**	-4	11	-10
	SD	1	1	1	2	0	1									1	2	1	3	0	0
PMHS	mm	49	-7	43	-2	13	-53									16	-22	45	-2	13	-33
	SD	19	12	10	1	7	21									13	18	14	1	4	11

Bold indicates value closer to PMHS

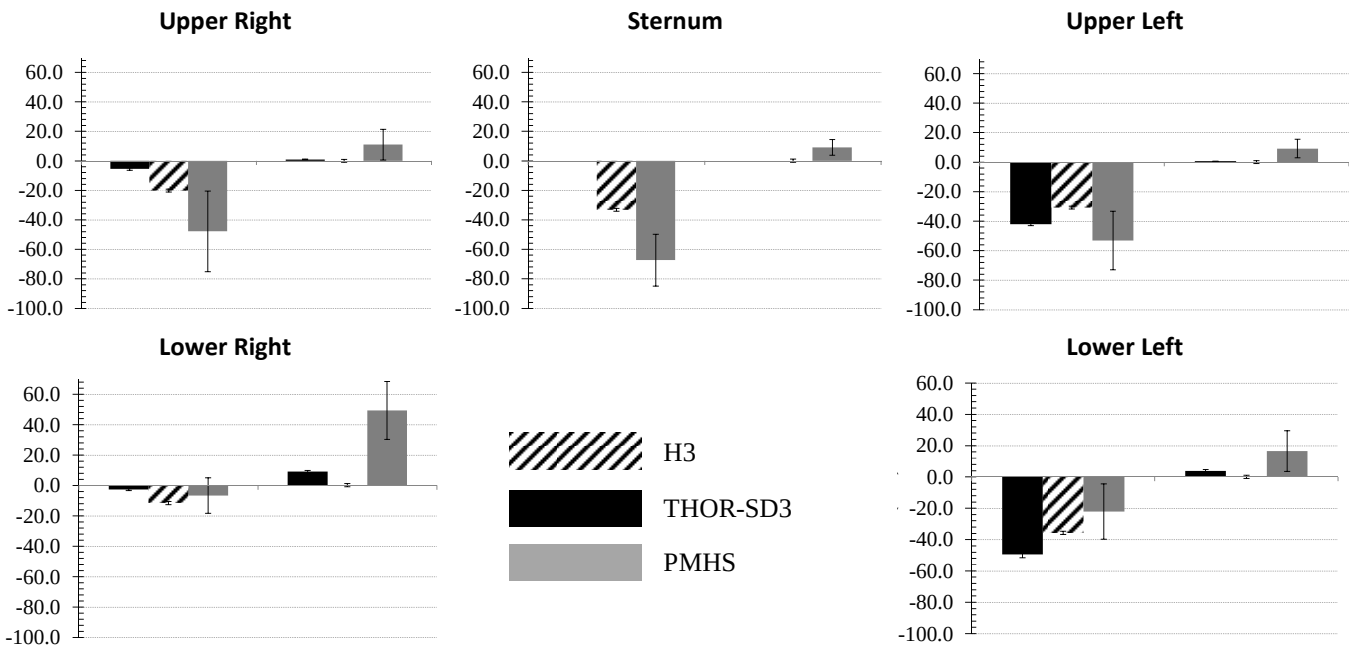

Figure 9. GS1 X-axis deflection. Average values with 1 SD.

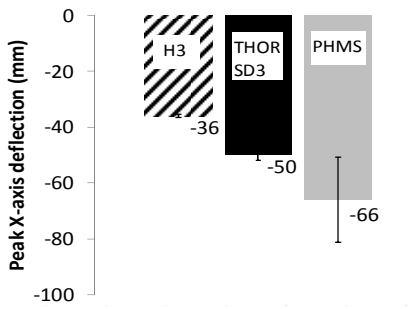

Figure 10. Peak X-axis deflection (with standard deviation) towards the spine, any site.

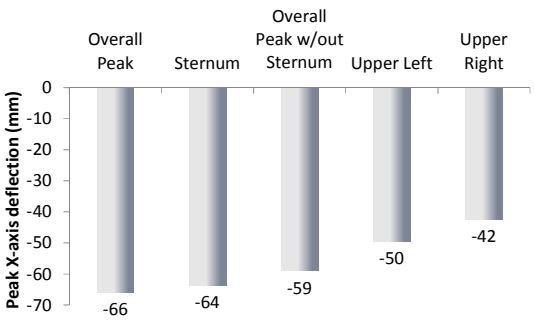

Figure 11. PMHS average X-axis peak deflections for the sternum and upper measurement sites.

Overall Peak	Average of peak values where ever they occur
Sternum	Average of sternal peak values only
Overall Peak w/out Sternum	Average of peak values where ever they occur excluding the sternum
Upper Left	Average of upper left peak values only
Upper Right	Average of upper right peak values only

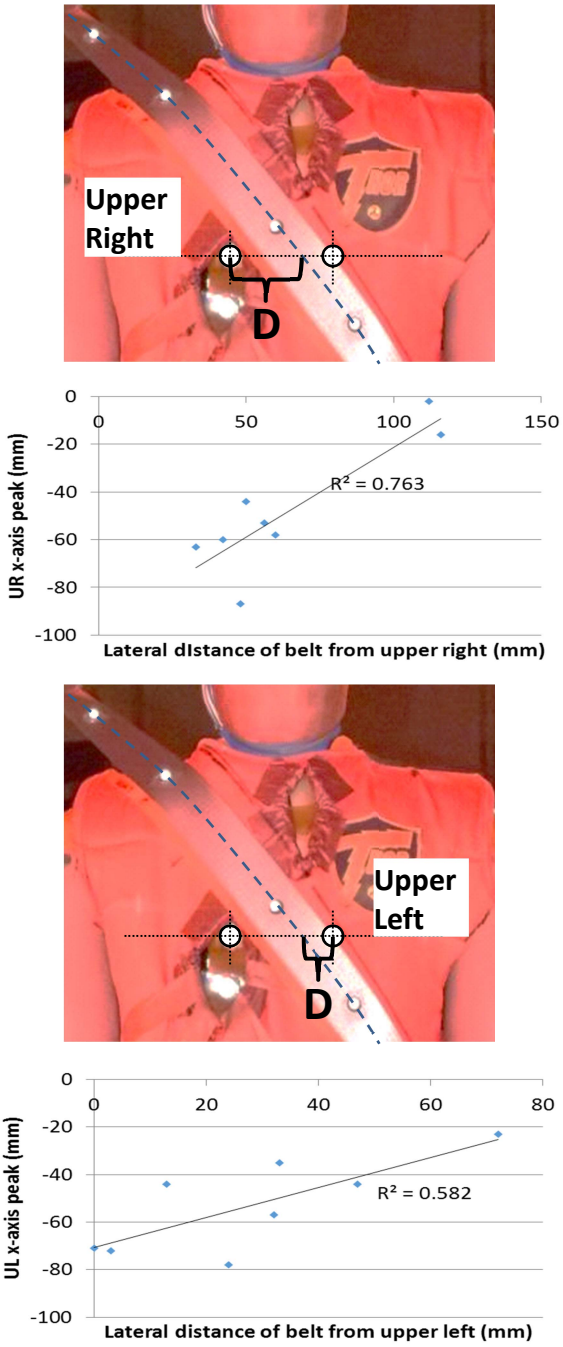

Figure 12 . Relationship between measurement site distance to belt path and peak deflection.

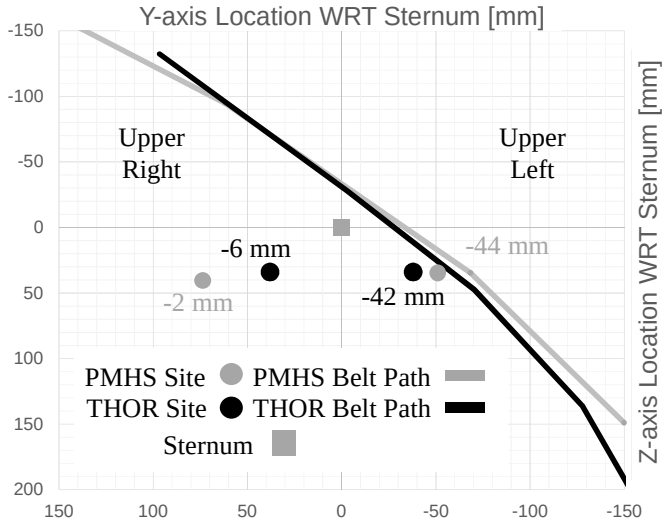

Figure 13. Belt paths, upper measurement sites, and X-axis deflections of a single PMHS and THOR.

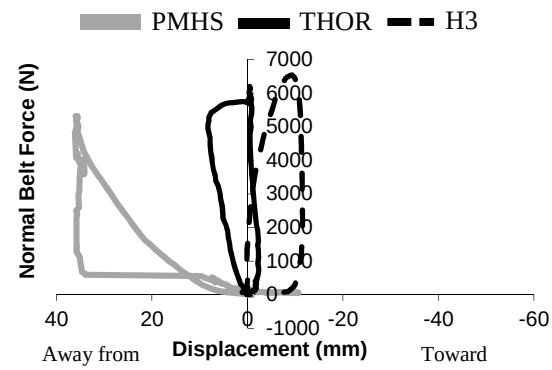

Lower Right

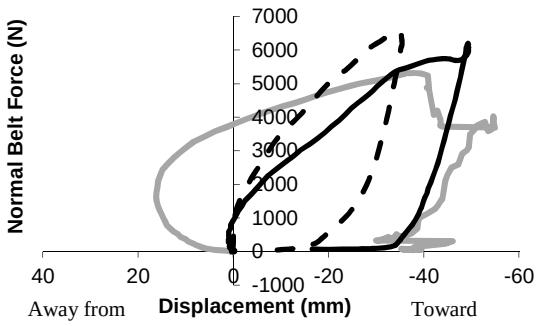

Lower Left

Figure 14. Total normal shoulder belt force relative to X-axis displacement.

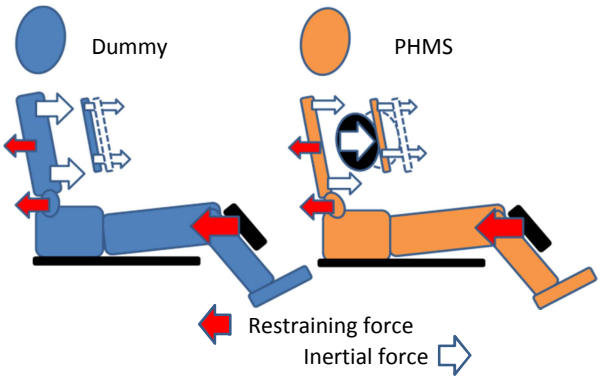

Figure 15. Forces acting to move anterior ribcage away from the spine.

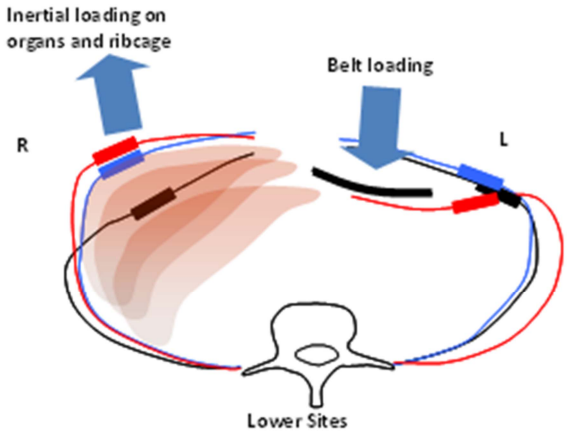

Figure 16. Bulge out for the lower right PMHS measurement site.

AN ADVANCED THORAX-SHOULDER DESIGN FOR THE THOR DUMMY

Paul Lemmen, Bernard Been
Humanetics Innovative Solutions
The Netherlands
Jolyon Carroll, David Hynd
Transport Research Laboratory
United Kingdom
Johan Davidsson
Chalmers University of Technology
Sweden
Luis Martinez, Antonio García
Universidad Politécnica de Madrid
Spain
Philippe Vezin
Laboratoire de Biomécanique et Mécanique des Chocs, University of Lyon, IFSTTAR
France
Andre Eggers
Federal Highway Research Institute (BASt)
Germany
Paper Number 13-0171

ABSTRACT

Thoracic injuries are one of the main causes of fatally and severely injured casualties in car crashes. Advances in restraint system technology and airbags may be needed to address this problem; however, the crash test dummies available today for studying these injuries have limitations that prevent them from being able to demonstrate the benefits of such innovations. THORAX-FP7 was a collaborative medium scale project under the European Seventh Framework. It focused on the mitigation and prevention of thoracic injuries through an improved understanding of the thoracic injury mechanisms and the implementation of this understanding in an updated design for the thorax-shoulder complex of the THOR dummy. The updated dummy should enable the design and evaluation of advanced restraint systems for a wide variety (gender, age and size) of car occupants.
The hardware development involved five steps: 1) Identification of the dominant thoracic injury types from field data, 2) Specification of biomechanical requirements, 3) Identification of injury parameters and necessary instrumentation, 4) Dummy hardware development and 5) Evaluation of the demonstrator dummy.
The activities resulted in the definition of new biofidelity and instrumentation requirements for an updated thorax-shoulder complex. Prototype versions were realised and implemented in three THOR dummies for biomechanical evaluation testing. This paper documents the hardware developments and biomechanical evaluation testing carried out.

INTRODUCTION

Data from the European Road Safety Observatory show that around 31,000 people were killed and more than 1.4 million injured in European road accidents in 2010 [1]. Although these figures continue the decline in road casualties observed since 20001, further efforts are needed to make European roads safer. In support of this the EU 7th Framework project THORAX (Thoracic injury assessment for improved vehicle safety) focused on reduction and prevention of thoracic trauma. As depicted in Figure 1, thoracic injuries are one of the leading causes of severe injuries and fatalities in car crashes.

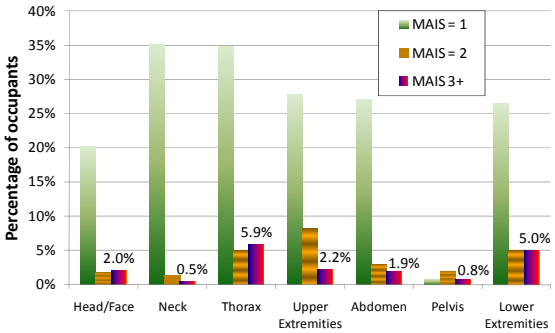

Figure 1 –MAIS injury level per body region (CCIS frontal impact sample n = 2,148 occupants) [2].

The THORAX consortium consisted of car manufacturers, suppliers, research groups and universities with wide experience in impact biomechanics. The main objectives of the project were:

- Identification of the two most relevant thoracic injury types for car occupants in view of societal relevance;
- Development of a mechanical demonstrator consisting of a new dummy thorax and shoulder design for the THOR NT dummy;
- Derivation of injury risk functions;
- Evaluation of the sensitivity of the demonstrator to modern vehicle safety systems.

This paper presents the demonstrator dummies developed including the biofidelity evaluations. The paper starts with a short summary of accident surveys and biomechanical studies which provided requirements for the dummy design.

BACKGROUND INFORMATION TO THE DESIGN

Outcome from accident surveys

Accident data were studied to identify the two most relevant thoracic injury types for car occupants and to provide detailed information on the type and severity of thoracic injuries in relation to impact type, restraint type, and occupant characteristics. The data were controlled for impact partner, impact severity, overlap and intrusion, and type of restraint system used. Results have been reported in detail in [3], [4], [5] and [6]. The data analysis showed that at the AIS ≥ 2 severity level, thoracic fractures are the torso injuries that occur most frequently. These occur to the ribs and sternum, and are observed often, particularly when AIS 1 rib fractures are counted. Lung injuries also occur frequently in frontal impact accidents (even though they are AIS ≥ 3) and are the most frequently observed injuries to an organ.

Biomechanical requirements definition

To ensure that a crash test dummy loads the vehicle and restraint system in a similar way to the human, biofidelity requirements are used to specify the dummy performance. In addition, these requirements are used to ensure that the response of the dummy to restraint system loading is relevant to be used in the prediction of injury risk in simulated crashes. Biofidelity requirements may be derived from human volunteer, PMHS (post-mortem human subject), or animal tests and the test conditions should be representative of real-world accidents.

As no full set of requirements and related biofidelity rating system was available for frontal impact dummies the THORAX project conducted an in-depth literature review to identify all available PMHS datasets relevant for frontal impacts. Criteria were developed for inclusion or exclusion of PMHS tests. When feasible, data were processed to account for differences in mass and age of the subjects. The test conditions for biomechanical evaluations included pendulum impactor, table top, static airbag and belt tests, quasi static volunteer shoulder tests and various sled tests. To ensure good performance under various loading conditions a much broader set of requirements was proposed when compared with those from the EEVC and NHTSA. The results of the literature review have been reported in [7]. The report includes a detailed description of each test configuration allowing for reproduction of the tests with the THOR dummy.

Injury criteria and dummy instrumentation

A study into injury criteria and risk curves that are independent of experimental parameters such as the apportionment of seatbelt and airbag loading was performed using a validated Human Body Model [8], [9]. The model was submitted to a wide range of loading types: impactor, static airbag, belt only restraint, airbag only restraint and combined belt and airbag restraint. For each loading type different severities were applied to generate different levels of rib fracture: from the absence of fractures to numerous fractured ribs. From these studies rib bending was identified as being the main loading resulting in fracture as opposed to torsion. Two injury criteria representing this pattern were formulated. The first one, called the Combined Deflection (Dc) criterion, uses chest displacements at four locations to compute overall and differential deflections resulting in bending strains. The second criterion, called Number of Fractured Ribs (NFR), uses locally measured strains at individual ribs to identify those ribs for which the bending strains at any location has exceeded a critical value. The Dc criterion requires displacement to be measured at four locations in the chest while the NFR requires local strains to be measured at individual ribs.

SHOULDER / THORAX DESIGN

Based on the findings of the accident surveys and the outcome of the biomechanical work a demonstrator dummy was designed. Extensive design and prototyping efforts were made to realise three demonstrator prototypes for evaluation testing and restraint sensitivity testing [10]. The main focus was on the updates to the SD2 shoulder, rib response tuning to corridors and the implementation of instrumentation to capture information for newly proposed injury criteria.

Shoulder and arm design

Various updates were made to the THOR SD2 shoulder which was originally developed by Törnvall [11]. The sterno-clavicular joint was redesigned to meet anthropometry requirements for the 50th percentile male described in [12]. The original SD2 design did not meet the anthropometric target position of ±20 mm lateral from mid saggital plane (it was ±44 mm).

Of particular importance is the update of the shoulder cover. As the SD2 design allows a complex and large range of shoulder motion, the original design applied left and right soft foam shoulder mouldings inside a dedicated jacket. The position and shape of the foam was not well defined and did not provide a repeatable position of and interaction with the belt. The updated SD shoulder employs a solid elastomer moulding, which is closer to the original NT part in geometry and firmness. The THOR jacket used with the updated SD shoulder is slightly modified to allow for the larger range of shoulder motion.

The THOR dummy had Hybrid III arms which did not match the anthropometry requirements in [12]. Moreover the arms were not well integrated in the SD2 shoulder design. To correct these discrepancies, a new upper arm was developed which is compatible with the shoulder design and meets the anthropometric targets. The new design includes load measurement capabilities at the middle of the humerus using a WorldSID 50th loadcell.

Finally, clavicle load cells were implemented in the updated shoulder design. Two-channel load cells can be installed at both ends of the clavicles to measure force in the forward and vertical directions.

The updated shoulder-arm design is shown in Figure 2 through Figure 4. It is being referred to as the SD3 shoulder.

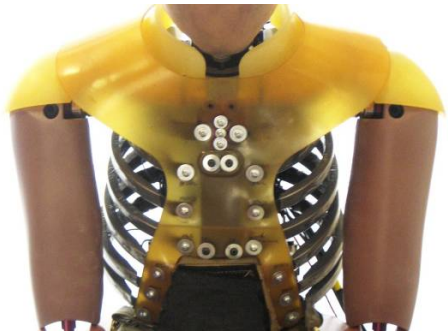

Figure 2 – SD3 shoulder and arms installed on demonstrator dummy.

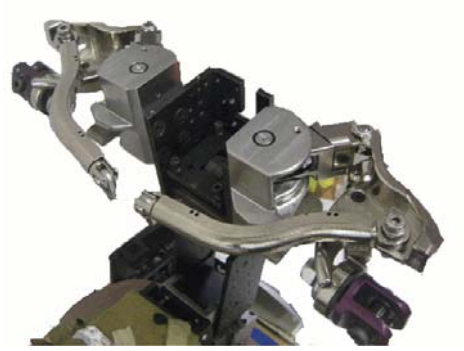

Figure 3 – The pivot mechanism.

Figure 4 – Updated arm design (flesh not shown).

Rib cage response tuning

To optimise the thorax response the sensitivity to rib stiffness and damping behaviour were investigated in pendulum impactor tests [9], [10]. The rib stiffness was gradually reduced first by damping thickness reduction, then by stepwise cutting the height of the metal. On this basis an optimal response with respect to the NHTSA (Kroell) biofidelity corridors was pursued as starting point for further biofidelity evaluations. Based on the outcome 3 rib sets were produced with 1.6 mm rib metal and 9 mm damping material gauge. An additional 6 mm foam pad was added inside the front jacket to increase damping and, to a small amount, the external deflections. In a first evaluation the demonstrator dummies were subjected to frontal and oblique pendulum impactor

tests (see Figure 5). Figure 6 shows responses from frontal pendulum impact tests for three dummies plotted against corridors based on Kroell [13]. The peak pendulum force is exceeded by less than half the corridor width and the peak compression is close to the mean. Some variability between the dummies is observed due to differences in the configuration of the demonstrator dummies as described below. Figure 7 shows the performance for oblique lower rib impact tests (15° about a vertical axis) and the NHTSA certification requirements for peak force and peak compression [14]. One dummy is inside the requirement while the other slightly exceededs the peak compression. This was considered close enough to the corridor to proceed with biofidelity evaluation.

Instrumentation

In conjunction with the injury criteria proposed, four 3D IR-Traccs in the thorax were adopted from the THOR mod-kit [15]. The IR-Traccs provide the required input to be used in calculating the Dc criterion. As input to the NFR criterion two of the demonstrator dummies were equipped with a total of 72 strain gauges on the ribs (see Figure 8). The gauges are implemented such that the influence on the chest dynamic response is negligible. From the second rib down, all six lower ribs have six strain gauges on both sides equally spaced in ratio to the length of the ribs.

THORAX demonstrators

Three demonstrators were built based on THOR donor dummies provided by THORAX partners IFSTTAR, Autoliv and TRL. All three included tuned rib sets, modified jackets and SD3 shoulders. The Autoliv and TRL dummies also included the Pelvis-Femur-Knee Mod Kit described in [15].

Figure 5 – Dummy in frontal and oblique pendulum impact test set-up (Jacket removed for photo).

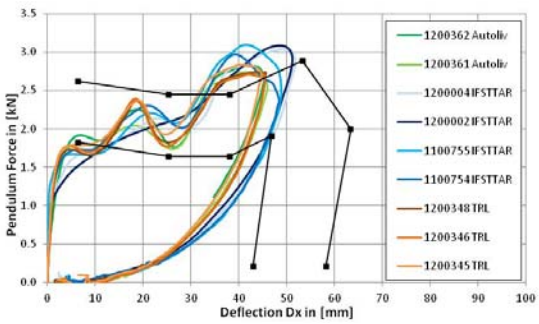

Figure 6 – Response for three THORAX demo dummies in frontal 4.3 m/s pendulum impact tests.

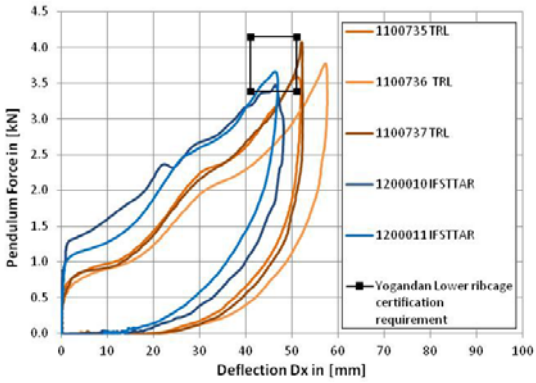

Figure 7 – Results for two THORAX demo dummies in oblique pendulum impact tests.

Figure 8 – Example of rib with gauges.

BIOMECHANICAL EVALUATION

In 2009, ISO/TC22/SC12 Working Group 5 started an effort defining frontal impact biofidelity targets in a world-wide expert group. The ISO Task Force led by ACEA and CEESAR contributed a literature review and also defined selection criteria to find biofidelity test configurations. In the end, the work focused on three test configurations and biofidelity targets were proposed by ACEA-TFD and CEESAR and released by Lebarbé and Petit [16], [17]. Their current proposal for biofidelity targets is being reviewed by ISO WG5, with a draft Technical Report

under revision. Acknowledging this effort and previous evaluation proposals by EEVC and NHTSA, the THORAX project sought further test conditions under which an advanced dummy thorax could be evaluated. In view of this the THORAX project considered a wide set of test conditions for the biomechanical evaluation of the demonstrator dummies [7]:

- Pendulum impactor (Lebarbé [17], Yoganandan [14]).
- Table top (Cesari & Bouquet [18], Kent [19]).
- Quasi static volunteer shoulder tests.
- Sled tests (Forman [20], Bolton [21], Shaw [22]).

In most cases matching tests with a Hybrid III and / or baseline THOR dummy were included. Where previous tests had been performed with one of those dummies, this was used to give confidence to the accuracy of the testing set-up. It also allowed analysis of the relative dummy performance.

Thorax pendulum tests

Pendulum impactor tests replicating the Kroell frontal sternum and Yoganandan oblique lower rib tests, were evaluated against corridors defined by Lebarbé [17] and, for the oblique impacts, by the THORAX project itself based on Yoganandan pendulum tests.

The requirements for the frontal sternum impacts were developed as part of the ACEA-TFD support of ISO Working Group 5. They define an external (surface of the chest) deflection measurement. As this can not be measured with the IR-Traccs inside the thorax the pendulum penetration was recorded with High Speed Video analysis. A standard 23.4 kg and 152 mm diameter pendulum was used at an impact speed of 4.3 m/s. The dummy was positioned according the PMHS test positions (see Figure 5). For the Yoganandan tests the pendulum was lined with 19 mm Rubatex foam, as specified.

Results for the upper thorax impact tests are given in Figure 9. The peak penetration in these tests was between 67 and 72 mm. The response is in fairly good correlation with corridors defined by Lebarbé [17]. The peak penetration corresponds well with the average found in PMHS tests. The peak pendulum force exceeds the target by around half the corridor width. The unloading phase is entirely within the corridor. In THORAX [7] the orginal Yoganandan [14] data was reanalysed and Moorhouse normalisation applied, which was found to reduce scatter more than other methods. An artefact of this method is that the corridors do not represent the variation of peak deflection seen in the original tests,

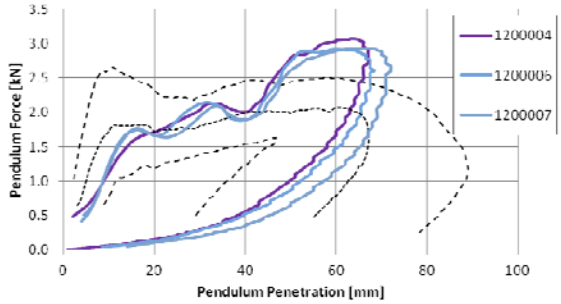

Figure 9 – Results Pendulum Force versus Pendulum Penetration. Corridors from Lebarbe [17].

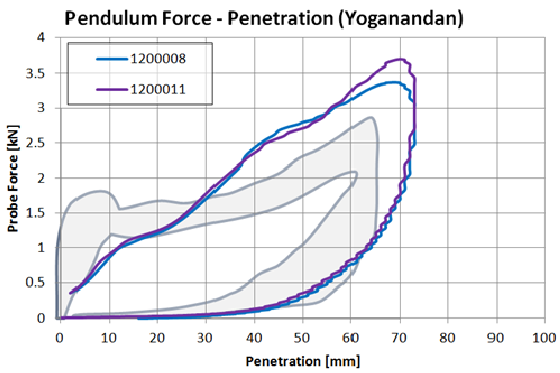

Figure 10 - Pendulum force – penetration for oblique impact tests on lower thorax. Normalised PMHS responses grey shaded [7].

and corridors are narrow at peak deflection. Figure 10 shows resulting corridors and the demonstrator dummy responses. Due to inaccuracy of the time zero of pendulum contact with the dummy, the penetration derived from high speed video analysis was possibly overestimated upto 17mm . The peak forces of the dummy exceed the PMHS responses. Considering that dummy peak penetrations were almost certainly overestimated, the penetration response was close to the requirement.

Cesari & Bouquet table top tests

As part of the evaluation the THORAX demonstrator was subjected to table-top conditions reported by Cesari and Bouquet [18] and previous authors. For this purpose a replica of the table-top rig as described in [18] was built. The new demonstrator dummy and the baseline THOR-NT were assessed on this rig with additional Hybrid III tests required to prove that the set-up was comparable with the original Cesari and Bouquet experimental work. In the original tests an impactor of mass 22.4 or 76.1 kg loaded the belt. Impact velocities ranged from 3 to 9 m/s. The two

Figure 11 – Image of table top set-up with THOR-NT

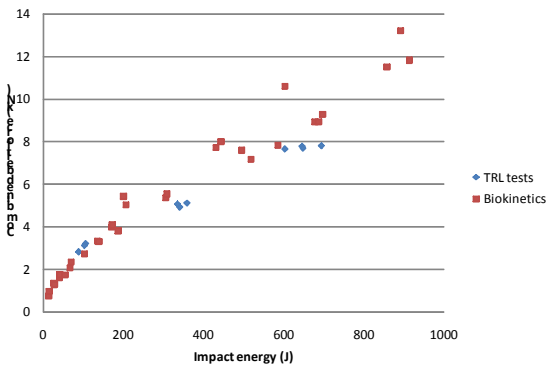

Figure 12 – Comparison of belt force for original set-up (red dots) and replica (blue dots) using Hybrid III [23].

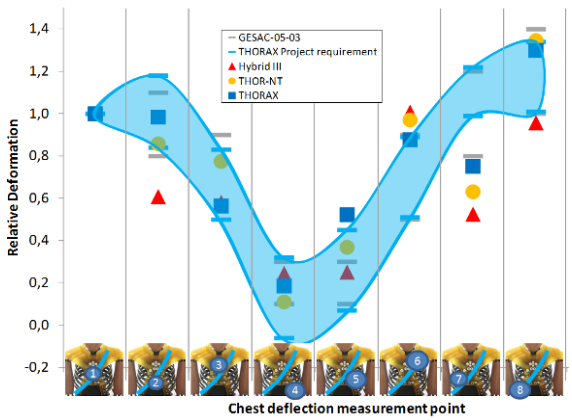

Figure 13 – Relative deflections for Hybrid III, THOR NT and THORAX demonstrator with SD3 in comparison to corridor from PMHS data.

ends of the seat belt passed through the table over low friction supports and were attached to a horizontal spreader bar. The movement of the bar was activated by a dynamic impactor. The force at each end of the belt was measured with a load cell before connection to the rod. The chest deflection was measured at eight different locations spread over the different ribs.

The behaviour of the new equipment was compared with the original behaviour via a comparison of test results with the Hybrid III dummy (see Figure 12). Slight differences were noted in the belt forces and external deflection measurements at the higher severity loading conditions. These differences were regarded as being acceptable for the intended purpose of comparing relative displacement measurements and hence regional stiffness and coupling.

A limitation of the set-up was in the accuracy with which the external measurement points were positioned around the thorax of the subject. The locations had to be manipulated in order to align them with realistic hard points throughout the thorax. Whilst efforts were taken to minimise those errors, it is considered that small variations in the positions of the external deflection measurement points could have an influence on the biofidelity results.

Results comparing the three different dummies in relation to corridors from the PMHS data are depicted in Figure 13. Results for both the THORAX demonstrator as well as the THOR-NT were found to be close to the response corridor. Results for both dummies are quite similar indicating no negative effect of the modifications to the chest and shoulder complex on the regional stiffness distribution as evaluated in this test condition.

Kent *et al.* table top tests

In addition to the Cesari and Bouquet tests the THORAX demonstrator was subjected to table-top conditions described in [19]. In their research, Kent *et al.* studied the effect of four different loading conditions on the biomechanical response of the human thorax using PMHS. For the purpose of the evaluation of the demonstrator, three of four loading conditions applied by Kent *et al.* were reproduced. These loadings conditons were: hub, single diagonal belt and double diagonal belt. The hub had the same geometry as the one used in Kent *et al.* The belt for the single and double diagonal belt loading conditions was positoned on the dummy chest similarly to the cadaver tests. The breadth of the belt used was a little smaller than the original belt (4.6 cm instead of 5 cm). The test rig was not reproduced identical to the original set-up but the positions and orientations of the loading devices as well as the loading conditions were identical to the PMHS tests. A universal tensile test machine was used to generate

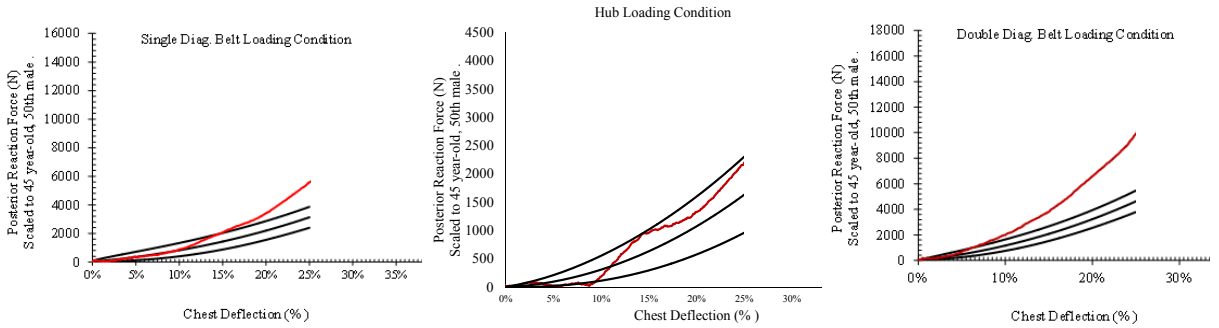

Figure 14 – Force deflection data for the THORAX demonstrator compare with the characteristic average and corridors of the PMHS for hub (left), single (middle) and double (right) diagonal belt. PMHS corridors are scaled to a 45 year-old, 50th percentile male.

chest deflection at a rate similar to the rate applied on the PMHS chest. This chest deflection is supposed to mimic the deflection of a restrained PMHS in 48 km/h frontal sled tests. This corresponds to a linear displacement with a constant velocity of 1 m/s. In order to replicate the PMHS protocol accurately, the pre-test 10-cycle preconditioning regime described in the Kent paper was also applied to precondition the thorax of the demonstrator. The dummy was positioned in the same way as the PMHS with its back lying on the table.

Applied and reaction force were recorded with the same sampling frequency as in the PMHS tests. In addition to the dummy instrumentation, the chest deflection at mid-sternum was also measured with a linear transducer (LVDT) to facilitate the comparison with the PMHS corridor established by Kent *et al.* [19]. Kent *et al.* performed non-injurious tests with the different loading condtions on each cadaver and a final injurious test with one of the four loading conditions for each PMHS. For the THORAX demonstrator, successive tests were performed by increasing the chest deflection from 10% up to 30%. The 30% of chest deflection corresponds roughly to the injurious tests performed on the PMHS. This allowed to check the repeatability of the demonstrator response and to avoid damage to the dummy by checking the rib conditions after each test and before increasing the deflection.

The responses of the demonstrator were compared with the PMHS corridors (see Figure 14). The demonstrator response is within the corridor for the hub loading condition. Nevertheless, for low chest deflection (<10%) the reaction force was low compared to cadavers. The reaction force increased rapidly between 10 and 15% and then the demonstrator followed the cadaver response with a value slightly higher than the average characteristics of the PMHS. For the single diagonal belt loading, the demonstrator behaviour fitted very well with the corridor up to 10% of chest deflection. Then, the stiffness of the dummy chest increased and became higher than the upper corridor above 15% of deflection. The THORAX demonstrator appears too stiff compared with the PMHS corridor with the double diagonal belt loading condition. It should be noted that permanent deformation of the lower ribs of the demonstrator were observed for this series, which is to be expected considering the peak load of 18 kN applied.

Quasi static volunteer shoulder tests

In the Thorax project a test rig for evaluation of the human shoulder stiffness was developed (see Figure 15). Belted volunteers were seated and their shoulder bone motions measured when loaded forward (0°), forward-upward (45°), upward (90°) and rearward (180°). The forward and upward loads to the shoulders were applied through the arms by means of arm brackets fastened to the elbows Rearward loads were applied by means of a padded strap wrapped around the shoulder complex. To block torso movement the volunteers were restrained by two shoulder belts, routed close to the neck, that were pre-tensioned to 100 N each. The arms or shoulders were statically loaded with 50 N increments to a maximum of 200 N/side. Each volunteer was exposed to three tests for each loading direction. The position of the shoulder complex was recorded by three digital cameras. The left acromion process relative to T1 displacements were used to calculate shoulder motion in 3D. Belt loads and seat back loads were recorded to facilitate a comparison between dummy interactions during testing as compared to those of the volunteers.

Tests were done with six volunteers and reproduced using the THORAX demonstrator dummies as well

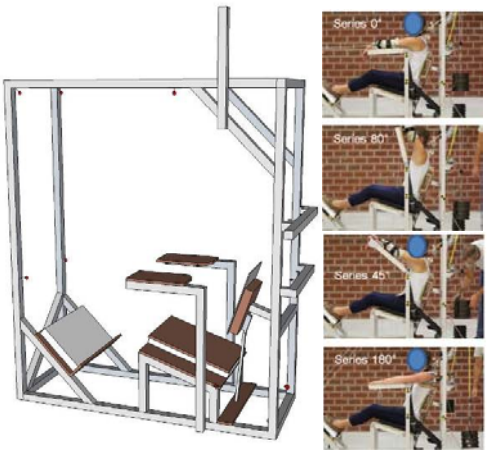

Figure 15 – Test rig used for shoulder stiffness tests

as a standard Hybrid III. Evaluation of the dummy performance in this loading condition is regarded as complimentary to PMHS sled tests like, for instance, the Gold Standard sled tests [24]. Average T1 change in position for each loading condition was below 32 mm forward-rearward and 14 mm upward-downward when maximum load was applied (both for volunteers and dummies). This means that the shoulder motion was more successfully isolated from other motions in this study than in similar previous studies [11] and therefore more suitable for evaluation of crash test dummy shoulders.

The THORAX demonstrator produced similar shoulder motions as the volunteers did when the loads were applied forward, oblique and upward (Figure 16). For series 0° the shoulder relative to T1 forward motion was 54 mm for the average volunteer, 45 mm for the THORAX demonstrator and 2 mm for the Hybrid III when maximum load was applied. For series 45° the resultant maximum shoulder relative to T1 motion was 68 mm for the average volunteer, 64 mm for the THORAX demonstrator and 2 mm for the Hybrid III. Both the THORAX demonstrator and the Hybrid III exhibited less than half the rearward shoulder motion of the volunteers in the 180° tests (Figure 16). For this loading condition the THORAX demonstrator exhibited 22 mm rearward motion whereas the average volunteer exhibited 47 mm.

Forman and Bolton sled tests

To replicate PMHS sled test configurations reported by Forman *et al.* [20] and Bolton *et al.* [21] a sled rig was developed (see Figure 17). The rig consists of a stiffened Ford Taurus buck equipped with airbags,

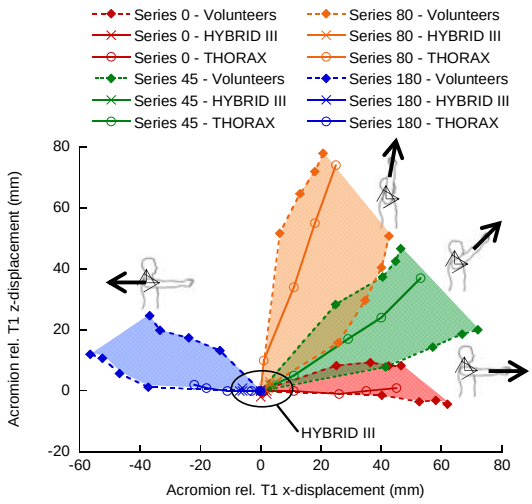

Figure 16 – THORAX project shoulder response corridors, Hybrid III and THORAX displacements in four loading directions.

safety belts, dashboard, seat, etc. Four front passenger sled test configurations were replicated using the Autoliv THORAX demonstrator dummy:

- No shoulder belt (2pt belt) + airbag.
- Only 3-point belt load, no airbag. 5 kN Shoulder belt load.
- 3-point belt (force limiter) + airbag. 5 kN Shoulder belt load.
- 3-point belt (no force limiter) + AB. 8 kN Shoulder belt load.

High speed filming with motion capture was applied to obtain dummy kinematics data. Dummy reponses were compared against global kinematics, thoracic spine accelerations and thoracic deformations obtained from the PMHS tests.

To derive the acceleration corridors, the original raw PMHS data from the tests performed by UVa have been used. PMHS corridors were derived for T1, T8 and T12/L1 resultant accelerations. An attempt was made to apply normalisation to the standard 50th percentile size [25]. However, the different temporal scaling factors between subjects appeared to generate different values resulting in a bi-modal mean response, which was not representative of any of the

Figure 17 – General view of the sled rig.

PMHS and cannot reasonably be reproduced by the dummy. Therefore normalisation was not applied for the corridors used in the performance comparisons. The acceleration versus time responses were obtained as the mean response with a corridor set at ± one standard deviation.

For T1 acceleration corridors, the positions of the accelerometers in the PMHS and in the dummy are different. To derive the T1 corridors, the PMHS response with three accelerations and three rotational velocities have been used to obtain the acceleration corridors for the position of the dummy T1 accelerometer. Therefore the T1 corridors presented in this paper are dummy specific corridors.

Furthermore, the kinematics behavior is analysed (trajectories of different targets on the head, T1 or hip) in order to perform a general comparison of the demonstrator dummy with respect to the PMHS.

The results from the two tests with the demonstrator dummy in each test configuration, together with the response corridors, are shown in Figure 18 to Figure 20. It is observed that:

- The general behaviour of the THOR kinematics is good. The lower part of the dummy underwent a greater excursion than the mean of the PMHSs. It is possible that the main factor was the knee to dashboard distance which, together with the forward displacement of the pelvis from condition to condition, was variable in the PMHS. The T1 and head excursions are well reproduced.

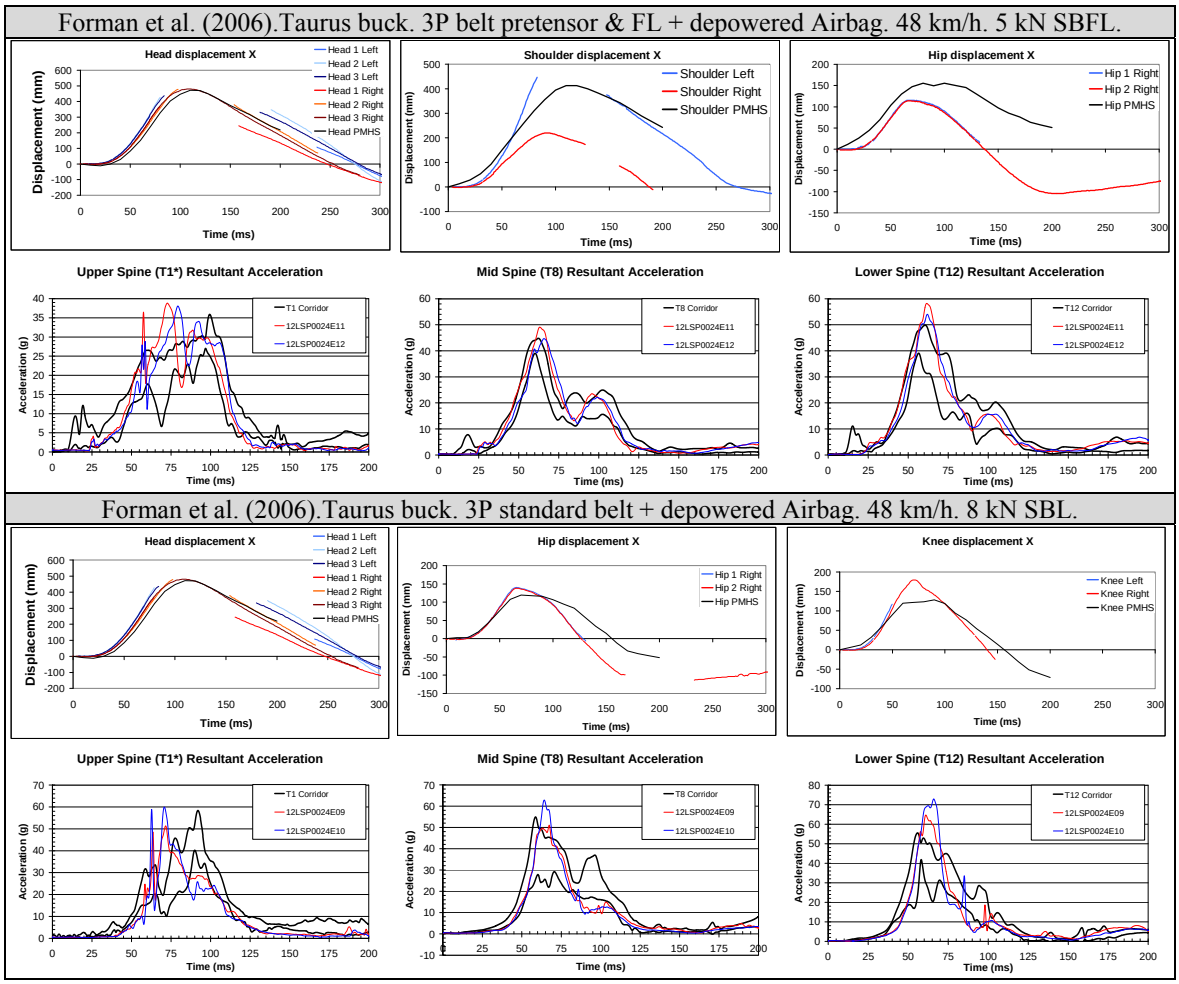

Figure 18 – Head, T1 and hip x-displacements; upper spine, mid spine and lower spine resultant accelerations for tests with 2 point belt and full powered airbag (top rows) by Bolton et al. [21] *and tests with 3 point belt without airbag (bottom rows) by Forman et al. et al.* [20].

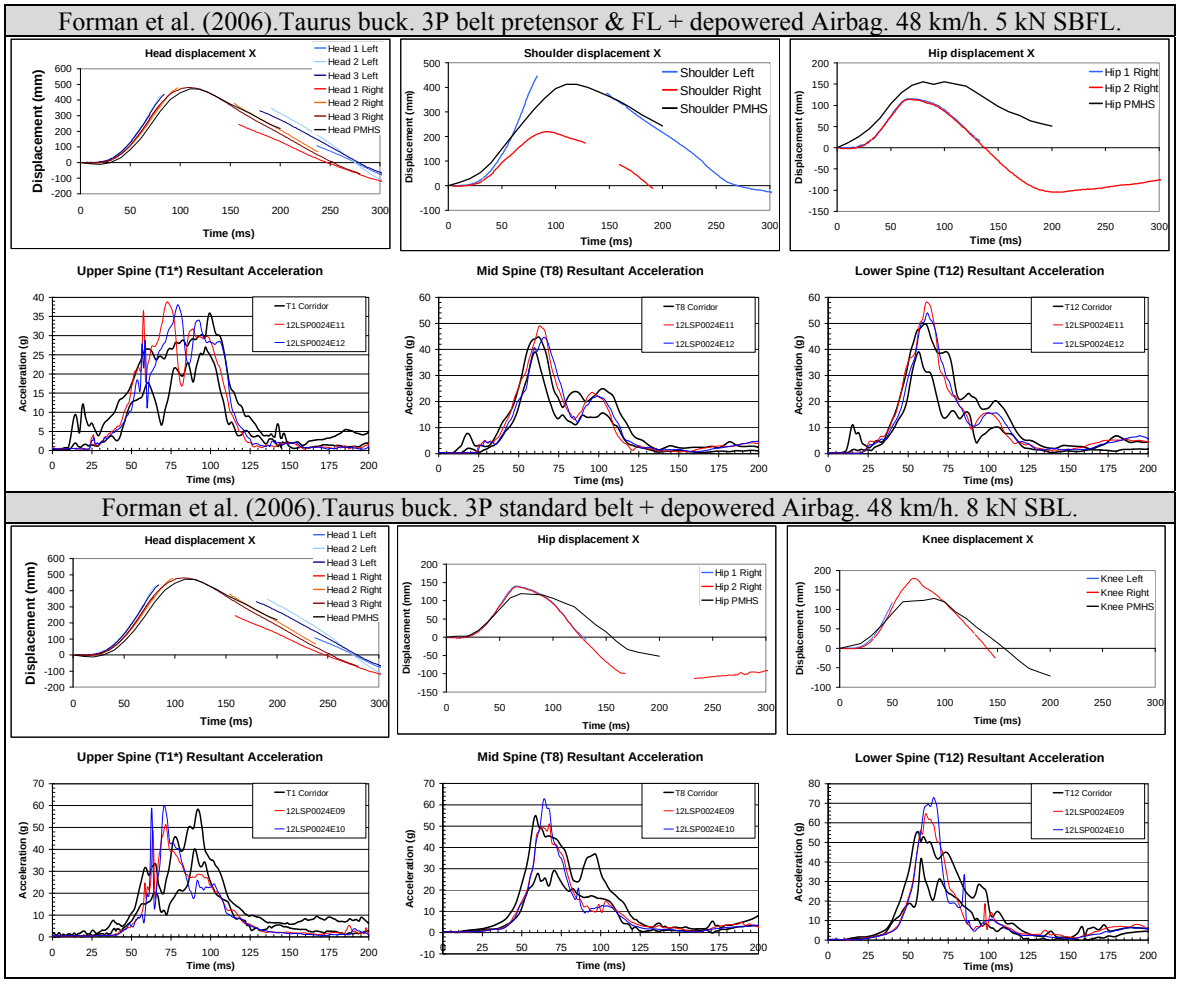

Figure 19 – Head, T1 and hip x-displacements; upper spine, mid spine and lower spine resultant accelerations for tests with 3-point force limiting belt (5 kN) and de-powered airbag (top rows) and tests with 3-point standard belt no-force limitation (maximum shoulder belt load of 8 kN) with de-powered airbag by Forman et al.[20].

2P belt + Full-powered Airbag			
	THOR	PMHS	THOR
	Right	Sternum	Left
Upper	-12.2%	-11.0%	-11.1%
Lower	-4.1% (5.9%)	-	-4.1% (6.3%)

3P belt pretensor & FL + depowered Airbag				
THOR	PMHS			THOR
Right	Right	Sternum	Left	Left
-10.4%	-25.9%	-27.6%	-24.8%	-17.0%
-4.4% (4.3%)	6.2%	-6.9%	-11.5%	-16.3% (1.7%)

3P standard belt + NO Airbag			
	THOR	PMHS	THOR
	Right	Sternum	Left
Upper	-6.7%	16%	-14.3%
Lower	-5.2% (2.4%)	7%	-13.0% (1.4%)

3P standard belt + depowered Airbag				
THOR	PMHS			THOR
Right	Right	Sternum	Left	Left
-16.7%	-33.5%	-34.1%	-38.0%	-18.5%
-6.6% (3.4%)	7.1%	-5.9%	-13.4%	-20.7% (2.7%)

Figure 20 – Comparison of chest x-deflections (as a percentage of the chest depth at measurement location) tests for all four passenger load conditions considered by Forman et al. [20] and *Bolton et al.* [21].

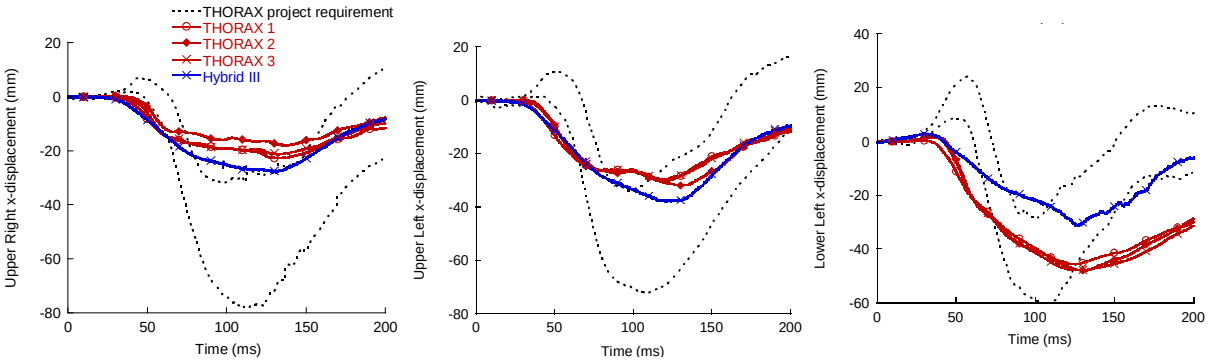

Figure 21 – Chest deformations relative T8 for THORAX demonstrator with SD3, Hybrid III compared with biofidelity target provided by Lebarbé and Petit [17].

- The resultant spine accelerations (T1, T8 and T12) gave good results. Dummy accelerations are greater than the PMHS, but the morphology and timing was well reproduced. The T8 and T12 dummy accelerations are influenced by the direct contact of the knees against the dashboard.
- The THOR dummy had less chest compression than the PMHS, especially for the more severe configurations. The dummy thoracic deformation was able to discriminate the configurations in terms of their severity. In the three-point belt loading, the PMHS had large uncoupled deflections (the upper compression was 2 to 4 times greater that the lower compression); however, the prototype dummy could not reproduce this. With the three-point belt, the lower left thoracic location had high deflection and the lower right location had very little deflection (even considering the local chest depth at that level) reproducing the behavior of the PMHS.

Gold Standard Shaw *et al.* sled tests

In a sled test series, commonly referred to as the 'Gold Standard', by Shaw *et al.* [26] and [27], eight PMHSs were positioned on a rigid planar seat with their torso and head supported by a matrix of wires. The subjects were restrained by a three-point shoulder and lap belt, using separate adjustable-length sections joined near the subject's left hip, tensioned to approximately 5 N and 50 N, respectively, prior to each test. In addition, a rigid knee bolster, adjusted to be in contact with the knees, and a footrest with ankle straps restrained the lower extremities. The sled and the PMHSs were subjected to a peak acceleration of 140 m/s^2 that resulted in a velocity change of 40 kph. Instrumentation was comprehensive and enabled the extraction of acromion, spine, and head displacements and chest compressions using video analysis [26], [27], [17].

The new THORAX demonstrator and Hybrid III dummy were subjected to Gold Standard sled tests using a replica of the original test rig [28]. Dummy rib cage deformations were measured using internal sensors and recalculated to the coordinate system used in the the Gold Standard series; anterior chest displacements in a T8 vertebra coordinate system. T8 location and coordinate system attitudes were transferred to dummy drawings from drawings of seated humans [12].

THORAX demonstrator upper chest deformations were larger than those of the THOR NT [28] but still lower than the response target (Figure 21). In the tests with the demonstrator dummy slightly larger belt downward sliding was observed compared to the original PMHS tests [27]. This off-loaded the left chest and may, to some degree, explain the smaller upper left chest deformations. For the belted shoulder, the clavicle of the PMHSs moved somewhat rearward and exposed the chest to belt loads. This was not fully reproduced by the demonstrator; the clavicle shielded the upper right chest to a higher degree in the demonstrator. In addition, the demonstrator exhibited slightly larger thorax rotation around its vertical axes and this could explain why the demonstrator exhibited relatively large lower left chest compressions as compared to those observed in the upper chest. Another reason for larger lower left chest deformations were differences in pelvis motions; the demonstrators moved on average 35 mm forward while the PMHSs only moved on average 25 mm.

The results indicate that the dummy chest may be slightly stiffer than that of the average PMHS in this loading condition.

Hybrid III chest deformations were uniform but also small; upper right and lower left chest deformations were smaller than the biofidelity targets (Figure 21).

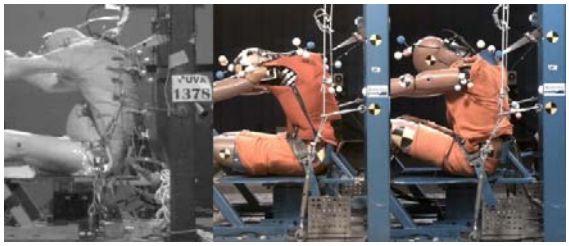

Figure 22 – Stills from high speed video of tests in Gold standard conditions with a respresentative PMHS, THORAX and Hybrid III at 120 ms.

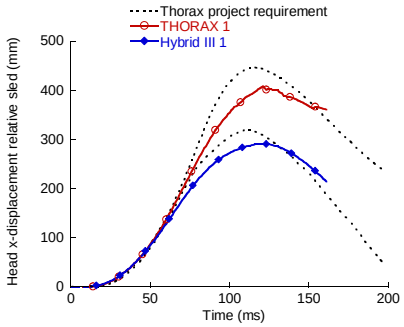

Figure 23 – Head displacement relative sled for THORAX demonstrator and Hybrid III compared with project requirments that were derived from Ash et al. [2012].

In addition to chest stiffness, two other factors highly influenced the chest response of the Hybrid III; the Hybrid III thorax spine is rigid and as a result the thorax did not flex as did the spine of the demonstrator and the PMHSs (Figure 22); the Hybrid III exhibited smaller head forward displacements than those specified in the project requirements (Figure 23). These differences may not seem to be important in this sled condition but influences restraint interactions in modern cars.
Neither the THORAX demonstrator nor the Hybrid III exhibited lower right chest bulge out as did the average PMHS. The THORAX demonstrator appears to be repeatable based on these three tests.

DISCUSSION

In the THORAX project a new shoulder-thorax complex to be fitted on the THOR-NT was developed and three demonstrator dummies were updated with this design. The dummies were then evaluated against a broad list of biomechanical requirements for the thorax and shoulder. Those requirements included, but were not limited to those published previously by NHTSA and Lebarbé. In summary the performance of the demonstrator dummies in each test condition was as follows:

1) In pendulum impactor tests generally a reasonable to good correlation between demonstrator dummy responses and corridors was obtained. Peak forces for frontal pendulum tests (Lebarbé) and oblique tests in the lower thorax region (Yoganandan) tended to be higher than the corridors. Penedulum penetration could not be determined accurately, however appeared to be a good match in both conditions.
2) In table-top tests the regional coupling, assessing the influence of loads in one part of the thorax on deflections in another part, was investigated. Comparison of the demonstrator dummy with corridors identified from PMHS table top tests by Cesari and Bouquet revealed that the dummy performs reasonably well compared with other dummies like the Hybrid III. However, slight deviations from the PMHS responses were still observed. Also, in sled tests, it appears that the balance of the upper to the lower measurement point deflections may not be the same as for PMHS. As injury risk development work now considers a combined deflection criterion incorporating the differential deflections from the four measurement points (left-right, top-bottom), it seems important that those efforts consider the biofidelity of the dummy. Implications of the performance of the dummy in terms of regional coupling and stiffness need to be viewed in relation to the injury criterion used.
3) In table-top tests considering the influence of loading condition (Kent), the demonstrator dummy also performed reasonably well. The stiffness of the dummy increased from the hub to the single diagonal belt to the double diagonal belt conditions as for the PMHS. Results were within the force-compression corridors for hub and initially for the diagonal belt loads while being too stiff for the double diagonal belt. This may indicate that the SD3 shoulder or the top of the thorax is too stiff compared to humans under the belt conditions tested. The consequences of this for the behavior in frontal impacts are not clear from this test environment though.
4) Very good correlation was obtained between dummy tests and corridors for the shoulder range of motion tests, matched with a new set of volunteer tests. The human shoulder motions in the forward and/or upward directions are represented well by the dummy including sufficient range. Rearward shoulder motions however, were found to be limited but still

showed a substantial improvement compared with the Hybrid III. The results for rearward shoulder loading with limited motion compared to volunteers might help explain the belt condition performance in the Kent table top tests, but this is to be investigated.

5) In sled tests (Forman, Bolton) representing various restraint conditions the demonstrator dummy generally shows good behaviour. Although, some differences with respect to the PMHS corridors were observed. It is to be noted that reproducing these test conditions is difficult in terms of finding representative test components like airbags, belts and seats. Furthermore for each restraint type only a very limited number of subjects were used to define the corridors. Therefore, the requirements could be biased to the specific subject characteristics and responses, for instance in their interaction with the knee bolster.
6) The gold standard tests were specified to address some of the limitations noted above by selecting subjects with anthropometry close to the average male. Also, the set-up was intended to be easily reproduced in other laboratories. In reproductions of these tests the demonstrator dummy showed improved overall kinematics in terms of head forward displacement and spine rotation and bending in comparison with the Hybrid III. Also the chest deformations were improved when compared to published THOR-NT results. However, the maximum upper right chest deformation was somewhat lower than the project requirements while the upper and lower left maximum deformations were within the required range. The reason for low upper left chest deformation may be due to higher stiffness of the upper ribcage quadrant but may also be due to the first rib-clavicle complex. This was also indicated in the comparisons with volunteer shoulder data, Kent table top test data, table top tests by Cesari and Bouquet and the Forman and Bolton sled test series.

Although for some of the individual test conditions the dummy response deviates from the project requirements, reasonable correlation is obtained over the broad range of conditions considered. Detailed comparison of chest deflections in various conditions indicates that the upper rib - clavicle complex appears stiffer than those of the PMHSs. No specific biomechanical data for this region was available and it is recommended to collect such data in future studies. The demonstrator exhibited differential displacements in upper and lower, as well as left to right thorax regions in line with PMHS data. The Hybrid III dummy also showed differential deflections but too a much lesser extent. These relative deflection components are input to injury criteria proposed in THORAX and regarded as important when distinguishing between different loading conditions. In defining such criteria the relatively stiff response in the upper thorax region should be kept in mind as it reduces dummy displacement readings in this part.

In some cases the lack of correlation could clearly be attributed to specifics of the set-up. As an example differences in kinematics in sled tests could be attributed to knee contact with the bolster which is highly dependent on subject size considered and seating position. This example also illustrates an aspect of certain test conditions which, other than table top and pendulum impactor, suffer from the fact that data for only a limited number of subjects are available. However, if broad evaluation in a variety of test conditions is deemed a priority, than also conditions of small subject count must be included. In this respect it should also be noted that at this stage of the research the comparison of the dummy responses with the biofidelity targets has been a subjective one. It is encouraged that future efforts will incorporate an objective validation of the dummy performance. This will require an approved set of requirements and assessment method, which are not formally available at the time of writing.

During the biofidelity evaluations it became evident that the THORAX demonstrator dummies showed sensitivity of the chest deflection measurements to the different restraint systems or loading devices used. This suggests that the THORAX demonstrator can be valuable as a tool to investigate performance differences between various types of restraint. However, to offer equivalent or comparable risk of injury predictions under localised or distributed loading a criterion which is independent of the restraint system should be used. The potential use of the THORAX demonstrators and injury criterion candidates is being investigated in sled tests using modern restraint systems within the final work package of the THORAX Project.

CONCLUSION

THORAX was a project under the European 7th Framework. Car manufacturers, suppliers, research groups and universities jointly investigated thoracic injury mechanisms and findings were implemented in

design tools meant to enable the design and evaluation of advanced occupant restraint systems.
Following accident surveys and biomechanical studies a new shoulder-thorax complex for the THOR-NT dummy was developed. This included a modified version of the SD shoulder representing realistic range of motion in this body section. Three demonstrator dummies were prepared for evaluation against a broad list of biomechanical requirements and test conditions. This included hub impactor tests, table-top tests and sled tests under various restraint conditions. Although in some individual tests differences between dummy response and corridors / requirements from PMHS tests were observed, the THORAX demonstrator generally shows reasonable to good correlation over a broad range of conditions.
The upper rib - clavicle complex seems stiffer though than those of the PMHSs in various conditions. As currently no specific biomechanical data for this region is available it is recommended to collect such data in future studies for further improvement of the dummy.

ACKNOWLEDGEMENT

The authors would like to thank the European Commission for commissioning and funding this research, the UK Department for Transport and to the Region of Madrid for the SEGVAUTO 2009 DPI-1509 programme for providing supporting funding. Thanks are also extended to the providers of the accident case data: the CCIS, the GIDAS and GIE RE PR as well as to the on board DAS systems providers for the dummies, Hentschel and Messring.

REFERENCES

[1] European Commission, “Road safety evolution in EU”,ec.europa.eu/transport/road_safety/ specialist/ statistics/index_en.htm, 2012.
[2] Carroll J., Adolph T., Chauvel C., Labrousse M., Trosseille X., “Overview of serious thorax injuries in European frontal car crash accidents and implications for crash test dummy development”, Proceedings of IRCOBI Conference, Hannover, Germany, pp 217-234, 2010.
[3] Adolph T., Eggers A., Pastor C., “Matrix of serious thorax injuries by occupant characteristics, impact conditions and restraint type and identification of the important injury mechanisms to be considered in THORAX and THOMO”, COVER project GA No. 218740, Deliverable D5-Annex II, 2009.
[4] Carroll J., “Matrix of serious thorax injuries by occupant characteristics, impact conditions and restraint type and identification of the important injury mechanisms to be considered in THORAX and THOMO”, COVER project GA No. 218740, Deliverable D5-Main summary report, 2009.
[5] Carroll J., Cuerden R., Richards D., Smith S., Cookson R., et al., “Matrix of serious thorax injuries by occupant characteristics, impact conditions and restraint type and identification of the important injury mechanisms to be considered in THORAX and THOMO”, COVER project GA No. 218740, D5-Annex I, 2009.
[6] Chauvel C., Labrousse M., “Matrix of serious thorax injuries by occupant characteristics, impact conditions and restraint type and identification of the important injury mechanisms to be considered in THORAX and THOMO”, COVER project GA No. 218740, Deliverable D5-Annex III, 2009.
[7] Hynd D., Carroll J., Davidsson J., Vezin P., “Biofidelity requirements for the THORAX project”, THORAX project GA No. 218516, D2.1, 2010.
[8] Song E., Troisseille X., Mendoza-Vazquez M., Davidsson J., Vezin P., “Definition of injury mechanism and related physical parameters based on datasets from PMHS tests and advanced HBM simulation”, THORAX project GA No. 218516, Deliverable D2.4, Version 1 (M12), 2010.
[9] Lemmen P., Been B., Carroll J., Hynd D., Davidsson J., Song E., Lecuyer E., “Development of an advanced frontal dummy thorax demonstrator”, Proceedings of IRCOBI Conference, Dublin, Ireland, 2012.
[10] Lemmen P., Been B., Carroll J., Hynd D., Davidsson J., Song E., Lecuyer E., “Development of an advanced thorax / shoulder complex for the THOR dummy”, Proceedings SIAT Conference, Pune, India, 2013.
[11] Törnvall F., “A New Shoulder for the THOR Dummy Intended for Oblique Collision, Vehicle Safety Division, Department of Applied Mechanics”, Chalmers University of Technology, Goteborg, Sweden, 2008.
[12] Schneider L., Robbins D., Pflug M., Snyder R., “Development of Anthropometrically based Design Specifications for an Advanced Adult Anthropomorphic Dummy Family”, Volume 2, University of Michigan Transportation Research Institute, 1983.
[13] Kroell C., Schneider D., Nahum A., “Impact tolerance and response of the human thorax”, Proceedings of 15th Stapp Car Crash Conference, San Diego, California, U.S.A., Paper number 710851, pp 84-134, 1971.

[14] Yoganandan N., Pintar F., Kumaresan S., Haffner M., Kuppa S., "Impact biomechanics of the human thorax-abdomen complex", IJCrash 2(2), pp 219-228, 1997.
[15] Ridella, S.A., Parent, D.,"Modifications to Improve the Durability, Usability and Biofidelity of the THOR-NT Dummy" Paper 0312, 22nd ESV International Technical Conference on the Enhanced Safety of Vehicles. Washington D.C. June 2011.
[16] Lebarbé M., "Contribution to the definition of biofidelity corridors in frontal impact for an adult male 50th percentile - Thorax Report - Rev 6", International Task Force for Frontal Biofidelity Requirements, ISO/TC22/SC12 – working group 5, 2011.
[17] Lebarbé M. Petit, P., "New Biofidelity Targets for the Thorax of a 50th Percentile Adult Male in Frontal Impact", Proceedings of IRCOBI Conference, Dublin, Ireland, 2012.
[18] Cesari D., Bouquet R., "Behaviour of human surrogates thorax under belt loading", Proceedings of 34th Stapp Car Crash Conference, Orlando, Florida, U.S.A., Paper number 902310, pp 73-81 1990.
[19] Kent R., Lessley D., Sherwood C., "Thoracic response to dynamic, non-impact loading from a hub, distributed belt, diagonal belt, and double diagonal belts", Proceedings of 48th Stapp Car Crash Conference, Nashville, Tennessee, U.S.A., Paper number 2004-22-0022, pp 495-519, 2004.
[20] Forman J., Lessley D., Kent R., Bostrom O., Pipkorn B., "Whole-body kinematic and dynamic response of restrained PMHS in frontal sled tests", Proc. of 50th Stapp Car Crash Conference, Dearborn, MI, U.S.A., Paper number 2006-22-0013, 2006.
[21] Bolton J., Kent R. and Crandall J., "Passenger Air Bag Impact and Injury Response using a Hybrid III Test Dummy and Human Surrogates", NHTSA Biomechanics Test Database, Tests 8377-8379, 2006.
[22] Shaw G., Crandall J. and Butcher J., "Biofidelity evaluation of the THOR advanced frontal crash test dummy", Proceedings of the IRCOBI Conference, Montpellier, France, pp 11-29, 2000.
[23] Carroll J., Hynd D., Davidsson J., Vezin P., Been B., Eggers A., Martinez L., "Dummy validation report", THORAX project GA No. 218516, D3.3, 2010.
[24] Shaw G., Parent D., Purtsezov S., Lessley D., Crandall J., *et al.*, "Impact response of restrained PMHS in frontal sled tests: skeletal deformation patterns under seat belt loading", Proceedings of 53rd Stapp Car Crash Conference, Savannah, Georgia, U.S.A., Paper number 2009-22-0001, 2009.
[25] Eppinger R., Marcus J. and Morgan R. "Development of dummy and injury index for NHTSAs thoracic side impact protection research program". SAE Government/Industry Meeting and Exposition, Washington, DC, USA, 21-24 May, 1984.
[26] Shaw G., *et al.* "Frontal Impact PMHS Sled Tests for FE Torso Model Development", Proceeding of the 2009 International IRCOBI Conference on the Biomechanics of Impact, September 7-10, York, UK, pp. 341-356.
[27] Shaw G. *et al.* "Impact response of restrained PMHS in frontal sled tests: skeletal deformation patterns under seat belt loading" 53rd STAPP Car Crash Conference, Savannah, Georgia, USA, 2-4 November, 2009.
[28] Crandall J., "ATD Thoracic Response Test Development", UVA1286, 1289, 1294, 1295, NHTSA Biomechanics Test Database, 2007.

THORACIC BIOFIDELITY ASSESSMENT OF THE THOR MOD KIT ATD

Daniel P. Parent
Matthew Craig
Stephen A. Ridella
Joseph D. McFadden
National Highway Traffic Safety Administration
United States of America
Paper Number 13-0327

ABSTRACT

During the upgrade of the 50th percentile male THOR anthropomorphic test device (ATD) from the Alpha level to the NT level, the low-speed Kroell hub impact corridor was selected as the design requirement for blunt thoracic impact response. Although this requirement was reiterated during the development of the THOR Mod Kit, it has been documented that the response of the thorax does not meet the design requirement. There were three objectives to this study: first, to quantify the thoracic biofidelity of frontal impact ATDs; second, to demonstrate that the Mod Kit design level of the THOR ATD meets the intended the low-speed blunt thoracic impact biomechanical response requirement; and third, to evaluate the influence of the SD-3 shoulder design on the performance of the THOR ATD in blunt thoracic impact. Data were collected from low-speed (4.3 meters per second) blunt thoracic impact tests of several variations of 50th percentile male ATDs: Hybrid III, THOR-NT, THOR Mod Kit, and THOR Metric. The latter two THOR variations were tested both with and without an updated shoulder ("SD-3") used in the European Union's THORAX project demonstrator. The thoracic force-deflection responses were qualitatively compared to the existing low-speed thoracic impact response corridors: the Kroell corridor, based on internal deflection, and the Lebarbé corridor, based on external defelction. The THOR-NT and THOR Mod Kit responses showed force levels similar to the biomechanical response requirements, but deflections lower than desired. The repeatability array carried out on one THOR Mod Kit ATD showed no notable variations in force or deflection. Quantitative comparison of the ATD impact response to the biofidelity corridors was carried out using a biofidelity ranking system, which was used to demonstrate that the response of the THOR ATDs are not differentiable from the human subjects used to develop the corridors. The low-speed blunt thoracic impact response requirement for the THOR Mod Kit design level was met both qualitatively and quantitatively. The installation of the SD-3 shoulder influenced the resulting biofidelity ranking system results, but did not change the order of ranking of either the THOR Mod Kit or the THOR Metric ATDs. This study is limited by the volume, quality, and specificity of the PMHS data.

INTRODUCTION

The National Highway Traffic Safety Administration (NHTSA) has been researching advanced anthropometric test devices (ATDs) to succeed the Hybrid III ATD since the early 1980s (Haffner, 2001). The primary design objective of this research was to represent the response of automotive occupants in sophisticated restraint systems developed since the advent of the Hybrid III, such as force-limited three-point belts and air bags. This research has culminated in the development of the Test Device for Human Occupant Restraint (THOR), first as the THOR Alpha (Haffner, 2001) and later upgraded to the THOR-NT (Shams, 2005). Most recently, in coordination with the Society for Automotive Engineers (SAE) THOR Evaluation Task Group, a modification package ("Mod Kit") intended to enhance the biofidelity, repeatability, durability, and usability of the THOR was introduced (Ridella, 2011) and installed as an upgrade kit on the NHTSA-owned fleet of THOR-NT ATDs. One of the primary requirements of the Mod Kit upgrade was to ensure thoracic biofidelity as assessed by the low-speed Kroell blunt hub impact corridor. Although this design requirement was first implemented during the upgrade from THOR Alpha to THOR-NT and reiterated during the development of the THOR Mod Kit, it has been documented that the response of the thorax does not meet this design requirement (Ridella, 2011; Mueller 2011).

Subsequent to the development of the THOR Mod Kit, an upgrade to the Chalmers shoulder assembly known as the "SD-3" was developed through the European Union's THORAX project (Lemmen, 2012). This shoulder assembly is currently being evaluated to determine its suitability for inclusion in the THOR drawing package. One step in this evaluation is to install the shoulder on the THOR ATD and compare the response to both the standard shoulder response and to the biomechanical response requirement.

There are three objectives in the current study: first, to quantify the thoracic biofidelity of frontal impact ATDs; second, to demonstrate that the Mod Kit design level of the THOR ATD meets the intended the low-speed blunt thoracic impact biomechanical response requirement; and third, to evaluate the influence of the SD-3 shoulder design on the performance of the THOR ATD in blunt thoracic impact.

Figure 1. THOR Metric ATD

METHODS

The first objective of this study can be addressed using a biofidelity ranking system, but to implement such a system in this case, several steps were necessary to prepare the both the existing biofidelity corridors and the collected test data (Figure 2). First, since the biofidelity corridor used as the primary THOR design requirement ("Kroell") exists as a force-deflection characteristic, it was necessary to develop internal (skeletal) deflection and force time history data before the biofidelity ranking system could be implemented. This was carried out using a three degree-of-freedom "Lobdell" model fit to the response corridor. Then, for each ATD configuration, at least one blunt thoracic impact test was carried out. The measured thoracic response was compared to the Kroell corridor time histories using the biofidelity ranking system. Next, in order to develop the external deflection for comparison to the Lebarbé corridor, a Lobdell model was fit to the response of the blunt thoracic impact test. This process resulted in four measurements of thoracic impact response biofidelity for each ATD.

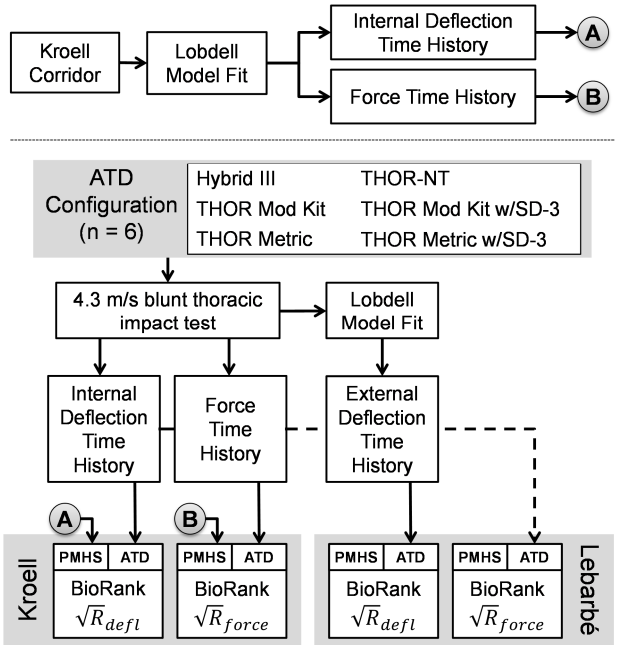

Figure 2. Methodology employed in this study to quantify biofidelity of thoracic impact response.

Blunt Thoracic Impact Tests

Low-speed blunt thoracic impact tests were carried on four different 50th percentile male ATDs: Hybrid III, THOR-NT, THOR Mod Kit, and THOR Metric. The THOR Mod Kit and the THOR Metric were tested both with the standard THOR-NT shoulder and with SD-3 shoulder, for a total of six configurations (Table 1). In each test, the response force imparted on the impact pendulum and the internal deflection time histories were recorded. In one test (THOR Mod Kit w/SD-3), high-speed video of the impact event was recorded from the side and film analysis was used to calculate external deflection by measuring the change in distance between the impactor face and the posterior aspect of the ATD starting at the time of first contact.

Anthropomorphic Test Devices

The THOR-NT, which was built by GESAC, Inc., was based on the drawing package released in 2005. The THOR Mod Kit was originally built as a THOR-NT by GESAC, Inc., and then subsequently modified by Humanetics Innovative Solutions, Inc. to the Mod Kit build level (Ridella, 2011). The THOR Metric (Figure 1) was built by Humanetics to the same design as the THOR Mod Kit, except that it was built from scratch instead of upgrading a THOR-NT. While there are some detailed differences between

the THOR Mod Kit and the THOR Metric, such as the imperial fasteners in the THOR Mod Kit compared to the metric fasteners in the THOR Metric, the performance requirements for both ATDs are based on the test conditions defined by the biomechanical response requirements and certification requirements of the THOR-NT (NHTSA, 2005a,b), with additional requirements specified during the development of the Mod Kit (Ridella, 2011).

Table 1. Test Objects

Identifier Description
Hybrid III As described in 49 CFR Part 572 Subpart E
THOR-NT As described in THOR-NT technical data package (http://www.nhtsa.gov/Research/Biomechanics+&+Trauma/>>THOR-NT+Advanced+Crash+Test+Dummy)
THOR Mod Kit As described in Ridella, 2011
THOR Mod Kit w/SD-3 As described in Ridella, 2011 except for the shoulder assembly. SD-3 shoulder assembly as described by Lemmen et al (2012) is installed
THOR Metric As described in Ridella, 2011 but with the remaining components soft-converted (exact unit conversion without change in precision or physical configuration) to metric dimensions and metric fasteners used throughout
THOR Metric w/SD-3 As described in Ridella, 2011 but with the remaining components soft-converted to metric dimensions and metric fasteners used throughout. Additionally, SD-3 shoulder assembly as described by Lemmen et al (2012) is installed

Biomechanical Response Requirements

The Biomechanical Response Requirements for the THOR ATD (NHTSA, 2005a) specify two test conditions that were used as design requirements. The first condition is a blunt thoracic impact, which consists of a 23.4 kilogram pendulum with a 152.4 millimeter diameter flat face impacting the center of the sternum at 4.3 meters per second. The 6.7 meter-per-second impact was originally included in the design requirements, but this requirement was relaxed during the development of the Mod Kit. The 6.7 meter-per-second condition remains as a certification condition, but primarily to assess the durability of the ATD. The second condition describes a 15 degree oblique impact to the lower thorax using the same impactor characteristics.

Calculation of Thoracic Deflection

In the design of the THOR-NT, the thoracic deflection instrumentation is initially aligned with the coordinate system of the pendulum. However, this is not necessarily effective for rib strain estimation, as this effectively measures the change in distance between the 4th rib and the 8th thoracic vertebral body. In this arrangement, rotation of the ribs about the spine can be measured as deflection, but such deflection does not necessarily relate to rib strain. In the design of the THOR Mod Kit, the upper thorax deflection instrumentation was attached to the same spine segment as the rib attachment, which is thought to be a more accurate representation of rib strain, which in turn is believed to be a predictor of rib fracture (Forman, 2012)

However, this presents an additional layer of processing difficulty, as the coordinate system used to measure skeletal deflection on the THOR Mod Kit is not parallel to the impactor in the blunt thoracic impact test, thus may not record the total skeletal deflection. As previously presented (Shaw, 2012), the methodology to process the IR-TRACC chest deflection instrumentation presents the three-dimensional deflections in the coordinate system of the upper spine, which is roughly 20 degrees forward of vertical. During the blunt thoracic impact event, the THOR rib cage compresses towards and rotates downward about the upper spine. This results in compression of the chest along the axis of the impactor that is not captured by the upper spine local X-axis. To account for this, both the local X- and Z-axes of deflection in the upper spine coordinate system must be evaluated (Appendix A).

Biofidelity Ranking

The biofidelity ranking system ("Bio Rank" for short) calculation assesses the biofidelity of an ATD by comparing the dummy response to the mean cadaver response. To account for the potentially large variability in individual cadaver responses, Bio Rank calculates a cumulative variance between the dummy response and the mean cadaver response (DCV) and normalizes this value by the cumulative variance between the mean cadaver response and the mean plus one standard deviation cadaver response (CCV) (Rhule, 2002). For example, given a fixed dummy response, the DCV/CCV value would be higher for a narrow corridor of cadaver response corridor compared to a wide corridor of cadaver response. For the current effort, the $\sqrt{R}$ terms for deflection and force are presented both individually and combined to allow multiple levels of comparison. The biofidelity targets for the deflection and force time-

histories are limited to the timeframe between 0 and 500 milliseconds, since the impactor is no longer in contact with the occupant. While the unloading portion of the event is important in that the unloading hysteresis is one representation of the viscoelastic properties of the occupant, including too much of the unloading portion could override response at peak force, which has a stronger relationship to injury risk.

Generation of Mean, +/- SD for Kroell Corridor

The design requirement for response to blunt thoracic impact for the THOR ATD was specified using the corridors known as the Kroell corridors, developed from several series of PMHS impacts in the early 1970s (Neathery, 1974). From these tests, a biofidelity corridor for low-speed (4.3 meters per second) blunt thoracic impact was developed through an oft-criticized "eyeball averaging" method, though subsequent reanalysis has not shown significant differences from this method (Lessley, 2004).

Since the Kroell corridor exists in the force-vs-deflection domain and not the time domain, the calculation of Bio Rank is not straight-forward. In order to achieve the time histories of force and deflection for the mean response, a simplified Lobdell model (Lobdell, 1973) was formulated (Figure 3). The simplified Lobdell model includes 8 variables and two constants (Table 2). This model was optimized to match the mid-points of the low-speed thoracic impact response corridor as defined in the THOR Biomechanical Response Requirements manual (Figure 4).

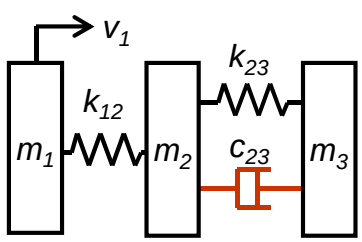

Figure 3. Simplified Lobdell model implemented in this study

Table 2. Variables in the Simplified Lobdell model of thorax response to blunt hub impact

Variable	Description
m_1	mass of impactor
m_2	mass of the sternum, anterior rib cage
m_3	mass of the remaining coupled mass of the body
k_{12}	stiffness of the skin/muscle in front of sternum
k_{23a}	stiffness of rib cage before k_{23s}
k_{23b}	stiffness of rib cage after k_{23s}
k_{23s}	inflection point of piecewise linear stiffness k_{23}
c_{23a}	viscous response of thorax compression
c_{23b}	viscous response of thorax extension
v_1	initial velocity of the impactor

The optimization was configured to minimize the objective function defined by the sum of the normalized distances from each target point (represented by red stars in each relevant plot) and the nearest point on the Lobdell model force-vs-deflection response. To ensure a global solution in the optimization, an initial design array was developed by generating 100,000 designs by randomizing variable values between 0.1 times and 10 times the values provided for the initial dummy targets (Lobdell, 1973). The design that demonstrated the best fit was then used as the input to a brute force optimization using the ranges defined by +/- 20% of each variable value.

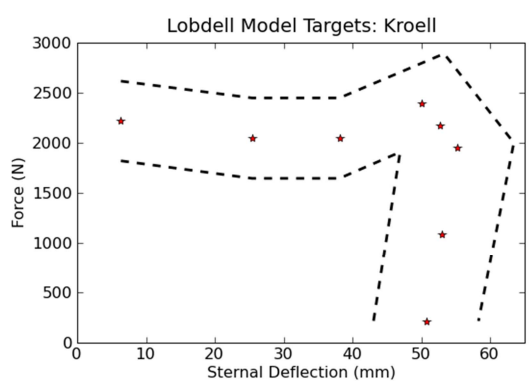

Figure 4. 4.3 meters per second blunt thoracic impact response requirement (NHTSA, 2005a) in dashed black line, along with optimization target points (red stars).

The mean response was then scaled in the deflection and force axes by 15% (as described in Neathery, 1974) to create the upper and lower boundaries of the force and deflection time-histories for use in the Bio Rank calculation.

Generation of Mean, +/- SD for Lebarbé Corridor

In support of the International Standards Organization (ISO) Frontal Biofidelity Specification

International Task Force (ISO/TC22/SC12/WG6), new biomechanical response targets were developed in the low-speed blunt thoracic impact condition (Lebarbé, 2012). These targets have since been adopted by the European Union's THORAX project, which aims to develop a thoracic impact response demonstrator which has been installed on a THOR ATD. The development of this corridor included a different normalization process, along with additional newer data sets, compared to the Kroell corridor. Since this corridor was developed by calculating the mean and standard deviations of the force and deflection time-histories, it is suitable for evaluation using Bio Rank. Nonetheless, a Lobdell model was optimized to the Lebarbé corridor to allow an apples-to-apples comparison with the Kroell corridor (Figure 5).

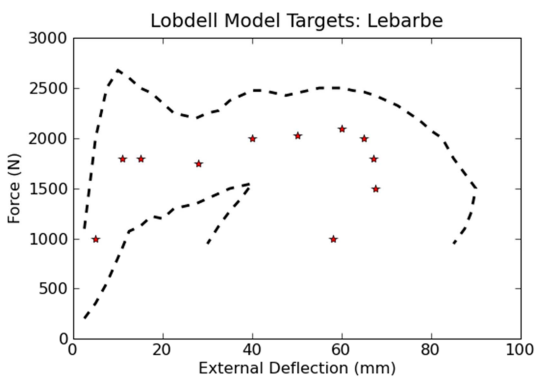

Figure 5. 4.3 meters per second blunt thoracic impact response target (Lebarbé, 2012) in dashed black line, along with optimization target points (red stars).

Estimation of External Deflection for THOR (based on THOR-K SD3 tests)

The two targets for blunt thoracic impact response differ in that the Kroell target is based on skeletal deflection, while the Lebarbé target is based on external deflection. Both the certification requirements and the biomechanical response requirements for the THOR ATD (NHTSA, 2005a,b) specify that internal (skeletal) deflection shall be measured. As such, a comparison to the Lebarbé target is not possible. To address this issue, a series of blunt thoracic impact tests were conducted, using both the THOR Mod Kit and the THOR Mod Kit with the SD-3 shoulder installed, which employed high-speed video to track the external deflection in addition to internal deflection measured by the thoracic IR-TRACC instrumentation.

Ideally, the external deflection measured should be related to the internal deflection by some transfer function. However, due to various nonlinearities, this cannot be calculated by a simple shifting and/or scaling of the internal deflection. Therefore, to address this issue, a Lobdell model was fit to the response of the THOR internal response the same way it was fit to the Kroell corridor, except this time the deflection time-history was used as the target. Once optimized to recreate the skeletal deflection using the differential motion of m_2 and m_3, the model can be used to predict external deflection based on the differential motion of m_1 and m_3. The quality of this prediction can be evaluated using the THOR Mod Kit with SD-3 test condition, where both internal and external deflections were measured.

RESULTS

Repeatability

For all of the ATDs included in this study, local repeatability (same ATD, same laboratory, consecutive tests) was excellent (Figure 6). Since the repeatability was good, the Bio Rank subsequent calculations were carried out using just one of the sets of test results for each ATD, since calculating an average of the response time-histories could result in smoothing or filtering of the responses if the timing was not identical, resulting in non-physical nonlinearities.

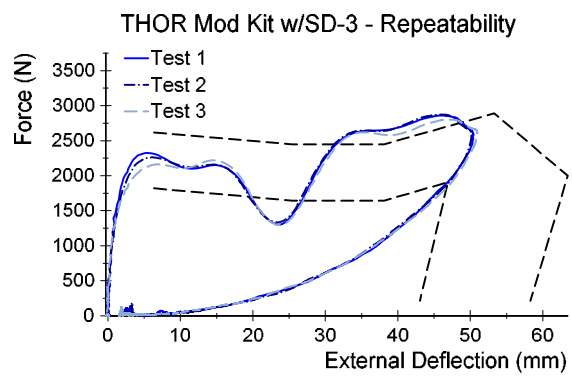

Figure 6. Three consecutive repeated blunt thoracic impact tests on a THOR Mod Kit w/SD-3 shoulder (S/N 16).

Response to Blunt Hub Impact

In a blunt thoracic impact with a 23.4 kilogram impactor at 4.3 meters per second, compared to the Kroell internal deflection corridor the Hybrid III shows the stiffest response, with a peak force about 1,000 Newtons higher than the corridor and a peak deflection 10 millimeters less than the peak of the lower boundary of the corridor (Figure 7). The THOR-NT response (Figure 8) is stiffer than the THOR Mod Kit response (Figure 9), which is in turn stiffer than the THOR Metric response (Figure 10). When installed on the THOR Mod Kit, the SD-3

shoulder resulted in a similar peak deflection as the standard shoulder, while some of the local peaks in force have been smoothed out. When installed on the THOR Metric, there peak deflection is reduced by roughly five millimeters, and the local peaks in force are similarly smoothed out.

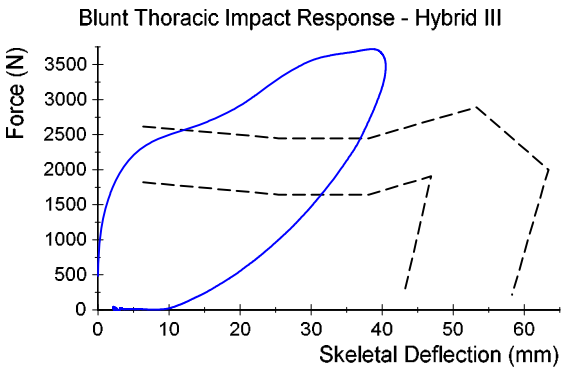

Figure 7. Force-deflection response of the Hybrid III under 23.4kg, 4.3m/s blunt thoracic impact.

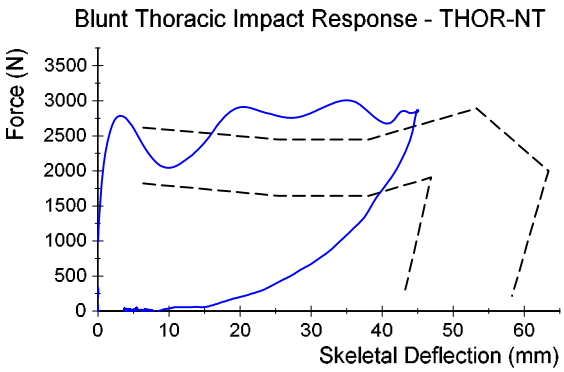

Figure 8. Force-deflection response of the THOR-NT under 23.4kg, 4.3m/s blunt thoracic impact.

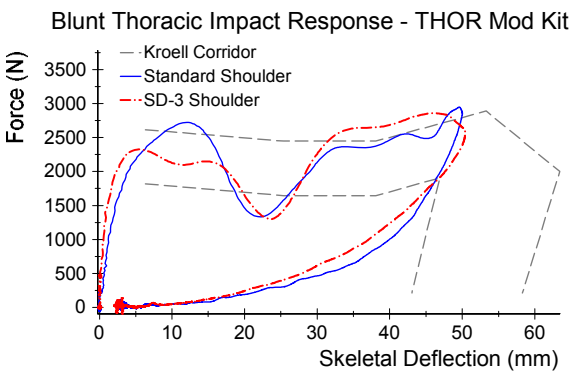

Figure 9. Force-deflection response of the THOR Mod Kit with and without the SD-3 shoulder under 23.4kg, 4.3m/s blunt thoracic impact.

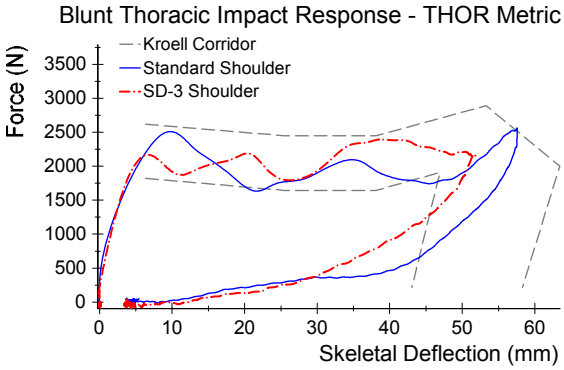

Figure 10. Force-deflection response of the THOR Metric with and without the SD-3 shoulder under 23.4kg, 4.3m/s blunt thoracic impact.

Generation of Mean, +/- SD for Kroell Corridor

The optimized Lobdell model of blunt thoracic impact achieved good qualitative and quantitative agreement with the center of the Kroell corridor (Figure 11). The scaled upper and lower boundaries generally conformed to the boundaries of the original Kroell corridor, though naturally the sharp creases were not able to be represented with the simple Lobdell model. The resulting skeletal deflection and force time-histories (Figure 12) were similar in shape to those of the Lebarbé targets (Figure 13). Note that both deflection time-histories show a very narrow corridor width at the onset of force and deflection, though only the Kroell force time-history narrows at the end of the force time-history

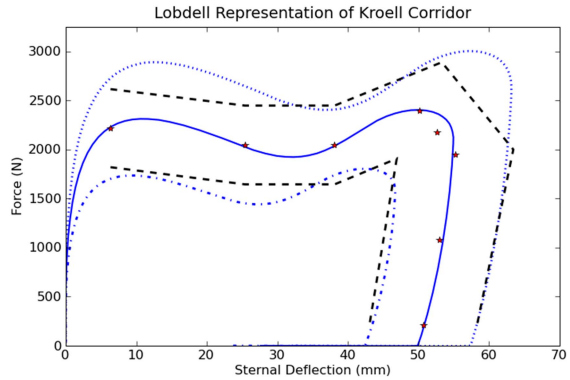

Figure 11. Lobdell model response that best fits the center of the Kroell corridor.

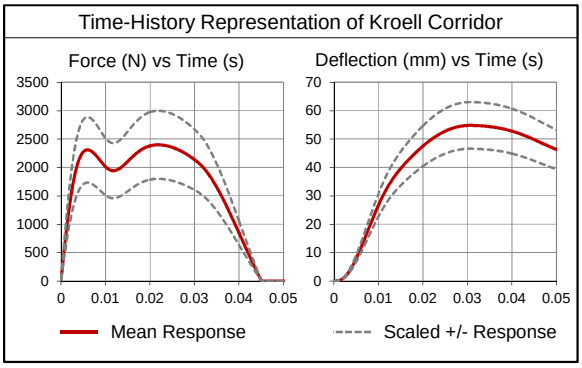

Figure 12. Representation of the force (left) and skeletal deflection (right) components of the Kroell corridor as a time-histories for use in Bio Rank calculations.

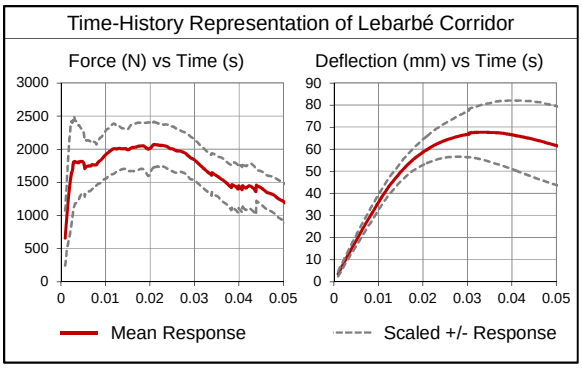

Figure 13. Representation of the force (left) and external deflection (right) components of the Lebarbé corridor as a time-histories for use in Bio Rank calculations.

Comparing the Lobdell model fits of the Kroell and Lebarbé corridors, the parameters resulting in optimal fit to the corridor centerline were noticeably different for the two conditions (Appendix B). However, the Kroell response, when represented in the same external deflection basis as the Lebarbé response, fits within the plus or minus standard deviation corridor for a majority of the response (Figure 14).

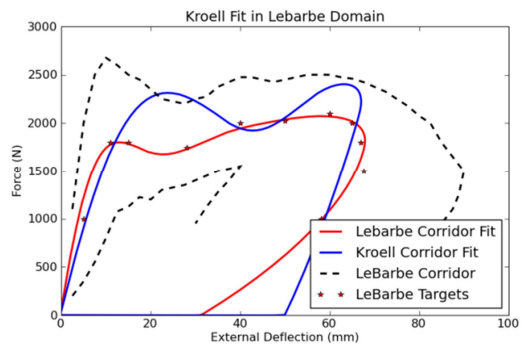

Figure 14. Lobdell model response that best fits the Lebarbé corridor mean response.

Estimation of External Deflection for THOR (based on THOR-K SD3 tests)

For each of the tests for which external deflection was not explicitly measured during a test with high-speed video, the external deflection was determined by first fitting a Lobdell model to the measured sternal deflection, then outputting the impactor-to-spine deflection predicted by this Lobdell model. To validate this methodology, the external deflection measured during the test of the THOR Mod Kit with SD-3 was compared to the Lobdell model prediction (Figure 15). The peak deflection predicted by the model is 60.5 millimeters, compared to 75.3 millimeters measured during the test. It should be noted that this measured deflection is based on post-processing of high-speed video data, which introduces numerous error sources including images resolution, lens distortion, and synchronization of test data and video data.

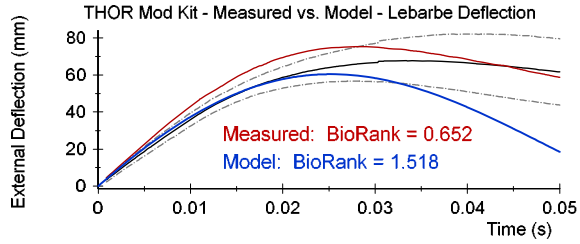

Figure 15. Comparison of the measured and predicted external deflection (and force-deflection response) of the THOR Mod Kit with SD-3 ATD.

The same trends in relative stiffness that appear in the Kroell corridor comparison (Figure 7 through Figure 10) are repeated in the Lebarbé corridor comparison (Figure 16 through Figure 19). Note that these responses present the force and external deflection time-histories predicated by the Lobdell model. Qualitatively, out of the ATDs included in this study the response of the THOR Metric with the SD-3 shoulder is the closest to meeting both the Lobdell (Figure 10) and the Lebarbé (Figure 19) corridors.

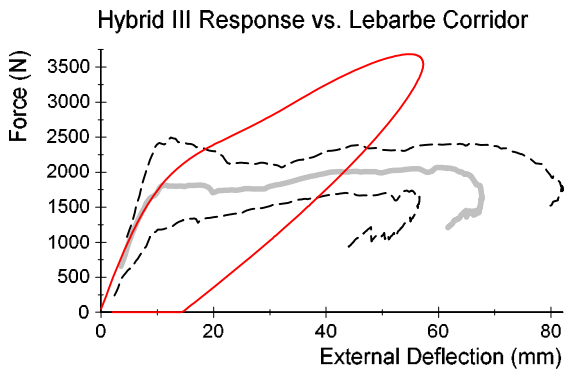

Figure 16. Force vs. external deflection response of the Hybrid III under 23.4kg, 4.3m/s blunt thoracic impact.

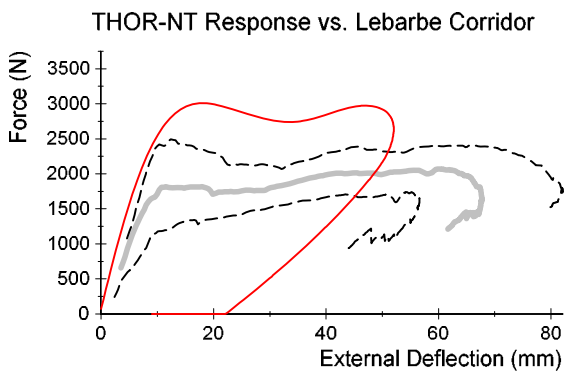

Figure 17. Force vs. external deflection response of the THOR-NT under 23.4kg, 4.3m/s blunt thoracic impact.

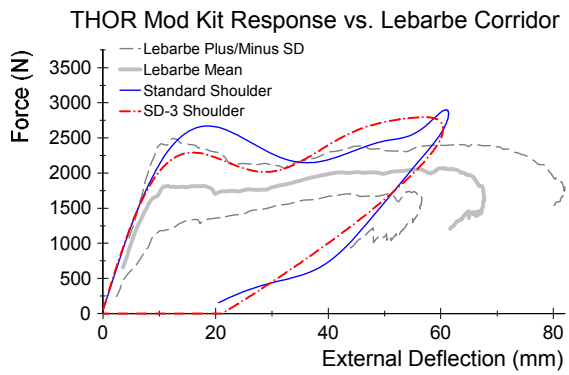

Figure 18. Force vs. external deflection response of the THOR Mod Kit with and without the SD-3 shoulder under 23.4kg, 4.3m/s blunt thoracic impact.

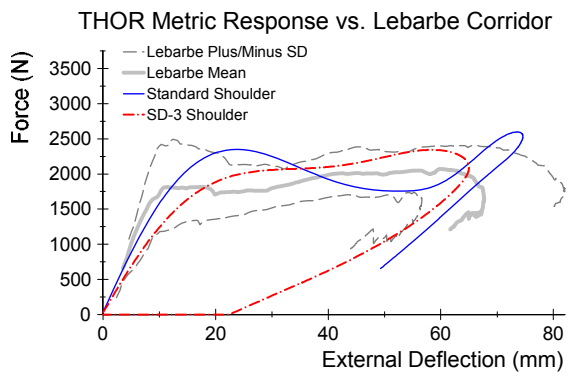

Figure 19. Force vs. external deflection response of the THOR Metric with and without the SD-3 shoulder under 23.4kg, 4.3m/s blunt thoracic impact.

Bio Rank

A Lobdell model was optimized to fit the force vs. skeletal deflection response of the Kroell 4.3 meters per second blunt thoracic impact response biofidelity corridor to allow the Bio Rank calculation of the individual force and deflection time histories measured in certification tests carried out for each of the ATDs included in this study. For the Bio Rank evaluation using the Kroell corridor as the biomechanical response basis (Table 3), the measured skeletal deflection was used (either the chest slider on the Hybrid III, the CRUX on the THOR-NT, or the IR-TRACC on the remaining THORs). For the Bio Rank evaluation using the Lebarbé corridor as the biomechanical response basis, the deflection used for all of the ATD responses was the external deflection output from a Lobdell model that was fit to the measured internal deflection (Table 4).

In the case of the THOR Mod Kit w/SD-3, the Bio Rank $\sqrt{R}_{defl}$ could be calculated for both the measured external deflection and the external deflection calculated using the Lobdell model fit to the ATD. In this condition, $\sqrt{R}_{defl}$ for the measured and predicted external deflections were 0.652 and 1.518, respectively. This discrepancy is likely due to the 20% difference noted in the peak external deflection calculated using the Lobdell model and the measured external deflection from the test of the THOR Mod Kit w/SD-3 (Figure 15).

In every Bio Rank calculation except for the $\sqrt{R}_{defl}$ for the Lebarbé corridor comparison, the THOR Metric with the SD-3 shoulder had the lowest $\sqrt{R}$, indicating the most biofidelic response. All of the THOR Mod Kit and Metric responses demonstrated $\sqrt{R}$ values below 2.0, suggesting that the ATD responds as much like the target corridor as would another human subject (Rhule, 2002).

Table 3. Bio Rank calculation using the Kroell corridor as the force and deflection target

Biomechanical Basis: Kroell			
ATD	$\sqrt{R}_{defl}$	$\sqrt{R}_{force}$	$\sqrt{R}_{avg}$
Hybrid III	2.648	1.844	2.246
THOR-NT	1.865	1.052	1.459
THOR Mod Kit	1.030	1.024	1.027
THOR Mod Kit w/SD-3	1.256	0.973	1.115
THOR Metric	0.266	1.267	0.767
THOR Metric w/SD-3	0.581	0.905	0.743

Table 4. Bio Rank calculation using the Lebarbé corridor as the force and deflection target

Biomechanical Basis: Lebarbé 2012			
ATD	$\sqrt{R}_{defl}$	$\sqrt{R}_{force}$	$\sqrt{R}_{avg}$
Hybrid III	2.364	2.923	2.644
THOR-NT	2.327	1.968	2.148
THOR Mod Kit	1.518	1.514	1.516
THOR Mod Kit w/SD-3	1.621	1.438	1.530
THOR Metric	0.495	0.985	0.740
THOR Metric w/SD-3	1.049	0.769	0.909

DISCUSSION AND LIMITATIONS

It is no surprise that in the low-speed blunt thoracic impact condition that was used as a primary design requirement for the THOR ATD, its biofidelity when assessed in the same condition shows improvement over the Hybrid III, for which the primary thoracic impact response requirement was a high-speed (6.7 meters per second) blunt thoracic impact. On the other hand, the quantification of biofidelity implemented in this study demonstrates that the THOR-NT blunt thoracic response is less biofidelic than the THOR Mod Kit design level, which is important because the same design requirement was used for the THOR-NT during the upgrade from the THOR Alpha version, yet the response of the THOR-NT would not be considered biofidelic under evaluation in the same condition.

When installed on the THOR Mod Kit or the THOR Metric, the SD-3 shoulder does not appreciably improve or degrade the biomechanical response in the blunt hub impact. The SD-3 was designed more for biofidelic range of motion and shoulder belt interaction than for blunt hub impact response, so this outcome was not unexpected since this increased range of motion assumedly results in the mass of the shoulders and arms being less coupled to the thorax. This assumption is supported by the Lobdell models fit to the THOR Mod Kit and THOR Metric with and without the SD-3 shoulder, as the variable m_3 indicates that the coupled mass of the thorax is lower with the SD-3 shoulder than with the standard shoulder (Appendix B). There are other variable differences as well, but it is difficult to compare directly since the value of variable k_{23s}, the switch between the piecewise linear stiffness of the rib cage, is markedly different.

Overall, the THOR Metric resulted in the lowest Bio Rank values of any of the frontal impact ATDs included in this study. Addition of the SD-3 shoulder to the THOR Metric resulted in some differences in the individual $\sqrt{R}$ values, as in both corridor comparisons the deflection values increased but the force values decreased. However, the average $\sqrt{R}$ values for both the Kroell and Lebarbé corridor comparisons for the Metric THOR with the SD-3 shoulder were below 1.0, suggesting that the response is indiscernible from the response of a human subject used to develop the biofidelity corridors.

The performance of the THOR under the low-speed blunt thoracic impact condition does not alone demonstrate sufficient biofidelity of the ATD, since this condition is not necessarily representative of the type of loading that the occupant may undergo during as a motor vehicle occupant during a frontal or oblique crash. One way to assess the thoracic biofidelity under such conditions is through an isolated sled test representing shoulder belt loading to the thorax, as carried out in the "Gold Standard" condition at the University of Virginia (Shaw, 2013). Preliminary results show that the chest deflection measured using the THOR Mod Kit w/SD-3 were more PMHS-like than those of the Hybrid III, though

there were some localized differences in the response of the loaded shoulder and associated upper chest quadrant, as well as differences in the chest deflection measurement locations between the Hybrid III and the PMHS.

There is a second thoracic impact response requirement in the THOR Biomechanical Response Requirements manual (NHTSA, 2005a): oblique impact to the lower thorax, based on tests carried out by Yoganandan et al (1997). The THOR manual includes mean and plus/minus standard deviation responses for both the force and deflection time-histories (NHTSA 2005a, Figures 21 and 22). This deflection time-history appears to be related to processed chestband deflection, though the force and deflection time-histories are only presented for one subject in the source referenced by the manual. The manual later states that the external deflection in the THOR tests was taken from a linear potentiometer measuring the impactor displacement, which is not ideal since it does not account for the spine moving away from the impact interface. Due to this lack of information, the oblique thoracic impact condition was not included in the present study.

There are several limitations to this study that are worth noting, mostly relating to the implementation of the Lobdell model. Though it has not been demonstrated herein, it is acknowledged that the optimization of the Lobdell model returns a non-unique solution. Specifically, the value of the variable k_{12}, which represents the stiffness of the impactor-to-chest response, could significantly influence the relationship between internal and external deflection. However, changes to k_{12} also influence the initial peak (between 0 and 10 millimeters of deflection) of the response, so care was taken in selecting the validation points to ensure that this portion of the response was captured. Nonetheless, it is understood that the predicted external deflection is not a single solution, thus the values of the Bio Rank $\sqrt{R}_{defl}$ in the Lebarbé condition should be used with caution.

FUTURE WORK

One of the potential applications of the THOR ATD is the assessment of injury risk in small overlap and oblique vehicle crash tests (Saunders, 2012). Since oblique loading of the thorax by the shoulder belt or steering wheel rim is possible in this test condition, it is important that the biomechanical response of the thorax in oblique loading is assessed. To confirm the biofidelity of the ATD, the THOR will be exercised in the same condition as the oblique thorax loading conditions referenced in the THOR Biomechanical Response Requirements manual.

CONCLUSIONS

Using the previously-developed Bio Rank methodology to assess frontal impact ATD thoracic biofidelity as defined using both the Kroell and the Lebarbé biomechanical response bases, the THOR Metric ATD demonstrates the best qualitative agreement with the available biofidelity corridors and resulted in a favorable quantitative biofidelity assessment compared to the Hybrid III and previous versions of the THOR ATD. Using the quantitative biofidelity ranking system, the THOR Mod Kit and Metric ATDs result in $\sqrt{R}$ values below 2.0, indicating that the ATDs respond as much like the target corridor as would another human subject. It was further demonstrated that the THOR Metric ATD showed the best overall thoracic impact response biofidelity. The installation of the SD-3 shoulder assembly resulted in better qualitative agreement and similar quantitative agreement with the biomechanical response corridors.

ACKNOWLEDGEMENTS

The authors would like to express appreciation for the contributions of the NHTSA Vehicle Research and Test Center staff including, but not limited to, Bruce Donnelly, Kevin Moorhouse, Alena Hagedorn, Jim Stricklin, Patrick Biondillo, and Dave Walker.

REFERENCES

[1] Haffner, M., Rangarajan, N., Artis, M., Beach, D., Eppinger, R., Shams, T., "Foundations and Elements of the NHTSA THOR Alpha ATD Design," 17th ESV Conference, Paper No. 458, 2001.

[2] Shams, T., Rangarajan, N., McDonald, J., Wang, Y., Platten, G., Spade, C., Pope, P., Haffner, M., "Development of THOR NT: Enhancement of THOR Alpha – the NHTSA Advanced Frontal Dummy," 19th ESV Conference, Paper No. 05-0455, 2005.

[3] Ridella, S., Parent, D., "Modifications to Improve the Durability, Usability, and Biofidelity of the THOR-NT Dummy," 22nd ESV Conference, Paper No. 11-0312, 2011.

[4] Mueller, B.C., Sherwood, C.P., Arbelaez, R.A., Zuby, D.S., Nolan, J.M., "Comparison of Hybrid III and THOR Dummies in Paired Small Overlap Tests," Proc. 55th Stapp Car Crash Conference, Dearborn, MI, November 2011.

[5] Yoganandan, N., Pintar, F., Kumaresan, S., Haffner, M., Kuppa, S. 1997. Impact biomechanics of the human thorax-abdomen complex. International Journal of Crash, Vol 2, No. 2, pp 219-228.

[6] Rhule, H.H., Maltese, M.R., Donnelly, B.R., Eppinger, R.H., Brunner, J.K., and Bolte, J.H.IV. (2002) Development of a New Biofidelity Ranking System for Anthropomorphic Test Devices. Stapp Car Crash Journal 46: 477-512.

[7] Shaw, G., Lessley, D., Ash, J., Crandall, J., "Development of an Alternative Frontal Impact Condition to Assess Thoracic Response Using the THOR Mod Kit Dummy," Proceedings of the 2012 JSAE Annual Congress (Spring), 2012.

[8] Forman, J.L., Kent, R.W., Mroz, K., Pipkorn, B., Bostrom, O., Segui-Gomez, M., "Predicting rib fracture risk with whole-body finite element models: development and preliminary evaluation of a probabilistic analytical framework," Annals of Advances in Automotive Medicine/Annual Scientific Conference. Vol. 56, 2012.

[9] Shaw, G., Parent, D., Purtsezov, S., Lessley, D., Crandall, J., Tornvall, F., "Torso Deformation in Frontal Sled Tests: Comparison Between THOR-NT, THOR-NT with the Chalmers SD-1 Shoulder, and PMHS," Proceedings of the International IRCOBI Conference, 2010.

[10] International Standards Organization, "WorldSID Instrumentation," ISO TC22/SC12/WG5, WorldSID TG N397, 2005.

[11] Society of Automotive Engineers, "Instrumentation for Impact Test – Part 1 – Electronic Instrumentation," SAE J211/1, July 2007.

[12] Moorhouse, K., Probst, E., "A Repeatability Assessment of the THOR-NT ATD Response and an Evaluation of the Certification Procedures," National Highway Traffic Safety Administration, Docket No. NHTSA-2008-0102, May 2007.

[13] Shaw, G., Lessley, D., Kent, R., Crandall, J., "Dummy Torso Response to Anterior Quasi-static Loading," 19th ESV Conference, Paper No. 05-0371, 2005.

[14] Schneider, L., King, A., Beebe, M., "Design Requirements and Specifications: Thorax-Abdomen Development Task. Interim Report: Trauma Assessment Device Development Program," DOT HS 807 511, November 1989.

[15] Neathery, R.F., "Analysis of Chest Impact Response Data and Scaled Performance Recommendations," Proceeding of the 18th Stapp Car Crash Conference, SAE Paper No. 741188, 1974.

[16] Lessley, D., Crandall, J., Shaw, G., Kent, R., Funk, J., "A Normalization Technique for Developing Corridors from Individual Subject Responses," Society of Automotive Engineers, Paper No. 2004-01-0288, 2004.

[17] Kent, RW, Bass, CR, Woods, WA, Salzar, RS, Lee, SH, Melvin, J., "The Role of Muscle Tensing on the Force-deflection Response of the Thorax and a Reassessment of Frontal Impact Thoracic Biofidelity Corridors," Journal of Automobile Engineering, Proceedings of the Institution of Mechanical Engineers, Vol. 220, No. 7, pp. 853-868, 2006.

[18] National Highway Traffic Safety Administration (a), "Biomechanical Response Requirements of the THOR NHTSA Advanced Frontal Dummy, Revision 2005.1," Report No: GESAC-05-03, U.S. Department of Transportation, Washington, DC, March 2005.

[19] National Highway Traffic Safety Administration (b), "THOR Certification Manual, Revision 2005.2," Report No: GESAC-05-04, U.S. Department of Transportation, Washington, DC, March 2005.

[20] Lebarbé, M., Petit, P., "New Biofidelity Targets for the Thorax of a 50th Percentile Adult Male in Frontal Impact," Proceedings of the 2012 IRCOBI Conference, 2012.

[21] Lemmen, P., Been, B., Carroll, J., Hynd, D., Davidsson, J., Song, E., Lecuyer, E., "Development of an advanced frontal dummy thorax demonstrator," Proceedings of the 2012 IRCOBI Conference, 2012.

[22] Saunders, J., Craig, M., Parent, D., "Moving Deformable Barrier Test Procedure for Evaluating Small Overlap/Oblique Crashes," SAE International Journal of Commercial Vehicles 5.1 (2012).

[23] Shaw, C.G., Lessley, D.J., Ash, J.H., Crandall, J.R., Parent, D.P., "Response Comparison for the Hybrid III, THOR Mod Kit with SD-3 Shoulder, and PMHS in a Simulated Frontal Crash," 23rd ESV Conference, Paper No. 13-0130, 2013.

APPENDIX A. THORAX DATA PROCESSING

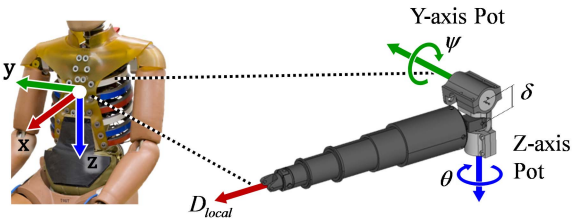

Figure A1. Diagram of the IR-TRACC configuration in the upper thorax of the THOR Mod Kit.

Upper Chest (IR-TRACC below pot; See Figure A1)		
X_{US} =	$D_{local}\cos\theta\cos\psi + \delta\sin\psi$	Eq. A1
Y_{US} =	$D_{local}\sin\theta$	Eq. A2
Z_{US} =	$-D_{local}\cos\theta\sin\psi + \delta\cos\psi$	Eq. A3
Lower Chest (IR-TRACC above pot)		
X_{LS} =	$D_{local}\cos\theta\cos\psi - \delta\sin\psi$	Eq. A4
Y_{LS} =	$D_{local}\sin\theta$	Eq. A5
Z_{LS} =	$-D_{local}\cos\theta\sin\psi - \delta\cos\psi$	Eq. A6

where:

D_{local}	=	Position of the anterior attachment point of the IR-TRACC tube relative to the attachment origin at the Z-axis potentiometer
θ	=	Angle time-history of Z-axis rotational potentiometer
ψ	=	Angle time-history of Y-axis rotational potentiometer
δ	=	Offset between centers of Z-axis and Y-axis potentiometers
XYZ_{US}	=	X, Y, or Z component relative to upper spine coordinate system
XYZ_{LS}	=	X, Y, or Z component relative to lower spine coordinate system

Pendulum coordinate system correction			
ϕ_{US}	=	$-17 + \phi_{LTS}$	Eq. A7
$\phi_{US,PEND}$	=	$\phi_{PEND} - \phi_{US} = \phi$	Eq. A8
$X_{PEND,L}$	=	$X_{US,L}\cos\phi - Z_{US,L}\sin\phi$	Eq. A9
$X_{PEND,R}$	=	$X_{US,R}\cos\phi - Z_{US,R}\sin\phi$	Eq. A10
$\bar{X}_{PEND}$	=	$\frac{X_{PEND,L} + X_{PEND,R}}{2}$	Eq. A11
$\bar{X}_{PEND,REL}$	=	$\bar{X}_{PEND} - \bar{X}_{PEND}(0)$	Eq. A12

where:

ϕ_{US}	=	Angle of the upper thoracic spine in the lab coordinate system
ϕ_{PEND}	=	Angle of the pendulum in the lab coordinate system (0˚)
ϕ_{LTS}	=	Y-axis angle measured by the lower thoracic spine tilt sensor
ϕ	=	Angle of transformation from US to PEND
$[X,Z]_{US,[L,R]}$	=	Left- and right-side upper spine X- and Z-axis position
$X_{PEND,[L,R]}$	=	Left- and right-side X-axis deflection in pendulum coordinate system
$\bar{X}_{PEND}$	=	Average of left- and right-side X-axis deflection in pendulum coordinate system
$\bar{X}_{PEND,REL}$	=	Relative X-axis deflection in pendulum coordinate system
$\bar{X}_{PEND}(0)$	=	Average of left- and right-side X-axis deflection in pendulum coordinate system at the time of initial impactor contact with the chest

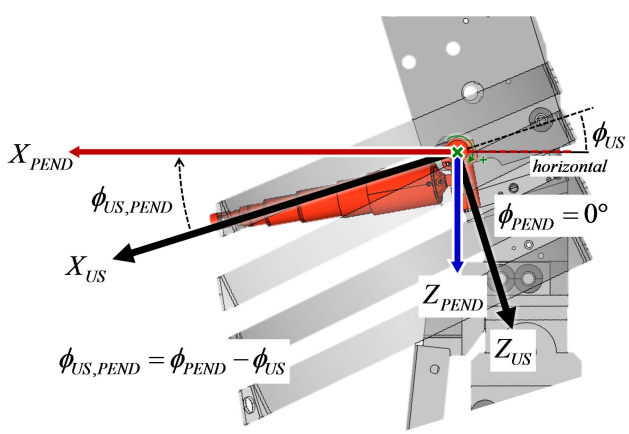

Figure A2. Schematic of the upper spine coordinate system relative to the pendulum coordinate system

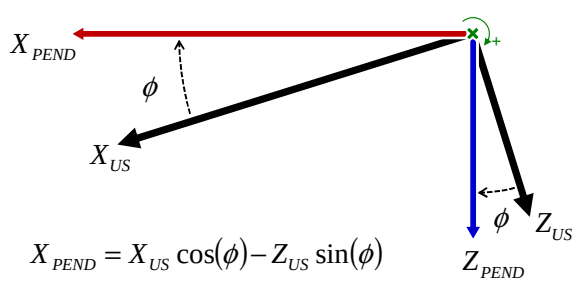

Figure A3. Representation of upper spine coordinate system components relative to the X-axis of the pendulum coordinate system

APPENDIX B. LOBDELL MODEL PARAMETERS

Lobdell model parameters for the conditions presented in this study.

Model Identifier	**Variable** / **Units**	m_2 kg	m_3 kg	k_{12} N/m	k_{23a} N/m	k_{23b} N/m	c_{23a} Ns	c_{23b} Ns	k_{23s} m
Kroell Mean Response		0.85	32.66	180000	8400	61600	520	2490	0.0231
Lebarbé Mean Response		0.35	28.20	270000	29300	100100	350	510	0.0640
Hybrid III		0.53	48.32	220000	87100	81900	500	610	0.0202
THOR-NT		0.74	36.04	330000	39000	76100	660	490	0.0220
THOR Mod Kit		0.99	36.52	250000	39100	129700	460	300	0.0408
THOR Mod Kit w/SD-3		0.64	33.79	260000	34400	59400	420	410	0.0160
THOR Metric		1.04	40.73	180000	16900	105900	460	190	0.0434
THOR Metric w/SD-3		0.84	26.24	140000	44300	33100	400	540	0.0325

APPENDIX C. BIO RANK RESULTS

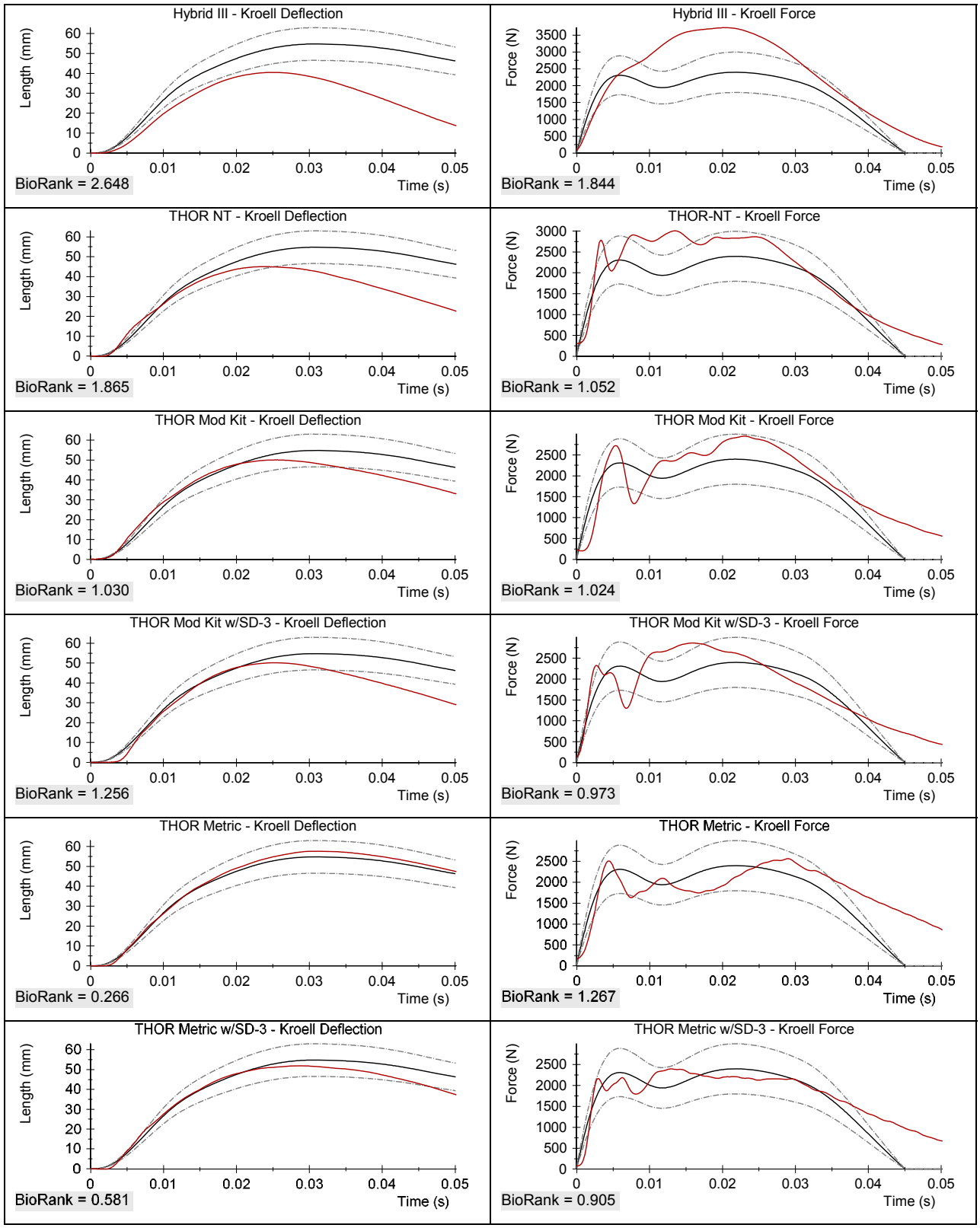

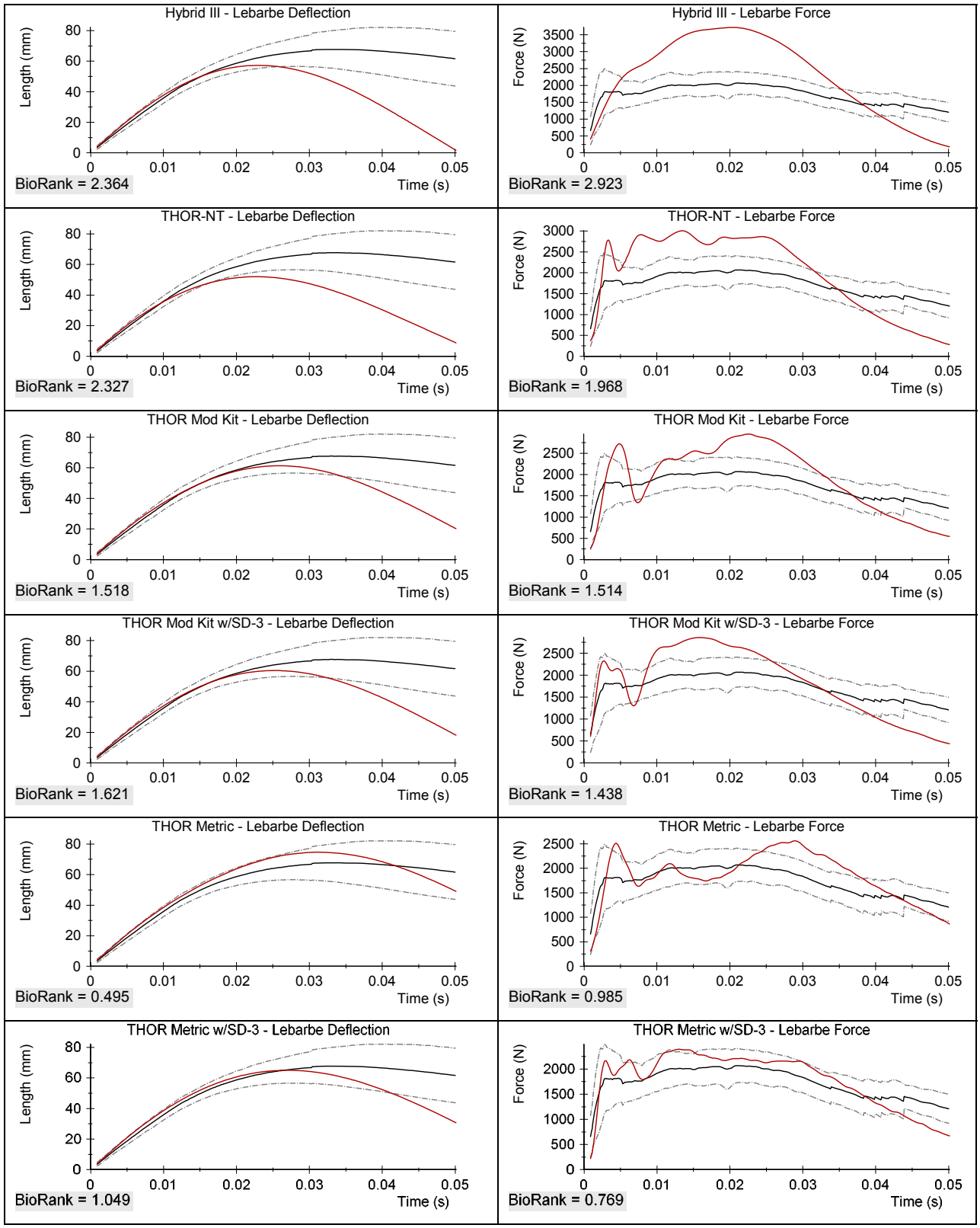
Hybrid III - Lebarbe Deflection
Length (mm)
Time (s)
BioRank = 2.364
Hybrid III - Lebarbe Force
Force (N)
Time (s)
BioRank = 2.923
THOR-NT - Lebarbe Deflection
Length (mm)
Time (s)
BioRank = 2.327
THOR-NT - Lebarbe Force
Force (N)
Time (s)
BioRank = 1.968
THOR Mod Kit - Lebarbe Deflection
Length (mm)
Time (s)
BioRank = 1.518
THOR Mod Kit - Lebarbe Force
Force (N)
Time (s)
BioRank = 1.514
THOR Mod Kit w/SD-3 - Lebarbe Deflection
Length (mm)
Time (s)
BioRank = 1.621
THOR Mod Kit w/SD-3 - Lebarbe Force
Force (N)
Time (s)
BioRank = 1.438
THOR Metric - Lebarbe Deflection
Length (mm)
Time (s)
BioRank = 0.495
THOR Metric - Lebarbe Force
Force (N)
Time (s)
BioRank = 0.985
THOR Metric w/SD-3 - Lebarbe Deflection
Length (mm)
Time (s)
BioRank = 1.049
THOR Metric w/SD-3 - Lebarbe Force
Force (N)
Time (s)
BioRank = 0.769

SENSITIVITY TO DIFFERENT SEATING POSITIONS OF THOR-NT AND HYBRID III IN SLED TESTING

Masayuki, Yaguchi
Koshiro, Ono
Japan Automobile Research Institute
Japan
Mitsutoshi, Masuda
Tatsuya, Fukushima
Japan Automobile Manufactures Association, Inc.
Japan
Paper Number 13-0333

ABSTRACT

In this study, the sensitivity to different seating positions of the THOR-NT and the Hybrid III in sled testing were evaluated. In the tests, the THOR-NT or the Hybrid III was installed on the driver seat of a vehicle body fixed on the sled, and a frontal impact of 15.6 m/s (56 km/h) was given to the sled. Dummy installation was subject to FMVSS 208 and UMTRI seating procedures. Furthermore, based on the FMVSS 208 procedure, the seat slide was adjusted forward 30 mm (MP-30).

In testing of the three seating positions of the THOR-NT, different responses in the head acceleration was shown. The head accelerations in FMVSS 208 and UMTRI exhibited a sharp high wave of about 110 ms, but that in the MP-30 did not exhibit such a wave. Applying the dummy injury values to provisional injury assessment reference values (IARVs) for THOR used in the research of the NHTSA, kinematic rotational brain injury criterion (BRIC) of the MP-30 was lower than FMVSS 208 and UMTRI. For the acetabulum force, it was large, in the order of the UMTRI, FMVSS 208, and MP-30. For inversion/eversion of the right ankle of the accelerator pedal side, it showed large angles, in the order of the FMVSS 208, MP-30, and UMTRI. Other injury values of the ankles showed large angles, in the order of the UMTRI, FMVSS 208, and MP-30.

The difference in the responses to the different seating positions was mainly observed in the head acceleration and lower extremity force responses for both the THOR-NT and the Hybrid III. However, comparing responses of the THOR-NT and the Hybrid III with the same conditions, the upper body of the THOR-NT moved forward more, compared to the Hybrid III, and the torsion about the z-axis was also larger than the Hybrid III. As a result, the head acceleration of the THOR-NT and the Hybrid III exhibited different responses.

INTRODUCTION

Currently, though the Hybrid III frontal crash test dummy is used worldwide, there is a neeed for a more advanced dummy with more biofidelity and higher measurement performance to more sensitively evaluate the advanced restraint devices, so as to further improve safety performance. Under these circumstances, in 2001 an advanced frontal crash test dummy THOR (Test Device for Human Occupant Restraint) - alpha version was developed in the United States [1]. In 2005, the THOR-NT version which exhibited improvement in durability and usability from the THOR-alpha was released [2]. In order to further improve the biofidelity and measurement performance of the THOR-NT, development of a new version THOR (THOR Mod Kit), under collaboration of NHTSA, EU THORAX, and other organizations came in progress [3]. In this study, it evaluates the sensitivity to different seating positions of the THOR-NT and the Hybrid III in sled testing. The objective is to obtain base data which is a comparative target for evaluating the THOR Mod Kit in the near future.

SLED TESTING

Test Condition

The THOR-NT or the Hybrid III was installed on the driver seat of a vehicle body fixed on the sled, and a frontal impact of 56 km/h was given to the sled. The vehicle body used in the sled tests was a four-door sedan passenger car (Figure 1). For the restraint system, the air bag, and a seatbelt with force limiter and a double pretensioner at the retractor and outer lap belt anchorage were used in this series of tests. Figure 2 shows the acceleration and the velocity curves of the sled.

Figure 1. Vehicle body of four-door sedan passenger car

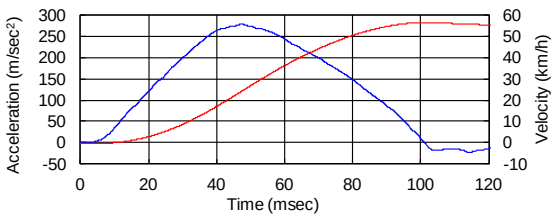

Figure 2. Sled pulse (acceleration and velocity)

Measurements

For the electrical measurements, the accelerations, deflections and forces of the dummies and the acceleration of the sled were recorded by a data acquisition system, and they were filtered in compliance to SAE J211 [4]. The detailed information of the instrumentation of the THOR-NT and Hybrid III is shown in the Appendix (Table A1). For the photogrammetry, two high-speed video cameras were used to take the kinematics of the dummy during the impact. Kinematics of the dummies were observed as follows: The motions of the markers attached to some parts on the dummy were recorded by the video camera, then these were converted into the displacements using a video analyzer.

Dummy Positioning

Dummy installation was subject to the following three seating procedures:

(1) FMVSS 208; specified for Hybrid III [5],
(2) UMTRI (University of Michigan Transportation Research Institute); the seat position depends on the driver occupant size, dimensions of steering wheel and accelerator pedal, and seat adjustment range [6],
(3) MP-30; based on FMVSS 208 procedure, the seat slide was adjusted forward 30 mm.

For FMVSS 208, the seat slide is in the mid position, and the seat lifter is in the lowest position. For UMTRI, the seat slide is rearward 49 mm relative to FMVSS 208, and the seat lifter is upward 14 mm. For MP-30, it is as described above.

Figures 3 and 4 show the comparison of the positioning in the X-Z coordinate system for the THOR-NT and the Hybrid III in each seating position according to three seating procedures. The x-axis is posterior and anterior direction, and the z-axis is superior and inferior direction. Figures 5 and 6 show the posture and the clearance between the instrument-panel and each body region, for the THOR-NT and the Hybrid III in each seating position. For both the dummies, depending on the difference in the seat position, dummy positioning differed in three conditions.

Kinematic Responses

Figures 7 and 8 illustrate the trajectories of the markers on each body region for the THOR-NT and the Hybrid III in three seating positions. Time of trajectories shown in these figures is when the dummies' head has reached to the maximum displacement with the x-direction. Table 1 shows the maximum displacement of each body region. For both the dummies, the trajectory in three seating positions was mostly similar. However, in reviewing the details, the forward movement of the upper body was larger as the dummy position was more in the rear position (UMTRI > 208 > MP-30) (see comparison of the values in the red-bordered boxes in Table 1). For the ankle, the

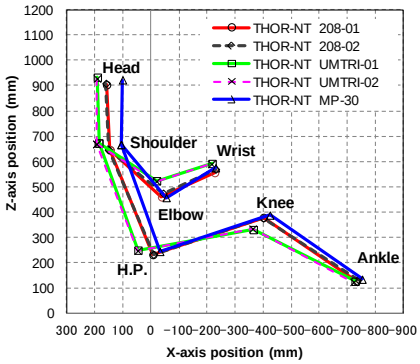

Figure 3. Comparison of the positioning in the X-Z coordinate system for the THOR-NT

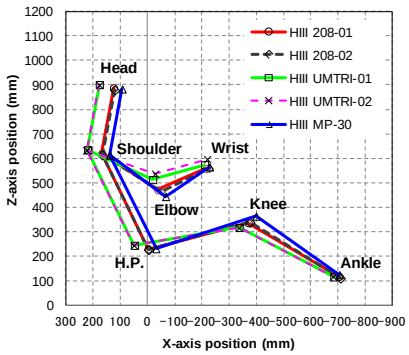

Figure 4. Comparison of the positioning in the X-Z coordinate system for the Hybrid III

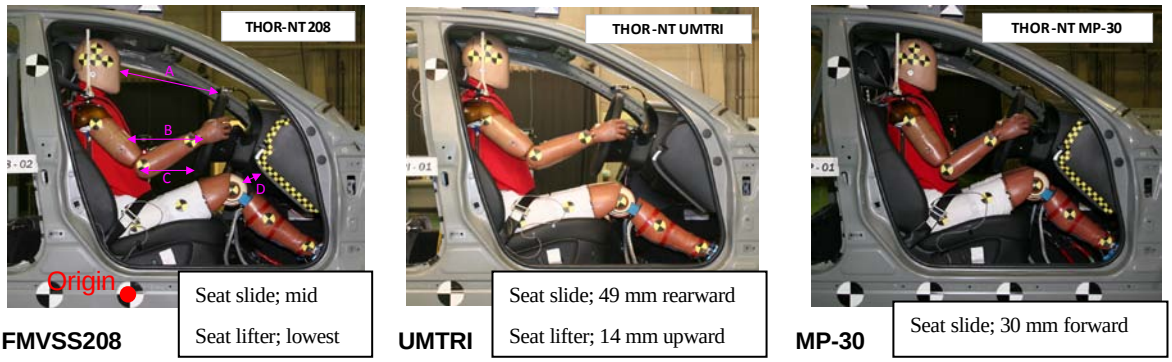

	Measurements	THOR-NT 208-01	THOR-NT 208-02	THOR-NT UMTRI-01	THOR-NT UMTRI-02	THOR-NT MP-30
A	Face to Steering Wheel Rim (Top) (mm)	442	442	471	469	380
B	Chest to Steering Wheel (Center) (mm)	337	338	365	361	278
C	Abdomen to Steering Wheel Rim (Bottom) (mm)	213	215	254	260	187
D	Knee to Dash Panel (mm)	60	63	122	123	40

Figure 5. Posture in each seating position and clearance between instrument panel and each body region for the THOR-NT

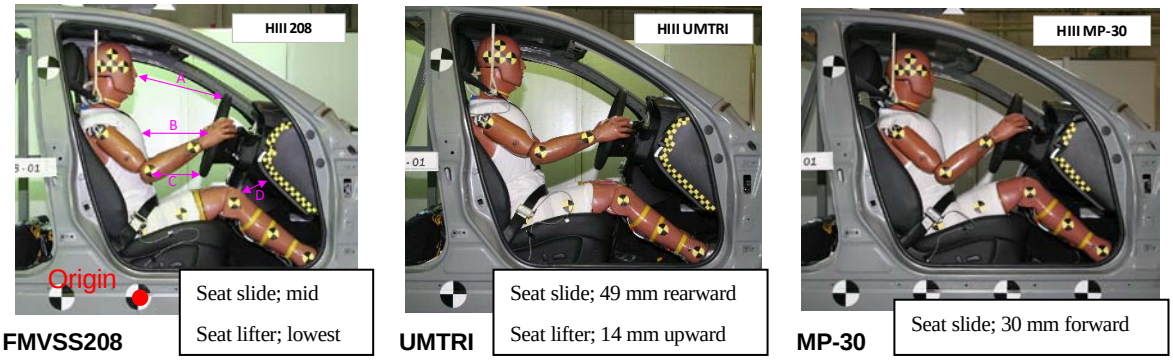

	Measurements	HIII 208-01	HIII 208-02	HIII UMTRI-01	HIII UMTRI-02	HIII MP-30
A	Face to Steering Wheel Rim (Top) (mm)	382	378	425	428	350
B	Chest to Steering Wheel (Center) (mm)	293	293	333	337	266
C	Abdomen to Steering Wheel Rim (Bottom) (mm)	217	212	264	268	185
D	Knee to Dash Panel (mm)	104	102	150	153	73

Figure 6. Posture in each seating position and clearance between instrument panel and each body region for the Hybrid III

difference in upward movement was remarkable (see comparison of the values in the blue-bordered boxes in Table 1). Figure 9 shows the comparisons of the trajectories of each body region for the THOR-NT and the Hybrid III in FMVSS 208 seating position. The upper body of the THOR-NT moved forward more, compared to the Hybrid III. Figure 10 shows forward displacement versus time curves for the right and left shoulders of the dummies based on the video analysis. With the THOR-NT, the left shoulder was still moving forward even when the right shoulder has rebounded. For the Hybrid III, the left shoulder also started moving rearward when the right shoulder has rebounded. These results showed that the torsion about the z-axis of the upper body of the THOR-NT was larger than that of the Hybrid III.

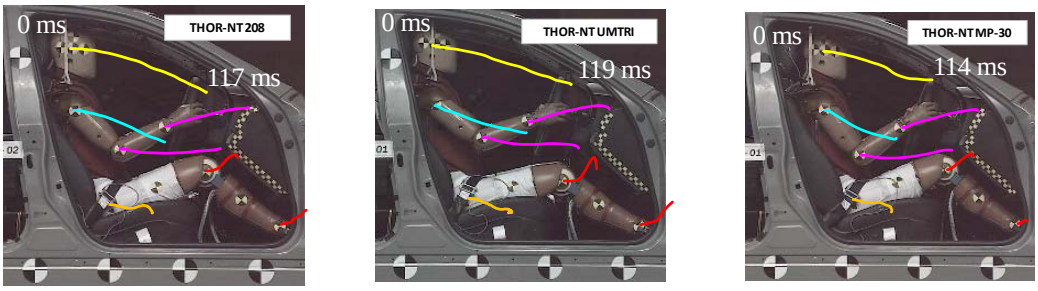

Figure 7. Trajectories of each body region of THOR-NT in three seating positions

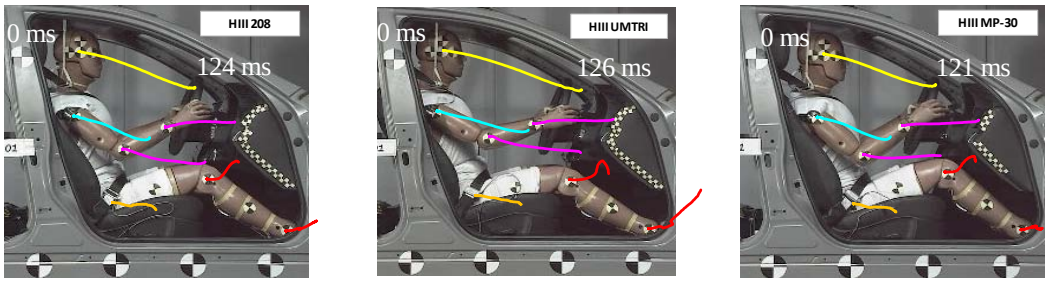

Figure 8. Trajectories of each body region of Hybrid III in three seating positions

Table 1. Maximum displacement of each body region

	THOR-NT						Hybrid III					
	THOR-NT 208		THOR-NT UMTRI		THOR-NT MP-30		HIII 208		HIII UMTRI		HIII MP-30	
	X	Z	X	Z	X	Z	X	Z	X	Z	X	Z
Head	568	−188	594	−171	467	−131	487	−160	592	−180	467	−141
Shoulder	376	−134	392	−120	310	−131	322	−107	390	−90	306	−95
Elbow	417	−20	413	−47	393	23	347	−64	391	−75	346	−19
Wrist	345	82	344	72	332	83	291	25	339	26	318	26
H.P.	177	−36	183	−65	166	−53	179	−33	192	−41	179	−37
Knee	125	73	141	102	112	70	135	77	168	86	128	72
Ankle	103	62	133	103	38	20	128	43	226	175	88	15

+ Direction Forward Upward mm

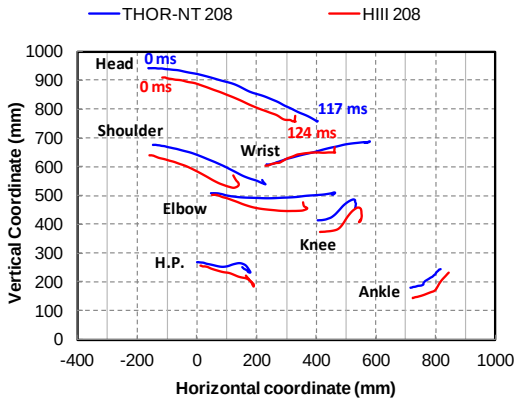

Figure 9. Trajectories of each body region of THOR-NT and Hybrid III in FMVSS 208 seating position

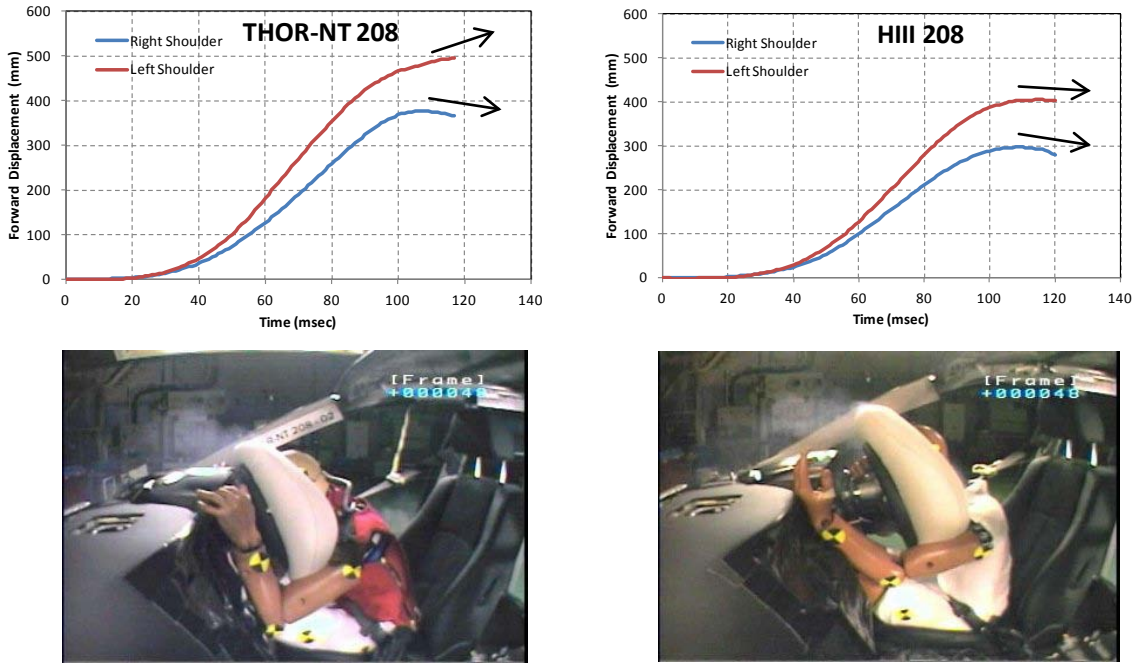

Figure 10. Forward displacement versus time curves for the right and left shoulders of THOR-NT and Hybrid III

Dynamic Responses

<u>Responses of THOR-NT</u>

Figures 11 to 16 show the comparison of dummy responses of the different seating positions for each body region. The head accelerations in FMVSS 208 and UMTRI exhibited sharp high wave of about 110 ms, but that in the MP-30 did not exhibit such wave (Figure 11). The response of chest deflection was similar in three seating positions (Figure 12). Acetabulum force between FMVSS 208 and MP-30 was similar, but the time of the maximum in UMTRI was later and the maximum value was larger than the others (Figure 13). For femur axial force, UMTRI exhibited stronger force than others in both compression and tension (Figure 14). Tibia axial force exhibited different responses between the three seating positions. The initial response of UMTRI was later than others but the force increase was the sharpest and the value was the largest. The initial response of MP-30 was earlier than others, exhibiting a flat curve between 40 ms and 80 ms, and the value was the lowest (Figure 15). For inversion/eversion of the right ankle of the accelerator pedal side, it showed large angles, in order of FMVSS 208, MP-30, and UMTRI (Figure 16).

Responses of Hybrid III

Figures 17 to 20 show the comparison of responses of the different seating positions for each body region.The head acceleration in UMTRI exhibited sharp high wave of about 110 ms, but the others did not exhibit such wave (Figure 17). The response of chest deflection was similar in the three seating positions (Figure 18). With the femur axial force, slight compression force was generated between 40 ms and 60 ms in all three seating positions, and the time of the maximum of UMTRI was later than the others (Figure 19). The tibia axial forces of FMVSS 208 and MP-30 exhibited one sharp wave while that of UMTRI exhibited two peaks (Figure 20).

Responses of THOR-NT versus Hybrid III

Figures 21 to 24 show the comparison of the responses of each body region for the THOR-NT and the Hybrid III in FMVSS 208 seating position. The head acceleration of the THOR-NT exhibited sharp wave of about 110 ms, but that of the Hybrid III did not exhibit such wave (Figure 21). The chest deflection in the left side (upper and lower) of the THOR-NT was similar to the Hybrid III (on the chest center) (Figure 22). The axial force to the femur of the THOR-NT was not significantly strong. For Hybrid III, tension force was larger than compression force (Figure 23). The tibia axial force of the Hybrid III exhibited sharp wave and value was larger than that of the THOR-NT (Figure 24).

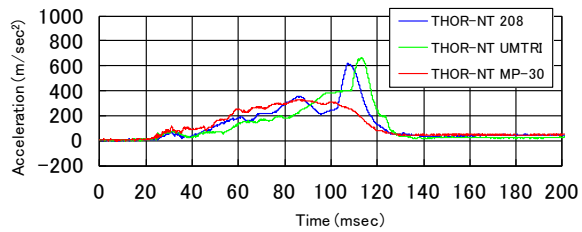

Figure 11. Head resultant acceleration of THOR-NT

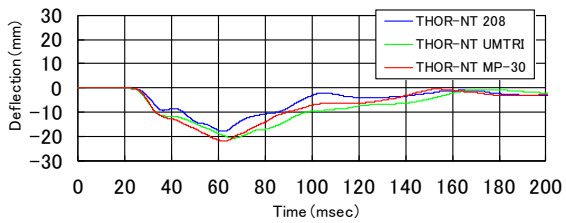

Figure 12. Chest deflection (upper right) of THOR-NT

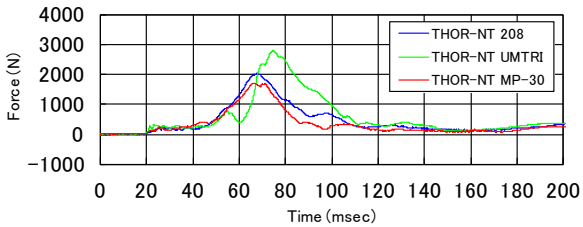

Figure 13. Right acetabular resultant force of THOR-NT

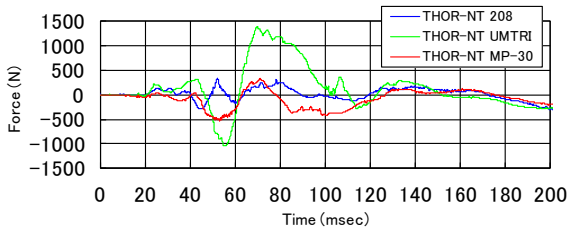

Figure 14. Right femur axial force of THOR-NT

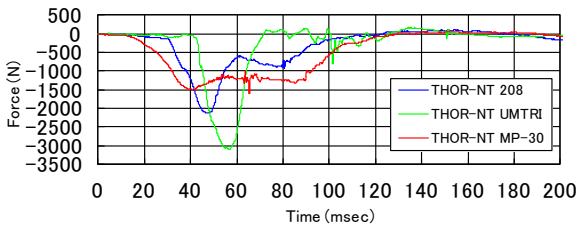

Figure 15. Right tibia axial force (lower) of THOR-NT

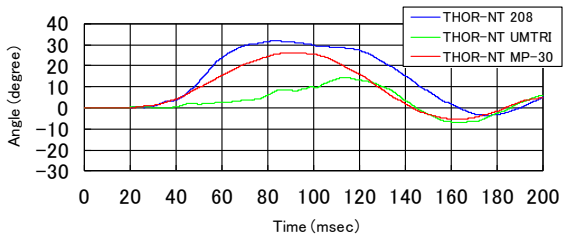

Figure 16. Right ankle rotation (inversion/eversion) of THOR-NT

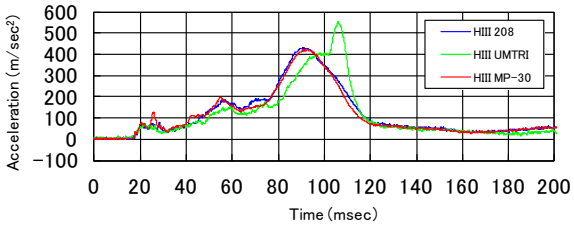

Figure 17. Head resultant acceleration of Hybrid III

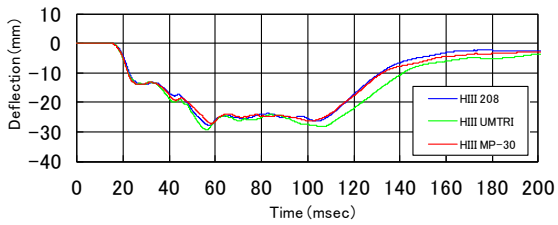

Figure 18. Chest deflection of Hybrid III

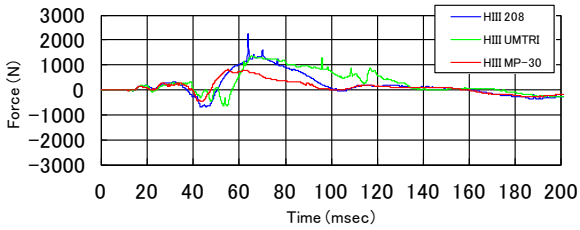

Figure 19. Right femur axial force of Hybrid III

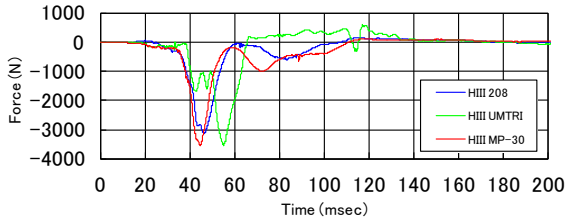

Figure 20. Right tibia axial force (lower) of Hybrid III

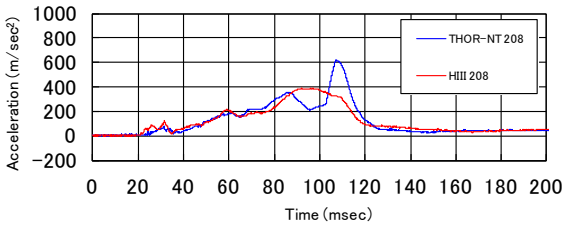

Figure 21. Head resultant acceleration of THOR-NT and Hybrid III

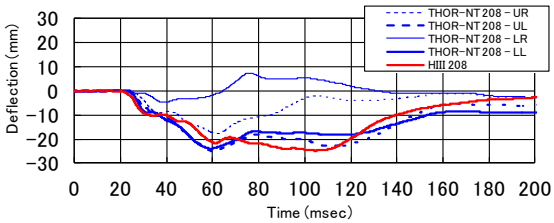

Figure 22. Chest deflection of THOR-NT and Hybrid III

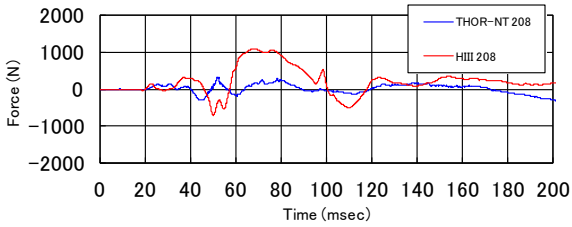

Figure 23. Right femur axial force of THOR-NT and Hybrid III

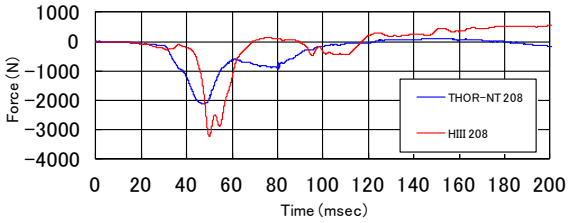

Figure 24. Right tibia axial force (lower) of THOR-NT and Hybrid III

<u>Dummy Injury Values</u>

Table 2 shows the injury values of THOR-NT in three seating positions. It also shows provisional injury assessment reference values (IARVs) for THOR used in the research of the NHTSA [7].

Applying the dummy injury values to IARVs for THOR, kinematic rotational brain injury criterion (BRIC) of MP-30 was lower than FMVSS 208 and UMTRI. For the acetabulum force, it was large, in the order of the UMTRI, FMVSS 208, and MP-30. For inversion/eversion of the right ankle of the accelerator pedal side, it showed large angles, in the order of the FMVSS 208, MP-30, and UMTRI. Other injury values of the ankles showed large angles, in the order of the UMTRI, FMVSS 208, and MP-30.

Table 2. Injury values of THOR-NT in three seating positions

		IARV	THOR-NT 208-01	THOR-NT 208-02	THOR UMTRI-01	THOR UMTRI-02	THOR-NT MP-30
Head	BRIC	1	0.55	0.52	0.55	0.49	0.44
	HIC 15ms	700	317.2	200.3	270.7	147.5	87.1
	3ms clip G	80	68.9	59.6	64.0	42.2	32.8
Upper Neck	Tension Force (N)	2520	867.4	892.3	864.4	874.7	1154.9
	Compression Force (N)	3600	281.4	274.2	173.7	219.5	260.0
	Flexion at OC (Nm)	48	5.0	6.5	9.5	14.4	1.9
	Extension at OC (Nm)	72	7.5	7.3	6.8	6.1	8.4
Chest	Deflection(Upper Right) (mm)	N/A	15.7	17.7	20.7	18.9	21.9
	Deflection(Upper Left) (mm)		25.6	24.8	21.0	18.8	24.8
	Deflection(Lower Right) (mm)		-8.4	-7.5	6.8	7.4	5.9
	Deflection(Lower Left) (mm)		25.6	23.9	25.4	22.7	25.5
	3ms clip G	60	34.2	32.7	28.6	29.1	31.0
Abdomen	Deflection (mm)	111	39.3	29.1	17.4	17.3	29.9
Acetabulum	Right Resultant Force (N)	3500	3118.8	2024.1	2789.5	2693.0	1712.9
	Left Resultant Force (N)		1731.5	1640.3	2173.6	2184.9	1567.6
Femur	Right Femur Force (N)	10000	330.9	294.9	1047.3	1045.5	524.3
	Left Femur Force (N)		1163.1	378.5	313.4	328.9	720.8
Tibia	Right Upper Tibia Index	1.16	0.41	0.38	0.32	0.34	0.39
	Left Upper Tibia Index		0.45	0.55	0.48	0.54	0.47
	Right Lower Tibia Index		0.33	0.34	0.34	0.35	0.31
	Left Lower Tibia Index		0.33	0.44	0.40	0.44	0.39
Ankle	Right Inversion/Eversion	35/35	33.9	32.0	14.4	8.4	26.1
	Right Dorsiflexion/Plantarflexion		21.8	23.0	23.4	27.3	14.5
	Left Inversion/Eversion		31.9	28.4	34.3	34.0	27.5
	Left Dorsiflexion/Plantarflexion		25.2	29.3	29.5	31.6	23.1

DISCUSSION

Difference in Dynamic Responses of THOR-NT

With regard to some differences of injury values among the three seating positions, the cause of the difference is considered.

Head Acceleration Response

As shown in Figure 11, the head accelerations in FMVSS 208 and UMTRI exhibited sharp high wave of about 110 ms, but that of the MP-30 did not exhibit such wave. With the high speed video analysis, the incline of the dummy upper body during impact in MP-30 was smaller than in FMVSS 208 (Figure 25). Thus, it was presumed that the contact force between head and airbag in MP-30 became lower than others, and the head acceleration was lower. As a result, it was presumed that BRIC in MP-30 was also lower than others (Table 2).

KTH and Lower Extremity Responses

As shown in Figures 13 to 15, the acetabulum, femur and tibia forces in UMTRI seating position differed from others. The cause of the difference is considered the following: The initial gap between the floor and lower extremity was wider as the H-point of the dummy was more in the rear position, and the peak values increased. In addition, the load path to the knee-thigh-hip and lower extremity differed with the difference in the angle of the knee during the load against the tibia from the accelerator pedal (Figure 26).

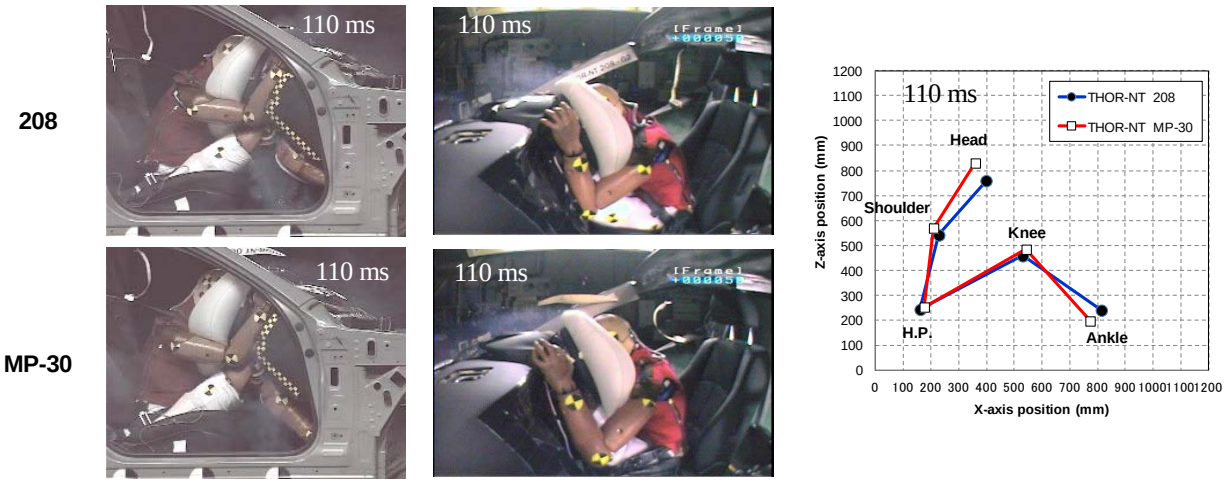

Figure 25. Behavior of upper body of THOR-NT

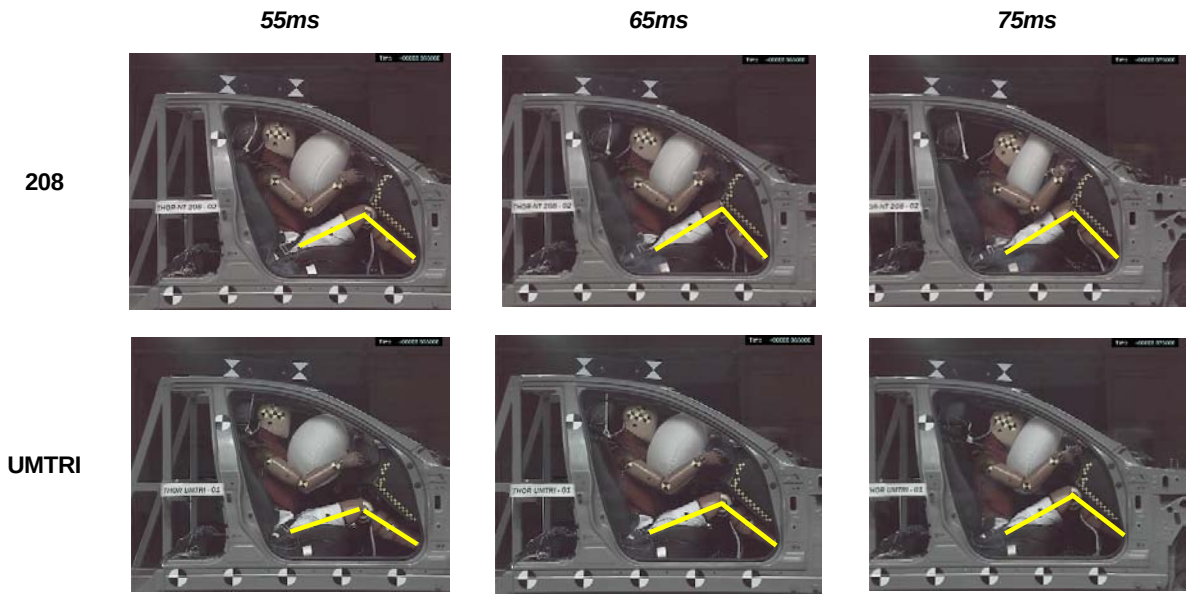

Figure 26. Behavior of KTH and lower extremity of THOR-NT

CONCLUSION

The difference in the responses to the different seating positions was mainly observed in the head acceleration and lower extremity force responses for both the THOR-NT and the Hybrid III. However, comparing responses of the THOR-NT and the Hybrid III with the same conditions, the upper body of the THOR-NT moved forward more, compared to the Hybrid III, and the torsion about the z-axis was also larger than the Hybrid III. As a result, the head acceleration of the THOR-NT and the Hybrid III exhibited different responses.

Development of the THOR seating procedure is in progress under SAE THOR Task Force, etc. Considering such differences in dummy responses as observation in this study, it is necessary that the THOR seating procedure is determined.

REFERENCES

[1] Haffner M., Eppinger R., Rangarajan N., Shams T., Artis M., Beach D. "Foundations and Elements of the NHTSA THOR Alpha ATD Design," Proceedings of the 17th International Technical Conference on the Enhanced Safety of Vehicles, 2001

[2] Shams T., Rangarajan N., McDonald J., Wang Y., Platten G., Spade C., Pope P., Haffner M. "Development of THOR-NT: Enhancement of THOR Alpha-the NHTSA Advanced Frontal Dummy," Proceedings of the 19th International Technical Conference on the Enhanced Safety of Vehicles, 2005

[3] Ridella S.A., Parent D.P. "Modifications to Improve the Durability, Usability and Biofidelity of the THOR-NT Dummy," Proceedings of the 22nd International Technical Conference on the Enhanced Safety of Vehicles, 2011

[4] SAE "(R) Instrumentation for Impact Test – Part 1 – Electronic Instrumentation," SAE J211-1 REV. JUL2007

[5] NHTSA "Code of Federal Regulations, 49 CFR Part 571 FMVSS No.208; Occupant Crash Protection," 2010

[6] IIHS "Guidelines for Using the UMTRI ATD Positioning Procedure for ATD and Seat Positioning (Version V)," 2004

[7] Saunders J., Craig M.J., Suway J. "NHTSA's Test Procedure Evaluations for Small Overlap/Oblique Crashes," Proceedings of the 22nd International Technical Conference on the Enhanced Safety of Vehicles, 2011

APPENDIX

Table A1. Comparison of the instrumentations of the THOR-NT and the Hybrid-III

	THOR-NT	Hybrid III(Typical Configuration)
Head	9 Uniaxial Accelerometers	**Yes** (1 Triaxial Accelerometer at Head C.G.)
	1 Biaxial Tilt Sensor	No
Face	Five Uniaxial Load Cells	No
Neck	Upper Neck Load Cell (6 channels)	**Yes**
	Lower Neck Load Cell (6 channels)	**Yes**
	Front Neck Cable Load Cell	No
	Rear Neck Cable Load Cell	No
	Head Rotation Potentiometer	No
Thorax	CRUX Deflection Units - 3 Dimensional Displacement at each of Four Locations (UL, UR, LL, LR)- 4 CRUX units @ 3 channels each;	**Yes** (One-directional Displacement String Potentiometer)
	1 Triaxial Accelerometer at the C.G.	**Yes**
Mid Sternum	1 Uniaxial Accelerometer	No
Upper Abdomen	Uni-directional Displacement String Potentiometer	No
	Uniaxial Accelerometer	No
Lower Abdomen	DGSP Deflection Units - 3 Dimensional Displacement at L & R Locations (2 DGSP units @ 3 channels each)	No
Spine	1 Triaxial Accelerometer at T1 location	No
	1 Triaxial Accelerometer at T12 location	No
	T12 Load Cell (5 channels)	**Yes**
	4 Biaxial Tilt Sensors	No
Pelvis	Acetabulum Load Cell (left and right, 3 channels each)	No
	Iliac Crest Load Cells (left and right, 1 channel each)	No
	1 Triaxial Accelerometer at Pelvis C.G.	**Yes**
Femur	Femur Load Cell (left and right, 6 channels each)	**Yes**
Knee	Knee Shear Displacement, L&R	**Yes**
Lower Extremity	Upper Tibia Load Cell (left and right, 4 channels each)	**Yes**
	Lower Tibia Load Cell (left and right, 5 channels each)	**Yes**
	Tibia Acceleration (left and right, 2channels each)	No
	Achilles Tendon Load Cell (left and right, 1 channels each)	No
	Ankle Joint Rotation Potentiometers (left and right, 3channels each)	No
	Foot Acceleration (left and right, 3 channels each)	No

PEDIATRIC HEAD AND NECK DYNAMICS IN FRONTAL IMPACT: ANALYSIS OF IMPORTANT MECHANICAL FACTORS AND PROPOSED NECK PERFORMANCE CORRIDORS FOR SIX AND TEN YEAR OLD ATDS

Alan T. Dibb
Hattie C. Cutcliffe
Jason F. Luck
Courtney A. Cox
Barry S. Myers
Cameron R. Bass
Roger W. Nightingale
Duke University, Department of Biomedical Engineering and Division of Orthopaedic Surgery
United States of America
Kristy B. Arbogast
Thomas Seacrist
Center for Injury Research and Prevention, Children's Hospital of Philadelphia
United States of America
Paper Number 13-0207

ABSTRACT

Traumatic injuries are the leading cause of death of children aged one to nineteen in the United States. These unintentional injuries are principally caused by motor vehicle collisions, with the head being the primary region injured. The neck, though not commonly injured, governs head kinematics and influences head impact location and velocity. Vehicle design improvements necessary to reduce or prevent these injuries are evaluated using anthropomorphic testing devices (ATDs). The head and neck properties of the current pediatric ATDs were established by scaling adult properties using the size differences between adults and children. Due to the paucity and limitations of pediatric head and neck biomechanical research, computational models are the only available methods that combine all existing biomechanical data to produce injury-relevant biofidelity specifications for pediatric ATDs. The purpose of this study is to provide the first frontal impact biofidelity corridors for neck flexion response of six and ten year olds using computational models incorporating pediatric cadaveric data. These corridors are compared with response of the Hybrid III (HIII) ATD necks and the Mertz flexion corridors.

Our six and ten year old head and neck multibody models used pediatric biomechanical properties obtained from pediatric cadaveric and radiological studies. The computations included the effect of passive and active musculature, and were validated with data including 3 g dynamic frontal impact responses using pediatric volunteer tests. Because ATD pendulum tests are used to calibrate HIII neck bending stiffness, we simulated these tests to compare the pediatric model and HIII ATD neck bending stiffness, and to compare the model flexion bending responses with the Mertz scaled neck flexion corridors. Additionally, pediatric response corridors for both pendulum calibration tests and high speed (15 g) frontal impacts were estimated through uncertainty analyses on primary model variables. For the frontal impacts, adult boundary conditions and muscle activations, validated against 15 g volunteer tests, were applied to the pediatric models. Response corridors for each loading scenario were calculated from the average ± standard deviation response over 650 simulations.

We found that the models were less stiff in dynamic anterioposterior bending than the pediatric ATDs, as the secant stiffness of the six and ten year old models was 53% and 67% less than that of the HIII ATDs. At higher rotation angles the ATDs exhibited nonlinear stiffening while the models demonstrated nonlinear softening. Consequently, the models did not remain within the Mertz scaled flexion bending corridors, especially for rotations above 60 degrees of flexion. The more compliant model necks suggest an increased potential for head impact via larger head excursions. In contrast with the Mertz corridors, no interactions between the head and chest were modeled in these simulations since the loading conditions used (pendulum calibration testing) do not include chin-on-chest contact. The pediatric anterioposterior bending corridors developed in this study are extensible to any frontal loading condition through calculation and sensitivity analysis. Our corridors are the first based on pediatric cadaveric data and provide the basis for future, more biofidelic designs of six and ten year old ATD necks.

INTRODUCTION

Traumatic injuries are the leading cause of death of children ages one to nineteen years in the United States (CDC 2007). The main source of these traumatic injuries is motor vehicle crashes (MVC), with the head being the primary body region injured (Durbin et al. 2001). The pediatric neck, although not commonly injured, governs head excursion and acceleration, thus influencing head impacts and injury during automobile collisions. Additionally, pediatric cervical spinal injuries are debilitating and often fatal. Of children sustaining these cervical injuries, the mortality rate was 27% and the overall incidence of neurological deficits was 66% (Platzer et al. 2007). While seating children in the rear seat of a vehicle in an age-specific restraint can decrease the likelihood of injury, additional pediatric MVC injuries can be prevented by design improvements to vehicle passenger compartments and restraint systems.

The principal tool used to evaluate these restraint systems and passenger compartment advances are anthropomorphic testing devices (ATD). While very useful, these child ATDs were developed with limited human pediatric biomechanical data. The head and neck dynamic response of the current pediatric ATDs are adult properties scaled using size differences between adults and children with limited incorporation of the material differences with age. The assessment of pediatric ATD biofidelity and injury criteria is limited by the paucity of pediatric head and neck biomechanical research. Common sources of this data include studies with human volunteers, cadavers, animal surrogates, and computer models. While valuable, each of these approaches has inherent limitations.

For instance, human volunteer studies are restricted to non-injurious loading scenarios. To date, only a single pediatric volunteer study at the Children's Hospital of Philadelphia (CHOP) has been published in which volunteers were subjected to frontal impact loading. During this study, adults and pediatric volunteers, aged six to fourteen years, were subjected to low-speed (<4 g) frontal impacts (Arbogast et al. 2009).

Moreover, cadaver studies are limited by the rare availability of pediatric cadavers, their lack of live-active musculature, and their inability to demonstrate minor injury, such as pain or loss of consciousness. Only a handful of pediatric cadaver studies of frontal impact tests have been conducted (Kallieris et al. 1976; Wismans et al. 1979; Dejeammes et al. 1984). Though the pediatric cadavers in these studies were less stiff than their respective ATDs, the authors conclude that determining ATD performance criteria and injury values from their results would be speculative.

Animal surrogate studies provide valuable insights into the biomechanical response of the cervical spine. However, they are limited by interspecies differences in functional anatomy and the absence of scaling relationships from animal to human responses.

In view of the above limitations, computational modeling of the pediatric head and neck may prove to be the best method to provide biofidelity requirements and injury assessment reference values for child ATDs. Experimentally validated models incorporating accurate pediatric properties can simulate numerous loading conditions to investigate injury potential. While numerous models of the adult 50th percentile male have been created, a limited number of pediatric models exist (de Lange et al. 2001; Liu and Yang 2002; Mizuno et al. 2005; Dupuis et al. 2006; Meyer et al. 2009).

Accuracy of the computational model results is limited by the parameters—geometric and mechanical—upon which the model is founded. Thus, validation is critical to assess model biofidelity. Validation is the correlation of model responses to experimentally obtained result corridors, either cadaver or volunteer. Computer models of the head and neck have principally relied upon frontal impact simulations for validation, such as adult volunteer frontal impact experiments performed at the Naval Biodynamics Laboratory (NBDL) (Ewing and Thomas 1972; Wismans et al. 1986; Thunnissen et al. 1995).

To ensure repeatable and biofidelic response, dummies are also certified against such experimental or computational/scaled corridors. For example, the head and neck of the Hybrid III family of ATDs is certified before use in a frontal impact loading scenario (49 CFR 572, Subpart E). The ATD head and neck are attached to the end of a pendulum, which is raised and released. The pendulum arm is allowed to rotate under gravity until it impacts a block of aluminum (49 CFR 572, Subpart E). The pendulum deceleration results in head and neck flexion similar to a frontal impact. Computational models of the ATD head and neck have simulated this test for model validation (Doherty and Paver 1988; Yang and Le 1992; Marzougui et al. 1997; Medri et al. 2004). Similarly, models of the pediatric head and neck have used this test to validate against

scaled flexion corridors (de Lange et al. 2001; Mizuno et al. 2005; Dupuis et al. 2006).

The objective of this study was to use validated pediatric head and neck computer models that incorporate biomechanical properties from pediatric volunteer and cadaver studies to provide frontal impact biofidelity corridors for pediatric ATDS. Specifically, neck dynamic bending corridors were developed using a statistical uncertainty analysis for six and ten year olds based on the dynamic bending stiffness response of validated pediatric computational models for the pendulum certification test and for 15 g frontal impacts. These corridors were compared to that of the adult, the Hybrid III pediatric ATDs, and the Irwin and Mertz (1997) scaled neck flexion corridor.

METHODS

Model Development

The adult 50th percentile male computational head and neck model developed and used in the current study is a hybrid multibody and finite element model (Dibb 2011), as shown in Figure 1. Previous models (Camacho 1998; Van Ee 2000; Chancey 2005) provided the foundation for the current model (Dibb 2011). The osteoligamentous cervical spine was modeled with rigid body vertebrae connected by six degree of freedom non-linear viscoelastic beam intervertebral joints. A viscoelastic finite element head was implemented for head impact studies but was modeled as a rigid body for the purpose of this study. The material and inertial properties for the head, vertebrae, and muscles were developed from literature. Cervical musculature was modeled using Hill-type discrete beams. Muscle models were rate sensitive and included passive and active musculature (Hill 1938). Muscle wrapping was implemented to account for the interactions between individual muscles and vertebrae during bending (Dibb et al. 2013). Modeling and analysis were performed using LS-DYNA (LSTC, Livermore, CA). This adult model was validated in low-speed (<4 g) frontal impacts (Dibb et al. 2013), using data from CHOP (Arbogast et al. 2009), and in 15 g frontal impacts, using from NBDL (Ewing and Thomas 1972).

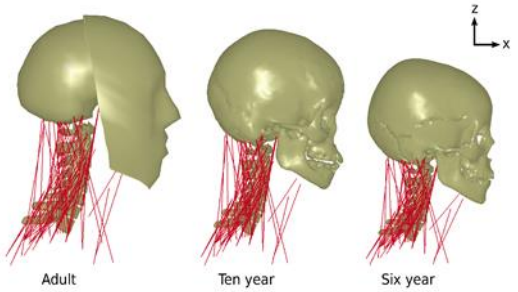

Figure 1. Lateral view of the adult and pediatric head and neck models.

The pediatric head and neck models of the current study (Figure 1) represent a 50th percentile six and ten year old and were created upon the same framework as the adult model, while incorporating pediatric biomechanical properties from pediatric volunteer and cadaver studies. The pediatric head models were developed using pediatric geometric and inertial properties reported by Loyd et al. (2010), while cervical vertebral geometric and inertial properties were developed from pediatric volunteer and cadaver radiology studies, respectively (Dibb 2011). Likewise, cervical muscle cross-sectional areas and attachment locations were developed from human pediatric and adult radiology studies (Dibb 2011). Intervertebral joint stiffnesses were derived from pediatric cadaver osteoligamentous cervical spine mechanical tests (Luck et al. 2008; Luck et al. 2012). These pediatric head and neck models were validated in frontal impacts (Dibb et al. 2013) using the only pediatric head and neck biofidelity validation currently available: the CHOP low-speed (<4 g) human volunteer tests (Arbogast et al. 2009).

Pendulum Certification Simulation

Simulations of the ATD neck pendulum calibration test with the adult and pediatric models were performed to compare the neck sagittal dynamic bending stiffness between the pediatric models and: the adult model, the pediatric Hybrid III ATD necks, and the Irwin and Mertz (1997) scaled neck flexion corridor. In these simulations, the pendulum was modeled as a rigid solid with physical and inertial dimensions as detailed in the Hybrid III 50th percentile male ATD test procedure (49 CFR 572, Subpart E). It was constrained to rotate about the y-axis only. The T1 vertebrae of the head and neck models were rigidly attached to the end of the pendulum such that the radial distance between the pivot and head CG was equivalent for the ATD and adult model. The pendulum with attached head and neck model was initiated in the vertical position, as specified in the certification test (49 CFR 572,

Subpart E), with the specified rotational velocity. Each model was ran with the appropriate pendulum impact velocity, according the model's age: 7.01 m/s as specified by the Hybrid III (HIII) 50th percentile male ATD (49 CFR 572, Subpart E) certification test procedure, 4.95 m/s as specified by the HIII six year old ATD (49 CFR 572, Subpart N) test procedure, or 6.10 m/s as specified by the HIII ten year old ATD (49 CFR 572, Subpart T) test procedure (Figure 2). Additionally, the adult and 10 year old models were ran at the HIII six year old certification velocity of 4.95 m/s for comparison between model responses. Decelerations were defined at the specified accelerometer attachment radius for both impact velocities.

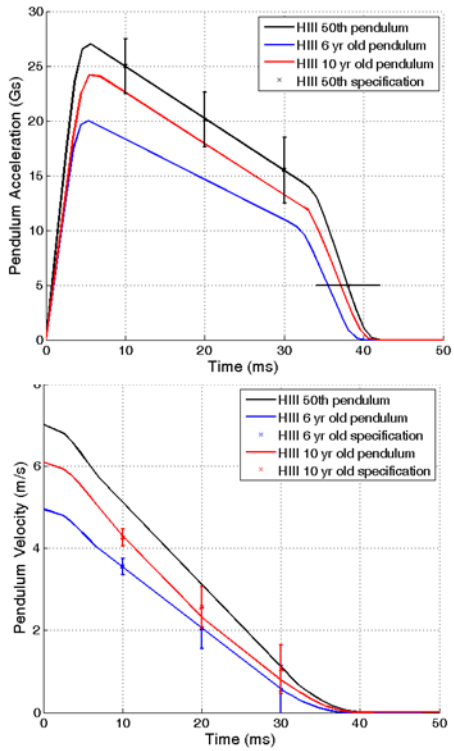

Figure 2. Applied pendulum deceleration and subsequent velocity time histories with the Hybrid III 50th percentile male, six year old ATD, and ten year old ATD certification specifications. The adult Hybrid III 50th percentile male standard specifies an acceleration corridor while the Hybrid III six and ten year old standards specify a velocity corridor. The corresponding pediatric acceleration and adult velocity profiles are plotted for comparison.

Biofidelity corridors for the pendulum certification tests were created from uncertainty analyses of the pediatric models with their corresponding pendulum velocity by varying the thirteen pediatric model input parameters ± one standard deviation (Table 1). These input values were scale factors developed from the ratio of the measured child to measured adult values for each parameter. For example, the adult model neck length, defined as the distance between the occipital condyle-C1 joint center of rotation and the C7-T1 joint center of rotation, was 14.08 cm. The ten and six year old model neck lengths were 12.35 and 9.80 cm, respectively. Input parameter values were selected using Latin hypercube sampling and 50 simulations were run per variable (Iman et al. 1981a; Iman et al. 1981b), for a total of 650 simulations. Correlation of stiffness to input variable was quantified through Pearson correlation with significance levels of $p < 0.05$. Model uncertainty corridors were created from the average ± one standard deviation over all simulations.

Muscle activations were initially set to a relaxed activation state (Dibb et al. 2013), since pediatric motor vehicle occupants are likely not aware of impending impacts. However, the dynamics result in muscle activations due to stretch mediated activation, so the extensor muscles as a group were activated to 100% at the pendulum impact, with no delay time. Muscle activation dynamics were modeled using Hill-type muscle models and two first-order systems (Hill 1938; Winters and Stark 1985; Winters and Stark 1988), and 100% was chosen to bracket the response. A delay time was not incorporated for the pendulum certification test. Similarly, chin-on-chest contact was not modeled in these simulations as this contact is not accounted for in the pendulum certification test, and thus peak head excursions in the simulation were unimpeded. Gravity was modeled in the inferior to superior direction to simulate an inverted posture, and simulations were run for 200 ms.

The model head rotation was measured relative to the pendulum longitudinal centerline. The model sagittal moment at the occipital condyle (OC) joint was calculated from the ligamentous joint and the sum of all the muscle moments about the O-C2 joint center of rotation (COR). Therefore, the OC moment reported in this study is the total neck moment (sum of the ligamentous loads and all muscle moments about the O-C2 joint COR), not the moment seen by the OC joint alone. Secant stiffness was calculated at peak OC moment, as the slope of the line between zero and peak on a plot of OC moment versus head rotation.

Table 1. Pediatric Head and Neck Uncertainty Analysis Parameters (average ± one standard deviation; each value given is a ratio of the pediatric to adult* value and thus is unitless)

Parameter	Age		
	Six Years	**Ten Years**	**Pediatric Value Reference**
Head mass	0.75 ± 0.02	0.80 ± 0.02	Loyd et al. 2010
Head inertia	0.58 ± 0.09	0.62 ± 0.10	Loyd et al. 2010
Head size x	0.92 ± 0.03	0.93 ± 0.03	Loyd et al. 2010
Head size y	0.92 ± 0.03	0.93 ± 0.03	Loyd et al. 2010
Head size z	0.74 ± 0.06	0.77 ± 0.06	Loyd et al. 2010
Vertebra mass	0.47 ± 0.07	0.62 ± 0.07	Dibb 2011
Vertebra inertia y	0.26 ± 0.05	0.44 ± 0.05	Dibb 2011
Vertebra size x	0.73 ± 0.08	0.80 ± 0.08	Dibb 2011
Vertebra size y	0.82 ± 0.06	0.85 ± 0.06	Dibb 2011
Vertebra size z	0.70 ± 0.09	0.88 ± 0.11	Dibb 2011
Intervertebral joint stiffness (Upper cervical spine)	0.44 ± 0.11	0.58 ± 0.09	Luck et al. 2008, Luck et al. 2012
Intervertebral joint stiffness (Lower cervical spine)	0.75 ± 0.12	0.88 ± 0.13	Luck et al. 2008, Luck et al. 2012
Muscle PCSA	0.47 ± 0.09	0.57 ± 0.12	Dibb 2011

*Adult values, previously cited during development of the Duke Adult Head and Neck Model, can be reviewed in Dibb 2011, Chancey 2005, Van Ee 2000, and Camacho 1998

NBDL 15 g Frontal Impact Simulation

The adult and pediatric head and neck models were subjected to 15 g frontal impact loading (Figure 3). To simulate this loading, the average T1 x-direction accelerations and y-direction rotational displacements from the NBDL volunteer tests (Ewing and Thomas 1972; Thunnissen et al. 1995) were applied to the T! vertebra of the models (Figure 3). The same adult volunteer NBDL T1 boundary conditions were applied to the pediatric models (Figure 3) as well as the same muscle activation dynamics (Figure 4) (Dibb 2011). Muscle activation dynamics were modeled using Hill-type muscle models and two first-order systems (Hill 1938; Winters and Stark 1985; Winters and Stark 1988). The simulations were initiated with relaxed muscle activation states that maintained an upright posture against gravity (Dibb 2011; e.g. Dibb et al. 2013). Extensor muscles were then activated to 100% (Figure 4), again chosen to bracket the response, after a reflex delay time. As muscle reflex delay times range in the literature from 10 to 120 ms (Colebatch et al. 1994; Foust et al. 1973; Reid et al. 1981; Schneider et al. 1975; Tennyson et al. 1977; Siegmund et al. 2003), a time of 50 ms was used in this simulation. Gravity was simulated as a constant body load in the superior to inferior direction.

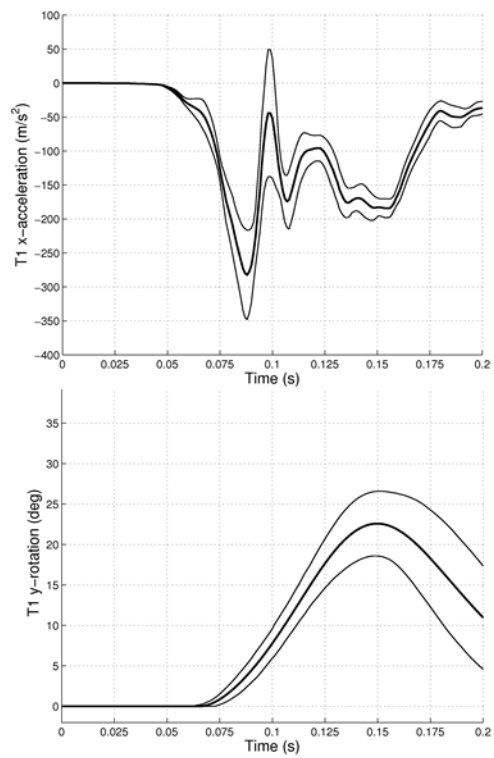

Figure 3. Imposed T1 horizontal acceleration and sagittal rotation time history from 15 g NBDL human male volunteer frontal impact tests, average ± one standard deviation (adapted from Thunnissen et al. 1995). The average histories were applied in all of our simulation.

Biofidelity response corridors were developed through uncertainty analyses of the adult and pediatric models, since pediatric volunteer high speed frontal impact experiments cannot be conducted due to the possibility of serious injury. The thirteen pediatric model input parameters were varied plus and minus one standard deviation (Table 1). Input parameter values were selected using Latin hypercube sampling and 50 simulations were run per variable (Iman et al. 1981a; Iman et al. 1981b), for a total of 650 simulations. The dependence of peak model responses and OC neck loads on input variables were quantified through Pearson correlation with significance levels of $p < 0.05$. Pediatric model response corridors were created from the average ± one standard deviation over all simulations.

Adult model kinematic and kinetic responses were validated against the NBDL volunteer response corridors (Dibb 2011) defined as the average response plus and minus the standard deviation (Thunnissen et al. 1995). Accelerations were defined relative to the global coordinate system while displacements were defined relative to a local coordinate system fixed to the midsagittal anterior-superior corner of the T1 vertebral body. Head accelerations and displacements were defined at the head CG. Neck rotations were defined as the rotation of a linkage that connected the T1 local coordinate origin to the OC center of rotation. Neck loads were calculated at the vertebral joints, including the OC, by summing the ligamentous and the muscular contribution about the vertebral joint COR. Neck loads were relative to the head anatomical coordinate system. The secant head and neck bending stiffness was calculated from the head rotation and OC joint neck moment.

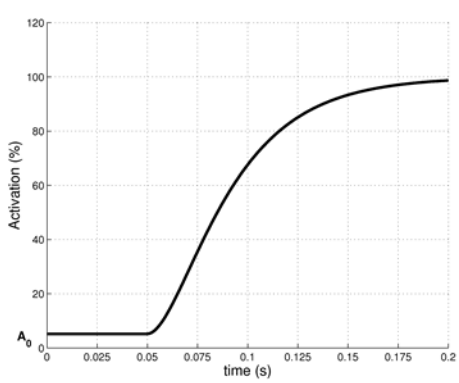

Figure 4. Activation dynamic time history of the extensors during 15 g frontal impact, modeled using Hill-type muscle models and two first-order systems. Initial activations, A_0, maintained an upright head posture against gravity. Activations were then increased to 100% after a reflex time (t = 50 ms).

RESULTS

Pendulum Certification Simulation

The response of the pediatric six and ten year old models during pendulum induced frontal impact with the HIII six year old certification velocity (49 CFR 527, Subpart N) was similar to the adult response at the same velocity (Figures 5 and 6). The adult 50th percentile male model first went into extension rotation, followed quickly by flexion rotation upon impact (Figure 6). Extension peaked at -4° head rotation. Peak head flexion of 111° occurred 97 ms after impact, while peak flexion moment of 51.2 Nm occurred earlier, at 85 ms after impact. The flexion moment reached 90% of its peak magnitude by 55 ms and increased the final 10% during the next 27 ms. OC moment decreased by 17% at the time of peak head rotation. The pediatric model heads also initially extended, reaching a peak of -3° head rotation. The head of the pediatric models then rotated into flexion with greater rotational displacements and lower OC flexion moments than the adult model, indicating that the pediatric necks were less stiff than the adult.

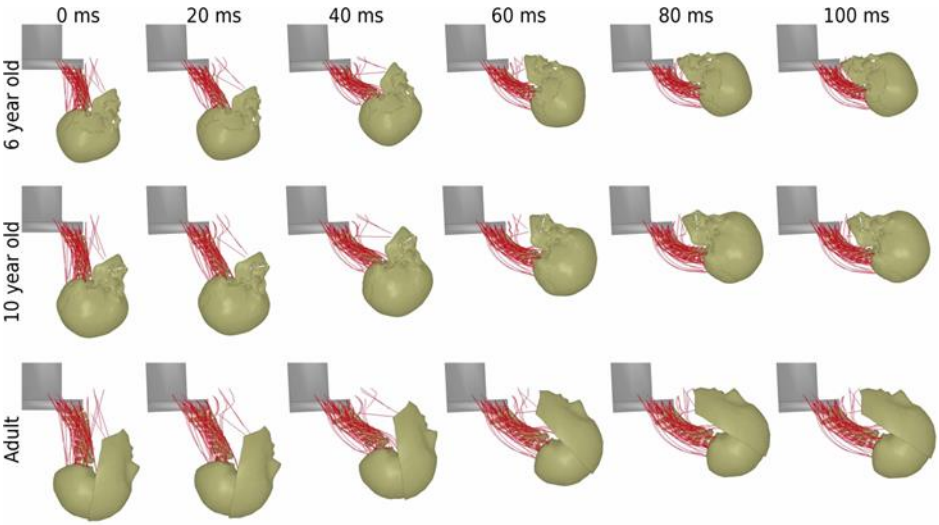

Figure 5. Adult and pediatric kinematic time-lapse during the six year old pendulum certification test. The pediatric models had larger peak head rotations than the adult.

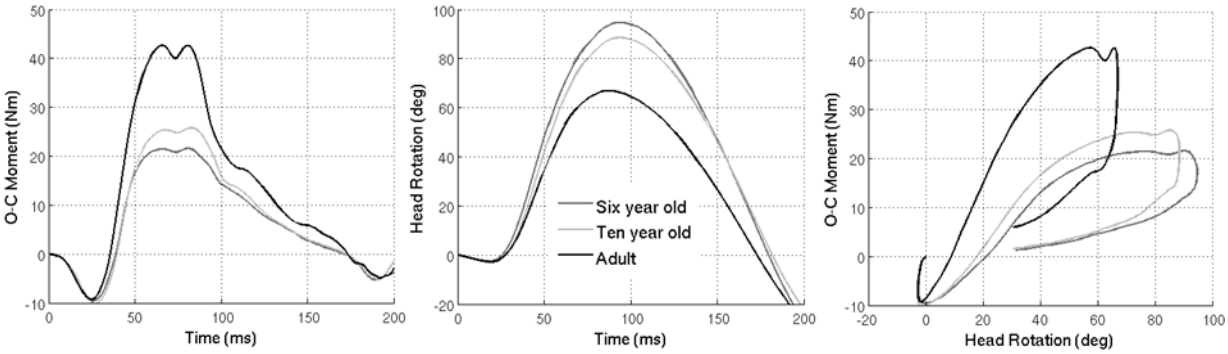

Figure 6. Pediatric and adult model head rotation and OC moment during the six year old pendulum certification test. The pediatric models are more compliant than the adult, as indicated by the slope of the loading curve. Both the pediatric and adult models rotated first into extension before rotating into flexion.

Pediatric model uncertainty analysis corridors are presented in Figure 7. The six year old average peak OC moment was 22 ± 1.7 Nm at 85 ± 10 degrees of head flexion. The ten year old average peak OC moment was 28 ± 2.1 Nm at 110 ± 14.6 degrees of head flexion. The average secant stiffness during the uncertainty analysis was 0.27 ± 0.05 Nm/deg for both the six and ten year old models, respectively. Pediatric model bending stiffnesses were most sensitive to muscle physiological cross-sectional area (PCSA). Increasing the muscle PCSA significantly increased the bending stiffness, as this increased the force-generating capacity of the muscles. Bending stiffness correlation coefficients to pediatric model parameters are presented in Table 2. The next most significant parameters were vertebral and head geometry scale factors in the x and z directions, which altered muscle attachment locations and thus their effective moment arms. Increasing these factors also increased the bending stiffness of the models. Increasing the osteoligamentous bending stiffness increased the neck bending stiffness too; however, the muscle parameters and geometric scale factors mentioned previously had greater effects.

The pediatric models with muscle tension were less stiff than the Hybrid III six year old (NHTSA 1998; Saul et al. 1998) and ten year old ATD (Mertz et al. 2001), as shown in Figure 8. The secant stiffness of the six year old model was 0.24 Nm/deg and of the ten year old was 0.25 Nm/deg. This was 53% and 67% less than the HIII six and ten year old ATD stiffnesses of 0.50 and 0.75 Nm/deg, respectively. In addition, the qualitative response of the model and the Hybrid III were different; the pediatric model flexion bending stiffnesses were nonlinear softening while the HIII were nonlinear stiffening. Due to these differences in nonlinearity, the pediatric models did not remain within the Irwin and Mertz (1997) scaled flexion bending corridors (Figure 8).

Table 2. Pediatric Model Bending Stiffness Pearson Correlation Coefficients During Pendulum Uncertainty Analysis (* indicates statistically significant; the three most important parameters for each model are in bold)

Parameter	Stiffness Correlation	
	Six Years	Ten Years
Vertebra geometry – x	**0.18***	0.11*
Vertebra geometry – y	-0.03	-0.07
Vertebra geometry – z	-0.16*	**-0.16***
Vertebra mass	0.07	0.07
Vertebra inertia	0.02	0.02
Head geometry – x	0.09	**0.12***
Head geometry – y	0.00	-0.01
Head geometry – z	**-0.18***	-0.10
Head mass	-0.07	-0.04
Head inertia	0.09	0.05
Intervertebral joint stiffness (Upper cervical spine)	-0.14*	-0.04
Intervertebral joint stiffness (Lower cervical spine)	-0.01	-0.01
Muscle PCSA	**0.88***	**0.88***

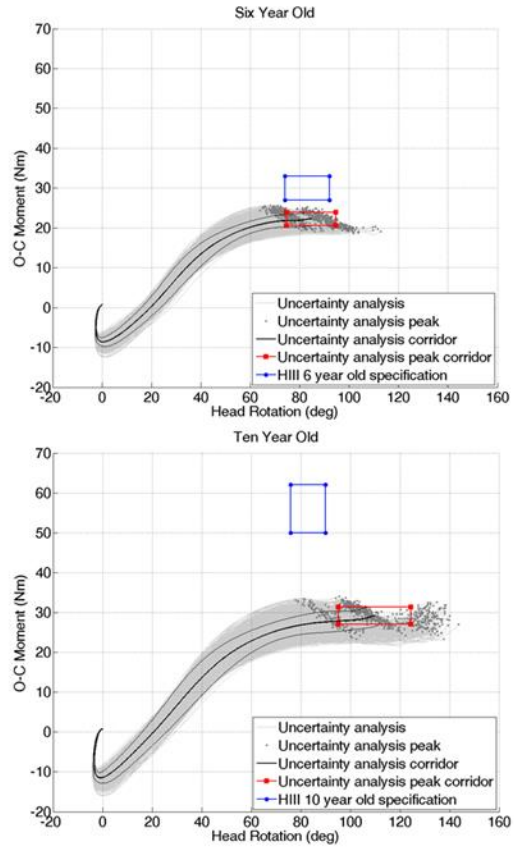

Figure 7. Pediatric model flexion stiffness uncertainty analysis corridors for pendulum certification tests. Plotted are all 650 simulations with response corridors created from the average ± standard deviation. Model stiffness for both pediatric models was most sensitive to muscle PCSA.

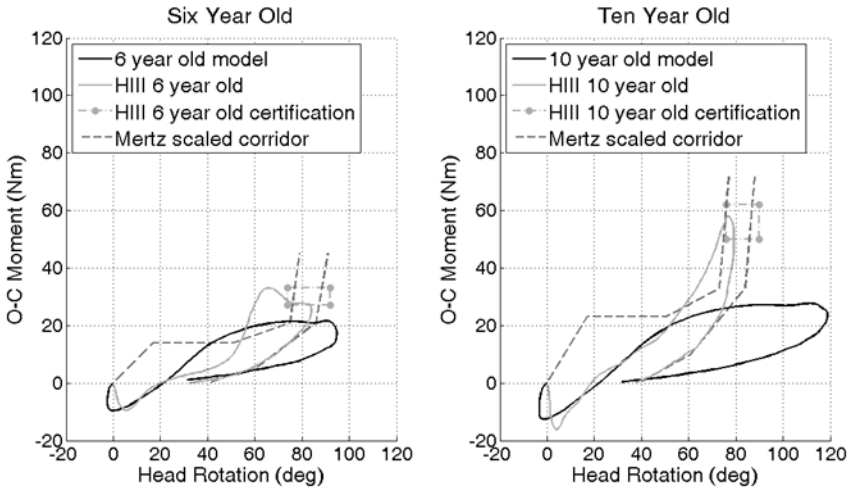

Figure 8. The pediatric head and neck models demonstrated qualitatively different behavior than the Hybrid III six and ten year old ATD in pendulum certification tests. The models were less stiff than the Hybrid III ATDs and their behavior was not predicted by the Irwin and Mertz (1997) scaled flexion corridor.

NBDL 15 g Frontal Impact Simulation

The response of the pediatric six and ten year old head and neck models to 15 g frontal impact was similar to the adult model response (Figure 9), which reproduced the kinematic response of adult human volunteers to 15 g frontal impact (Dibb 2011). During the first 80 ms there was little head motion and the relaxed state muscles maintained an upright posture against gravity. From 80 to 106 ms, the head began to translate but did not begin to rotate. This 26 ms delay in head rotation is termed head lag. Afterwards, the head rotated into flexion. After reaching peak angular displacement, the head started rebounding.

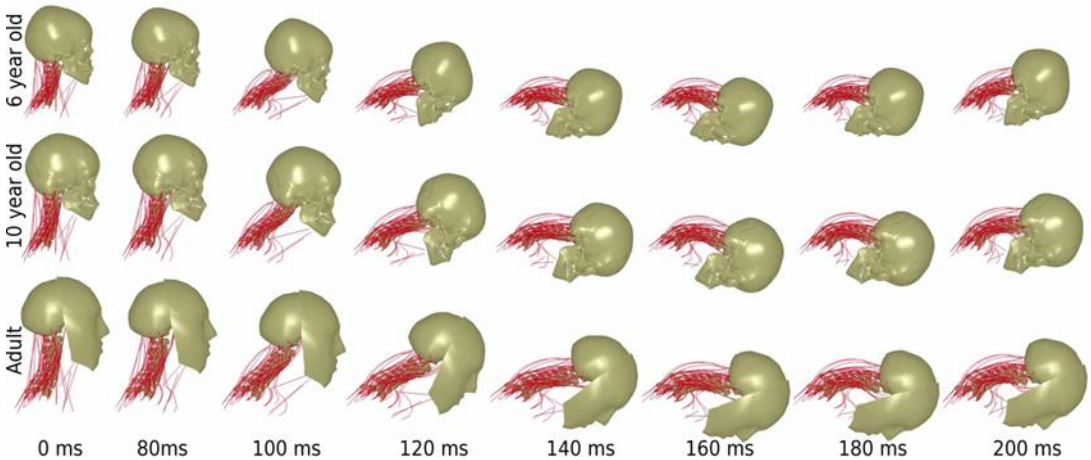

Figure 9. Pediatric and adult model response time-lapse in 15 g frontal impact. The pediatric models had larger peak head rotations than the adult.

As in the pendulum certification tests, the pediatric models had smaller head excursions but greater rotations than the adult (Table 3 and Figure 10). Specifically, the six and ten year old models displaced 30% and 14% less in the x-direction and 21% and 5% less in the z-direction. This is not unexpected given the shorter overall lengths of the pediatric necks. The head of both the six and ten year old models rotated 11% more than the adult. This is not unexpected, since rotation is dependent on the head mass and moment of inertia (MOI). The ratio of head MOI to head mass is very similar for the six and ten year old models, leading to a very similar amount of rotation. On the other hand, the adult ratio of head MOI to head mass is less than that of the pediatric models, and consequently demonstrates less rotation.

The pediatric models had greater head translational and rotational accelerations than the adult (Table 3 and Figure 10). Head x-direction translational accelerations for the six and ten year old models were 17% and 6% greater than the adult, respectively. Head sagittal rotational accelerations for the six and ten year old model were 68% and 44% greater than the adult, respectively. These higher accelerations resulted in earlier peak excursions and rotations, and the six and ten year old models reached peak head rotation 19 and 11 ms earlier than the adult.

Table 3. Pediatric and Adult Model Peak Responses During 15 g Frontal Impact

Response	Six Years	Ten Years	Adult
Head displacement x	10.1 cm	12.5 cm	14.5 cm
Head displacement z	12.2 cm	14.6 cm	15.4 cm
Head rotation	76.1 deg	76.2 deg	68.4 deg
Head acceleration x	286 m/s^2	258 m/s^2	243 m/s^2
Head acceleration z	174m/s^2	185 m/s^2	172 m/s^2
Head rot. acceleration	2571 rad/s^2	2208 rad/s^2	1534 rad/s^2
Neck rotation	65.6 deg	67.9 deg	62.5 deg
Head lag	26 ms	26 ms	26 ms

Furthermore, the pediatric models sustained lower cross-sectional neck flexion moment and tensile loads than the adult (Figure 11). The total cross-sectional peak flexion moment at the OC was only 20.9 and 25.5 Nm in the six and ten year old models compared to 46.5 Nm in the adult. The total cross-sectional peak tensile force at the OC was 648 and 713 N in the six and ten year old models compared to 859 N in the adult. On the other hand, the pediatric models sustained higher peak shear loads than the

adult model. The total cross-sectional peak shear force at the OC was 950 and 861 N for the six and ten year old models compared to 835 N for the adult.

In all models, the neck muscles were the primary moment and force-carrying component of the total neck during 15 g frontal impacts (Figure 11). As illustrated by comparing the ligamentous, muscular, and total F_z neck loads, the osteoligamentous spine was loaded in compression during peak neck flexion at the same time the total neck was loaded in tension.

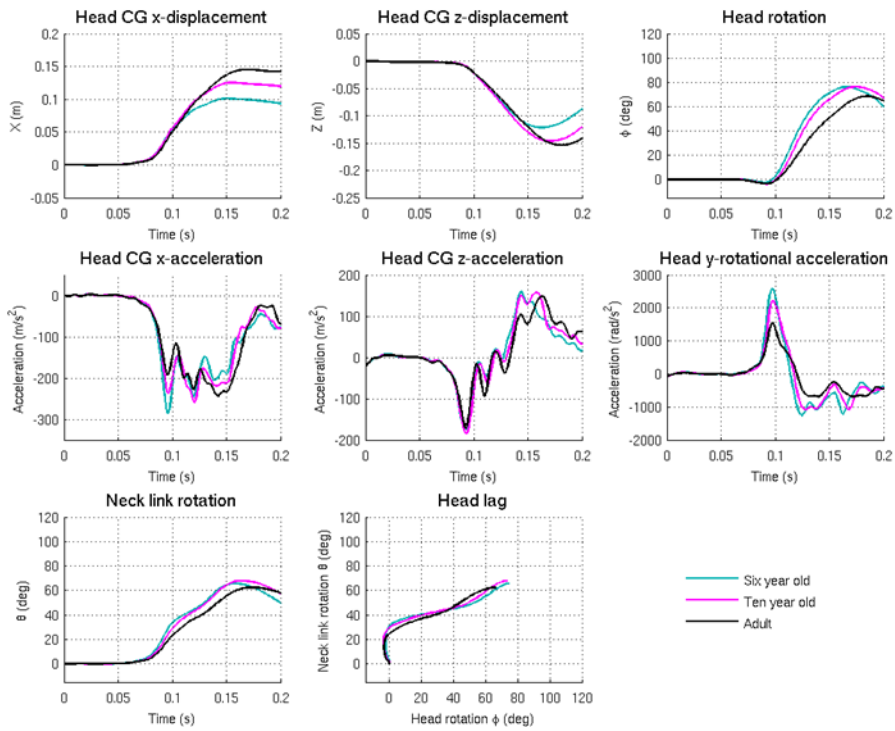

Figure 10. Pediatric and adult model kinematic response to 15 g frontal impact. The heads of the six and ten year old models displaced less but rotated more than the adult.

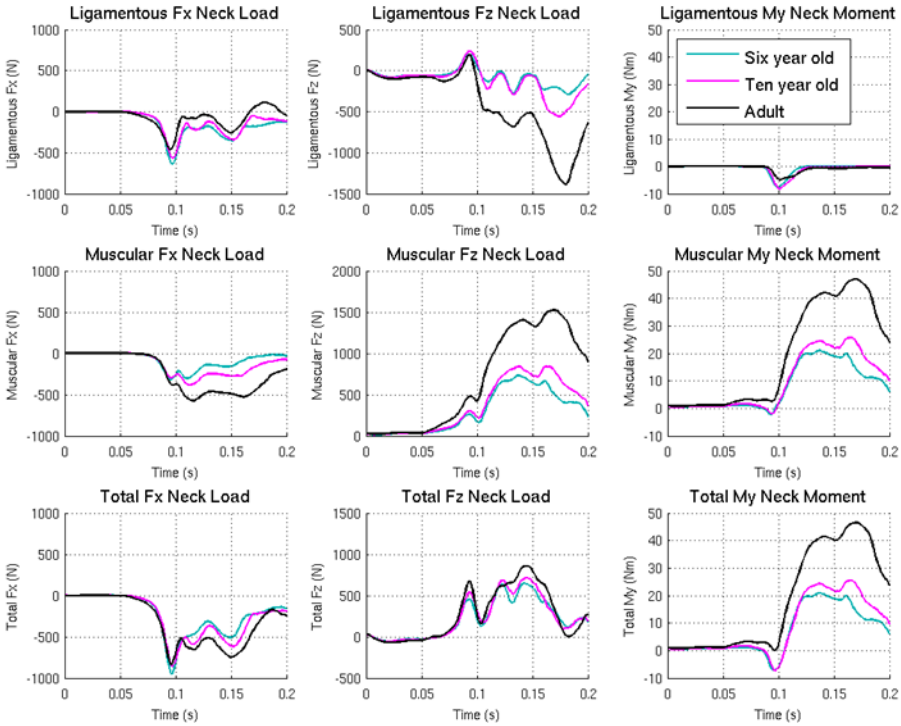

Figure 11. Pediatric and adult model O-C2 spinal segment osteoligamentous, muscular, and total neck loads during 15 g frontal impact. The cervical muscles bore a majority of the loading during this impact. At peak neck flexion, the osteoligamentous spine was loaded in compression while the total neck was loaded in tension.

From the uncertainty analysis, the kinematic response of the pediatric models was most sensitive to the z-direction vertebral geometry scale factor. Correlation coefficients of model parameters to kinematic responses are presented in Table 4. Increasing the z-direction scale factor—which in turn increased the length of the pediatric neck—significantly increased peak head displacements, head rotation, and z-direction translational accelerations; increasing this value also significantly decreased the peak x-direction translational acceleration and head rotational acceleration.

The next most significant parameters affecting the kinematic response were muscle PCSA and the z-direction head geometry scale factors. Increasing these scale factors increased the muscle size and the muscle attachment distance from the spine, or moment arm. Increases in these parameters significantly decreased peak head flexion rotation and decreased head rotational accelerations. Increasing the intervertebral joint stiffness did not significantly affect peak head excursion or rotations; however, increasing the joint stiffnesses did increase peak head accelerations. Additionally, cross-sectional neck loads measured at the OC spinal segment were most sensitive to pediatric muscle PCSA, vertebral and head z-direction geometry, and head inertial property scale factors (Table 5). As before, intervertebral joint stiffnesses only significantly affected peak OC tensile forces.

Six and ten year old pediatric response corridors during 15 g frontal impact are presented in Figures 12 and 13.

Table 4. Pediatric Model Uncertainty Analyses Kinematic Pearson Correlation Coefficients During 15 g Frontal Impact, Presented and Ranked Against Other Model Parameters
(* indicates statistically significant; the top three parameters in each column of each age are in bold)

	Parameter	Peak CG displace-ment x	Peak CG displace-ment z	Peak head rot.	Peak CG accel. x	Peak CG accel. z	Peak head rot. accel.	Peak neck rot.	Head lag time
Six Years	Vertebra geometry - x	-0.08	-0.22*	**-0.24***	-0.02	**-0.45***	-0.07	**-0.43***	-0.33*
	Vertebra geometry - y	0.04	0.07	0.05	0.00	0.04	0.04	0.09	0.13*
	Vertebra geometry - z	**0.94***	**0.76***	**0.37***	**-0.73***	**0.69***	**-0.41***	**0.63***	**0.59***
	Vertebra mass	0.01	-0.01	-0.04	-0.04	-0.01	-0.04	0.01	0.03
	Vertebra inertia	0.00	-0.01	0.00	0.01	-0.01	-0.06	-0.04	0.02
	Head geometry - x	**-0.08**	-0.06	-0.14*	0.07	-0.05	0.00	0.01	-0.01
	Head geometry - y	0.05	0.03	0.01	-0.08	0.04	-0.01	0.00	-0.05
	Head geometry - z	**0.28***	**0.25***	0.23*	**-0.33***	-0.13*	-0.06	0.08	**-0.34***
	Head mass	0.00	0.10	0.13*	0.04	0.07	0.18*	0.17*	0.01
	Head inertia	-0.02	0.04	0.14*	0.24*	-0.28*	**-0.53***	-0.08	**0.47***
	Joint stiffness - upper cerv. spine	0.01	0.02	0.01	0.05	0.08	0.20*	0.03	-0.14*
	Joint stiffness - lower cerv. spine	0.01	-0.09	-0.03	0.04	**0.33***	0.08	-0.28*	-0.09
	Muscle PCSA	-0.07	**-0.55***	**-0.85***	**-0.43***	-0.21*	**-0.65***	**-0.54***	-0.08
Ten Years	Vertebra geometry - x	-0.07	-0.19*	-0.19*	-0.39*	**-0.52***	-0.10	**-0.36***	-0.19*
	Vertebra geometry – y	0.05	0.06	0.05	0.05	0.07	0.03	0.08	0.10
	Vertebra geometry - z	**0.96***	**0.78***	**0.43***	**-0.41***	**0.73***	**-0.45***	**0.66***	**0.71***
	Vertebra mass	0.01	-0.01	-0.04	-0.01	0.01	-0.03	0.00	0.04
	Vertebra inertia	0.00	0.00	0.01	-0.01	-0.01	-0.06	-0.03	0.01
	Head geometry - x	-0.09	-0.06	-0.12*	-0.07	-0.03	0.01	-0.02	-0.04
	Head geometry - y	0.05	0.02	0.01	0.07	0.02	-0.01	0.01	-0.03
	Head geometry - z	**0.23***	**0.21***	**0.24***	**0.27***	-0.18*	-0.08	0.06	**-0.29***
	Head mass	0.01	0.09	0.11	-0.08	0.04	0.16*	0.15*	-0.03
	Head inertia	-0.01	0.05	0.12*	-0.25*	-0.11	**-0.51***	-0.03	**0.47***
	Joint stiffness - upper cerv. spine	0.01	0.01	0.01	**0.28***	-0.05	0.12*	0.02	-0.10
	Joint stiffness - lower cerv. spine	0.02	-0.06	-0.01	0.25*	**0.30***	0.04	-0.19*	-0.04
	Muscle PCSA	**-0.13***	**-0.57***	**-0.85***	-0.04	-0.28*	**-0.65***	**-0.62***	-0.07

Table 5. Pediatric Model Uncertainty Analyses Kinetic Pearson Correlation Coefficients During 15 g Frontal Impact, Presented and Ranked Against Other Model Parameters
(* indicates statistically significant; the top three parameters in each column of each age are in bold)

	Parameter	Peak OC Shear Force	Peak OC Tensile Force	Peak OC Flexion Moment
Six Years	Vertebra geometry - x	0.02	-0.07	0.10
	Vertebra geometry - y	0.00	-0.05	-0.04
	Vertebra geometry - z	**0.48***	0.01	**-0.15***
	Vertebra mass	0.02	-0.04	0.05
	Vertebra inertia	-0.02	0.03	0.01
	Head geometry - x	-0.05	-0.28*	0.08
	Head geometry - y	0.07	0.07	0.01
	Head geometry - z	**0.40***	**0.53***	0.12*
	Head mass	-0.37*	0.30*	-0.03
	Head inertia	-0.26*	**0.35***	**0.15***
	Intervertebral joint stiffness – upper cervical spine	0.01	**0.31***	-0.02
	Intervertebral joint stiffness – lower cervical spine	-0.06	0.21*	0.06
	Muscle PCSA	**0.58***	-0.25*	**0.95***
Ten Years	Vertebra geometry - x	0.03	-0.21*	-0.01
	Vertebra geometry – y	-0.01	-0.01	-0.04
	Vertebra geometry - z	**0.60***	0.20*	-0.04
	Vertebra mass	0.02	-0.04	0.04
	Vertebra inertia	-0.01	0.02	0.01
	Head geometry - x	-0.09	-0.20*	**0.11**
	Head geometry - y	0.07	0.06	0.03
	Head geometry - z	**0.33***	**0.56***	**0.28***
	Head mass	-0.31*	**0.28***	-0.02
	Head inertia	-0.21*	0.10	0.05
	Intervertebral joint stiffness – upper cervical spine	0.02	0.20*	0.03
	Intervertebral joint stiffness – lower cervical spine	0.01	0.13*	0.06
	Muscle PCSA	**0.57***	**-0.49***	**0.93***

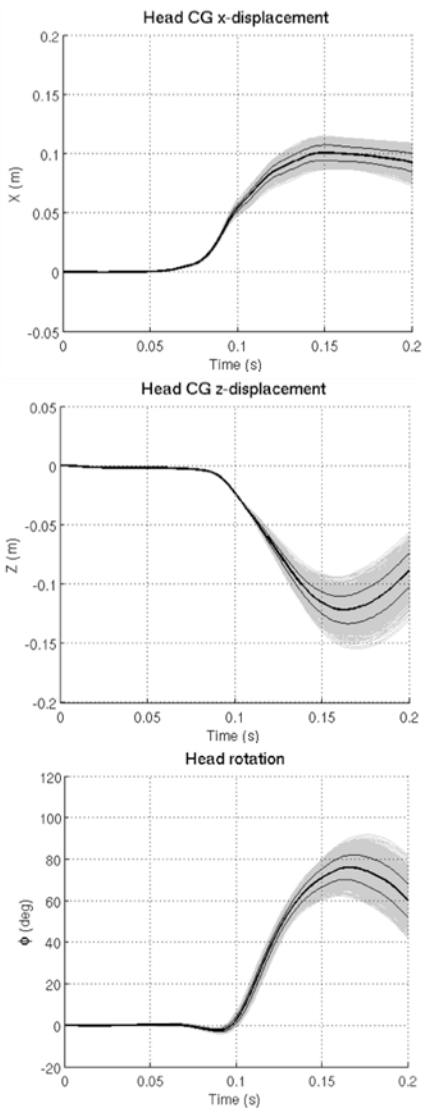

Figure 12. Six year old model head CG translational and rotational responses during 15 g frontal impact uncertainty analysis. Plotted are all 650 simulations with the corridor created from the average ± standard deviation.

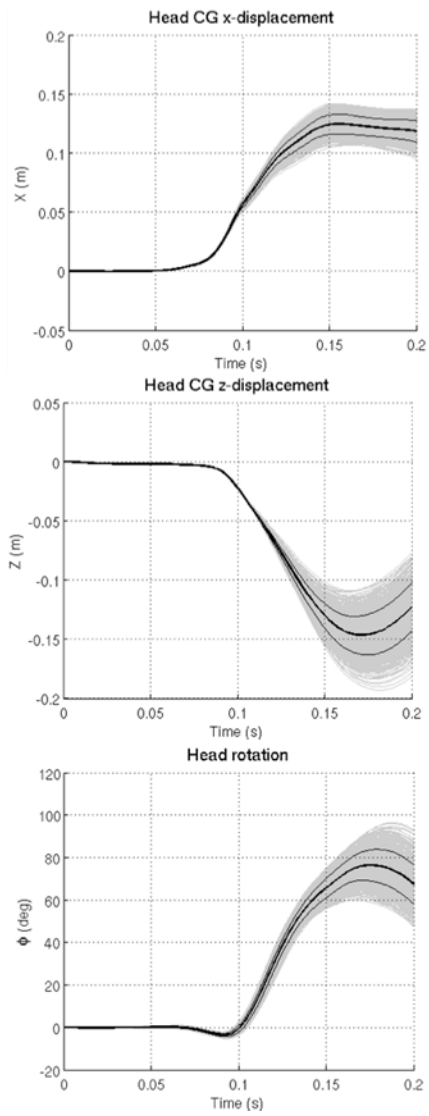

Figure 13. Ten year old model head CG translational and rotational responses during 15 g frontal impact uncertainty analysis. Plotted are all 650 simulations with the corridor created from the average ± standard deviation.

DISCUSSION

The purpose of this study was to utilize a pediatric head and neck multibody and finite element model to investigate the head kinematics and dynamic flexion bending response and stiffness of the neck during ATD neck certification pendulum testing. Also created and studied were flexion biofidelity corridors for future pediatric ATD design for both pendulum certification tests and 15 G frontal impacts.

In the pendulum certification tests, the pediatric neck was less stiff than the adult neck. Likewise, the pediatric necks were less stiff in flexion bending than the Hybrid III ATD necks: the six year old was 53% less stiff than the ATD while the ten year old was 67% less stiff. The difference between ATD and model bending stiffness was minimal below 40° of head flexion, while greater differences occurred at higher rotations. At higher rotations the ATD stiffness nonlinearly increased while the model stiffness nonlinearly decreased. The muscles and their strain rate dependence can explain this nonlinear softening of the models. Muscle force increases at higher elongation strain rates in both the passive and active elements (Hill 1938; Myers et al. 1998; Winters 1990; Winters 1995). Since higher muscle strain rates occurred during the higher head rotational velocities of the initial loading phase, and then decreased until peak head rotational displacement was reached, the muscle force decreased as peak head rotational displacements were reached. This is illustrated by the OC moment time histories (Figure 6). The moments increased rapidly during the high muscle strain rate of the initial loading and peaked prior to peak rotational displacement, then decreased by peak rotation. A secondary explanation of the softening of model bending stiffness is the decrease in stress of the active muscle with increased strains (Hill 1938; Myers et al. 1998; Winters 1990; Winters 1995). However, the active muscle strain dependence was less of a factor since muscle strains were relatively low with an average peak extensor strain of only 11%. Therefore, an important difference in stiffness between the models and the HIII ATD necks is the strain rate dependent effects that are not accounted for in the design of the ATD necks.

In a similar fashion, the pediatric and adult model flexion bending response all passed outside of the Mertz corridors, primarily at higher head rotations. This is because the model bending stiffness did not increase at higher rotations, and instead decreased. This behavior was consistent for both the six and the ten year old, and illustrates that the Mertz corridors predict qualitatively different behavior than the neck models display.

Though chin-on-chest contact was not modeled in these simulations, the pendulum flexion bending biofidelity response corridors created from uncertainty analysis of the models' response (Figure 7) are appropriate since this contact is not accounted for in the Hybrid III pendulum certification test. Therefore, these corridors represent the response of validated, biofidelic models under the same loading conditions used to certify the ATD neck, and can be used for future pediatric ATD neck design specification. Importantly, both the head extension, which occurs prior to flexion, and the nonlinear softening behavior were included in the corridors. Neither of these effects is represented by the current HIII ATD necks. Muscle parameters had the greatest effect on neck bending stiffness. Increasing the force generating capacity, effective moment arm, and stiffness of the muscles significantly increased the bending stiffness.

Similarly, the first 15 g frontal impact pediatric biofidelity response corridors (Figures 12 and 13) were created for future pediatric ATD neck design specifications from uncertainty analysis of the models in this loading scenario. Uncertainty analysis demonstrated that the z-direction vertebral geometry scale factor had the largest effect on the pediatric kinematic translation response, as increasing this value increased the length of the pediatric neck. As can be expected because of their smaller neck length, the heads of the pediatric models translated less than the adult. Peak x-direction CG translations were 70% and 86% of the adult peak translations, which were essentially the same percentage as the vertebral z-direction scale factors used to create the six and ten year old models, respectively. For the kinematic rotation response, the most significant parameter was muscle PCSA. Increasing this value decreased the peak head rotation, which is likely the result of an increased bending stiffness due to an increased muscle PCSA. As the ratio of head MOI to head mass is very similar for the two pediatric models, they experienced very similar flexion rotations. Additionally, since this ratio was larger in the pediatric models than in the adult, the pediatric model heads experienced more flexion rotation than the adult, each rotating 11% more than the adult.

Both the pediatric six and ten year old models had higher head translational and rotational head accelerations than the adult, with the six year old having the highest accelerations. This can be explained by a simple mass spring on a moving base

model. Increasing the spring stiffness of the mass-spring model decreases the acceleration of the mass. This was demonstrated during the uncertainty analysis in which increasing the muscle PCSA, which increased the neck bending stiffness, significantly decreased head accelerations. This is important as higher pediatric head accelerations could lead to pediatric head injuries that would not have caused adult injury under identical loading scenarios. However, further work needs to be done to understand pediatric accelerational head injuries to fully study this possibility. Currently, the Head Injury Criterion (HIC) threshold for the six year old is the same as the adult (Eppinger et al. 1999).

Notably, in all models (pediatric and adult), the neck muscle protected the osteoligamentous spine by bearing a large portion of the cross-sectional neck loads during 15 g frontal impacts (Figure 11). At peak neck flexion, the overall neck was loaded in tension. However, at this point the osteoligamentous cervical spine was loaded in compression due to the tension in the muscles. Additionally, nearly all of the moment experienced by the total neck in 15 g frontal impacts was carried by the muscles. As a result, the moments experienced by the osteoligamentous spine were small, indicating that in frontal impacts the osteoligamentous spine is unlikely to fail in this mode. In fact, the high compressive loads experienced by the osteoligamentous spine suggest that the primary mode of neck failure in frontal impacts is compression.

Finally, this study is not without limitation. For one, a limitation of the comparison of model responses during pendulum certification tests to the Mertz corridors was that head and chest interactions were not modeled in the simulations. The Mertz corridors were created from cadaver frontal impact sled tests in which the OC moment was calculated from inverse dynamics of head accelerations and included "the summation of the moments of the neck and chin forces" (Mertz and Patrick 1971). Mertz and Patrick reported a volunteer static head flexion rotation limit of 66 degrees and a dynamic rotation limit of 70 degrees. The adult model surpassed these limits with a peak head rotation greater than 110 degrees, which would not have occurred with chin contact providing "a stop for forward head rotation" (Mertz and Patrick 1971). Another limitation of this study was that during the 15 g frontal impact simulation, the same T1 boundary conditions were applied to the pediatric models as those measured from adult volunteers. While doing this enables direct comparisons between adult and pediatric head and neck kinematics and kinetics, subjecting children and adults to the same sled accelerations would likely result in different T1 accelerations, as demonstrated in low speed frontal sled tests (Arbogast et al. 2009). This study also removed the effects of muscle activation dynamics from the comparison by applying the same activation histories to the pediatric models as those of the adult model for 15 g frontal impacts.

CONCLUSION

Pediatric head and neck models were used to investigate the dynamic bending stiffness of the pediatric human neck during frontal impact induced via Hybrid III ATD neck certification pendulum loading. The neck response of both pediatric models (six and ten years old) was found to be qualitatively different from the pediatric HIII ATDs: the models demonstrated nonlinear softening behavior while the HIII ATDs experienced nonlinear stiffening. Additionally, the pediatric models' response was less stiff than that of the pediatric HIII ATD: Specifically, the pediatric six and ten year old models were 53% and 67% less stiff than the HIII ATD, respectively. As a result, the models' response was not predicted by the Irwin and Mertz (1997) scaled neck flexion corridors. Moreover, these validated pediatric models based on human pediatric biomechanical properties were used to create the first pendulum certification and 15 g frontal impact biofidelity corridors for future ATD design.

REFERENCES

[1] Arbogast K, Balasubramanian S, Seacrist T, Maltese M, García-España J, Hopely T, Constans E, Lopez-Valdes F, Kent R, and Tanji H. 2009. "Comparison of kinematic responses of the head and spine for children and adults in low-speed frontal sled tests." Stapp Car Crash Journal 53:329-372
[2] Camacho DLA. 1998. "Dynamic Response of the Head and Cervical Spine to Near-vertex Head Impact: An Experimental and Computational Study." Ph.D. Thesis, Department of Biomedical Engineering, Duke University, Durham, North Carolina
[3] CDC. 2007. WISQARS (Web-based Injury Statistics Query and Reporting System) Centers for Disease Control and Prevention
[4] Chancey VC. 2005. "Strength of the human neck: understanding the contributions of the ligamentous and muscular spine in tension and bending." Ph.D. Thesis, Department of Biomedical Engineering, Duke University, Durham, North Carolina
[5] Colebatch JG, Halmagyi GM, Skuse NF. 1994. "Myogenic potentials generated by a click-evoked vestibulocollic reflex." Journal of Neurology,

Neurosurgery, and Psychiatry 57:190-197
[6] de Lange R, van der Made R, Feustel JR, Subbian T, and van Hoof J. 2001. "Development and evaluation of MADYMO child occupant dummy models." In Proceedings of the 4th North American MADYMO User's Meeting, pp. 1-13
[7] Dejeammes M, Tarri C, Thomas C, and Kallieris D. 1984. "Exploration of Biomechanical Data Towards a Better Evaluation of Tolerance for Children Involved in Automotive Accidents." In Proceedings of the 28th Stapp Car Crash Conference, SAE 840530, pp. 427-440
[8] Dibb AT. 2011. "Pediatric Head and Neck Dynamic Response: A Computational Study." Ph.D. Thesis, Department of Biomedical Engineering, Duke University, Durham, North Carolina
[9] Dibb A, Cox C, Nightingale R, Jason L, Cutcliffe H, Myers B, Arbogast K, Seacrist T, and Bass C. 2013. "Importance of Muscle Activations for Biofidelic Pediatric Neck Response in Computational Models." Traffic Injury Prevention (in review)
[10] Doherty B and Paver J. 1988. "Mathematical modeling of the hybrid III manikin head-neck structure." Mathematical and Computer Modelling 11:430-435
[11] Dupuis R, Meyer F, Deck C, and Willinger R. 2006. "Three-year-old child neck finite element modelization." European Journal of Orthopaedic Surgery & Traumatology 16(3):193-202
[12] Durbin DR, Chen I, Smith R, Elliott MR, and Winston FK. 2005. "Effects of Seating Position and Appropriate Restraint Use on the Risk of Injury to Children in Motor Vehicle Crashes." Pediatrics 115(3):305-309
[13] Ewing CL and Thomas DJ. 1972. "Human head and neck response to impact acceleration, NAMRL monograph, 21". Naval Aerospace Medical Research Laboratory, Naval Aerospace Medical Institute, Naval Aerospace and Regional Medical Center, Pensacola, Fla
[14] Federal Motor Vehicle Safety Standard - Part 572 - Subpart E - Hybrid III Test Dummy. Code of Federal Regulations, Title 49 - Transportation. 2011
[15] Federal Motor Vehicle Safety Standard - Part 572 - Subpart N - Hybrid III Six-year-old Child Test Dummy. Code of Federal Regulations, Title 49 - Transportation. 2011
[16] Foust DR, Chaffin DB, Snyder RG, Baum JK. 1973. "Cervical range of motion and dynamic response and strength of cervical muscles." In Proceedings of the 17th Stapp Car Crash Conference, SAE 730975, pp. 285-308
[17] Hill AV. 1938. "The Heat of Shortening and the Dynamic Constants of Muscle. Proceedings of the Royal Society of London." Series B, Biological Sciences 126(843):136-195
[18] Iman R, Campbell J, and Helton J. 1981a. "An approach to sensitivity analysis of computer models. Part I—Introduction, input, variable selection and preliminary variable assessment." Journal of Quality Technology 13(4):174-183
[19] Iman R, Helton J, and Campbell J. 1981b. "An approach to sensitivity analysis of computer models: Part II—Ranking of input variables, response surface validation, distribution effect and technique synopsis." Journal of Quality Technology 13(4):232-240
[20] Irwin A and Mertz HJ. 1997. "Biomechanical basis for the CRABI and Hybrid III child dummies." Technical Report, Society of Automotive Engineers SAE 973317
[21] Kallieris D, Barz J, Schmidt G, Heess G, and Mattern R. 1976. "Comparison Between Child Cadavers and Child Dummy By Using Child Restraint Systems in Simulated Collisions." In Proceedings of the 20th Stapp Car Crash Conference, SAE 760815, pp. 513-542
[22] Liu XJ and Yang JK. 2002. "Development of Child Pedestrian Mathematical Models and Evaluation with Accident Reconstruction." Traffic Injury Prevention 3(4):321-329
[23] Loyd AM, Nightingale RW, Lee C, Bass CR, Frush D, Daniel C, Marcus J, Mukundan S, and Myers BS. 2010. "Pediatric Head Contours and Inertial Properties for ATD Design." Stapp Car Crash Journal 54:167-196
[24] Luck, J.F., R.W. Nightingale, Y. Song, J.R. Kait, A.M. Loyd, B.S. Myers, and C.R. Bass. 2012. "Tensile failure properties of the perinatal, neonatal and pediatric cadaveric cervical spine." Spine [accepted – DOI: 10.1097/BRS.0b013e3182793873]
[25] Luck JF, Nightingale RW, Loyd AM, Prange MT, Dibb AT, Song Y, Fronheiser L, and Myers BS. 2008. "Tensile mechanical properties of the perinatal and pediatric PMHS osteoligamentous cervical spine." Stapp Car Crash Journal 52:107-134
[26] Marzougui D, Kan C, and Bedewi N. 1997. "Development and validation of an NCAP simulation using LS-DYNA3D." In Proceedings of the Fourth International LS-DYNA3D Conference, at Minneapolis, Minnesota, pp. 319-332
[27] Medri M, Zhou Q, DiMasi F, and Bandak F. 2004. "Head–neck finite element model of the crash test dummy THOR." International Journal of Crashworthiness 9(2):175-186
[28] Mertz H, Jarrett K, Moss S, Salloum M, and Zhao Y. 2001. "The Hybrid III 10-Year-Old Dummy." Stapp Car Crash Journal 45:319-328
[29] Mertz HJ and Patrick LM. 1971. "Strength and Response of the Human Neck." In Proceedings of the 15th Stapp Car Crash Conference, SAE 710855, pp.

2903-2928
[30] Meyer F, Roth S, and Willinger R. 2009. "Child neck FE model development and validation." International Journal of Human Factors Modelling and Simulation 1(2):244-257
[31] Mizuno K, Iwata K, Deguchi T, Ikami T, and Kubota M. 2005. "Development of a three-year-old child FE model." Traffic Injury Prevention 6(4):361-371
[32] Myers BS, Woolley CT, Garrett WEJr., Slotter TL, Best TM. 1998. "The Influence of Strain Rate on the Passive and Stimulated Engineering Stress-Large Strain Constitutive Behavior of Skeletal Muscle." J Biomechanical Engineering 120(1):126-132
[33] NHTSA. 1998. "Development and Evaluation of the Hybrid III type Six-Year-Old Child Dummy." Technical Report, Office of Crashworthiness Standards and Vehicle Research and Test Center: National Highway Traffic Safety Administration Docket Number 98-3972
[34] Platzer P, Jaindl M, Thalhammer G, Dittrich S, Kutscha-Lissberg F, Vecsei V, and Gaebler C. 2007. "Cervical Spine Injuries in Pediatric Patients." The Journal of Trauma 62(2):389
[35] Reid SE, Raviv G, Reid SEJr. 1981. "Neck muscle resistance to head impact." Aviation, Space, and Environmental Medicine, pp. 78-84
[36] Saul RA, Pritz HB, McFadden J, Backaitis SH, Hallenbeck H, and Rhule D. 1998. "Description and performance of the Hybrid III three-year-old, six-year-old and small female test dummies in restraint system and out-of-position air bag environments." In Proceedings of the 16th International Technical Conference on the Enhanced Safety of Vehicles, pp. 1513-1531
[37] Schneider LW, Foust DR, Bowman BM, Snyder RG, Chaffin DB, Abdelnour TA, Baum JK. 1975. "Biomechanical properties of the numan neck in lateral flexion." In Proceedings of the 19th Stapp Car Crash Conference, SAE 751156, pp. 455-485
[38] Siegmund GP, Sanderson DJ, Myers BS, Inglis JT. 2003. "Awareness affects the response of human subjects exposed to a single whiplash-like perturbation." Spine 28(7):671-679
[39] Tennyson SA, Mital NK, King AI. 1977. "Electromyographic signals of the spinal musculature during +Gz impact acceleration." Orthopedic Clinics of North America 8:97-119
[40] Thunnissen J, Wismans J, Ewing CL, and Thomas DJ. 1995. "Human Volunteer Head-Neck Response in Frontal Flexion: A New Analysis." In Proceedings of the 39th Stapp Car Crash Conference, SAE 952721, pp. 439-460
[41] Van Ee CA. 2000. "Tensile Properties of the Human Muscular and Ligamentous Cervical Spine." Ph.D. Thesis, Department of Biomedical Engineering, Duke University, Durham, North Carolina
[42] Winters JM. 1990. "Hill-based muscle models: a systems engineering perspective." In Multiple muscle systems: biomechanics and movement organization, edited by J. M. Winters, pp. 69–93. Springer-Verlag, New York City
[43] Winters JM. 1995. "How detailed should muscle models be to understand multi-joint movement coordination?" Human Movement Science 14(4-5):401-442
[44] Winters JM and Stark L. 1985. "Analysis of fundamental human movement patterns through the use of in-depth antagonistic muscle models." IEEE transactions on biomedical engineering 32(10):826-39
[45] Winters JM and Stark L. 1988. "Estimated mechanical properties of synergistic muscles involved in movements of a variety of human joints." Journal of Biomechanics 21(12):1027-1041
[46] Wismans J, Maltha J, Melvin JW, and Stalnaker RL. 1979. "Child Restraint Evaluation By Experimental and Mathematical Simulation." In Proceedings of the 23rd Stapp Car Crash Conference, SAE 791017, pp. 383-415
[47] Wismans J, van Oorschot E, and Woltring JH. 1986. "Omni-Directional Human Head-Neck Response." In Proceedings of the 30th Stapp Car Crash Conference, SAE 861893, pp. 313-331
[48] Yang K and Le J. 1992. "Finite element modeling of Hybrid III head-neck complex." In Proceedings of the 36th Stapp Car Crash Conference, SAE 922526, pp. 219-233

SEAT PAN LOADING DIFFERENCES USING A NEW TEST APPARATUS

John J. DeRosia
Frank A. Pintar
Dale E. Halloway
Mark A. Meyer
Narayan Yoganandan
Medical College of Wisconsin
and VA Medical Center
Milwaukee, WI
USA
Paper Number 13-0102

ABSTRACT

Despite decreases in mortality and overall injury in the last 15 years, in that same time lower thoracic and upper lumbar spine fractures have not decreased, and there is growing evidence that these fractures are actually increasing in frontal impact collisions. Due to the usual upward inclination of passenger seats and structural features added to optimize frontal impact performance, there is a question as to how much the construction of the seat pan might contribute to the incidence of thoraco-lumbar fractures. A seat testing apparatus was designed and evaluated to determine the static stiffness of any vehicle seat when it was loaded in a forward direction. The device used an appropriately pre-weighted seat form to load the vehicle seat and moved the seat form forward relative to the seat cushion. As the seat loading device interacted with the seat, horizontal and vertical forces were generated by the increasing load due to the inclination of the seat and the under cushion structure. While paired same model seats exhibited similar loading patterns and values, there was a variable response from different model seats. Of the five different models tested, maximum vertical loadings varied from 1082 N to 5655 N. After disassembly, structural differences were found between the tested seat models that could account for the difference in seat reaction loads. The device proved that the differences in stiffness between seat models could be evaluated in a non-destructive and timely manner.

BACKGROUND

Research and mitigation strategies regarding injury due to frontal impacts has concentrated on protecting the head, neck and thorax of front seat occupants (Mertz, Irwin et al. 2003). The development of airbags and three point seatbelts has been instrumental in reducing mortality and injury severity in collisions. Mortality rates while wearing only a seatbelt were reduced by 51% compared with users utilizing no restraint devices. The mortality rate of those utilizing an airbag only, without belts, had a 32% reduction, but the rate for those users protected by both airbag and seatbelt had a 67% drop (Cummins, Koval et al. 2011). Injury severity scores showed a similar pattern. However, while the use of both seatbelts and airbags has decreased the probability of sustaining many injuries, the occurrence of spine fractures in front seat occupants has not decreased between 1994 and 2002 (Wang, Pintar et al. 2009).

Although thoracolumbar injuries due to axial compression have been known to occur due to frontal impacts, the mechanism of injury to the spinal column is somewhat elusive (Begeman, King et al. 1973). Begeman used a series of sled tests of lap and shoulder belted cadavers placed on a welded steel chair with a load cell under the seat to monitor axial forces from the spine. In a series of frontal braking tests of up to 15g, they found that the vertebral column suffered wedging or compression fractures at L1, T9, or T7. The authors felt that the fractures were the result of the straightening of the spine curvature during a frontal impact.

Huelke et al. found that, vertebral fractures can occur to lap-shoulder belted front car occupants in frontal crashes, and that thoracolumbar fractures can happen during low speed crashes without the occupant's head striking the interior of the car. They hypothesized that the fractures were due to the submarining of the occupant's pelvis under the lap belt with a pre-flexed lumbar spine (Huelke, Mackay et al. 1995). In a study involving 37 patients with thoracolumbar fractures, Ball found that of those wearing three point restraints, 80% sustained burst fractures

while 28.6% of patients wearing lap belts alone had burst fractures (Ball, Vacarro et al. 2000). They stated that the thoracic spine would straighten "suddenly and forcefully" as the torso was restrained by the shoulder belt. Bilston used NASS data to identify AIS2+ spinal injuries among restrained vehicle passengers. The study identified risk factors for thoracolumbar fractures such as higher severity crashes, crashes into fixed objects, and crashes in the presence of intrusion (Bilston, Clarke et al. 2010).

Pintar et al. studied NASS data and performed an in-depth study of the US-DOT NHTSA Crash Injury Research and Engineering Network (CIREN) database to identify crashes that involved the potential for seat pan and lap belt interaction with the pelvis. (Pintar, Yoganandan et al. 2012) They identified 73 cases from the CIREN database that met the criteria: frontal direction; fractured spine at T10 or below; fracture due to compressive loads (burst, overall compression, or wedge-type with more anterior than posterior involvement); no rollover greater than two quarter turns; row one occupants only. Exclusion factors included occupants who had a history of previous thoracic and/or lumbar surgery and occupants who were in sub-optimal posture at impact. They found that 73% of the Delta-V's occurred at 56 km/h or less and that the location of the crash was approximately half on-road and half off. The vehicles were predominantly (75%) late-model between 2000 to 2010 model years. They noted some interesting relationships between the location of the fracture and type of object struck: five of the ten occupants with T10 or T11 fractures struck a heavy truck, eight of the ten that struck a fixed hard object had L1 fractures, and 17 of the 30 tree/pole impacts suffered fractures at L2 or below. Given the detailed crash descriptions in the CIREN results, it was possible to identify many direct planar frontal impacts with no obvious upward component. As pointed out by Pintar et al. this implies that the seating components of the car are implicated in producing significant upward compressive loads on the distal spine. The structure of the modern automobile seat, in particular the seat pan and forward frame components such as thigh-bars, should be examined for interaction with the lumbar region of restrained occupants. To investigate the potential for seat pan involvement in generating vertical spine loads, a seat testing apparatus to determine static stiffness for vehicle seats was designed and evaluated.

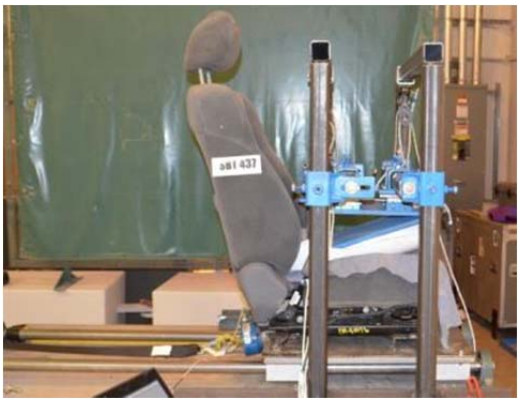

Photo 1. **Seat mounted in test fixture. Test platform angle is adjustable relative to seat form. Seat was pulled rearward during test.**

APPARATUS

The static seat testing (SST) device was intended to test the resistance of vehicle seats to forward motion of an occupant during a forward, planar collision. The test apparatus was constrained to remain in a horizontal plane while the seat was pulled out from beneath. The device incorporated a cart fastened to linear bearings riding on two parallel, large diameter (38.1 mm) round rods enabling free forward and back motion (Photo 1). The vehicle seat to be tested was bolted to the cart with the seat tracks parallel to the cart's plane of travel. A seat form of fiberglass composite was fabricated that matched the contours of a standard H-Point machine. The shaped form was rigidly mounted to a base plate. The plate was hinged to a second plate along its front edge to vary the angle of the device relative to the seat being tested while keeping four 3-axis load cells mounted above the upper plate horizontal (Photo 2). Two lateral beams were mounted to the upper surface of the front and rear pairs of load cells. The beams extended to a solid fixed frame rigidly mounted around the movable seat and cart. The vertical position of the two beams could be varied, then fixed in position. The cart with vehicle seat was pulled rearward using a manual winch through a single axis load cell. The total weight of the movable portion of the SST was, at 134 pounds (60.8 kg), equal to the sitting weight (total weight less the feet, lower legs and one half of the upper leg) of a Hybrid 3 dummy. The signals from all load cells were collected and recorded by a TDAS PRO (Diversified Technical Services, Seal Beach, CA, USA) data acquisition system. As the test was quasi static, the sample rate was

1000 samples per second with a duration of 60 seconds.

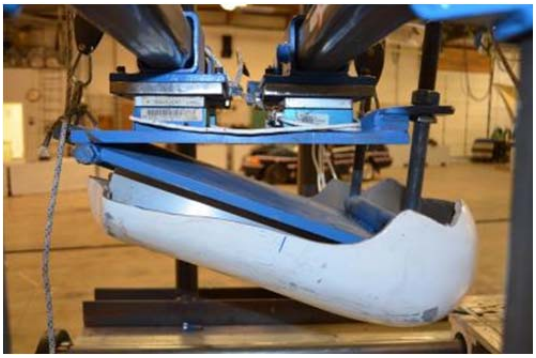

Photo 2. **Fiberglas seat form mounted to instrumented platform.**

METHODS

In this preliminary series of tests eight seats were tested. All seats were bucket seats with fabric covers. Six of the seats were previously used and two were from recently crash tested vehicles. The six used seats were from three different car models with two seats from each model. The vehicle model year of the six used seats ranged from 2006 through 2012. The two new seats were made available from NCAP tested vehicles. Each of the those seats were from the passenger side of 2012 model year vehicles that had been used for a side impact test to the opposite side and a side airbag occupant out-of-position test using SID-2s 5th percentile female dummies. Those seats had not been subjected to either the loading of frontal tests or the wear and tear of used seats. The seats represented five different models, each model with different seat frame designs, seat suspensions, and foam thicknesses.

Before testing, the seats were fixed to a plate with the seat track level, and seat centerline centered on the plate. If the seat pan angle was adjustable, it was set per FMVSS 208 guidelines. For consistency between pairs of seats, if only one seat of a pair was adjustable, it was adjusted to match the seat angle of the unadjustable seat. For each test setup, the seat form and load cell assembly were placed in the vehicle seat over a fabric sheet similar to the dummy setting procedure outlines in the FMVSS 208. The seat was brought forward into contact with the rear of the seat form. Additional weights were placed on top of the assembly to bring the total weight resting on the seat to 930 N. The portion of the device representing the ischial tuberosities location of a human occupant was allowed to rest into the rear of the seat cushion while the front of the device was stabilized in a fixed position to maintain an upward angle of the seat bottom of approximately 20 degrees with a level reference plane for the load cells. The outboard ends of the lateral beams on the pairs of load cells were then tightened into position while monitoring a real time output from the load cells to avoid introducing any significant preload into the system during the tightening. The seat was pulled slowly rearward using a manual winch, pausing every 50 mm of travel. The process was repeated until the seat was pulled free of the seat-form loading assembly. Care was taken to avoid maintaining the loading of the seat cushion for longer than 15 minutes, and the seat cushion was allowed to rest unloaded for a minimum of 30 minutes between repeat tests. Each seat was tested at least twice to assess repeatability. Results of the repeated tests of each seat were compared by summing the vertical loads recorded by the four load cells. The mean difference between peak seat pan loading between repeated tests was 5.2% (SD 4.9%).

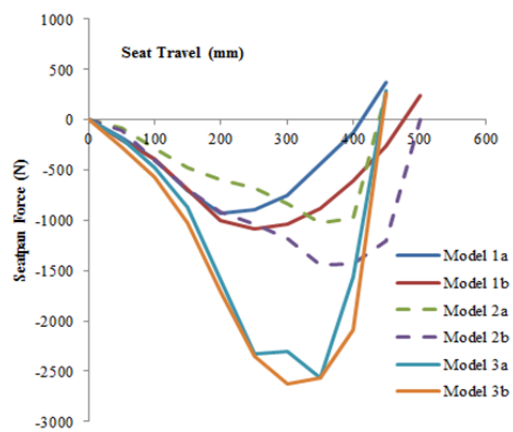

Figure 1. **Comparison of tests of three model seats.**

The loading responses between the paired seats were compared. For each seat, the mean of the maximum seat pan loading of the repeated tests was compared to the similar values calculated for the other seat of the pair. For Model 1 and Model 2 the differences between the two seats were 9.0% and 2.5% respectively, while the same comparison for the Model 3 seats was 32%. Combined, the mean difference was 14.6% (SD 12.8%). An explanation for the larger difference in peak loading within pairs of seats was found by examining the tested seats. Two seats of the third pair, although they were externally similar, had considerably different foam cushions (Figure 1). The age and condition

of the seat foam seemed to be a factor in the stiffness of the tested seats.

RESULTS

Each of the seat models displayed different stiffness behaviors with respect to the position of the loading device (Figure 2). The Model 1 and 2 seats exhibited linear stiffening to approximately 250 mm of seat travel. While seat Model 1 gradually decreased in stiffness, seat Model 2 did not reach peak stiffness until approximately 400 mm of travel. Both models unloaded smoothly after reaching the peak. The Model 3 seat was considerably stiffer than the first two (Table 1). It also exhibited a smooth unloading phase after its peak at 300 mm. The Model 4 seat paralleled the behavior of Models 1 and 2 until 200 mm, after which the stiffness rapidly rose to a peak higher than the three previous seats at 350 mm, then began to unload smoothly. The Model 5 seat showed a considerably different behavior. For the first 100 mm, Model 5 was initially only marginally stiffer than other seats, but the stiffness increased at a higher rate and reached a considerably higher peak at 350 mm. It remained stiff for 50 mm before dropping off suddenly.

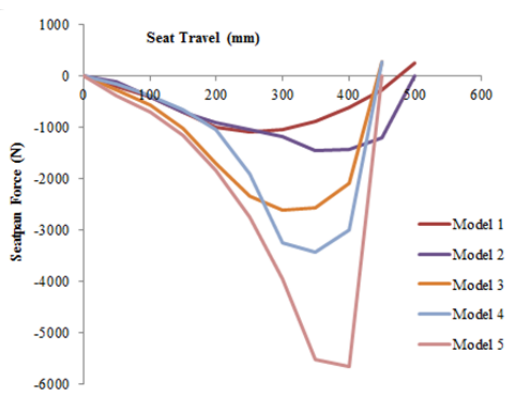

Figure 2. **Comparison of five different model seats.**

The horizontal force (X axis) required to move the seat pan out from under the test device was proportional to the seat pan force at approximately half of the Z axis load.

SEAT CONSTRUCTION

The construction of the Model 1 through 4 seats was generally similar but with important differences in detail. The seats utilized stamped sheet metal side frames fastened to movable tracks that allowed fore and aft adjustment of the seat in the vehicle.

Table 1. Matrix of test results.

Seat	Max Seat-pan Load [N]	Max Horizontal Pull [N]	X/Z
Model 1	-1081.8	-580.2	54%
Model 2	-1442.0	-809.0	56%
Model 3	-2621.3	-1429.3	54%
Model 4	-3437.9	-1696.0	49%
Model 5	-5655.2	-2698.4	47%

The two sides were fastened together with a tubular member across the back and a front structure consisting of another tube and/or other structure. A wire upholstery spring suspension was used to suspend the rear of the seat by clipping onto the rear tubular cross-member. At the front of all the seats a stamped sheet metal cover fastened over the front cross-member and springs (Photo 3).

Photo 3. **Cross-section of typical car seat construction. Under fabric upholstery and cushion is sheet metal cover on front of seat (to right) and a portion wire spring suspension is shown. Two side pieces are connected by a round tube in the rear and a second tube toward the front under the front cover.**

A foam rubber cushion then covered the metal portion of the seat, and fabric upholstery encased the foam cushions. Due to the spring suspension in the rearward portion of the cushion, the seats were more yielding under the buttocks of the vehicle occupant. During testing, as the testing device moved toward the front of the seat, the device compressed the foam cushion of the seat to the point that the structure of the seat under the cushion played a role in its relative stiffness.

The higher stiffness seats were constructed with more and heavier bracing between the side rail framework in the forward third of the seats. For instance, while Model 1 utilized a thin (0.67 mm thick) stamped steel forward cover and a 25 mm diameter tubular cross-tube beneath the cover, the cover was fastened to the side structures by four relatively small mechanical fasteners. Conversely, Model 3 was constructed with a thicker (1.0 mm) front upper metal cover over the top front corner of the seat frame that was welded to the side frames

***Photo 4*. Model 1 structure. Sheet metal front cover over front frame tube wire seat suspension springs wrapped around rear tube.**

Rather than the single steel tube connecting the two sides under the front cover sheet metal, Model 3 seat also had a considerably more rigid stamped sheet metal member fastened between the two sides. It used a closed section welded sheet metal beam of thicker (1.4 mm) construction connecting the two sides beneath the upper cover. Model 3 was more than twice as stiff as the Model 1 shown in Photo 3.

In addition to the normal seat components, Seats 4 and 5 also were equipped with seat cushion airbags. Neither seat bolster bag was deployed before or during the testing. While the Model 4 used a wire spring suspension system Model 5 used a considerably different approach (Photo 5).

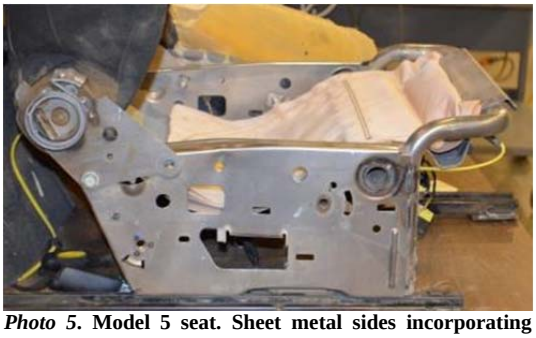

***Photo 5*. Model 5 seat. Sheet metal sides incorporating three cross-tubes.**

The side members of the seat were larger and taller than the other seats. Front and rear cross-tubes connected the two sides. In addition, a tubular frame rose from the floor level, up the front of the seat side frames, bent forward to extend the front of the seat, then laterally to form a rigid frame around the front of the seat. Rather than springs, a sheet metal pan spanned from the front tubular structure, rearward over the front tube, down to form a depression for the seat, then back to the rear tube (Photo 6). The pan was not attached to the sides but was welded to all three tubes. The airbag lay on top of the pan, under the cushion.

***Photo 6*. Airbag folded forward to show seat pan.**

DISCUSSION

Three factors were identified as being involved in the disparate stiffness of the seat models tested. The original angle of the seat cushion affected the measured stiffness of the seats. An increased angle of seat cushion brought the interaction of the test device with the under structure of the seat earlier and to a greater extent. Model 1, the least stiff seat, had a total seat cushion angle of six degrees, while Model 3 seat was 8.3 degrees and Model 5, the stiffest seat, was 10.9 degrees. Structurally, the stiffness of the front structure of the seat contributed to the overall stiffness as the load was moved

forward. For the seats with a stiffer front structure, stiffness increased as the seat form encountered the hard structures. The condition of the foam also influenced the tested stiffness although it was less of a factor than the seat geometry and structure.

In the small sample of seats tested, the unique design of Model 5 stood out. The unyielding seat pan was initially stiffer than the other seats and increased in stiffness in a nonlinear fashion until it reached a peak stiffness, 61% higher than the next most stiff. The front tubular structure was more forward and higher relative to the other seats. The effect of this structure was that it formed a rigid barrier at the front structure of the seat. An example of this effect was the abrupt fall off of force once the test device cleared the front structure. The resistance of the seat pan to forward motion of the occupant's pelvis may be significantly altered with under-seat airbag deployment by tightening the occupant against the lap belt, preventing appreciable forward interaction between the pelvis and hard structures of the seat pan.

There were limitations to conducting only static testing of the seats. As mentioned above, there is no opportunity to judge the effect of the under-seat airbags and how they would affect forward motion of the lower body. The small number of seats available to be tested is a drawback that will hopefully be addressed in the near future. Finally, it cannot be assumed at this point that a given seat that was evaluated with a higher stiffness will be more prone to inducing thoracolumbar spinal fractures. The dynamic nature of a crash and the interaction of the human pelvis with the seat pan have not been considered in this study.

CONCLUSIONS

As the rate of thoracolumbar spine fractures is increasing in more modern designs of automobiles, the contribution of seating systems to the problem should be addressed. A test device was developed and evaluated to determine the relative stiffness of automobile seats.

The device was able to measure differences in the vertical load resistance of an occupant surrogate between designs of modern seats. The device should be useful in determining which seating systems are more likely to cause high axial loading into the spine of an occupant. The next phase of the study will evaluate the most and least stiff seats subjected to more dynamic tests to verify the potential for spinal injury.

ACKNOWLEDGMENTS

This research was supported in part by US DOT NHTSA CIREN research funds DTNH22-10-H-00292 and by the Department of Veterans Affairs Medical Research. The views expressed are those of the authors and do not represent those of the funding agency. We gratefully acknowledge the work of Joe Frank and Chuck Bokath in the construction of the apparatus.

REFERENCES

Ball, S., A. Vacarro, et al. (2000). "Injuries to the T-L spine associated w restraint use.pdf>." Journal of Spinal Disorders **13**(4): 297-304.

Begeman, P., A. King, et al. (1973). "Spinal Loads Resulting from -Gx Acceleration." Stapp Car Crash J.: 343-360.

Bilston, L. E., E. C. Clarke, et al. (2010). "Spinal injury in car crashes: crash factors and the effects of occupant age." Injury Prevention **17**(4): 228-232.

Cummins, J., K. Koval, et al. (2011). "Do seat belts and air bags reduce mortality and injury severity after car accidents?" Am J Orthop (Belle Mead NJ). **40**(3): E26-29.

Huelke, D., G. Mackay, et al. (1995). "Vertebral column injuries and lap-shoulder belts." J Trauma. **38**(4): 547-556.

Mertz, H., A. Irwin, et al. (2003). "Biomechanical and scaling bases for frontal and side impact injury assessment reference values." Stapp Car Crash J. **47**: 155-188.

Pintar, F., N. Yoganandan, et al. (2012). "Thoracolumbar spine fractures in frontal impact crashes." Ann Adv Automot Med. **56**: 277-283.

Wang, M. C., F. Pintar, et al. (2009). "The continued burden of spine fractures after motor vehicle crashes." Journal of Neurosurgery: Spine **10**(2): 86-92.

DEVELOPMENT OF THE Q10 10 YEAR-OLD CHILD CRASH TEST DUMMY

Paul Lemmen, Kees Waagmeester, Mark Burleigh, Apoorva Lakshminarayana, Karl Korschdon
Humanetics Innovative Solutions
The Netherlands
Costandinos Visvikis, Jolyon Carroll, David Hynd, Mark Pitcher
Transport Research Laboratory
United Kingdom
Paper Number 13-0438

ABSTRACT

In Europe, the law requires children up to 12 years or up to 150 (or 135) centimetres to be restrained in a child restraint system (CRS) when travelling in cars. The EC FP7 project EPOCh developed test procedures and tools for impact tests for CRS designed to protect older and larger children in vehicle collisions. The EPOCh project involved TRL, Humanetics, IDIADA, DOREL and University of Surrey. One of the main EPOCH deliverables was the development of a prototype 10-year-old Q dummy.
This paper reports on the development and assessment of the Q10 dummy within the EPOCh project, as well as the subsequent refinement and evaluation of the dummy based on third party testing.

INTRODUCTION

According to data from the European Road Safety Observatory [1], the latest data available for child fatal injuries is the year 2011. For that year 815 children in the age below 15 years old were killed on European roads. Since 1995 the figure has dropped around 56%. Whilst this is a good achievement, there is still a need to reduce the level of child fatalities and all types of child injury in the EU in the various transport modes. Child fatality numbers for some EU Member States in 2011 are provided in Figure 1.
Motivated by these numbers the EU FP7 projects CASPER [2] and EPOCh [3] addressed the safety of children transported in passenger cars. While CASPER worked on improvements of existing Q-series dummies, their application in test procedures and development of numerical models, including Human body models, the EPOCh project realised a Q family member representing adolescents and investigated its application in UN Regulation No. 44 and NPACS type test procedures.

The paper will outline the development of the Q10, including: a summary of anthropometry and biofidelity specifications, prototype design realisation, prototype performance and proposals for injury thresholds obtained by scaling values from adult and smaller child dummies. A brief list of findings from testing by OEMs, suppliers and test houses world-wide will be provided followed by design updates implemented in a production version of the Q10 dummy. First results on the performance of the production version dummy are included as well. Finally, recent work to evaluate abdomen loading sensors related to the detection of belt penetration in the pelvis-thigh region will be presented. The sensors were developed in CASPER and transferred to the Q10 dummy.

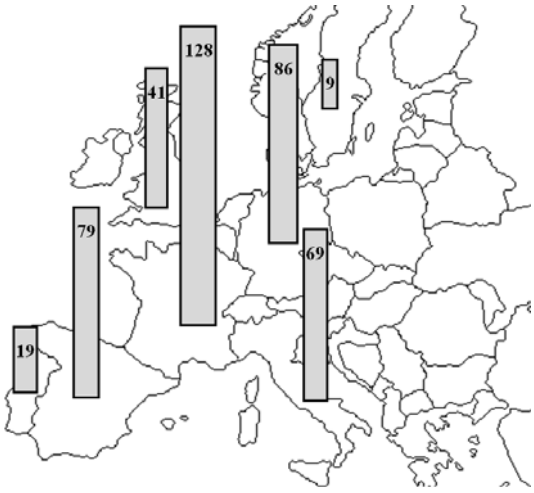

Figure 1. Numbers of child fatal injuries for the year 2011 in some Member States (source: www.erso.eu).

SIZE SELECTION

Under the current regulation (2003-20-EC) countries have an option to select the maximum size of a child that has to use a CRS when traveling in a car. Two different statures are mentioned in the regulation: 135 or 150 cm. This corresponds roughly with 50th percentile children of 8.9 and 11.6 Years Old (further indicated as YO) respectively. The current regulation

specifies a P10 dummy (Stature 1.38 m, mass 32 kg, approximately 50th percentile 9.4 YO). The EPOCh team presented their recommendation on the size selection in a stakeholder's forum meeting in June 2009. The conclusion from extensive discussions was that the age of 10.5 YO was felt to be most appropriate to represent the group of oldest CRS users [4].

REQUIREMENTS AND PROTOTYPE DESIGN

Anthropometry

The dummy was sized according to the 50th percentile anthropometry of the selected age: stature 1443 mm, seating height 748 mm, shoulder height 473 mm and total body mass 35.5 kg. In line with the rest of the Q-dummy family the Q10 anthropometry was based on CANDAT (Child ANthropometry DATabase) [5]. Figure 2 provides data for mass versus seating height. The yellow boxes give envelops for 5th to 95th percentile extremes according to CANDAT around the Q-dummy ages 1, 1.5, 3, 6 and 10.5 and 11.6 YO. Note that the latter relates to the age with average stature of 150 cm in CANDAT. Dimensions and masses as abstracted from the database are included in Table 1 and Table 2. References to the measures included in Table 1 are depicted in Figure 3. Additional information related to the skeletal geometry of the pelvis was obtained from [6]. This reference specifies coordinates for important landmarks in the pelvis, based on CT scans from 81 children of 5 to 11 years old. A full description of the dimensional requirements is included in the Q10 design brief [4, 7].

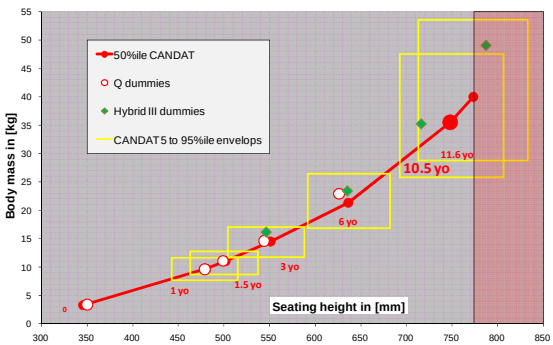

Figure 2. Mass versus seated height for the Q and Hybrid III series with the 5th to 95th percentile envelopes for 1, 1.5, 3, 6, 10.5 and 11.6 YO.

Biofidelity

In defining the Q10 dummy, priority was put on the frontal impact performance because the current UN Regulation No. 44 addresses frontal impacts only.

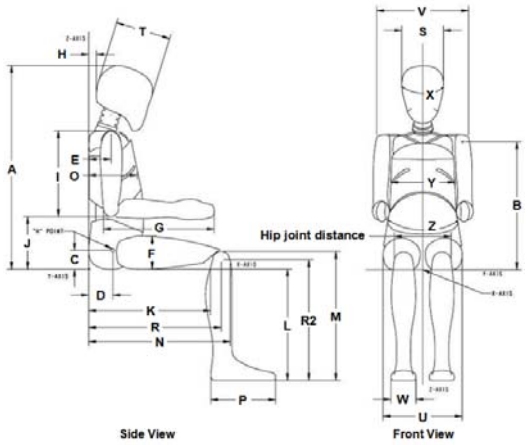

Figure 3. Q10 Overall dimensions.

Table 1. Q10 anthropometry requirements and realised dimensions in the prototypes from EPOCh

Description	Requir. [mm]	Actual [mm]
A1 – Seated Height (head tilt)	747.6	733.7
A2 – Seated Height (via T1)	747.6	748.4
B - Shoulder Height (top of arm)	473	472.5
C - Hip Pivot Height	65.9	65.9
D - Hip Pivot from Back Plane	90.4[1]	90.4
- Hip Joint Distance	130.0[1]	132.0
F - Thigh Height	114.0	114.0
G - Lower Arm & Hand Length	374.7	374.2
I - Shoulder to Elbow Length	292.9	291.6
J - Elbow Rest Height	189.6	181.0
K - Buttock Popliteal Length	417.5	414.9
L - Popliteal Height	405.7	405.7
M - Floor to Top of Knee	445.6	446.0
N - Buttock to Knee Length	488.4	485.4
O - Chest Depth at Nipples	171.2	171.0
P - Foot Length	220.0	220.0
- Standing Height (head tilt)	1442.5	1441.2
- Standing Height (via T1)	1442.5	1455.5
R - Buttock to Knee Joint	(none)	445.7
R2 - Floor to Knee Joint	(none)	414.0
S - Head Breadth	143.9	144.0
T - Head Depth	187.4	186.5
U - Hip Breadth	270.4	271.5
V - Shoulder Breadth	337.8	337.8
W - Foot Breadth	86.0	86.0
X - Head Circumference	534.5	534.0
Y - Chest Circum at Axilla	687.3	604.6
- Chest Circum at Nipples	684.9	633.6
Z - Waist Circumference	593.5	664.6

1) The data from Reed *et al.* [6] are transformed from standing to sitting and scaled from 10 YO stature of 137.4 cm to 144.3 cm for Q10.

Table 2. Q10 mass requirements and actual values prototypes and ballasted versions used for testing

Body part	Required [kg]	Original prototype [kg]	Ballasted prototype [kg]
Head	3.59	3.59	3.59
Neck	0.60	0.63	0.63
Upper torso	5.15	5.14	5.14
Lower torso	9.70	8.04	9.02
Upper arm[1]	1.09	1.05	1.10
Lower arm[1,2]	0.90	0.83	0.90
Upper leg[1]	3.71	3.70	3.70
Lower leg[1,2]	2.53	2.44	2.44
Total mass	**35.5**	**33.4**	**34.7**

1) Each arm / leg
2) Including hands / feet respectively

Nonetheless provisions were included for side impact applications wherever possible. This includes for instance a pelvis design based on the WorldSID 5th dummy and a neck design based on the Q3s.
With regards to frontal biofidelity targets the approach defined for other members of the Q family was adopted. It consists of scaling of adult targets based on anthropometry and bone properties. By applying this approach Q-dummy research results from the previous EU FP projects CREST [8] and CHILD [9] become applicable for the Q10.
Biomechanical requirements for the various body parts were described in [10]. As an example, scaled performance corridors for neck My moment versus flexion and thorax force versus deflection for 4.27 m/s frontal impact are provided in Figure 4 and Figure 5 respectively. For the thorax impact tests an impactor with a mass of 8.76 kg is defined. Corridors for Q6 and Hybrid III 50th percentile male are given for reference. It can be observed that the Q10 targets are in between those of the smaller child and the adult dummy.

Instrumentation

In the development of the prototype Q10 the following provisions for instrumentation were included:

- 2D Displacements –Upper and lower rib cage.
- 3D Linear accelerations – Head, spine T4 and T12, sternum and Pelvis.
- 3D Angular rate sensors – Head, thorax and Pelvis.
- 6 axis loadcells – Upper and lower neck, Lower lumbar spine, Sacro-Iliac and Femur.
- Single axis loadcell – Pubic force.

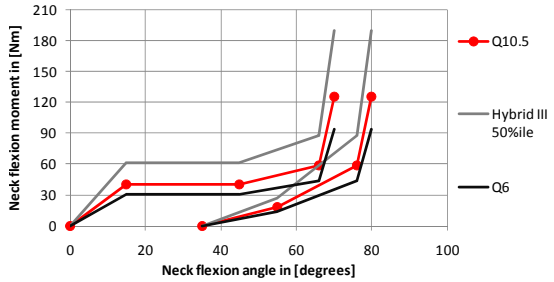

Figure 4. Q10 Neck flexion corridors.

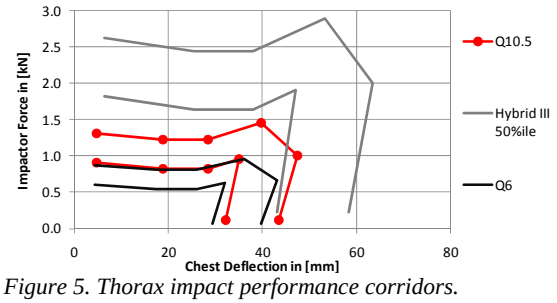

Figure 5. Thorax impact performance corridors.

For side impact application provision for alternative channels was implemented, such as 2-D chest displacement, T1 Ay acceleration and pubic symphysis load.
In addition to the above provisions for tilt sensors were included in various locations to facilitate positioning of the dummy.

Prototype Design Realisation

Using the requirements defined above, three prototype dummies were realised in the EPOCh project. The design and prototype evaluation are described in [10] and [11]. Figure 6 through Figure 9 give some impressions of the prototype design. The following summarises the performance of the prototypes realised as well as some key features of the Q10.
A comparison of the realised dimensions of the prototypes with the targets is given in Table 1. In Table 2 the actual mass distribution is compared with the requirements. As can be seen actual dimensions and masses correlate well with specifications set.
An apparent deviation in sitting and standing height is explained by the fact that these dimensions are measured in a fully erect posture while the dummy is assembled with the head tilted 27° forward. To enable comparison with an erect posture the dimensions measured via T1 are included in Table 1 as well. For this dimension good correlation is obtained.

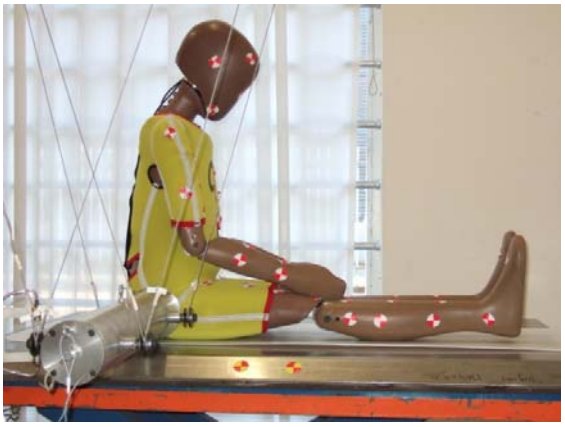

Figure 6. Q10 Prototype in pelvis certification test.

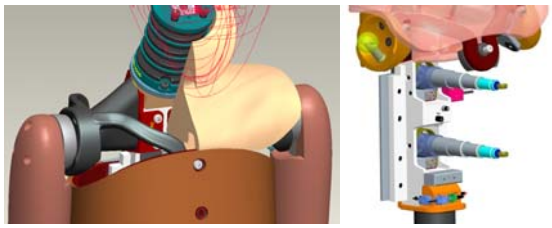

Figure 7. Shoulder design (initial concept) and double IR-Traccs in thorax.

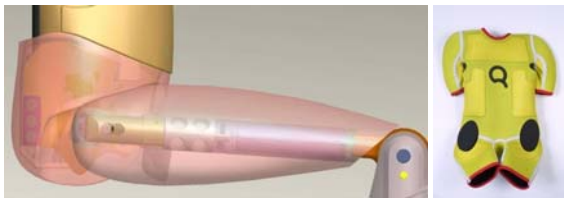

Figure 8. Detail of sit-standing pelvis design and suit with patches intended to prevent belt intrusion.

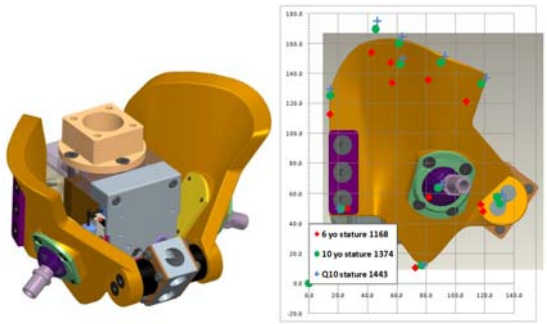

Figure 9. Pelvis design based on WorldSID 5th and comparison against bone anthropometry data from [6].

In addition to the sitting and standing height the chest circumferences show deviations. Actual dimensions are smaller than specified values because the soft muscle tissue at nipple and axilla level is not represented in the dummy. When considering the thickness of the suit (6 mm) which, to a degree, represents the flesh dummy values are much closer to the target.

The mass of some prototype parts revealed to be low within the mass tolerance for the upper and lower arms. With an addition of some ballast items to the upper arms, ~50 gram each, lower arms, ~70 gram each, and pelvis, ~980 grams, the mass was increased close to nominal weight. In design updates for the production version this was corrected adding mass to the related body parts.

For the head biofidelity three criteria for drop tests on a rigid plate were defined and evaluated [10]:

- Frontal 130 mm drop height: Biofidelity corridor limits based on EEVC scaling 113.1 – 194.2 *g*.
- Lateral 130 mm drop height: Biofidelity corridor limits based on EEVC scaling 116.4 – 200.0 *g*.
- Lateral 200 mm drop height: Biofidelity corridor limits based on ISO TR9790 107 – 161 *g*.

Figure 10 gives resulting accelerations for these conditions together with the corridors. The head of the prototype meets the frontal (130 mm) and lateral (130 mm) low in the EEVC corridors and meets the lateral (200 mm) high in the ISO/TR9790 corridor. During the prototype evaluation the approach to aim for simultaneously compliance with the EEVC and ISO/TR9790 corridor was found to be not feasible, therefore the EEVC corridors were selected to be the priority. As the skin stiffness generally will increase over time it was recommended to increase the stiffness of the head such that its performance is at the lower side close to the middle corridor [11].

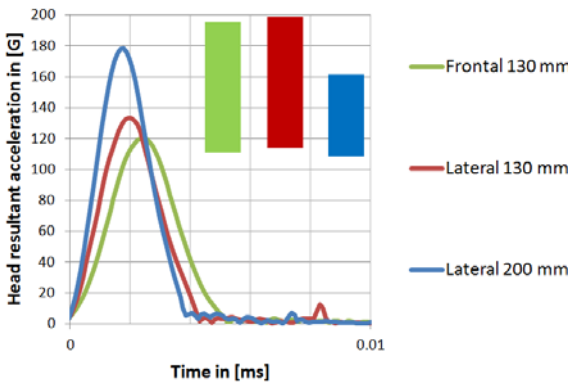

Figure 10. Head drop biofidelity results.

For the neck biofidelity requirements in flexion, extension and lateral flexion were defined. Figure 11 shows neck flexion bending performance in a Part

572 pendulum test with respect to the corridors defined [11]. The flexion response is in the lower range of the corridor and the rise in stiffness that should occur around 35° of head rotation is slightly late, starting around 45°. The slope in stiffness rise is correct. An improved performance could be obtained by increasing the rubber stiffness, but that would affect the fracture toughness and therefore the durability of the part. Another possibility is to change the neck mould, but this may affect the response in other directions which was not preferred.
Figure 12 gives neck extension bending performance in a Part 572 pendulum test in comparison with the biofidelity corridor [11]. It can be concluded that the extension performance fits the corridor very well. No further adjustment was deemed necessary.
Figure 13 shows the neck lateral flexion bending performance in a Part 572 pendulum test in comparison with the biofidelity corridor [11]. Up to 45° of head lateral flexion the performance is in the right order of magnitude but the rise in stiffness for large rotations is not followed.

Figure 14 shows shoulder pendulum force versus timein comparison with the biofidelity corridor. The test is done using an 8.76 kg pendulum at an impact speed of 4.5 m/s. It can be observed that the initial response of the shoulder is too stiff. In relation to this

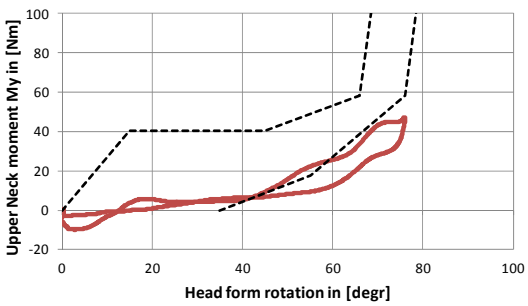

Figure 11. Neck flexion moment versus head rotation at 6.6 m/s.

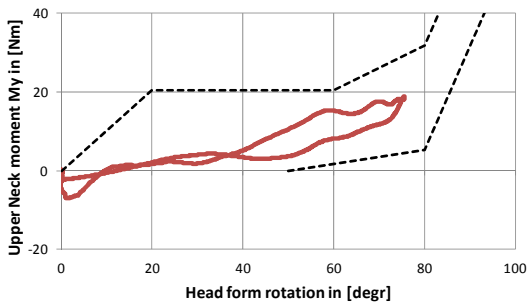

Figure 12. Neck extension moment versus head rotation at 4.3m/s.

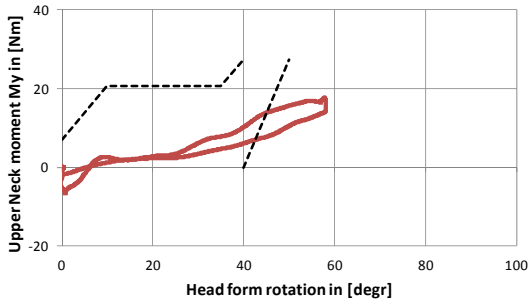

Figure 13. Neck lateral flexion moment versus head rotation at 3.9 m/s.

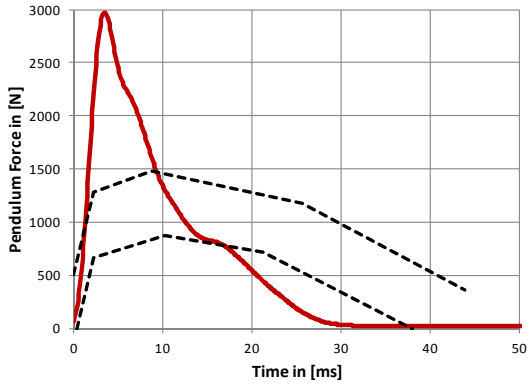

Figure 14. Lateral shoulder impact force versus time.

result it should be noted that the Q10 is an omni-directional dummy and performance tuning in either direction will affect the performance in the other direction. In the EPOCh project an optimal balance was sought in both directions with the focus on frontal impact. As shown below identical trends with regards to lateral impact performance are observed for thorax and pelvis region. Hence the stiffness distribution in side is balanced between these body regions, avoiding dominance of a single body segment in absorbing loads.

For the frontal biofidelity of the thorax two pendulum test impact speeds were specified: 4.31 and 6.71 m/s. Figure 15 provides pendulum force versus rib displacement in impact direction. Rib displacements are obtained by averaging the measured values in upper and lower chest IR-Traccs. It can be observed that the rib cage response meets the corridors reasonably well, especially for the 6.71 m/s impact. For the lower impact speed at 4.31 m/s the response is somewhat above the corridor. However, compared to other Q family members the frontal thorax performance is much better [12].

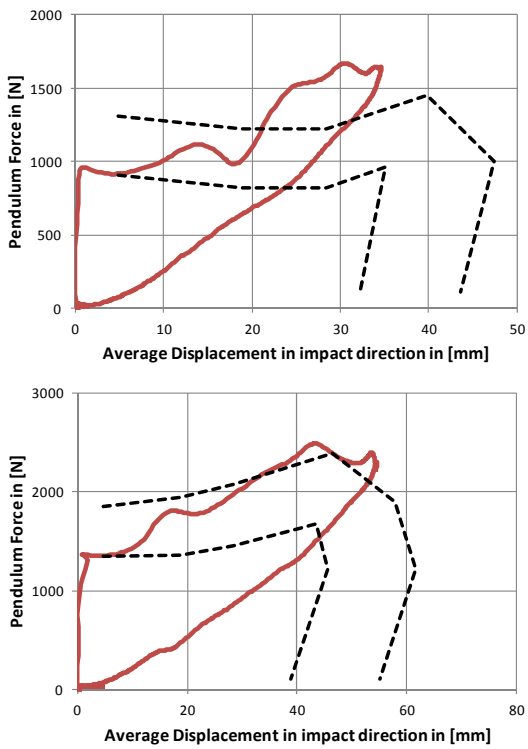

Figure 15. Thorax frontal pendulum impact 4.31 m/s (top) and 6,71 m/s (bottom).

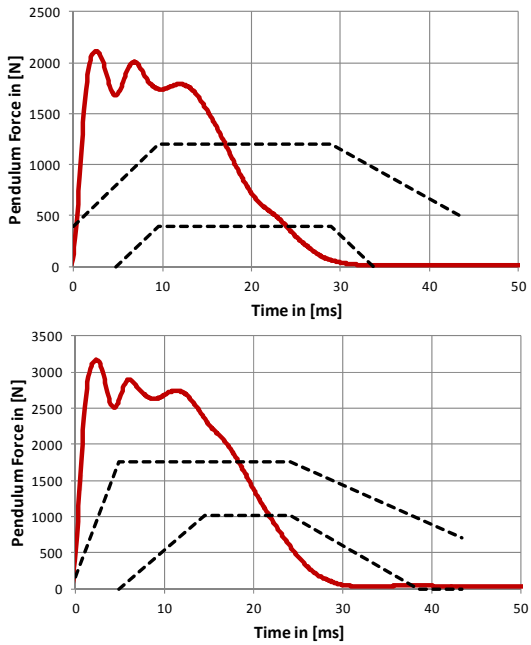

Figure 16. Thorax lateral pendulum impact 4.31 m/s (top) and 6,71 m/s (bottom).

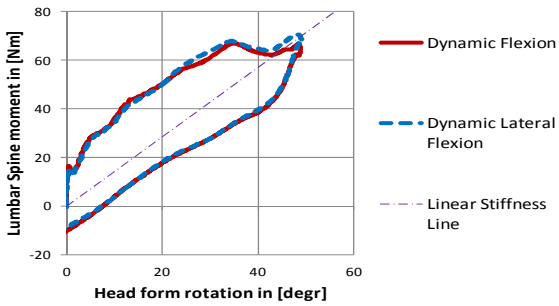

Figure 17. Lumbar Spine dynamic and static stiffness's (pendulum impact speed 4.53 m/s).

For the lateral biofidelity of the thorax two pendulum test impact speeds were specified: 4.31 and 6.71 m/s. Figure 16 gives results in comparison to the biofidelity corridors [11]. As for the shoulder the initial response overestimates the stiffness. Although performance tuning might be applied this would affect the frontal performance and introduce an imbalance with the shoulder and pelvis performance under lateral loadings.

The lumbar spine is made of a cylindrical rubber column; hence performances in frontal and lateral flexion are identical. Figure 17 gives test results obtained from pendulum impact tests. The dynamic stiffness is about 80 Nm/56° = 81.9 Nm/rad. This is slightly higher than the targets set for flexion (68.6 Nm/rad) and for lateral flexion 71.4 Nm/rad [11]. This result was considered to be acceptable.

Figure 18 gives the lateral pelvis impact performance in terms of pendulum force versus time. Again results are shown in comparison with the biofidelity corridor [11]. The pelvis response is in line with the lateral shoulder and thorax responses, showing too high stiffness. During the lateral pelvis impact tests a bottoming-out contact between the iliac wing and the sacrum block was observed for impact speeds of 4.0 m/s and above. This should not occur until the impact speed exceeds 5.2 m/s.

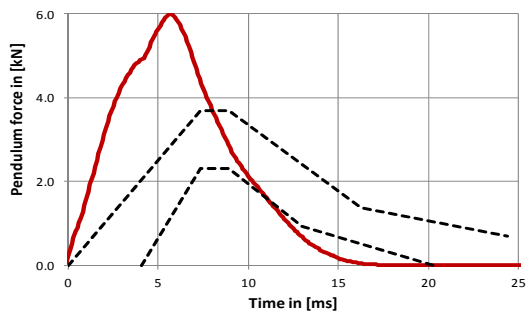

Figure 18. Pelvis lateral pendulum impact at 5.2 m/s.

When considering the side impact performance in the different regions it can be concluded that shoulder, thorax and pelvis pendulum impact responses largely exceed corridors in the initial phase. The stiffness in all regions is too high and further improvements for this configuration is needed (and being worked on as described below).

INJURY RISK FUNCTIONS

To apply the dummy it is necessary to specify injury criteria, risk functions and thresholds which are appropriate to this age and size of occupant. With adult humans the conventional approach taken to derive injury risk functions has been to conduct representative tests around the injury threshold with Post-Mortem Human Subjects (PMHS). These tests are then repeated with the dummy and the relevant dummy output compared against the observed risk of injury for the PMHS. By following this process, dummy-specific injury risk functions are defined directly relating a dummy measurement with the risk of injury for a human. Unlike the adult situation, however, there is very little biomechanical data from which specific injury risk functions for children can be derived. As alternatives, two approaches have been used [12]:

- Perform accident reconstructions using the child dummy under development.
- Scale adult injury risk functions and/or criteria to be relevant to the child size (dummy) being investigated.

The European Enhanced Vehicle-safety Committee (EEVC) Working Groups 12 and 18 used the accident reconstruction data developed within the European Commission (EC) CREST and CHILD projects to help develop risk functions for the Q3 dummy [12]. These functions were updated within the CASPER project [13].

Accident reconstructions with the newly developed Q10 were beyond the scope of the EPOCh project. As an alternative the EPOCh project took the second approach and scaled adult injury risk functions in an attempt to make them relevant for the older child dummy. To provide a comparison, the risk functions developed for the Q3 by EEVC WGs 12 and 18 were scaled up to the Q10 using the same formulae.

Previously, many authors have published techniques for scaling biomechanical measurements to different sizes of subject [14], [15], [16], [17]. While the general principle behind the scaling remains consistent, each of the publications seems to adopt different specific details. EPOCh therefore reviewed available scaling methods for each body region and dummy measurement. The review considered whether there are any new material property data available to aid the scaling process and if the output was reasonable.

Table 3. Proposed injury criteria for use with the Q10 dummy in UN Regulation No. 44 frontal impact conditions [11]

Measurement	Threshold
Head 3 ms exceedence	80 *g*
Head horizontal excursion	465 mm
Head vertical excursion	885 mm
Neck tension	†
Neck flexion	125 Nm
Neck extension	37 Nm
Chest deflection (either IR-Tracc)	56 mm
Chest 3 ms exceedence	45 *g*

† To be set after further testing with the Q10

The scaled injury risk functions or criteria were then compared with initial test results with the Q10 dummy under Regulation 44 conditions. Associated with this comparison has been an assessment of the feasibility for CRS manufacturers to meet prospective criteria. This has also been balanced with pragmatic expectations of how well the criteria may relate to current CRS performance and real world accidental injury incidence. The limits for the Q10 dummy resulting from this approach and to be used in UN Regulation No. 44 frontal impact conditions are summarised in Table 3. A more detailed description of the full EPOCh injury risk review is provided in [11]. Further work on the thresholds is needed to arrive at final values for frontal and derive values for side impact.

THIRD PARTY EVALUATION

Following the EPOCh evaluations two instrumented Q10 prototype dummies were made available to third parties for further evaluation testing. A wide variety of tests were performed by research labs, restraint manufacturers, OEMs and consumer organisations world-wide to check on the dummy performance in a vehicle environment. The tests included sled tests on a body in white as well as full-scale crash tests. Different restraint configurations were tested considering belts with and without pretensioner and belts with and without load limiter in combination with different child restraint types. Variations in test conditions included tests with sled buck rotation left

and right, with and without seat in front and partial overlap to the left and right. In some tests the dummies were equipped with add-on features, such as abdomen sensors and lap shields to prevent belt intrusion between the pelvis and the thigh.

Figure 20 shows some typical test results. Values for head 3 ms exceedence and upper neck bending My are depicted in cross plots against chest 3 ms exceedence. Results are normalised with respect to thresholds from Table 3. Results from the EPOCh project are included for reference (grey coloured markers). Chest acceleration 3 ms is generally high in NPACS sled tests (45 to 70 *g*) performed in EPOCh and low in BIW sled tests (35 to 30 *g*). The UN Regulation No. 44 tests performed in EPOCh show values in the middle range (25 to 50 *g*). For the upper neck My (extension) high values are observed in some tests. In most cases this can be attributed to impact loads upon rebound. In tests with pretensioner and load limiter a high extension moment may occur at the end of the loading phase (see e.g. Figure 19). Studies using a detailed finite element model of the Q10 dummy are on-going to investigate the root cause of this phenomenon. The high head acceleration 3 ms exceedence results found in some tests was also attributed to rebound impacts.

Feedback was provided on several dummy performance issues, the most important of which included:

1) Belt interaction in the pelvis region: lap belt penetrating between pelvis and thigh;
2) Belt slip towards the neck: observed after introducing Cordura top layer in the suit for durability;
3) Side impact performance: to be improved and, if possible, instrumentation to be added in shoulder region (e.g. shoulder load cell);
4) Durability of various dummy parts.

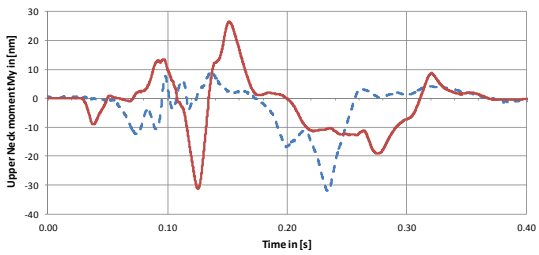

Figure 19. Upper Neck moment My for test with pretensioner and load limiter (red, solid line) and without (blue, dashed line).

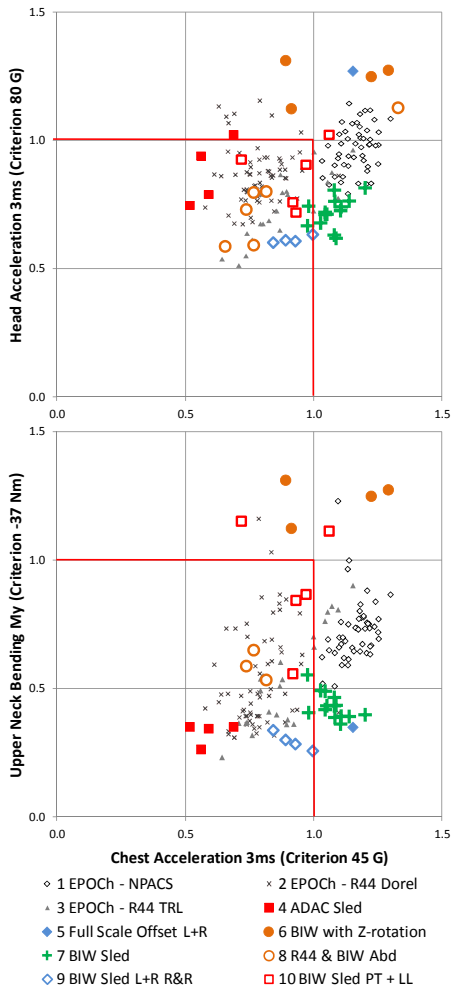

Figure 20. Maximum parameter values in EPOCh and 3rd party tests (normalised w.r.t. criteria set): Head acceleration 3 ms exceedence versus chest acceleration 3 ms (top); and upper neck My versus chest acceleration 3 ms exceedence (bottom).

DUMMY UPDATES FOR Q10 PRODUCTION VERSION

Following the testing with prototypes efforts were made to develop a production version Q10 dummy. Remarks related to durability, performance and handling of the dummy forwarded by the EPOCh and third party test programs were addressed. In the following a brief overview of the main changes is provided. A full overview is provided in [18].

Head and Neck - Additional dimple markers were added to the head for accurate dummy positioning.

Also the biofidelity was aligned with the EEVC requirements by making the response stiffer.
For neck no changes were introduced other than adding a lifting strap for handling, and reorientation of some of the washers.

Thorax / shoulder complex - The rib cage of the prototype dummies was produced using Ureol material which was recently banned under the REACH regulation. The new material formulation, also applied in other Q dummies was adopted. Figure 21 and Figure 22 compare the performance of production version rib cages with new material to the prototypes in frontal and lateral impactor biofidelity tests. Essentially identical responses are obtained.
Shoulder durability issues were reported, with the rubber tearing from the end plate. This failure was caused by high belt loading at top of arm in tests with the belt slipping over the shoulder onto the arm. As a countermeasure a stronger internal wire was applied in combination with a stress relief at the attachment of the rubber to the end plate (see Figure 23). This updated design was already used in the third party testing program. No further failures were reported, indicating that durability was improved.

Abdomen and Lumbar Spine - During tests with the prototypes severe ballooning of the abdomen was observed (see Figure 24). This part consists of a foam block with PVC skin. It is probable that air could not escape from the single vent hole fast enough, so six more holes were added evenly to the top rear and bottom of the skin. As the abdomen is soft it is not expected that this modification influences the dynamic response. However, this is to be evaluated in future testing. The lumbar spine only had very minor changes (e.g. change to screws with socket heads).

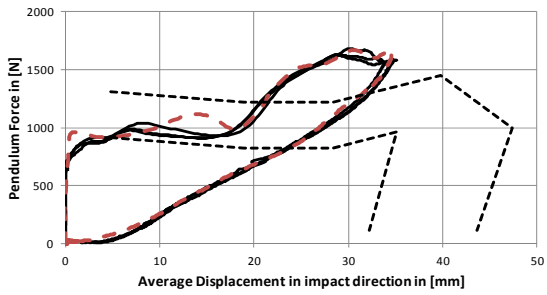

Figure 21. Performance of production version dummy in frontal thorax biofidelity test (solid black lines production dummy tests (3 off), dashed red line prototype).

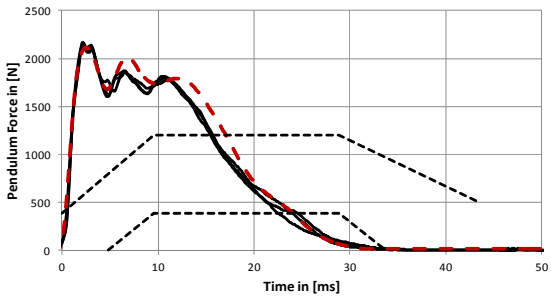

Figure 22. Performance of production version dummy in lateral thorax biofidelity test (solid black lines production dummy tests (3 off), dashed red line prototype).

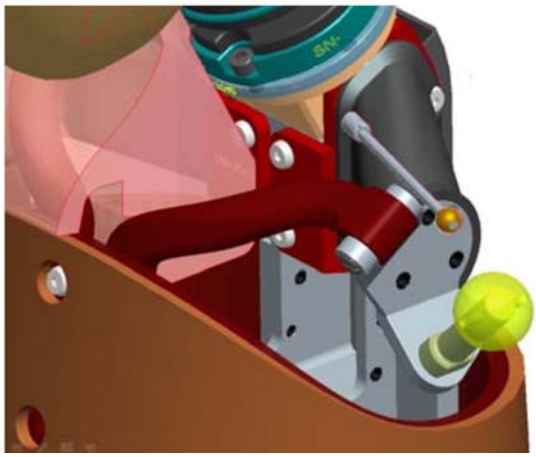

Figure 23. To reinforce the shoulder under loads from outboard belts the internal cable was reinforced and oriented more horizontally.

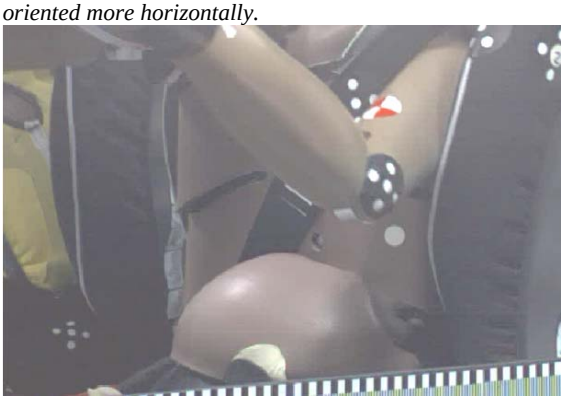

Figure 24 –Test without suit showing ballooning of the abdomen.

Pelvis - In the lower torso region the prototypes were 1660 grams too light and a temporary ballast weight (980 grams) was added to the pelvis to compensate. For the production dummy mass was added to the abdomen, pelvis flesh and pelvis bones, and some steel parts in the pelvis were replaced with tungsten.

DAS ballast was also added to allow for DAS integration into the sacrum. The changes resulted in a total mass increase of ~1550 grams bringing the total mass of the lower torso up to 9590 grams. This is close to target (9700 grams) specified in Table 2. The remaining 110 grams is consumed by the wire mass.
As with the thorax the pelvis flesh and bone material was banned due to the REACH regulation. Replacement materials as applied in the other Q dummies were introduced and tuned to provide identical performance and improved durability.
In lateral pelvis impactor tests contact between the iliac wing and the sacrum block was observed from impact speeds of 4.0 m/s onwards. To raise this contact to a higher impact speed the clearance between iliac wings and sacrum block was increased. Also the pubic buffers were stiffened. Future lateral pelvis testing is planned to evaluate the performance of these updates.

Arms - In the third party testing fracturing of the lower arm flesh at the wrist section occurred upon impact against the front seat. To resolve this failure tougher flesh material has been introduced in combination with rounded edges to the lower arm bone end. Like other items the performance of this solution is to be investigated in future testing. In case fracturing in the wrist section remains it might be decided to change the geometry of the hands from stretched to fist configuration.
Other modifications to the arms included the introduction of locking threads for the shoulder joint screws to maintain 1 *g* friction and adding friction screws on both sides of the elbow to balance loading and prevent damage in this joint. For handling purposes marker dimples were added to the wrist.
Mass was raised to the weight specified in Table 2, avoiding the ballast weights applied in the prototypes.

Legs - As for the arms tougher flesh material was introduced to the lower leg improve durability. Also the lower leg bone was extended for this purpose. In various tests excessive sliding of the upper leg flesh along the femur bone towards the knee was observed, introducing damage to the flesh in the pelvis area. To prevent sliding of the flesh along the metal bones observed in the production version, the flesh is locked to the bone by adding a retainer in an access hole for the femur load cell (see Figure 25).
Various minor modifications were introduced in the knee such as anti-fretting plastic washers and friction stops to the knee stop pins.
Mass was raised to the weight specified in Table 2.

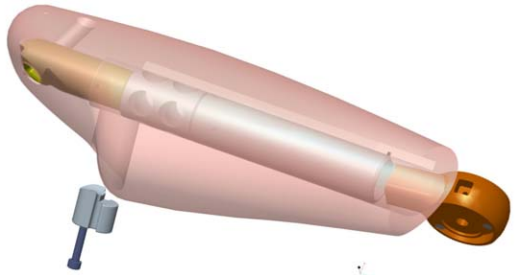

Figure 25. Upper leg flesh with insert.

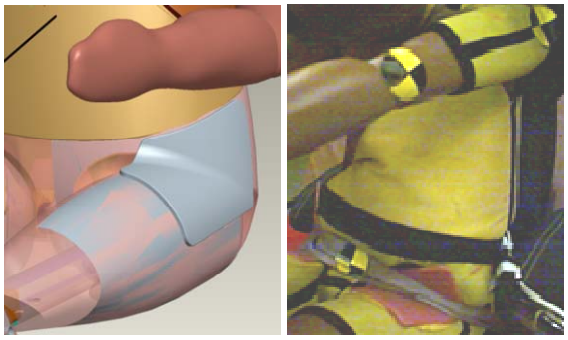

Figure 26. Lap belt shield design (left) and shield performance in dynamic condition (right).

Suit - In the prototype, hip patches where introduced to try and prevent lap belt intrusion into the hip pelvis gap. This did not work and profiled, stiffer, hip shields have been incorporated for further evaluation testing (see Figure 26).
A zip was added in the abdomen area to help with fitting and umbilical wire access. The front chest panel was covered with Cordura for better durability.

SIDE IMPACT PERFORMANCE – FE STUDY

In an attempt to define future improvements for side impact performance a finite element study into possible concepts has been conducted (see Figure 27). The initial focus was on the shoulder and thorax performance for interaction with vehicle restraint systems. To avoid any negative effects on the frontal impact performance it is proposed to introduce a side impact kit with a minimal number of components that are to be exchanged for side impact applications. The configuration evaluated through simulation included:

1) Omitting the lower arms;
2) Plastic upper arm bone (instead of aluminium);
3) Softened shoulder rubber and arm flesh.

Results for shoulder pendulum impact forces are depicted in Figure 28. Omitting the lower arm only

does not have a significant influence of the shoulder impact force as this part is remote from the impact location and due to interaction of the stiff arm (aluminium bone) with the thorax. When introducing a plastic bone in the upper arm (as used for the WorldSID 5th female dummy), shoulder forces were reduced. Softening of the shoulder rubber and arm flesh results in a further reduction, bringing forces close to the corridor. This design concept for improved side impact performance will be explored in more detail and if feasible realised in hardware for further evaluations.

An additional item for the side impact performance is the realisation of a shoulder load cell. Initial design efforts have started (see Figure 29). However, due to the shoulder concept with ball joint on an oblique pin, issues arise related to cross talk, non-linearity and hysteresis. Further efforts will be needed to realise an adequate solution.

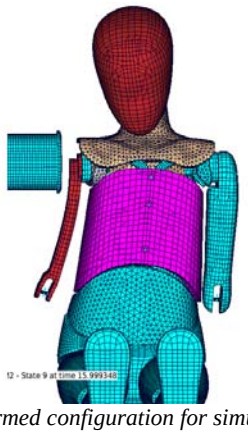

Figure 27. Deformed configuration for simulation with lower arms removed and upper arms realised with plastic bone (arm flesh in left arm removed for visualisation).

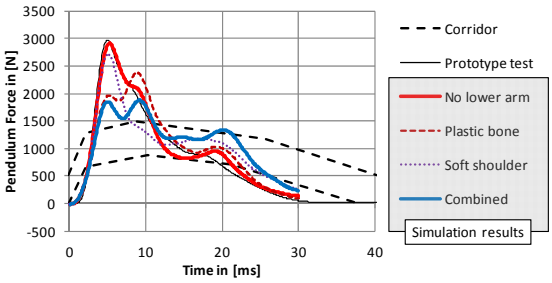

Figure 28. Shoulder impact pendulum force versus time Prototype test result (for reference) and simulation results: No lower arm, No lower arm + Plastic upper arm, No lower arm + Soft shoulder rubber and all three measures combined.

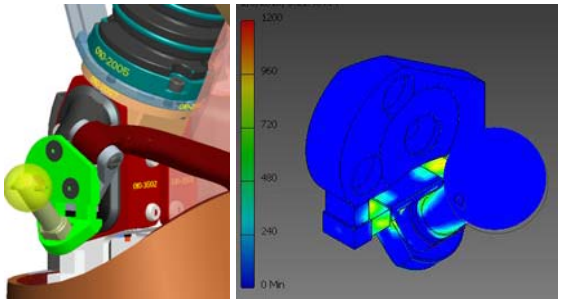

Figure 29. Shoulder load cell (green item in left plot) concept packaging and feasibility study.

MEASURING ABDOMEN LOADING WITH THE Q10 – FIRST STEPS

UN Regulation No. 44 specifies performance requirements for head excursion, chest acceleration and abdomen loading (by means of a clay insert between the lumbar spine and the foam abdomen block), using the P-Series dummies. Collision studies undertaken by EEVC WG 12 and 18, the CASPER and EPOCh projects indicate that it would be desirable to maintain the assessment of child restraint system performance at these body regions when the Q-Series is introduced into legislation [12, 19, and 20]. At present, the Q dummies have no method for detecting abdomen loading. It cannot be fitted with a clay insert and will require another solution. A potential solution is provided by the Abdominal Pressure Twin Sensors (APTS) developed at IFSTTAR during the CHILD and CASPER projects [21]. The APTS sensor consists of two cylindrical soft polyurethane bladders filled with a gel solution (see Figure 30). They are closed by aluminium caps in which pressure sensors are located. The bladders are implanted in holes drilled in the abdominal block of the dummy. In the CASPER project, risk curves were derived for sensors installed in the Q3 and Q6 [e.g. 13]. Risk curves for the Q10 are yet to be developed.

Various studies have shown that the lap part of the seat belt can become trapped in the gap between the legs and the pelvis in the Q-Series dummies [22]. The pelvis design of the Q10 differs from that of the other Q-Series dummies and minimises this gap. In addition, patches were stitched into the suit of the prototype Q10 to further limit belt intrusion. Nevertheless, the phenomenon was observed by participants in the third-party testing described earlier and a new solution has been developed consisting profiled hip shields (see Figure 26).

To investigate the use of the APTS sensors with the Q10 dummy and the capacity of the hip shields to

prevent belt intrusion into the gap between the legs and the pelvis a programme of three impact sled experiments was carried out. The Q10 was seated in a non-integral ISOFIX child restraint system (a booster seat) on the test bench defined in the draft new UN Regulation on "Enhanced Child Restraint Systems". It was exposed to a pulse defined in the draft Regulation (which is identical to that it UN Regulation 44). Three tests were done:

- Test #1: Reference test, no APTS or hip shields
- Test #2: Using APTS sensor but no hip shields
- Test #3: Using both APTS sensor and hip shields

The booster seat did not feature guides for the lap part of the seat belt, although severe abdomen loading was not expected in these experiments because the seat was approved to UN Regulation 44.

Figure 32 shows the interaction between the dummy and the seat-belt during each experiment. The abdomen sensors did not seem to influence the kinematics of the dummy or the way it interacted with the seat-belt (tests 1 and 2). The lap parts of the belt intruded partially into the gaps between the legs and the pelvis, but not to the same extent as that reported for other Q-Series dummies [see e.g. 18]. The abdomen 'ballooned' over the lap belt, but this seemed to reduce when the hip shields were used (test 3). The hip shields also helped to keep the lap part of the belt higher on the pelvis and away from the gap between the legs and the pelvis. Table 4 compares some of the main dummy measurements from the sled experiments. The Q10 had been used extensively prior to these experiments as part of the third-party testing described earlier. Although the dummy was inspected for damage, its schedule between the laboratories did not allow for regular certification and hence these data should be viewed in that context. The table shows that the abdomen sensors and the hip shields in this small programme, did not tend to influence the broader dummy measurements, but there were some exceptions and it would be worthwhile to continue to investigate this further.

Figure 30. APTS Abdominal pressure sensor (left) and abdomen with APTS inserted (right).

Evaluation tests as done by Takata in the third party testing programme also showed small changes in dummy readings when using the hip shields. See Figure 31. This was explained by small changes in the dummy kinematics when using the shields.

Relatively low levels of pressure were recorded by the APTS sensors, which was consistent with the low levels of abdomen loading observed in the videos and highlighted in Figure 32. The pressure was higher on the right side of the dummy, on the buckle-side of the seat belt. Beillas *et al.* [21] also reported low levels of abdomen pressure in booster seats that were used correctly, under UN Regulation 44 conditions; test bench and pulse.

These experiments were part of a wider programme supported by the European Commission (DG Enterprise and Industry) with the aim of investigating the state-of-the-art of the Q-Series dummies and sensors for measuring and assessing abdomen loading in the draft new UN Regulation. Further experiments and analyses by TRL and other members of the UN Informal Working Group on Child Restraint Systems are on-going with a view to proposing and validating a solution that can be implemented in the new Regulation.

Table 4. Q10 dummy measurements during the experiments

	Test #1 No sensor, no shield	**Test #2 Sensor, no shield**	**Test #3 Sensor and shield**
Head exc. (mm)	350	326	346
Head acc. 3ms (g)	62.9	66.3	78.6
Upper neck Fx (kN)	-0.98	-1.00	-1.17
Upper neck Fz (kN)	3.63	3.79	4.80
Upper neck My (Nm)	-16.6	-13.5	-18.5
Chest acc. 3ms (g)	34.0	32.8	35.4
Chest def. upp. (mm)	49.1	47.9	47.3
Chest def. low. (mm)	47.2	42.4	39.7
APTS left (bar)	No sensor	0.72	0.68
APTS right (bar)	No sensor	1.22	1.27

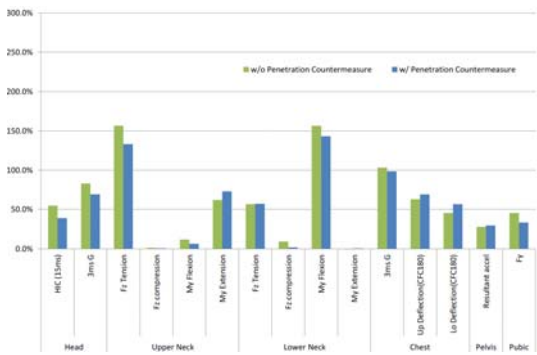

Figure 31. Influence of hip shields on dummy reading (data provided by Takata)

Figure 32. Q10 interaction with the seat belt: Test #1 No abdomen sensor and no hip shields (left); Test #2 Abdomen sensors without hip shields (middle); Test # 3 Abdomen sensors and hip shields (right).

DISCUSSION

Real-world car crash records shows that good achievements have been made over the past decades in reducing the number of fatally and severely injured children on European roads. Nonetheless further efforts are needed to improve the safety for this group of road users. The EU FP7 project EPOCh contributed to this by developing a Q10 dummy that represents adolescents.

In the EPOCh project prototype Q10 dummies were realised and extensively evaluated in UN Regulation No. 44 and NPACS test conditions [11]. Subsequently two dummies were forwarded to OEM's, suppliers and test houses world-wide to evaluate the dummy performance in a vehicle environment. Feedback and recommendations on design updates were collected for implementation in a production version of the Q10 dummy. The main remarks on the dummy performance included:

1) Belt interaction in the pelvis region: lap belt penetrating between pelvis and thigh;
2) Belt slip towards the neck: observed after introducing Cordura top layer in the suit for durability;
3) Side impact performance: to be improved and, ir possible, instrumentation to be added in shoulder region (e.g. shoulder load cell);
4) Durability of various dummy parts.

Various studies have shown that the lap part of the seat-belt can become trapped in the gap between the legs and the pelvis in the Q-Series dummies [22]. Based on this experience the pelvis of the Q10 was designed to have a minimal gap while maintaining the sit-standing concept of the Q dummies. This, even in combination with patches stitched into the suit, did not prevent the belt entrapment. A solution consisting of a profiled hip shields (see Figure 26) was developed and first evaluations do indicate that belt entrapment is reduced (see Figure 32). Sled tests also showed that the shields may affect dummy readings to some extent, requiring further investigations.

The shoulder belt slippage towards the neck was not that profound in EPOCh testing when a soft neoprene suit was used. To prevent reported damage to the suit under belt loading a Cordura top layer was added for use in the third-party testing programme. This resulted in an improved durability (no damage was reported). However, the reduced friction between belt and suit might promote the belt slippage towards the neck. Further studies are necessary on this item also considering location of the instrumentation in the dummy chest as well as the influence of external items like belt geometry. Recent studies have shown the influence of the belt position on the belt slippage in other Q dummies [23].

A key item for future improvement concerns performance in side impact. Although it is generally recognised and acknowledged that the dummy design was focused on frontal performance, updates in side impact were recommended to support restraint design for this configuration. To avoid any negative effects on the frontal impact performance it is proposed to introduce a side impact kit with modified arm and shoulder rubber which are to be exchanged for side impact applications. Concepts are being explored using a finite element model of the Q10. Simulations show that a significant improvement of the side performance can be obtained, with shoulder impact

loads close to the corridor, but this is to be further evaluated by realising a design. In view of the size of the Q10 dummy, being close to an adult, it is also proposed to evaluate its performance in a full-body side impact configuration. Previous PMHS tests from Wayne State University on small females may serve as basis for this. Results from these tests in which the shoulder, thorax and pelvis were impacted simultaneously in well-defined conditions served as basis for the requirement definition of the small female WorldSID 5th dummy. For application to the Q10 dummy response data and requirements are to be scaled assuming changes in material properties and geometry and test should be repeated using the Q10 dummy to evaluate its performance in the distributed loading conditions. In support of these activities a shoulder load cell is currently being developed.

During the EPOCh and third party testing various issues related to durability and handling of the Q10 dummy were listed. Issues on the shoulder as raised by EPOCh were implemented before testing by third parties and found to be effective (no further damage was reported). Various other items like local failures in the flesh are being addressed in the production version of the dummy which is currently being realised.

First proposals for frontal injury criteria were made by the EPOCh project considering scaling of existing adult data. Results were cross checked by scaling available child data. As for studies in risk curves and thresholds in general caveats had to be taken into consideration when defining these first proposals for the limits. Each of the scaling approaches available from literature makes numerous approximations to keep the formula relatively simple to calculate. As an example geometric similitude is often cited as an assumption, so that the smaller body is the same as the larger in all aspects but size. Such assumptions and approximations will affect the scaling ratios and results. However, it is hoped that those effects are relatively small to the other aspects being taken into consideration.
In view of the above it can be concluded that further work on proposed criteria and thresholds is needed. In this work pragmatic decisions based on an expected real world performance of CRS could be considered.

CONCLUSION

The Q-Series dummy family is being completed with the development of a Q10 dummy representing larger children. Prototype dummies were developed and evaluated in the EU FP7 EPOCh project in UN Regulation No. 44 and NPACS conditions. Further testing was performed by OEM's, suppliers and test houses world-wide to explore the performance of the dummy in a vehicle environment. The testing resulted in various items for improvement which are currently being realised in a production version of the dummy. Further work is needed though to improve the performance of the dummy in side impact. For frontal impact phenomena related to belt slip on the thorax, belt penetration in the pelvis region, neck loadings observed when using advanced restraints and the implementation of abdominal sensors need further investigations. In parallel further work is needed on injury criteria and thresholds, including establishing means for abdominal loadings.

ACKNOWLEDGEMENT

The authors would like to thank the European Commission for commissioning and funding the EPOCh project in which the Q10 prototype dummies were developed. The authors would also like to thank the Commission for funding the experiments to measure abdomen loading with the Q10. Any views expressed in this paper are not necessarily those of the European Commission. Special thanks also to all those that contributed to the evaluation testing of the Q10 dummy providing valuable feedback on the dummy design.

REFERENCES

[1] Data from the European Road Safety Observatory. See www.erso.eu
[2] CASPER-project deliverables, CASPER – Child Advanced Safety Project for European Roads, EC-Project number SCP7-GA-2009-218564 (www.casper-project.eu)
[3] EPOCh-project deliverables, EPOCh – Enabling Protection for Older Children, EC-Project number SCP7-GA-2009-218744 (www.epochfp7.org)
[4] Waagmeester, C.D., Mark Burleigh, M., Hynd, M., Longton, A., Salters, E., Girard, B., (2009). Q10 dummy Development Status Review, Protection of Children in Cars Conference, Munich December 2009

[5] Twisk, D. and Beusenberg, M.C. (1993). "Anthropometry of Children for Dummy Design", ECOSA Product Safety Research Conference, Amsterdam, The Netherlands.
[6] Reed, M.P., Sochor, M.M.,Rupp, J.D., Klinich, K.D. and Manary M.M. (2009). Anthropometric Specification of Child Crash Dummy Pelves through Statistical Analysis of the Skeletal Geometry, Journal of Biomechanics 42.
[7] Waagmeester, K., Burleigh, M. and Lemmen, P. (2009). EPOCh Project Deliverable D1.2 – Biomechanical Requirements and Design Brief.
[8] CREST-project final report (2000), CHEST - Child Restraint System for Cars, EC-Project number SMT4-CT95-2019
[9] CHILD-project final report (2006), CHILD – Child Injury Led Design, EC-Project number G3RD-CT-2002-00791
[10] Waagmeester, C.D., Mark Burleigh, M., Hynd, M., Longton, A., Salters, E., Girard, B. (2010). Q10 dummy Development Status Review – Biofidelity Performance Validation, Protection of Children in Cars Conference, Munich, Germany.
[11] Hynd, M., McGrath, M., Waagmeester, C.D., Salters, E., Longton, A., Cirovic, S. (2011). EPOCh Project Dissemination, Protection of Children in Cars Conference, Munich, Germany.
[12] Wismans, J., Waagmeester, K., Le Claire, M., Hynd, D., de Jager, K., Palisson, A., van Ratingen, M., and Troisseille, X. (2008). Q-dummies report: advanced child dummies and injury criteria for frontal impact. Retrieved November 8, 2012 from: http://eevc.org/publicdocs/publicdocs.htm
[13] Johannsen H., Trosseille, X., Lesire, P., Beillas, P. (2012). Estimating Q-Dummy Injury Criteria Using the CASPER Project Results and Scaling Adult Reference Values, Proceedings of IRCOBI Conference, Dublin, Ireland, 2012.
[14] van Ratingen, M. R., Twisk, D., Schrooten, M., Beusenberg, M. C., Barnes, A. and Platten, G. (1997). Biomechanically based design and performance targets for a 3-year old child crash dummy for frontal and side impact. Child occupant protection 2nd symposium proceedings, 12 November 1997 (SAE technical paper 973316), Orlando, Florida, U.S.A.: Society of Automotive Engineers, Inc. (SAE): Warrendale, PA, U.S.A.
[15] Irwin, A. and Mertz, H. J. (1997). Biomechanical basis for the CRABI and Hybrid III child dummies. Child occupant protection 2nd symposium proceedings, 12 November 1997 (SAE technical paper 973317), Florida, U.S.A.: Society of Automotive Engineers, Inc., 400 Commonwealth Drive, Warrendale, Pennsylvania, U.S.A.
[16] NHTSA (1996). Technique for developing child dummy protection reference values. Child injury protection team.
[17] Mertz, H. J., Irwin, A. L. and Prasad, P. (2003). Biomechanical and scaling basis for frontal and side impact injury assessment reference values. Stapp car crash journal volume 47: papers presented at the 47th Stapp car crash conference (SAE technical paper 2003-22-0009): Society of Automotive Engineers, Inc. (SAE): Warrendale, Pennsylvania, U.S.A.
[18] Product Information from Humanetics Innovative Solutions (2013). Q10 Users Manual, Rev-A, Plymouth, MI, USA
[19] Kirk, A. (2012). Summary of CASPER accident database. Paper presented at Cover Child Safety Final Workshop: CASPER and EPOCh, 13-15 June 2012, Berlin. Retrieved October 17, 2012 from: http://www.biomechanics-coordination.eu/site/en/documenten.php
[20] Visvikis, C., Pitcher, M., Girard, B., Longton, A. and Hynd, M. (2009). Literature review, accident analysis and injury mechanisms. EPOCh Project Deliverable, Work Package 1, Task 1, May 2009 Retrieved October 18, from: http://www.epochfp7.org/Publications.aspx
[21] Beillas, P. , Alonzo, F., Chevalier, M., Johannsen, H., Renaudin, F., Lesire, P. (2012), Abdominal Pressure Twin Sensors for the Q dummies: from Q3 to Q10, Proceedings Icrash Conference, Milan, Italy.
[22] Beillas, P. and Alonzo, F. (2010). Report associated with the deliverable D.1.2: auxiliary equipment for Q3 and Q6 to improve belt interaction response. Retrieved October 8, 2012 from: http://www.casper-project.eu/results/
[23] Johanssen, H. and Holtz, J. (2013), "Proposal for Belt Anchorage Points", Presentation to the GRSP Informal Group on Child Restraint Systems, 36th meeting, 29-01-2013, Paris, France.

TESTING OF THE WORLDSID-5F TO SUPPORT INJURY RISK FUNCTION DEVELOPMENT AND ASSESSMENT OF OTHER PERFORMANCE ISSUES

Jolyon Carroll
Oliver Goodacre
David Hynd
TRL
United Kingdom
Audrey Petitjean
Centre Européen d'Etudes de Sécurité et d'Analyse des Risques (CEESAR)
France
Paper Number 13-0193

ABSTRACT

Global Technical Regulation Informal Groups have directed a WorldSID Technical Evaluation Group to document the performance of the WorldSID-50M (50th percentile male) and 5F (5th percentile female).

This research contributes to the evaluation of the WorldSID-5F. It documents pendulum and sled tests carried out to aid both the biofidelity assessment by the WorldSID Informal Group and injury risk development by ISO/TC22/SC12 Working Group 6 (WG6).

Issues concerning contacts between the pelvis bone and lumbar-sacral components, and interaction between the pelvis flesh and lowest rib, were also investigated.

The WorldSID-5F test programme consisted of 26 sled and 51 pendulum tests, in a variety of impact configurations, matching the biofidelity and injury risk test requirements specified by ISO.

The WorldSID-5F generally performed as expected. The dummy biofidelity was shown to be outside of several ISO targets. However, this performance has been demonstrated previously with the Revision 1 release of the dummy and may still represent an improvement over other, currently available, side impact dummies.

Dummy handling was found to be good at typical vehicle test severities. Test-to-test use of the dummy was straightforward; however, durability is predicted to be a problem when trying to achieve the high test severities needed in the development of injury risk functions.

Contacts were detected between the pubic symphysis and anterior-inferior corner of the sacral load cell mounting and between the iliac wing and the lumbar spine mounting bracket. These contacts occurred in sled and pendulum tests at severity levels substantially below those specified for many of the biofidelity and injury risk tests.

In the pendulum test programme contacts were also detected between the shoulder and the neck bracket. Such a contact provides an uninstrumented load path.

INTRODUCTION

The WorldSID 50th percentile male crash test dummy (WorldSID-50M) was developed by a world-wide collaborative effort that was managed by the ISO WorldSID Task Force under a tri-chair representing Europe, the Americas, and Asia-Pacific. With an overall ISO biofidelity rating of 7.6 the WorldSID-50M offers a biofidelity improvement over other currently available side impact dummies such as the BioSID, ES-2, EuroSID-1 and USDOT-SID [1].

More recently, the WorldSID 5th percentile female dummy (WorldSID-5F) was developed by the European FP6 project APROSYS. The design of the 5F dummy was based on the 50M with the objective to create a family of dummies that give a consistent direction to the design of vehicle safety

structures and restraint systems. Eggers *et al.* [2] reported that the WorldSID-5F has an overall ISO biofidelity rating of 7.6, equal to the 50M. Other aspects of the WorldSID-5F dummy performance, such as repeatability and reproducibility (R&R), were intended to be comparable with the WorldSID-50M performance.

The objectives of the work described in this paper were to:

- Contribute to the assessment of WorldSID-5F biofidelity by:
    - Contributing to the ISO WG6 work to scale side impact biofidelity test conditions
    - Contributing pendulum impactor and sled biofidelity tests to complement the testing carried out by other participants in the GTR WorldSID Informal Group
- Contribute to the development of injury risk functions for the WorldSID-5F by:
    - Contributing to the ISO WG6 work to define injury risk functions for the WorldSID-5F
    - Contributing pendulum impactor or sled injury risk tests to complement the testing carried out by other contributors to the GTR WorldSID Informal Group.

This paper documents the TRL test work undertaken on behalf of the European Commission with the WorldSID-5F (Build level = SBL C, Serial number SN002). It was performed whilst collaborating closely with ISO Working Groups 5 and 6 and their efforts to define the biofidelity targets and injury risk functions for use with the WorldSID-5F. The next section of the paper documents the process used by ISO WG6 and the whole body of testing that would be completed ideally with each new side impact dummy.

ISO WORKING GROUP 6 REQUIREMENTS

As mentioned, the WorldSID-5F tests performed by TRL were used in the construction of injury risk curves specific to this dummy.

The method used for the development of the WorldSID-50M dummy injury risk curves (ISO/TC22/SC12/Technical Report TR12350: 2010E [3]) was applied to the WorldSID-5F female dummy. Dummy responses and injuries from paired dummy and Post-Mortem Human Subject (PMHS) tests, performed in similar test configurations were required. However, there were not enough 5th percentile female PMHS tests available in the literature. As a consequence, the samples of PMHS used to build injury risk curves for the WorldSID-50M were considered. The PMHS test configurations considered in ISO/TC22/SC12/TR12350 are presented in the Appendix in Tables 2 and 3.

It was necessary to determine the test conditions equivalent for a 50th percentile male and a 5th percentile female to be able to pair the WorldSID-5F responses and the PMHS injuries. The anthropometry from Schneider *et al.* [4] was used to calculate the scaling factors. The test conditions were defined by the impact surface geometry and the impact speed, plus the impactor mass for impactor tests.

The geometry of the impact surface was scaled in order to load the same body region for a 50th percentile male and a 5th percentile female occupant (some examples from the scaling of the Wayne State University sled test force plates are provided in Table 1). An equivalent test condition also means that the risk of injury is the same for a 50th percentile male and 5th percentile female occupant. This was made possible by scaling both the impact speed and impactor mass. The impactor mass was scaled based on the total body mass of a 50th percentile male and 5th percentile female. Based on a mass-spring-mass model, and given the scaling of the impactor mass, the impact speed was identical for a 50th percentile male and 5th percentile female.

Using the example of a thoracic impactor test, the test condition was considered to be equivalent if the same ribs were loaded for the 50th percentile male and the 5th percentile female and if the thoracic compression (deflection as a percentage of the chest depth) was the same.

Table 1.
Wayne State University sled test force plate dimensions

WSU, along the axis of the seat pan	Allowance for mid-sized male (mm)	Dimensions for UMTRI 5th percentile (mm)
Pelvis plate length from the seat back	284	242
Centre of the knee plate relative to seatback	542	461
Knee plate width	102	87
Knee plate height	203	173

The scaled test configurations were agreed on within the ISO/TC22/SC12/WG6 group and volunteering biomechanical experts.

In some cases, the new scaled test configurations for injury risk curve development deviated slightly from those previously generated for biofidelity assessments of small female dummies. Where differences occurred, priority was given to the test set-up needed for the injury risk work, as the biofidelity of the WorldSID-5F has been assessed previously [2].

EXPERIMENTAL WORK

To help meet the testing requirements specified by ISO WGs 5 and 6, pendulum and sled tests were carried out at TRL with the WorldSID-5F dummy. The methods used and the results derived from the ensuing tests are described in the next few sections. It should be noted that some of the original PMHS tests used a linearly guided impactor. Before undertaking the test programme, it was agreed with ISO WG6 that it would be acceptable to replicate these tests with a pendulum rather than have to use a linear impactor.

Pendulum testing

As mentioned earlier, the pendulum tests to be replicated for injury risk function development are described in ISO TR12350 [3]. The tests carried out at TRL with the WorldSID-5F are described below.

INRETS shoulder tests: a series of shoulder impactor tests. In the original testing, each PMHS was seated upright, without back support. Where an upright position with the WorldSID-5F is described, the thorax tilt sensor was positioned to read 20 degrees, approximately. This is because in the upright position the spine is about 20 degrees more upright than in the standard seated position. For the PMHS tests, the impactor face was centred on the glenohumeral joint. Each subject was impacted in the pure lateral direction, 15° rearward of lateral, and 15° forward of lateral. These three impact configurations were reproduced. For the WorldSID-5F in the lateral test, the impactor alignment was 17 mm anterior (forward) and 4 mm superior (above) to the centre of the three arm mounting bolts.

The impactor speed for the oblique tests was 1.5 m/s. The pure lateral tests were conducted at the three different speeds; 1.5, 3.5 and 6 m/s.

WSU shoulder tests: another series of impactor tests to the shoulder. For the PMHS the impact face was centred on the acromion of the subject and each PMHS was impacted in the pure lateral direction. To give a similar alignment for the WorldSID-5F, the centre of the impactor was aligned 43.5 mm superior to the centre of the three arm mounting bolts. The test speed for the WSU impacts was 4.5 m/s.

ISO TR 9790 Shoulder Test 1, as described in the ISO Technical Report 9790 [5], this is based on impactor tests conducted by the APR. The axis of the impactor was aligned with the centre of the shoulder joint (the centre of the three arm mounting bolts). The impact velocity was 4.45 m/s.
The requirements for this test specify the use of a 14 kg pendulum impactor. However, because the results from this test type are also useful for injury risk function development, the dummy was tested with a 14.7 kg pendulum. It is expected that the force and deflection recorded in these tests were greater than would be the case if the test had been performed with the prescribed 14 kg impactor.

ISO TR 9790 Thorax Test 1; For ISO Thorax Test 1 tests the dummy was seated upright with its arm raised so that the side of its thorax was clear to

be impacted. The face of the impactor was centred on the lateral aspect of the thoracic rib structure and the dummy's thorax was impacted laterally at velocities of 0.9, 4.3 and 6.1 m/s.
Regarding the vertical alignment, additional tests were carried out to investigate whether differences could be noticed between two subtly different alignments. The two options were:

1. Align the centre of the impactor with the middle of the 2nd thoracic rib
2. Align the lower border of the impactor with the lower border of the 3rd thoracic rib (position about 5 mm higher than Option 1)

In either case the arm did not interfere with the thoracic loading.

As noted in the previous section on the shoulder test, these thorax requirements specify the use of a 14 kg pendulum impactor. However, because the results from this test type are also useful for injury risk function development, the dummy was tested with a 14.7 kg pendulum. Again, it is expected that the force and deflection recorded in these tests were greater than would be the case if the test had been performed with the prescribed 14 kg impactor.

WSU/GM thorax tests use a setup very similar to that used for the ISO (HSRI-based) tests. The key difference between these and the other thorax tests, was the requirement to conduct these obliquely, 30 degrees forward of lateral. This was achieved by sitting the dummy on the bench normally, then rotating the bench through 30 degrees relative to the line of the pendulum action (so as to rotate the dummy about its z-axis). The alignment then translated around the thorax so as to still be centred horizontally to strike the most lateral aspect of the thorax. The vertical alignment was the same as the previous tests, taking the approach of picking the level which would be centred with the middle of the middle thoracic rib, if it had been struck laterally.

The impact speed for this test configuration was 6 m/s. Additionally, the original tests also indicate that a test at 8.7 m/s should be carried out. This higher test speed was not possible within the facility at TRL and without the likelihood of causing damage to the dummy and its instrumentation. Therefore, alternative tests were performed at tests speeds of 2, 3, 4, 5, 5.5 and 6 m/s to support the scaling up of results to predict output at 8.7 m/s.

The peak y-displacement against test speed is shown in Figure 1. The results show that there is a reasonable linear correlation between test speed and rib displacement and therefore it should be possible to use this method for extrapolation to higher test speeds.

UMTRI thorax tests: In the original series, each PMHS was suspended in a seated position, either with the arms positioned above the shoulder and the hands above the head or with the arms down. The metal impact face had various materials affixed to it to produce different force-time histories and load distributions. However, only the bare-faced impactor tests were reproduced with the WorldSID-5F. The test speed was 2 m/s with a pure lateral impact direction.

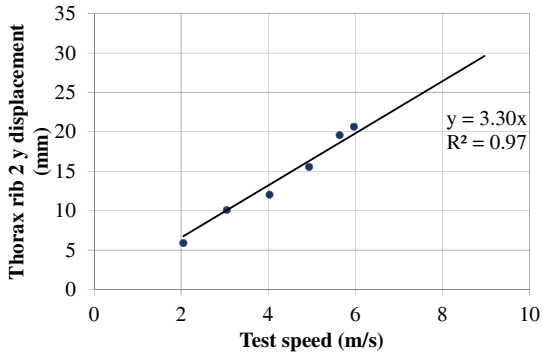

Figure 1. Peak y-axis displacement against test speed for WSU/GM thorax pendulum tests.

WSU/GM pelvis tests: Each PMHS was suspended in a standing position, with the arms positioned above the shoulder and the hands above the head. For the pelvis impacts, the impact face was centred on the greater trochanter. For the WorldSID 5th this was reproduced with the impactor aligned 9 mm forward and 29 mm inferior (downwards) to the H-point.

This test series required a test at 10m/s, however this speed could not be reached by the TRL pendulum. Therefore a series of tests were performed at lower speeds to investigate whether the data could be extrapolated to higher speeds.

The tests speeds chosen were 3, 4, 5, 6 and 7 m/s. Figure 2 shows the lateral acceleration and pubic force against test speed.

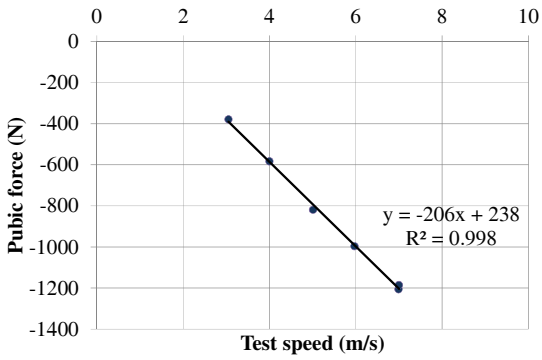

Figure 2. Pubic force against test speed for WSU/GM pelvis tests.

The results show that there is a linear correlation, however this would not pass through the origin, and therefore at test speeds lower than 3m/s the extrapolation may not be accurate enough. Similar results were obtained for the lateral acceleration, lateral iliac force and x-axis iliac moment.

Sled testing

Currently, there are three sled test conditions selected by ISO for use in the biofidelity assessment of, and injury risk function development for, side impact dummies. These conditions are taken from test series conducted with PMHS which have been reported in the literature. The three conditions can be described by the laboratory at which the work was undertaken, and are:

- Heidelberg (University of…)
- WSU (Wayne State University)
- MCW (Medical College of Wisconsin)

The sled bench design used in this project is capable of replicating the set-up conditions of all three test types.

Heidelberg: The oldest of the three test conditions is that reported by Marcus *et al.* [6]. It was intended to recreate the rigid wall tests at both 24 km/h (6.7 m/s) and 32 km/h (8.9 m/s).

Wayne State University: According to Cavanaugh *et al.* [7], the subjects from the WSU tests were positioned on a Heidelberg-type seat fixture. The seat was mounted to a sled and accelerated up to velocities of 6.6 to 10.5 m/s.

The subset of the original WSU tests recreated at TRL with the WorldSID-5F was the rigid wall tests, specified by ISO to have speeds of either 6.3 or 8.9 m/s. As in the original tests, the subject sat against a two-bar seat back. For those tests, the hands were placed in the lap of the subject. To replicate the position of the upper arms the WorldSID-5F half-arms were positioned slightly anteriorly to the mid-axillary line so that they did not bridge over the thorax ribs.

Medical College, Wisconsin: The Medical College of Wisconsin (MCW) and the NHTSA Vehicle Research and Test Centre (VRTC) performed a suite of side impact tests. According to Maltese *et al.* [8], they were conducted at two different speeds (6.7 and 8.9 m/s), with and without impact surface padding, and using a variety of impact wall geometries. At TRL only the rigid wall tests were reproduced, as the padding material was not readily available.

The sled apparatus was of the Heidelberg design. Test subjects were seated on the bench of the impact sled approximately one metre from the load wall. Just after the sled achieved the prescribed velocity change, the occupant contacted the load wall. The TRL recreation of the MCW conditions incorporated the load wall on the sled.

The load wall for the MCW tests was divided into four sections, one each to contact the thorax, abdomen, pelvis and legs. The change in sled velocity was either 6.7 or 8.9 (± 0.3) m/s. Load plates were either fixed in the same plane, or the thoracic or pelvic plate was offset, one at a time per test, toward the occupant. In flat wall and pelvic offset tests, the WorldSID-5F was seated with arms down, such that the arm was interposed between the thorax and load wall. In thoracic and abdominal offset tests, arms were raised to expose the thorax and abdomen directly to impact from the load wall. This was to match the PMHS positions in the offset wall tests, with the hands positioned up on the opposite shoulder.

RESULTS

As described in the introduction, one of the purposes for conducting these tests was to pass the results to ISO WG6 for use in the development of injury risk functions for the WorldSID-5F. The data from these tests have been made available to that group for that purpose. The tables of peak values are too large to be shown in this paper. However, they are available in the project report prepared for the European Commission [9].

Pendulum test results

Further to the production of test results for use in the development of injury risk functions, other interesting results from the pendulum testing are described in the following sections.

Shoulder biofidelity: the ISO (APR) shoulder test is used to assess shoulder biofidelity, according to ISO TR 9790.

The requirement for peak shoulder deflection is that the resulting value lies between 28 and 33 mm. The filtered shoulder deflections from two tests with the WorldSID-5F gave a mean peak value of 31.1 mm. This is within the required range. However, when the responses are normalised according to the ISO description, the mean peak value drops to 25.8 mm; below the lower boundary of the requirement.

The pendulum force response also suffers through the normalisation process with the filtered responses prior to normalisation lying closer to the required corridor than the normalised curves. These pendulum force results from the same two shoulder tests are shown in Figure 3.

Due to a conflict between the biofidelity and injury risk test specification, these tests were performed with a pendulum that was five percent heavier than that specified for the biofidelity evaluation. The force and deflection would be expected to be lower if conducted with the correct mass of impactor. This would help to bring the pendulum force response and the normalised shoulder deflection peak values closer to the corridor. However, the magnitude of the change is unlikely to bring the normalised results within the corridor.

On the basis of these results it seems as though the shoulder of the dummy is slightly too stiff.

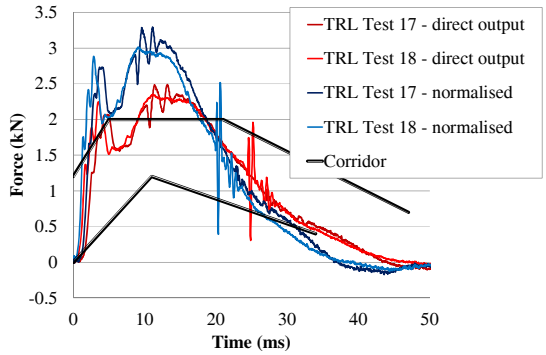

Figure 3. Shoulder test pendulum force response at 4.5 m/s.

Thorax biofidelity: As thorax pendulum tests were carried out using the ISO TR 9790 Thorax Test 1 set-up it is possible to comment on the thorax biofidelity of the WorldSID-5F in these tests. The biofidelity requirements from these tests concern the impactor force and the upper thoracic spine acceleration. Typically, an accelerometer at the T1 position is used to give the thoracic spine acceleration. However, with this WorldSID-5F only the T4 position was available for analysis. Therefore, Figure 4 shows the impactor force response from these tests compared with the requirement and Figure 5 shows the T4 lateral acceleration plotted against the upper thoracic spine acceleration corridor.

As described earlier, two different alignments of the impactor were tried with this test set-up. Firstly the middle of the impactor was aligned with the middle of the mid-thoracic rib and alternatively, the lower edge of the impactor was aligned with the lower edge of the third thoracic rib. Results from these two variations in set-up are shown in the following two figures.

When considering the force it is clear that the dummy does not meet this requirement. The duration of the response is too short for the corridor and depending on whether the response is normalised or not the peak force is either just inside the upper corridor limit or too high, respectively.

The influence of the impactor alignment is a reduction in peak force with the bottom edge of the impactor aligned with the lower edge of the third thoracic rib. The extent of this effect with the WorldSID-5F is sufficient to bring the impactor peak force within the limits of the biofidelity corridor.

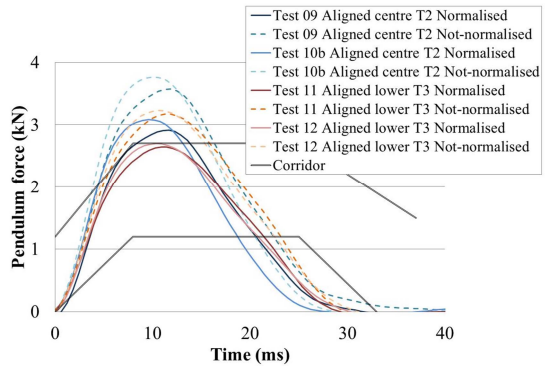

Figure 4. Thorax pendulum test impactor force response.

When considering the spinal accelerations then again the duration of the dummy response is too short. Also the peak acceleration, either normalised or not, is above the upper corridor limit. With the thoracic acceleration there seems to be less influence from the impactor alignment than was the case with the pendulum forces.

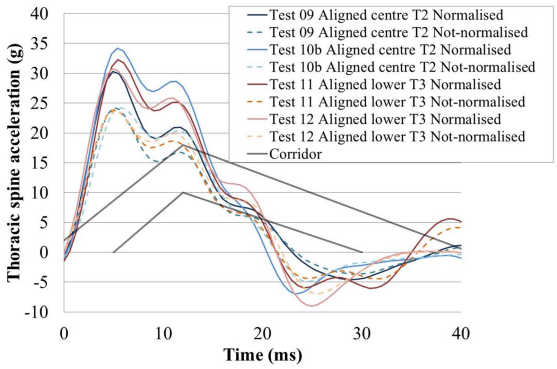

Figure 5. Thorax pendulum test upper thoracic spine acceleration.

These thorax biofidelity tests were carried out with a 14.7 kg pendulum rather than the 14 kg impactor specified in the requirements. The effect of testing with a heavier pendulum would be expected to give higher peak forces and accelerations than testing with a lighter impactor. This may help bring the pendulum force responses closer to the corridor. However, the 0.7 kg difference in this test set-up would be unlikely to account for the deviation in spine acceleration response from the required corridor.

Sled test results

It was expected that sled tests at 6.7 or 8.9 m/s would be conducted. However, due to concerns over the dummy's robustness under these conditions and the ability to provide meaningful measurements without damaging the instrumentation (i.e. reaching mechanical limits of measurement with the 2D IR-TRACCs), no tests were carried out above 6.3 m/s. To provide data for impacts above 6.3 m/s extrapolation has been used, where possible.

For the shoulder deflection it appeared that a mechanical limit of about 41 mm of deflection was reached in the Wayne State University (WSU) test at 6.3 m/s.

The consequence of reaching a mechanical limit is that whilst the impact speed shoulder deflection relationship may be linear up to this point, a plateau would be expected in deflection values at higher speeds. This is shown in Figure 6 where a linear line of best fit can be imagined for test speeds between 0 and 6 m/s. Above this speed the mechanical limit, as demonstrated at 6.3 m/s, would be expected to prevent further increases in shoulder deflection values. However, it is still possible to extrapolate beyond the point even though in practice the dummy cannot measure further deflection. This extrapolation can be considered as the best estimate of what would happen if the shoulder contact preventing further deflection was avoided. It is with this idea in mind, and using the linear relationship of the best fit trendline, that extrapolated shoulder deflection values for the higher severity WSU tests were derived.

When looking for potential sources of the mechanical contact preventing more than about 40 mm of shoulder deflection it became clear that contact could occur between the shoulder load cell and the lower edge of the neck bracket (Figure 7).

The bottom of the neck bracket in the WorldSID-5F increases in width from the top of the spine box upwards. This means that when there is no vertical displacement of the shoulder rib, it could be compressed until the shoulder load cell went all the way to the spine box. However, the more vertical displacement there is of the rib, the less y-axis deformation is possible. The extreme situation is that which occurred in the WSU tests where only 40 mm of lateral deformation is possible. In this case the shoulder load cell seems to have contacted the widest part of the neck bracket.

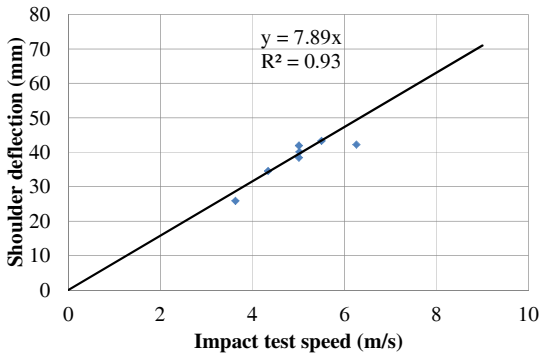

Figure 6. Peak shoulder deflection values from WSU sled tests at various impact speeds.

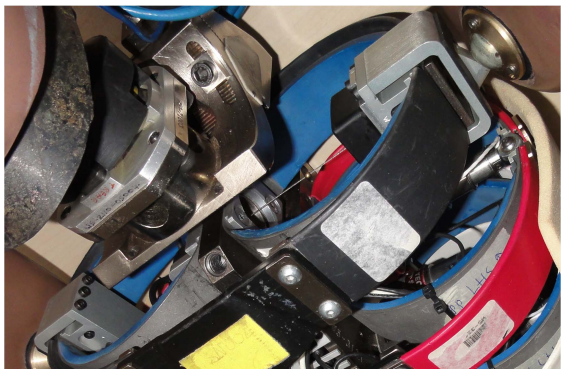

Figure 7. Neck and upper thorax of WorldSID-5F.

In the Heidelberg tests, higher shoulder deflection values were recorded than in the WSU tests. It may be that differences in the force plate configurations between the WSU and Heidelberg setups allow the hard limit for shoulder deflection to be avoided during the Heidelberg tests. It is assumed that some feature of the Heidelberg tests produces less vertical displacement of the shoulder rib than was the case in the WSU tests. Hence more lateral displacement is possible before a hard contact is made with the neck bracket.

With the variety of impact speeds for the rigid, flat wall Medical College of Wisconsin (MCW) tests similar extrapolation can be set-up as for the WSU tests. A similar approach has also been used for the other configurations. However, it should be noted that not all conditions were tested at more than one impact speed. This means that the extrapolation is reliant on one real data point and forcing the line of regression to go through the origin. This is not a robust method for determining expected values at higher severities.

With the y-axis rib deflection measurements, the line of best fit through the peak values from the sled tests supported a negative deflection intercept value at 0 m/s. Assuming that the physical meaning of this negative intercept is not plausible, this suggests that at low speeds the relationship between peak value and impact speed changes from that observed for the range of speeds tested. This serves to illustrate the danger of assuming constant behavioural relationships beyond the spread of test conditions evaluated. In terms of the test results, this behaviour means extrapolated values cannot be provided for test conditions without more than one impact speed.

The relationship between impact speed and x-axis Viscous Criterion (V*C) did not give a high r^2 correlation coefficient (0.42). Hence, extrapolation from these data was not appropriate. However, the MCW tests provided a much higher correlation value, $r^2 = 0.93$, though again the intercept was negative. In contrast, the left (struck) side sacro-iliac moment about the x-axis from the MCW flat wall tests did not provide a high correlation with impact speed ($r^2 = 0.05$), whereas the WSU tests provided a good correlation for this measure ($r^2 = 0.96$).

Thorax biofidelity: Heidelberg testing is used within ISO TR 9790 to assess both thorax and pelvis biofidelity. A 6.8 m/s test is required for Thorax Test 5. In the sled test programme carried out at TRL, impacts above 6.3 m/s were not carried out because of concerns over dummy breakages. Instead, 5 m/s was used as a reference speed which could be performed safely (without substantial risk of dummy breakages) with each of the three setups.

Heidelberg tests were only performed at 5 m/s. With regard to biofidelity, it is expected that the test at 5 m/s can provide some useful information. The thorax plate force response, with and without normalisation, is shown in Figure 8.

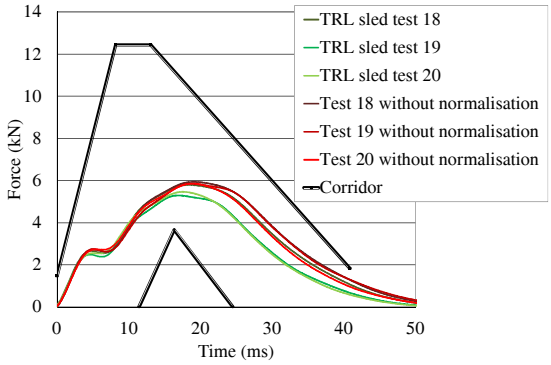

Figure 8. Heidelberg thorax plate response (5 m/s rigid plate tests, corridor for 6.8 m/s response).

It is clear from Figure 8 that at the reduced impact speed of 5 m/s, the WorldSID-5F meets the thorax plate force response corridor. It is expected that the response at the correct biofidelity test speed of 6.8 m/s could also remain within the corridor limits. However, it would be much closer to the upper corridor boundary.

Within the thorax biofidelity assessment there are also specifications for the subject accelerations. Accelerations are intended to be matched with requirements for the upper and lower spine. With the WorldSID-5F, accelerations from T4 and T12 have been used for this purpose. There is also a target for the peak lateral acceleration from the impacted rib. In this case the peak lateral acceleration values from Thorax ribs two and three are reported. A 100 Hz Finite Impulse Response filter was used to process the dummy acceleration signals prior to the peak value being taken. They have also been normalised using the ratio derived from the effective and standard mass estimates (R_a = 1.02 to 1.11).

The acceleration results showed that the peak spine acceleration is too low for the ISO target boundaries; whereas, the rib acceleration is just on the limit, though only if the higher acceleration value from Thorax rib 3 is dismissed. Again, it should be remembered that this test was conducted at 5 m/s and not the 6.8 m/s expected for use with these requirements. It should be expected that the acceleration values would increase when tested at a higher speed. This would move the spine accelerations closer to the targets whilst probably not achieving the required shift to produce values within the limits. Any increase in the rib acceleration would take it beyond the upper boundary limit. In essence it seems as though the rib acceleration is too high, whereas the spine acceleration of the WorldSID-5F is too low. This behaviour may be a consequence of the large spine box in the small female WorldSID which, apparently, had to be kept at the same size as the spine box in the 50th percentile dummy to house the data acquisition modules. The consequence of this is that proportionally more mass is located in the spine of the WorldSID-5F than in the larger 50M or would be expected in a human.

Abdomen biofidelity: The only abdomen biofidelity requirements set for the tests carried out at TRL were for the Wayne State University sled tests. Requirements are available for both 6.8 and 8.9 m/s rigid wall tests. However, the WorldSID-5F was only tested at speeds up to 6.3 m/s.

To give some indication of how the dummy response scales with impact speed a variety of test speeds up to the peak of 6.3 m/s were used. The abdomen results from these tests are plotted against the 6.8 m/s corridor in Figure 9.

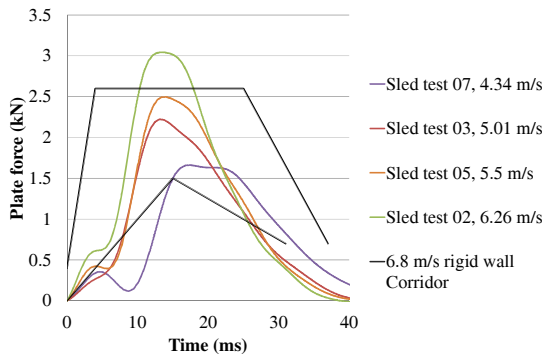

Figure 9. Wayne State University abdomen plate response (6.8 m/s rigid plate test requirement).

The force measured at the abdomen load plate increases with increasing impact speed. When tested at 6.3 m/s it had already exceeded the upper boundary of the biofidelity corridor. This indicates that the abdomen of the dummy is too stiff for the required response.

Pelvis biofidelity: The Heidelberg sled tests are also used in the evaluation of the pelvis biofidelity of side impact test dummies. Again, it must be noted that the target impact speed for the flat, rigid wall Heidelberg tests is either 6.8 or 8.9 m/s. As such, the test severity used to produce these results is substantially lower than expected for comparison with the biofidelity requirements. For this reason only the 6.8 m/s requirements are considered here.

From these results the pelvis acceleration is slightly too low when tested at a lower severity. This would improve as the impact speed is increased towards the necessary level. However, the pelvis plate force is already above the upper limit. This will move further from the requirements at a higher severity.

It was noted that at 5 m/s there was contact between the lower pelvis iliac wing and the sacro-iliac load cell and cable cover. However, there was no contact recorded between the upper central pelvis iliac wing and the lumbar spine mounting plate. The positions of the contact switches used to determine this are described later.

For the Wayne State University (WSU) tests, pelvis response requirements are also given for both 6.8 m/s and 8.9 m/s rigid wall impacts. As tests with the WorldSID-5F were not carried out above 6.3 m/s only the lower severity requirements are considered.

The peak lateral pelvis acceleration result is within the boundaries of the desired response. It is also likely that this could still be met even when the impact speed is increased by nine per cent.

The other part of the WSU pelvis biofidelity requirement concerns the pelvis plate force. The dummy responses from the range of impact speeds tested are shown against the biofidelity corridor in Figure 10. Unfortunately, for the test at 3.63 m/s the dummy had leaned substantially towards the impact wall by the time it made contact; hence the pelvis response is quite different to the other tests.

It can be seen that when an impact speed of 6.3 m/s is reached, the pelvis response has a peak already above the upper limit of the corridor. In agreement with the Heidelberg pelvis evaluation this suggests that the WorldSID-5F behaviour transfers more force through the pelvis than is expected based on the biofidelity requirements.

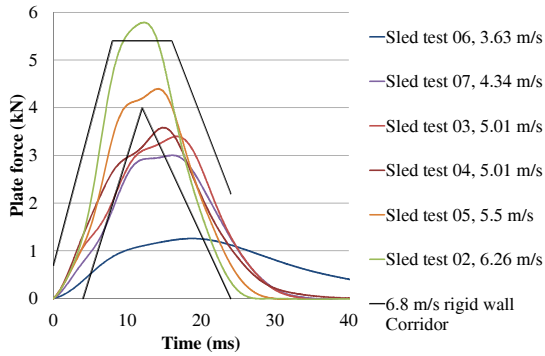

Figure 10. Wayne State University pelvis plate response (6.8 m/s rigid plate test requirement).

Pelvis interaction

Concerns had been raised in the WorldSID-5F Technical Evaluation Group over a non-instrumented load path in the pelvis. Contact reportedly occurred between the pelvis bone and the metal pelvis insert (which provides the mounting for the pelvis instrumentation and spine attachment). To detect contact, and the duration of that contact, a solution has been demonstrated where self-adhesive conductive foil is wrapped around the appropriate part of the pelvic bone to make a contact switch with the pelvis insert. A similar approach was taken at TRL to detect such a contact, in the following areas:

- The lower pelvis iliac wing with the sacro-iliac load cell and lumbar load cell cable cover
- The upper central pelvis iliac wing with the lumbar spine mounting plate

These areas and the corresponding area of the lumbar and sacro-iliac structure were fitted with the contact switches.

To provide input for possible future redesigns of the dummy pelvis components, a series of pendulum tests to impact the pelvis was used to evaluate the severity of test at which the contact occurs. The dummy was seated on a metal bench and impacted with a 14.7 kg 145 mm circular faced pendulum. The test speed was increased in increments of 1 m/s from 3 m/s to 7 m/s.

Humanetics provided modified parts with smaller volumes in critical areas to evaluate whether this improved the situation. The modified parts were fitted to the dummy and the testing series was repeated. The results from the contact switches are shown in Table 1.

Table 1.

Results of testing with original and modified pelvis-iliac and lumbar spine components

	Original parts			
Test speed (m/s)	Upper contact	Duration (ms)	Lower contact	Duration (ms)
3	No	-	-	-
4	No	-	Yes	8
5	Yes	7	Yes	10
6	Yes	10	Yes	13
7	Yes	10	Yes	14

	Modified parts			
Test speed (m/s)	Upper contact	Duration (ms)	Lower contact	Duration (ms)
3	No	-	No	-
4	No	-	No	-
5	No	-	Yes	5
6	Yes	3	Yes	2
7	-	-	-	-

The results show that there is contact at the lower part of the pelvis bone with the sacro-iliac load cell from 4 m/s and upwards. There is contact with the upper part of the pelvis bone and lumbar spine mounting plate from 5 m/s and upwards. These results were improved with the modified parts to 5 m/s and 6 m/s respectively.

Pelvis-rib interaction

In previous tests with the WorldSID-50M it had been noted that it may be possible to accidently seat the dummy with either:

- The lower abdomen rib on the flat upper face of the anterior pelvis flesh
- The anterior pelvis flesh pushed behind or "tucked under" the lower abdomen rib

In order to investigate the effect of this and a possible solution to the problem, additional tests were performed with the WorldSID-5F dummy. The tests performed were sled tests at 5 m/s with just the MCW abdomen plate and load cells on the impact face. Each test was repeated.

To push the anterior pelvis flesh under the lower abdomen rib, the dummy had to be leaned forward on the seat, the pelvis flesh tucked under the rib, and then the dummy leaned back into position. The dummy pelvis when tucked under the lowest ribs and the sternum is shown in Figure 11. The required steps to obtain this position were considered to be relatively extreme in the context of usual dummy positioning in a vehicle seat.

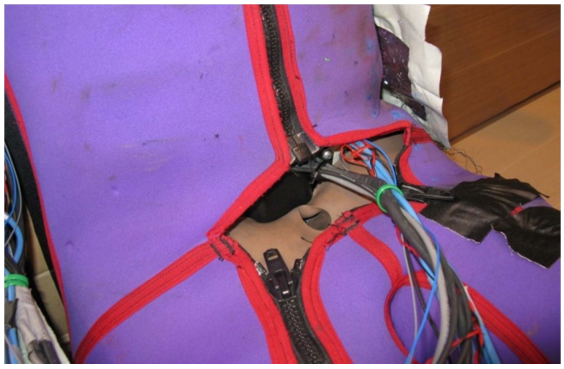

Figure 11. Dummy setup with pelvis-rib interaction.

The lower abdomen rib rotation and change in length in IR-TRACC are shown in Figures 12 and 13. In the test with forced pelvis-rib interaction (with the pelvis flesh deliberately pushed under the abdominal rib) there is less rotation, but greater change in IR-TRACC length than in the standard test.

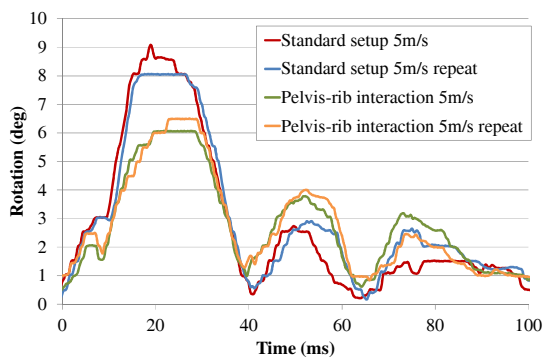

Figure 12. Lower abdomen IR-TRACC rotation for standard dummy setup and setup with pelvis-rib interaction.

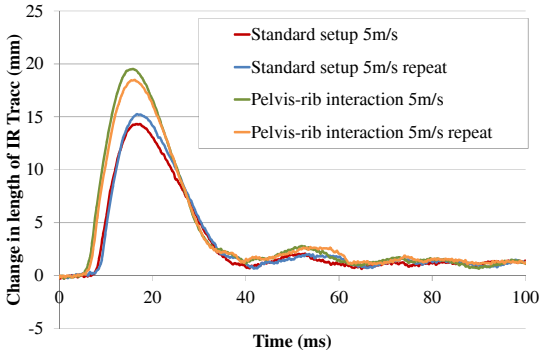

Figure 13. Change in length of lower abdomen IR-TRACC for standard dummy setup and setup with pelvis-rib interaction.

In order to reduce the possibility of accidently seating the dummy with the pelvis flesh interacting with the lower abdomen rib, modifications were made by TRL to the anterior pelvis flesh. Parts of the flesh were cut away to reduce the volume of the flesh in this region. The profile of the anterior surface was not affected by the removal of the foam behind it, although the stiffness of this part of the pelvis flesh would be reduced. Figures 14 and 15 show the flesh before and after the modification.

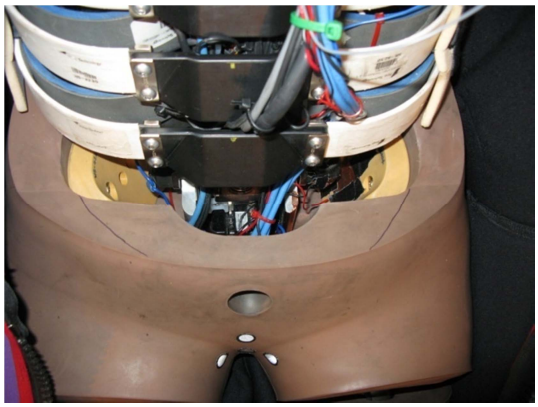

Figure 14. Anterior pelvis flesh before modification.

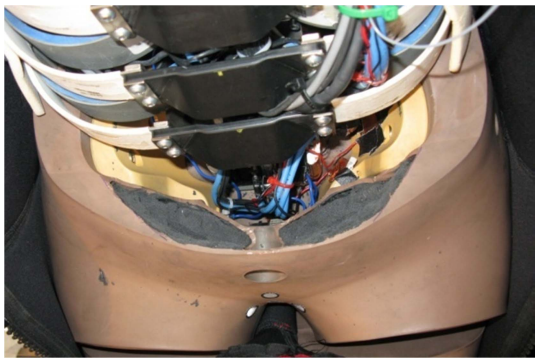

Figure 15. Anterior pelvis flesh after modification.

After making the modifications to the pelvis flesh the dummy was re-tested. With the modified flesh, the lower abdomen rib rotation and change in length of the IR-TRACC were greater than with the standard dummy, there was also a greater resultant displacement. This indicates the standard dummy pelvis constrains the motion of the lower abdominal rib in this sled test condition. If it is possible for the rib to become caught up on top of the flesh, as in the simulated pelvis-rib interaction tests, then the motion is further constrained and there can be an increase in the plate force measured by the load cell wall.

DISCUSSION

Results from this test work have already been presented to the WorldSID Informal Group (IG). Test data have also been offered to ISO WG6.

Based on the discussions held within the Informal Group, the manufacturer of the WorldSID-5F has proposed to revise the shoulder and pelvis of the dummy. Depending on the exact modifications an opportunity may come about to evaluate experimentally the dummy at higher severities. Therefore more of the severe injury risk tests could be performed perhaps leading to the development of improved risk functions.

All tests were made with one WorldSID-5F dummy, so there has been no evaluation of the dummy reproducibility in this work. It is hoped that these results will be compared with results from other dummies. Until that point there remains the risk that the dummy used by TRL is not representative of other WorldSID-5Fs.

Handling

As a result of the robustness issues and wanting to investigate the benefit of new pelvis designs, much time was spent working on the dummy and assembly/disassembly. Based on these experiences it has become clear that some comments are warranted regarding the ease of using the WorldSID-5F.

1. The pelvis was disassembled and reassembled four times during the testing programme. This is an extremely time-consuming task. There appears to be no easy way of sliding the pelvic bone back into the pelvis flesh. As a result it is very easy to put a lot of strain onto the cables running between the upper body of the dummy and the pelvis. Consideration should be given to making this task easier for the sake of protecting instrumentation and easing the process for the technician.
2. It is not clear why the cabling running from the data acquisition modules in the upper body of the dummy to the pelvis and legs cannot be split where the dummy is split. This seems as though it would be an extremely useful design feature to mitigate the risk of instrumentation damage when working on the dummy, whilst being separated top to bottom. At the very least sufficient cable lengths should be supplied to allow a reasonable distance between the two dummy portions.
3. It is very difficult to attach the bolts that hold the femoral heads into the acetabula of the pelvic bone with the full complement of instrumentation in the dummy pelvis.

CONCLUSIONS

A large programme of side impact sled and impactor tests has been conducted. The data will be used in the assessment of the WorldSID-5F biofidelity and also in specifying injury risk functions to be used with this dummy.

The dummy was used in 26 sled tests and 51 pendulum impacts. Throughout this test programme the dummy functioned well.

- The dummy biofidelity was shown to be outside of the ISO requirements in a number of areas. However, this performance has been demonstrated previously with the Revision 1 release of the dummy and may still represent a ‘good’ rating compared with other side impact dummies.
- Test-to-test use of the dummy is straight forward and no significant issues occurred with the data acquisition system, etc.

Durability is a problem when trying to achieve test severities needed for the development of injury risk functions.

- Sled tests were limited to impact speeds less than required for the higher severity biofidelity tests
- Whilst the highest severity injury risk tests may be outside the range of normal reasonable use of the dummy, there is still the need to provide dummy measurements in equivalent tests in order to generate robust injury risk functions
- Without dummy measurements from high severity tests it may be difficult to generate robust injury risk functions for this dummy

Dummy design changes which seem to be necessary to be able to perform these tests are:

- Improved displacement and angle range of motion for the 2D IR-TRACCs
- Removal of the contact potential between the shoulder load cell and the neck bracket
- Greater space for iliac wing bending without contact occurring with the sacro-iliac load cell or lumbar spine mounting in the pelvis

Results from this test work have already been presented to the WorldSID Informal Group (IG). Humanetics has already proposed to revise the dummy. The revisions will be based on this test work and similar findings from other groups participating in the TEG.

ACKNOWLEDGEMENTS

The authors wish to acknowledge the European Commission for funding this project and the experimental work described in this paper. Also, Humanetics Europe for the loan of the WorldSID-5F, and Transport Canada and PMG Technologies, Inc. for the loan of the sacro-iliac loadcell.

REFERENCES

[1] EEVC WG12. 2009. "Status of WorldSID 50th percentile male side impact dummy." EEVC WG12 Report Doc. 547. European Enhanced Vehicle-safety Committee (EEVC) Working Group 12

[2] Eggers, A., Schnottale, B., Been, B., Waagmeester, K., Hynd, D., Carroll, J. and Martinez, L. 2009. "Biofidelity of the WorldSID small female revision 1 dummy." In 21st International Technical Conference on the Enhanced Safety of Vehicles (Stuttgart, Germany, 15-18 June, 2009). US Department of Transportation, National Highway Traffic Safety Administration,

[3] ISO. 2010. "ISO/TR 12350:2010 Road vehicles - injury risk curves to evaluate occupant protection in side impact." ISO

[4] Schneider, L., Robbins, D., Pflüg, M. and Snyder, R. 1983. "Anthropometry of Motor Vehicle Occupants." University of Michigan Transportation Research Institute

[5] ISO. 1999. "ISO TR 9790: Road vehicles - anthropomorphic side impact dummy - lateral response requirements to assess the biofidelity of the dummy." ISO

[6] Marcus, J., Morgan, R., Eppinger, R., Kallieris, D., Mattern, R. and Schmidt, G. 1983. "Human response to and injury from lateral impact." In 27th Stapp Car Crash Conference (San Diego, California, USA, 17th to 19th October, 1983). Society of Automotive Engineers, Warrendale, PA, USA, 831634, 419-432

[7] Cavanaugh, J., Zhu, Y., Huang, Y. and King, A. 1993. "Injury and response of the thorax in side impact cadaveric tests." In 37th Stapp Car Crash Conference (San Antonio, Texas, USA, 8-10 November, 1993). Society of Automotive Engineers, Warrendale, PA, USA, 933127, 199-221

[8] Maltese, M., Eppinger, R., Rhule, H., Donnelly, B., Pintar, F. and Yoganandan, N. 2002. "Response corridors of human surrogates in lateral impacts." In 46th Stapp Car Crash Conference (Ponte Vedra Beach, Florida, USA, 11-13 November, 2002). Society of Automotive Engineers, Warrendale, PA, USA, 2002-22-0017, 321-351

[9] Carroll, J. A., Goodacre, O. and Hynd, D. 2012. "Global impact dummies - assessment concerning WorldSID in future regulatory applications." Client Project Report, CPR1317. Transport Research Laboratory

[10] Bendjellal, F., Walfisch, G., Fayon, A. and Tarrière, C. 1984. "A.P.R. Biomechanical Data." Association Peugeot-Renault.

[11] Compigne, S., Caire, Y., Quesnel, T. and Verriest, J.-P. 2004. "Non-injurious and injurious impact response of the human shoulder three-dimensional analysis of kinematics and detmerination of injnury threshold." Stapp Car Crash Journal. 2004-22-0005. 89-123

[12] Bolte, J. H., Hines, M. H., McFadden, J. D. and Saul, R. A. 2000. "Shoulder response characteristics and injury due to lateral glenohumeral joint impacts." Stapp Car Crash Journal. 2000-01-SC18. 261-280

[13] Bolte, J. H., Hines, M. H., Herriott, R. G., McFadden, J. D. and Donnelly, B. R. 2003. "Shoulder impact response and injury due to lateral and oblique loading." Stapp Car Crash Journal. 2003-22-0003. 35-53

[14] Marth, D. R. 2002. "Biomechanics of the shoulder in lateral impact." MS Thesis, Wayne State University

[15] Robbins, D., Lehman, R., Nusholtz, G., Melvin, J., Benson, J., Stalnaker, R. and Culver, R. 1982. "Quantification of Thoracic Response and Injury: the Gathering of Data; Final Report."

[16] Viano, D. C. 1989. "Biomechanical responses and injuries in blunt lateral impact." In 33rd Stapp car crash conference (Washington, D.C., U.S.A., 4-7 October 1989). Society of Automotive Engineers, Inc. (SAE), Warrendale, Pennsylvania, U.S.A., SAE technical paper 892432, 113-142

[17] Shaw, J., Herriott, R., McFadden, J., Donnelly, B. and Bolte, J. 2006. "Oblique and lateral impact response of the PMHS thorax." In 50th Stapp Car Crash Conference (Dearborn, MI, USA, 6-8 November, 2006). Society of Automotive Engineers, Warrendale, PA, USA, 2006-22-0007, 147-167

[18] Nusholtz, G. S. and Kaiker, P. S. 1985. "Experimental data for development of finite element models: Head/thoraco-abdomen/pelvis, Volume II: Thoraco-abdomen." The University of Michigan Transportation Research Institute

[19] Saul, R. A. 1996. "Development of a methodology for prediction of liver injury due to side impact loading in motor vehicle accidents." MS Thesis, Ohio State University

[20] Cesari, D. and Ramet, M. 1982. "Pelvic tolerance and protection criteria in side impact." In Proceedings of the 26th Stapp Car Crash Conference (Ann Arbor, Michigan, U.S.A., 20-21 October 1982). Society of Automotive Engineers, Inc., 400 Commonwealth Drive, Warrendale, Pennsylvania, U.S.A., 821159, 145-155

[21] Nusholtz, G. S. and Kaiker, P. S. 1985. "Experimental data for development of finite element models: Head/thoraco-abdomen/pelvis, Volume III: Pelvis." The University of Michigan Transportation Research Institute

[22] Bouquet, R., Ramet, M., Bermond, F., Caire, Y., Talantikite, Y., Robin, S. and Voiglio, E. 1998. "Pelvis human response to lateral impact." In 16th International Technical Conference on the Enhanced Safety of Vehicles (Windsor, Ontario, Canada, 31 May to 4 June, 1998). US Department of Transportation, National Highway Traffic Safety Administration, 98-S7-W-16, 1665-1686

[23] Cavanaugh, J., Walilko, T., Malhotra, A., Zhu, Y. and King, A. 1990. "Biomechanical response and injury tolerance of the thorax in twelve sled side impacts." In the proceedings of the 34th Stapp Car Crash Conference (Orlando, Florida, USA, 4-7 November, 1990). Society of Automotive Engineers, Warrendale, PA, USA, 902307, 23-38

[24] Cavanaugh, J., Walilko, T., Malhotra, A., Zhu, Y. and King, A. 1990. "Biomechanical response and injury tolerance of the pelvis in twelve sled side impacts." In the proceedings of the 34th Stapp Car Crash Conference (Orlando, Florida, USA, 4-7 November, 1990). Society of Automotive Engineers, Warrendale, PA, USA, 902305, 1-12

[25] Kuppa, S., Eppinger, R. H., McKoy, F., Nguyen, T., Pintar, F. A. and Yoganandan, N. 2003. "Development of side impact thoracic injury criteria and their applications to the modified ES-2 dummy with rib extensions (ES-2re)." Stapp Car Crash Journal. 2003-22-0010. 189-210

APPENDIX – ISO TEST SERIES

Table 2.

Original Test Series Of PMHS Impactor Tests

Test Series	Direction	Impact surface	Impactor face geometry	Range of impact speed (m/s)
Shoulder impactor tests				
APR [10]	Lateral	Rigid	circular	4.2-4.6
INRETS [11]	Lateral, forward and rearward from lateral	Rigid	rectangular	1.3-6.1
OSU series 1 [12]	Lateral	Padded	rectangular	3.7-6.8
OSU series 2 [13]	Lateral and forward from lateral	Padded	rectangular	4-7.6
WSU [14]	Lateral	Rigid	circular	4.3-7.0
Thoracic impactor tests				
HSRI [15]	Lateral	Rigid	circular	0.9-6.1
WSU [16]	Forward from lateral	Rigid	circular	6.0-8.7
OSU [17]	Lateral and forward from lateral	Rigid	circular	2.5
UMTRI [18]	Lateral and forward from lateral	Rigid or padded	circular	1.9-8.5
Abdomen impactor tests				
WSU [16]	Forward from lateral	Rigid	circular	9.8
OSU [19]	Lateral	Padded	rectangular	6.0-12.3
Pelvis impactor tests				
WSU [16]	Lateral	Rigid	circular	4.0-10.3
ONSER [20]	Lateral	Rigid	circular	5.8-14.0
UMTRI [21]	Lateral	Rigid or padded	circular	5.1-26
INRETS [22]	Lateral	Rigid	rectangular	3.2-13.7

Table 3.

Original Test Series Of PMHS Sled Tests

Test Series	Description of Sled Tests
Heidelberg [6]	8.2 m/s impacts into a flat impact surface with separate instrumented plates for the thorax and pelvis. The impact surface was rigid.
WSU [23], [24]	6.7 to 8.9 m/s impacts into rigid or padded plates for the shoulder, thorax, abdomen, pelvis and knee.
MCW & OSU [25]	6.7 to 8.9 m/s impacts into rigid or padded plates for the thorax, abdomen, pelvis and lower extremity. The plates were either flat, one plate offset by 110-mm, or the thorax and abdomen plates were angled.

A METHODOLOGY FOR GENERATING OBJECTIVE TARGETS FOR QUANTITATIVELY ASSESSING THE BIOFIDELITY OF CRASH TEST DUMMIES

Heather Rhule
Bruce Donnelly
Kevin Moorhouse
National Highway Traffic Safety Administration
Yun Seok Kang
The Ohio State University
United States
Paper Number 13-0138

ABSTRACT

A set of analysis tools and a procedure are presented for generating objective biofidelity targets derived from post-mortem human subject (PMHS) test response data and quantitatively assessing the biofidelity of crash test dummies. Using response time history data from PMHS tests (Maltese et al., 2002), this paper presents a methodology for creating PMHS response targets that have a statistical basis and then using those targets for quantitative evaluation of crash dummy biofidelity. The first step in the methodology is to normalize the response data to remove variation associated with anthropometric differences and match the size of the dummy to be assessed (e.g., 50th percentile male). After the data is normalized the phase differences are minimized for all responses using the cross-correlation functions and the Lagrange Multiplier technique. The resulting phase-adjusted set of time histories can be averaged, point by point, to obtain a "typical" response. The average phase shift is utilized to locate the mean PMHS response in time. The typical response, or mean curve, can then be bracketed with plus and minus one standard deviation curves resulting in a biofidelity target specification for a dummy response. A single average standard deviation value is used to encompass the mean curve rather than using the point by point standard deviation values, which eliminates "necking" at crossing points. To quantitatively determine the quality of the dummy biofidelity, each dummy response is evaluated for biofidelity in terms of shape and magnitude (SM) and phase (P). First, phase differences between the dummy and mean PMHS response are minimized by using the cross-correlation function to find the phase shift, or lag, that minimizes the squared difference between the two curves. Then the difference between the phase-minimized dummy response and the target mean is measured using a cumulative variance ratio (DCV/CCV) to describe the response shape and magnitude biofidelity. In addition, the dummy phase response biofidelity is assessed utilizing a ratio of the minimizing lag (dummy phase shift) divided by a standard acceptable lag. The acceptable lag is found by shifting the PMHS mean curve in time with respect to itself and determining the lag between the shifted and unshifted PMHS mean curves that results in a DCV/CCV equal to 1.0. The values for shape and magnitude biofidelity (SM) and phase biofidelity (P) are combined using a root mean square (RMS) methodology (the resultant or orthogonal vector addition) to provide a sense of the total biofidelity quality of each channel time history. The RMS values for each response measurement are averaged for each test condition to obtain the test condition rank; the test condition ranks are averaged to obtain the body region rank; and the body region ranks are averaged to obtain the External or Internal Biofidelity Rank; the External and Internal Biofidelity Ranks are then averaged to obtain the Overall Biofidelity Rank. Results consist of example PMHS biofidelity targets for lateral sled impact tests and two side impact dummies are ranked using this revised BioRank system.

INTRODUCTION

In 2002 Rhule et al. presented a new Biofidelity Ranking System (BRS) which quantifies 1) the ability of a dummy to load a vehicle as a cadaver does - External Biofidelity and 2) the ability of a dummy to replicate those cadaver responses that best predict injury potential - Internal Biofidelity. External Biofidelity is calculated using measures of the environment that the dummy and human subject are loading (i.e., thorax load wall force); Internal Biofidelity is calculated using measures from the dummy or human subject response. The essence of the biofidelity rank lies in the comparison of each selected dummy response to its corresponding mean human subject response. Equation 1 shows the calculation presented in 2002

for generating biofidelity ranks, where R (also known as DCV/CCV) is the ratio of the cumulative variance between the dummy response and mean human response (DCV) over the cumulative variance between the mean human response and the mean plus one standard deviation (CCV) (Morgan et al., 1986, Rhule et al., 2002).

$$B = \frac{\sum_{j=1}^{m}\left(V_j * \left(\frac{\sum_{k=1}^{n}\sqrt{R_{j,k}}}{n}\right)\right)}{\sum_{j=1}^{m} V_j} \quad (1)$$

where

B = Biofidelity Rank, either External or Internal
R = Response Measurement Comparison Value (DCV/CCV)
V = Test Condition Weight
j = test condition
k = response measurement
m = number of test conditions
n = number of response measurements per test condition

For any given response measurement in a biofidelity test the R value is calculated and its square root is taken to provide a biofidelity score for that response measurement. The $\sqrt{R}$ value represents the difference between the dummy response and the PMHS mean response in multiples of standard deviation, and thus a lower value represents better biofidelity.

In 2009 Rhule et al. presented updates to the BRS, including removal of all Test Condition Weights and inclusion of all available internal PMHS or dummy measures, not just those used for injury criteria. Internal dummy measures for which there are matching human subject response targets are useful for biofidelity evaluation. The Test Condition Weights were justifiably criticized for being subjective and were removed from the algorithm. A rigorous assessment of the relevance of the tests selected for biofidelity evaluation and the robustness of their corresponding human subject response targets should occur prior to using the objective Biofidelity Ranking System. Equation 2 shows the calculation presented in 2009 for generating biofidelity ranks.

$$B = \frac{\sum_{i=1}^{l}\left(\frac{\sum_{j=1}^{m}\left(\frac{\sum_{k=1}^{n}\sqrt{R_{i,j,k}}}{n}\right)}{m}\right)}{l} \quad (2)$$

where

B = Biofidelity Rank, either External or Internal
R = Response Measurement Comparison Value (DCV/CCV)
i = body region
j = test condition
k = response measurement
l = number of body regions
m = number of test conditions
n = number of response measurements per test condition

Since the 2009 presentation of the BRS, updates have been made to include an approach for minimizing phase differences among PMHS responses prior to generating human subject response targets as well as an independent measure of dummy phase biofidelity. This paper provides a set of tools and a procedure for generating objective biofidelity targets derived from post-mortem human subject test response data and quantitatively assessing the biofidelity of crash test dummies using an improved BRS.

METHODS

Biofidelity target generation and dummy ranking involves normalizing the PMHS data to a standard size, minimizing phase differences among multiple PMHS time histories, building human subject response targets, and scoring crash test dummy biofidelity using the BRS. The Results section of the paper presents an exemplar set of data after performing each step in the methodology, ending with example biofidelity ranks for two side impact crash test dummies.

Normalization

The first step in the methodology is to normalize the response data to remove variation associated with anthropometric differences and match the size of the dummy to be assessed (e.g., 50th percentile male). Moorhouse (2013) quantified the effectiveness of several methods of normalization by applying them to various sets of data. The methods evaluated include mass-based normalization as described by Eppinger et al. (1984) and impulse momentum-based normalization as described for single mass systems (e.g., sled & drop tests) by Mertz (1984) and for two-mass systems (e.g., pendulum tests) by Viano (1989).

Moorhouse developed a potential improvement to the impulse-momentum based normalization technique

by using an estimate of the effective stiffness calculated from the response data. The calculation for effective stiffness is shown in Equation (3):

$$\int F dx = \frac{1}{2} k_{eff} x_{\max}^2 \quad \Rightarrow \quad k_{eff} = \frac{2\int F dx}{x_{\max}^2} \qquad (3)$$

where k_{eff} is the effective stiffness, F is the force during impact, and $x_{\max}$ is the maximum displacement during the impact. The value of standard effective stiffness is estimated by first calculating the ratio of each subject's effective stiffness to its characteristic length (e.g., chest breadth for a thoracic side impact). Then the average ratio is determined and multiplied by the characteristic length of the population to which the data is to be normalized.

Example results of the normalization effectiveness evaluation are shown in Figure 1, where the effective mass-effective stiffness technique for normalizing PMHS response data resulted in the greatest improvement of signal groupings as indicated by the $\%CV_{ellipse}$ value (see Moorhouse 2013). The effective mass-effective stiffness method for normalizing PMHS response data yielded the smallest $\%CV_{ellipse}$ value in 21 out of 26 signal groups examined, and is selected as the technique of choice for normalizing data prior to building mean response curves in this study.

Phase Optimization

After the data is normalized, the phase differences among all responses are simultaneously minimized using an optimization technique (Donnelly and Moorhouse 2012) based on the cross-correlation function and the Lagrange Multiplier method. The phase shifts, or lags, of each PMHS curve are also averaged to locate the mean curve with respect to time zero so that appropriate timing of the response is not lost.

Kang et al. (2012) utilized the technique to perform phase optimization on rear impact PMHS data and present examples of mean response curves constructed prior to and after phase optimization (Figures 2 and 3, respectively). The mean response curve after phase optimization, shown in Figure 3, is much more like each individual PMHS response than is the non-phase optimized mean response curve of Figure 2.

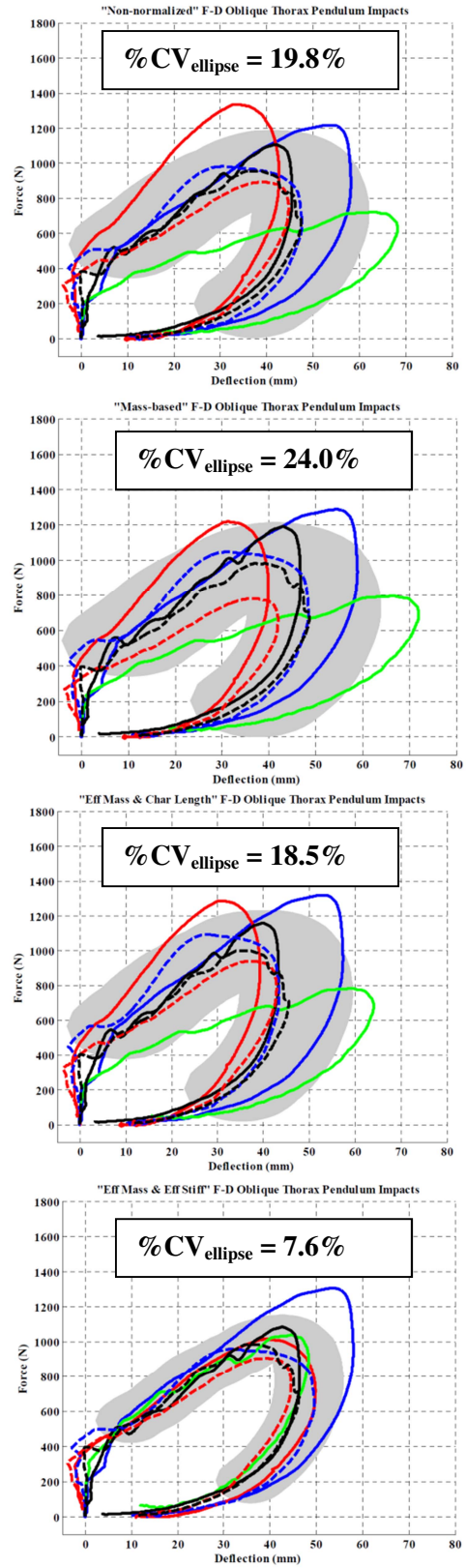

Figure 1. Results from Moorhouse (2013) evaluation of normalization methods as compared to the non-normalized PMHS data

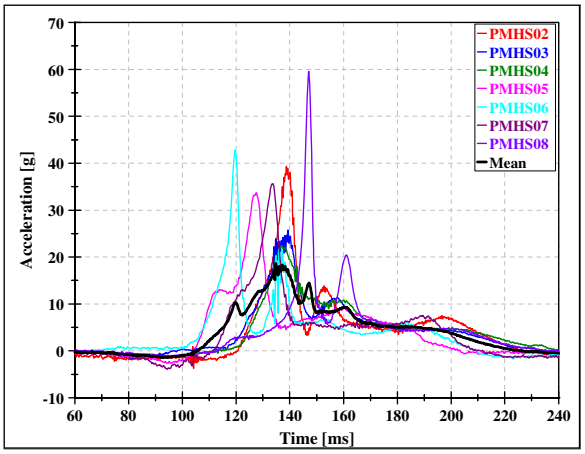

Figure 2. PMHS and mean (solid black line) responses before phase optimization

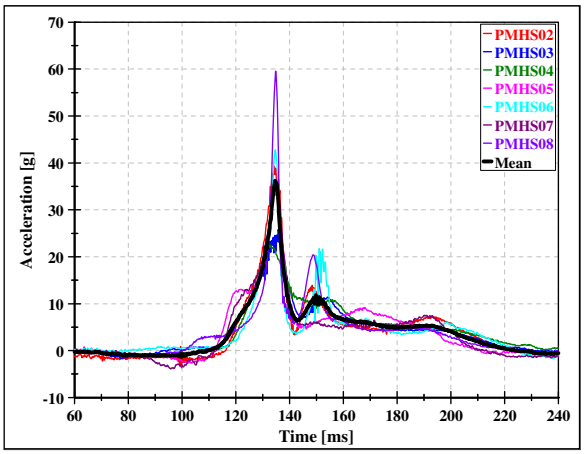

Figure 3. PMHS and mean (solid black line) responses after phase optimization

It should be noted that the timing of the responses can be affected by the normalization process since time is normalized as well as force, acceleration and deflection. Therefore normalization is performed prior to phase optimization. Performing phase optimization prior to normalization would be moot since the normalization would alter the timing of the signals, possibly causing the need for phase optimization to be performed again. Further, the optimization technique provides the time shifts that are averaged to locate the mean curve in time, and normalizing after this is accomplished would invalidate the location in time of the mean curve.

Target Building

Mean Response Curve The resulting phase-adjusted set of time histories can be averaged, point by point, to obtain a "typical" response.

The Mean Response and Standard Deviation Tolerance Curves The typical response, or mean curve, can then be bracketed with plus and minus one standard deviation curves resulting in a biofidelity target specification for a dummy response. Standard deviation curves obtained by using the point by point standard deviation values often result in "necking" at points where the original curves happen to be similar in value: usually where PMHS curves cross. To eliminate this issue, a single standard deviation value is obtained by averaging the point by point standard deviation values, and the single average standard deviation value is used to encompass the mean curve. Also, to focus on the most relevant portion of the target, the standard deviation curves are only calculated for the upper 80% of the mean response (i.e., for values of the mean response that are greater than 20% of the peak magnitude of the mean curve).

Figures 4 and 5 show examples of one standard deviation curves calculated at each point and averaged across all points, respectively. It should be noted that these mean and standard deviation curves will ultimately be used to calculate the CCV portion of the DCV/CCV value used to obtain $\sqrt{R}$ (Rhule et al., 2002, 2009) for the assessment of dummy biofidelity (see next section), and that for this calculation it does not matter whether the standard deviation is calculated at each point or the average standard deviation is used because the resulting CCV values will be the same. Although the resulting $\sqrt{R}$ values are not affected, using the average standard deviation makes the targets look more uniform.

Biofidelity Assessment

In the previously published versions of the BRS (Rhule et al. 2002; 2009), a dummy's biofidelity was assessed by calculating the $\sqrt{R}$ for the dummy response, regardless of the relative timing between the dummy response and the PMHS biomechanical response target. However, Moorhouse et al (2012) recently identified some cases where the calculation of the $\sqrt{R}$ value in this manner does not produce an outcome that accurately reflects the relative biofidelity of the dummies being evaluated. In particular this can occur when the PMHS and dummies exhibit short duration high peak responses, and the timing of the dummy response differs from the PMHS target.

Consider a PMHS response target with a large magnitude force peak such as seen in Figure 6, and

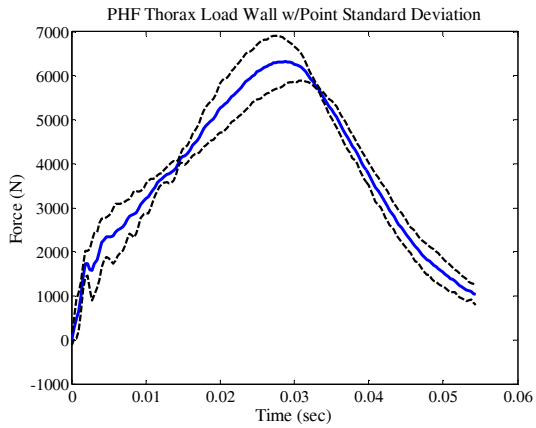

Figure 4. Thorax load wall PMHS mean response curve (thick blue) and plus- and minus-one standard deviation (thin black) targets (calculated at each point in time) for padded high speed flat wall (PHF) tests (Maltese et al., 2002)

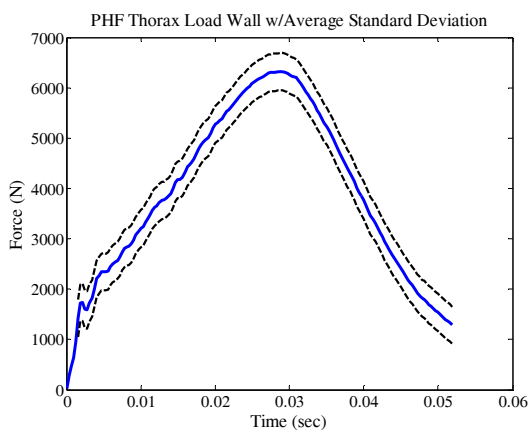

Figure 5. Thorax load wall PMHS mean response curve (thick blue) and plus- and minus-one standard deviation (thin black) targets (averaged across all points) for padded high speed flat wall (PHF) tests (Maltese et al., 2002)

three different dummies that are being compared to that PMHS target. Dummy 2 has a force peak similar in magnitude but out of phase and the other two dummies have essentially no force peak. Clearly a dummy that exhibits the proper force response, even if out of phase, is superior to one that generates no comparable force response, but the $\sqrt{R}$ values as calculated using the methods from Rhule et al. (2002, 2009) indicate only slightly better biofidelity for Dummy 2 (Figure 6). However, if the phase differences between each dummy and the mean PMHS response curve are first minimized prior to calculating the $\sqrt{R}$ value, the score of Dummy 2 improves and more clearly demonstrates the best biofidelity (Figure 7).

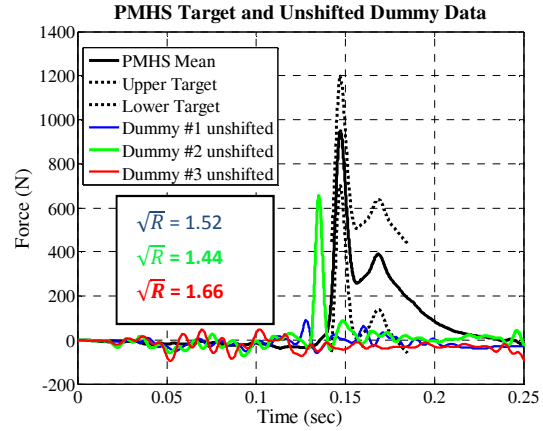

Figure 6. PMHS response target and three different dummy responses (unshifted), of which only one contains a peak response similar to that of the target, but out of phase. $\sqrt{R}$ values are shown.

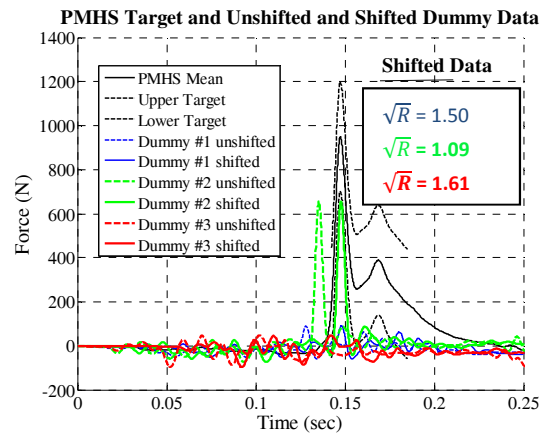

Figure 7. PMHS response target and three different dummy responses (unshifted and shifted shown). $\sqrt{R}$ values for shifted curves are shown.

Note that minimizing phase differences prior to calculation of $\sqrt{R}$ effectively assesses a dummy's biofidelity with respect to shape and magnitude only, and does not account for differences in the timing of the dummy response. However, with advanced restraints and countermeasures of modern vehicles the timing of a dummy response is also important and should be accounted for in a dummy's biofidelity assessment.

The example provided in Figures 6 and 7, along with the need to account for the timing of the dummy response, identifies the need for an improved method for assessing dummy biofidelity. An improvement to the BRS which accomplishes this is presented below.

Shape and Magnitude (SM value) In order to assess a dummy's biofidelity with respect to response shape and magnitude, the $\sqrt{R}$ calculation (Rhule et al., 2002, 2009) is performed after the dummy response is phase-minimized with respect to the mean PMHS response curve. The phase minimization is accomplished using the cross-correlation function to find the phase shift, or lag, that minimizes the squared difference between the two curves, and then the dummy response is shifted toward the PMHS mean response by that amount. The resulting $\sqrt{R}$ value between the shifted dummy response and the PMHS mean response is referred to as the Shape and Magnitude Response Comparison Value (SM). The SM value represents the difference between the dummy response and the PMHS mean response in multiples of standard deviation similar to the $\sqrt{R}$ value in previous versions of the BRS (Rhule et al., 2002; 2009), although the SM value only considers differences in shape and magnitude. Note that this calculation is only performed for the upper 80% of the mean PMHS response, which is the portion of the response for which the standard deviation curves were generated.

Phase (P value) In order to quantitatively assess the biofidelity of the phasing of a dummy response, a ratio metric is developed in which the minimizing lag (dummy phase shift) is divided by a standard acceptable lag such that large ratios represent poor phasing and small ratios represent good phasing. The acceptable lag is found by shifting the PMHS mean curve in time with respect to itself and determining the lag between the shifted and unshifted PMHS mean curves that results in a $\sqrt{R}$ value equal to 1.0. The absolute value of the minimizing dummy lag is divided by this standard acceptable lag to obtain a measure of phase quality. If the value of this ratio, the Phase Response Comparison Value (P), is less than 1.0, the dummy phasing is within a tolerance of one standard deviation of the PMHS mean response curve. If P is larger than 1.0, the value relates to multiple standard deviations in the same sense that multiples of the $\sqrt{R}$ value relate to a standard deviation.

Channel Biofidelity For each response measurement, or channel, selected for biofidelity assessment there will be a Phase Response Comparison Value (P) and a Shape and Magnitude Response Comparison Value (SM). The values for phase biofidelity, P, and shape and magnitude biofidelity, SM, are combined using a root mean square (RMS) methodology (the resultant or orthogonal vector addition) to provide a sense of the total biofidelity quality of each channel time history. The root mean square methodology is appropriate because each part, the P and the SM, measures biofidelity independently and without any interaction between the two. This is analogous to vector components in space where the resultant of the X and Y components is the magnitude of the vector. Note that both the P and the SM values are based on multiples of one cumulative standard deviation of the mean PMHS time history and thus have the same units and can be combined.

Biofidelity Rank Calculation For illustration purposes, Figures 8 and 9 show a schematic of how the Internal and External Biofidelity Ranks are calculated. For instance, if two test conditions (TC1 and TC2 in Figures 8 and 9) are selected to assess a dummy's biofidelity, and each test condition includes three internal thorax measurements (CH1, CH2, and CH3 in Figure 8), and one internal measurement for each of the abdomen and pelvis body regions (CH4 and CH5 in Figure 8), the internal biofidelity ranking schematic would look like Figure 8. Similarly, if one external measurement was recorded for each of two test conditions, the external biofidelity ranking schematic would look like Figure 9. For each response measurement there is a Phase Response Comparison Value (P) and a Shape and Magnitude Response Comparison Value (SM), which are combined using the RMS method for each response measurement (RMS in Figures 8 and 9). For each test condition the RMS values are averaged. For example, the RMS values for response measurements CH1, CH2 and CH3 are averaged to get the biofidelity rank for test condition 1 (TC 1) in Figure 8. Moving up Figures 8 and 9 to the body region level (orange, blue, and purple shading for thorax, abdomen, and pelvis body regions, respectively), each body region rank consists of the average of the test condition ranks. To obtain the Overall Internal (or External) Biofidelity Rank, the body region ranks are averaged. To obtain the Overall Biofidelity ranks, the Overall Internal and External Biofidelity Ranks are averaged.

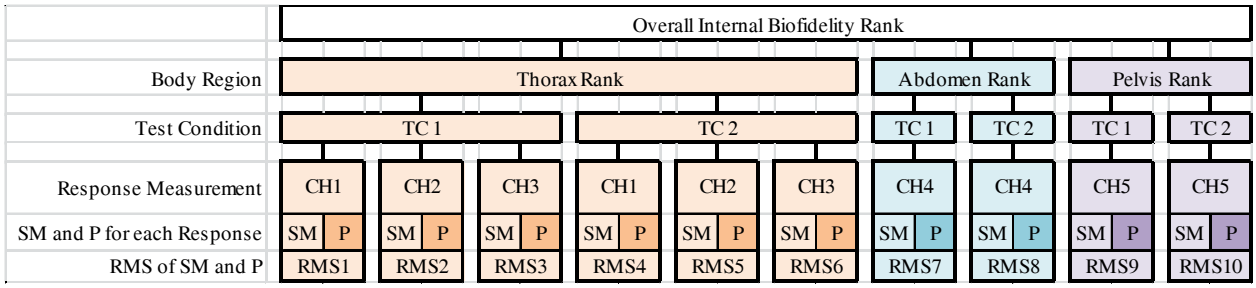

Figure 8. Schematic of how Internal Biofidelity Ranks are calculated

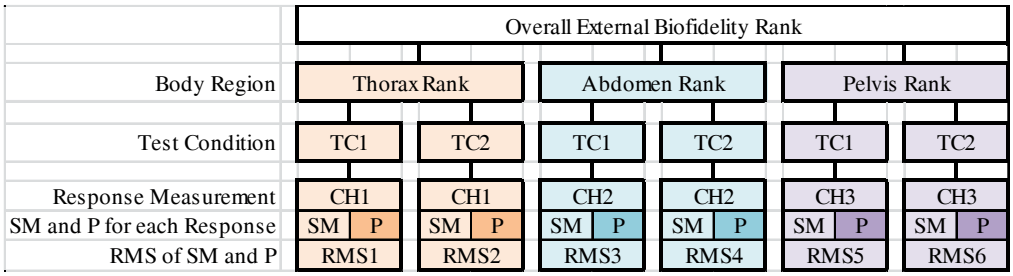

Figure 9. Schematic of how External Biofidelity ranks are calculated

RESULTS

The padded high speed flat wall (PHF) and rigid low speed flat wall (RLF) test conditions from Maltese et al. (2002) were selected to illustrate the usage of the tools for generating PMHS response targets and the procedure for assessing dummy biofidelity. Each step of the new tool box is illustrated using the RLF thorax deflection responses.

Normalization

Figures 10 and 11 show the non-normalized and normalized responses, respectively, of the three PMHS for the thorax deflection measurement in the RLF test condition.

Phase Optimization

Figure 12 shows the normalized PMHS thorax deflection responses after optimizing the phase responses.

Target Building

After the PMHS responses are normalized and the phase differences are minimized, the PMHS mean curve is calculated at each point in time (black curve in Figure 13) and the point-by-point standard deviations are averaged for the upper 80% of the mean PMHS response (black dotted curves in Figure 13) and plotted along with the mean PMHS

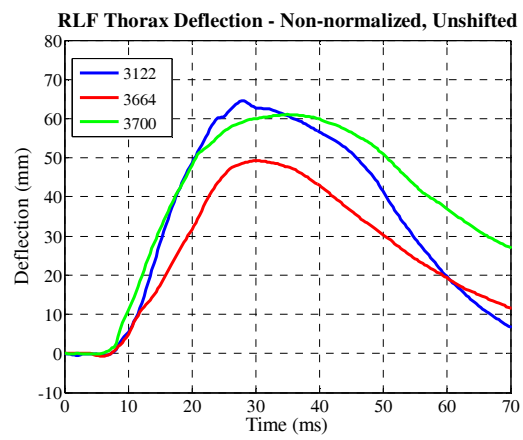

Figure 10. Non-normalized thorax deflection responses for three PMHS in RLF test condition.

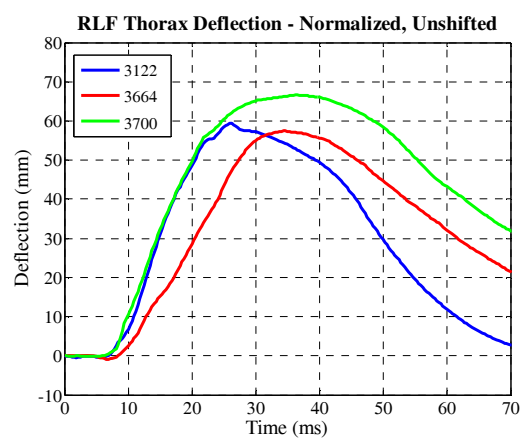

Figure 11. Normalized thorax deflection responses for three PMHS in RLF test condition.

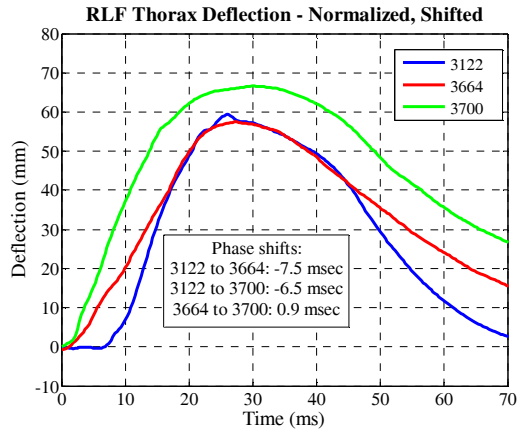

Figure 12. Normalized thorax deflection responses for three PMHS in RLF test condition after minimizing phase differences

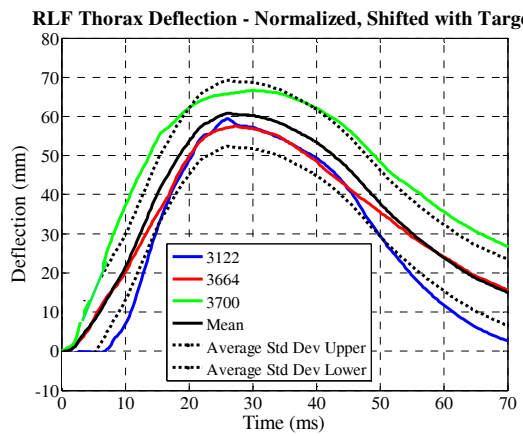

Figure 13. Mean and average standard deviation PMHS response target for RLF thorax deflection with three normalized and shifted PMHS curves

curve. The mean and average standard deviation curves represent the PMHS response and dummy biofidelity target.

Biofidelity Assessment

To assess dummy biofidelity, the dummy response is first phase-minimized with the mean PMHS response. Figure 14 shows the PMHS response target with the dummy curve unshifted (dashed pink) and shifted by 6 ms (solid pink) to minimize the phase difference. Also shown in Figure 14 is the $\sqrt{R}$ value for the unshifted curve (as calculated in previous versions of the BRS), the $\sqrt{R}$ value for the shifted dummy curve (SM value), the ratio of the dummy lag and the mean curve lag (P), and the RMS value. Note that the quantitative assessment of dummy biofidelity for this response would yield a value of 1.1 ($\sqrt{R}$) using the previous BRS and a value of 0.9 (RMS) using the new methodology.

The entire set of PHF and RLF targets with shifted dummy responses and P and SM values are shown in the appendix.

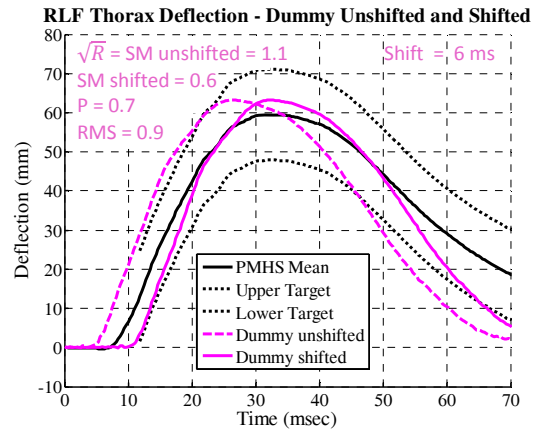

Figure 14. PMHS response target with a dummy curve unshifted and shifted with BRS values for RLF thorax deflection

<u>Biofidelity Rank Calculation</u> Figures 15-18 show the SM, P, and RMS values for each response measurement included in the demonstration of the updated BRS for Dummies A and B. The External Biofidelity response measurements include thorax, abdomen and pelvis load wall forces. The Internal Biofidelity responses include T1 and T12 lateral accelerations, the average of the upper and lower thorax half chest deflections, mid abdomen half deflection and pelvis lateral acceleration. Any P or SM value over 2.0 is highlighted in red, indicating a response that varies from the mean PMHS by more than two cumulative standard deviations.

Both dummies exhibit better Internal Biofidelity than External Biofidelity, probably because they were designed to be biofidelic in measurements related to injury criteria – typically those internal to the dummy. It appears that the thorax of both dummies could be improved in the shape/magnitude component of their external biofidelity responses, indicated by the SM values over 2.0; however, the phase biofidelity is good. The abdomen and pelvis of both dummies performed well (under 2.0) in both shape/magnitude and phase for one test condition and poorly in both shape/magnitude and phase for the other test condition. The RMS values for each response measurement appropriately reflect the combined biofidelity of the shape/magnitude and phase components.

	Dummy A External Biofidelity Rank												
	2.53												
Body Region	Thorax				Abdomen				Pelvis				
	3.07				2.07				2.44				
Test Condition	PHF		RLF		PHF		RLF		PHF		RLF		
	3.89		2.26		3.22		0.91		3.21		1.66		
Response Measurement	Thorax Plate		Thorax Plate		Abdomen Plate		Abdomen Plate		Pelvis Plate		Pelvis Plate		
	SM	P	SM	P	SM	P	SM	P	SM	P	SM	P	
	3.72	1.14	2.19	0.55	2.39	2.16	0.88	0.24	2.34	2.20	1.33	1.00	
RMS of SM and P	3.89		2.26		3.22		0.91		3.21		1.66		

Figure 15. SM, P, and RMS values for Dummy A for each external biofidelity response measurement, and biofidelity ranks for test condition, body region and external biofidelity levels.

	Dummy A Internal Biofidelity Rank																	
	1.42																	
Body Region	Thorax												Abdomen				Pelvis			
	1.19												1.97				1.08			
Test Condition	PHF						RLF						PHF		RLF		PHF		RLF	
	1.05						1.33						1.53		2.41		1.21		0.96	
Response Measurement	T1 Lat		T12 Lat		Thx Defl		T1 Lat		T12 Lat		Thx Defl		Abd Defl		Abd Defl		Pelvis Lat		Pelvis Lat	
	SM	P	SM	P	SM	P	SM	P	SM	P	SM	P	SM	P	SM	P	SM	P	SM	P
	0.69	0.00	0.60	1.46	0.86	0.21	0.59	1.93	1.08	0.11	0.60	0.67	1.48	0.40	2.34	0.56	1.16	0.35	0.85	0.44
RMS of SM and P	0.69		1.58		0.89		2.02		1.09		0.90		1.53		2.41		1.21		0.96	

Figure 16. SM, P, and RMS values for Dummy A for each internal biofidelity response measurement, and biofidelity ranks for test condition, body region and internal biofidelity levels.

	Dummy B External Biofidelity Rank											
	2.95											
Body Region	Thorax				Abdomen				Pelvis			
	3.34				2.20				3.30			
Test Condition	PHF		RLF		PHF		RLF		PHF		RLF	
	4.26		2.42		3.51		0.89		4.51		2.09	
Response Measurement	Thorax Plate		Thorax Plate		Abdomen Plate		Abdomen Plate		Pelvis Plate		Pelvis Plate	
	SM	P	SM	P	SM	P	SM	P	SM	P	SM	P
	3.96	1.57	2.42	0.11	2.63	2.33	0.85	0.28	3.69	2.60	1.84	1.00
RMS of SM and P	4.26		2.42		3.51		0.89		4.51		2.09	

Figure 17. SM, P, and RMS values for Dummy B for each external biofidelity response measurement, and biofidelity ranks for test condition, body region and external biofidelity levels.

	Dummy B Internal Biofidelity Rank																							
	1.53																							
Body Region	Thorax												Abdomen				Pelvis							
	1.37												2.24				0.97							
Test Condition	PHF						RLF						PHF		RLF		PHF		RLF					
	1.24						1.49						1.47		3.01		1.05		0.89					
Response Measurement	T1 Lat Acc		T12 Lat Acc		Thx Defl		T1 Lat Acc		T12 Lat Acc		Thx Defl		Abd Defl		Abd Defl		Pelvis Lat Acc		Pelvis Lat Acc					
	SM	P	SM	P	SM	P	SM	P	SM	P	SM	P	SM	P	SM	P	SM	P	SM	P				
	0.56	0.15	0.55	1.46	1.59	0.12	0.62	0.93	0.92	1.50	1.56	0.32	1.45	0.26	2.84	1.00	0.99	0.35	0.88	0.11				
RMS of SM and P	0.58		1.56		1.59		1.12		1.76		1.59		1.47		3.01		1.05		0.89					

Figure 18. SM, P, and RMS values for Dummy B for each internal biofidelity response measurement, and biofidelity ranks for test condition, body region and internal biofidelity levels.

Table 1 shows that the External Biofidelity Rank of Dummy A is better than that of Dummy B and their Internal Biofidelity Ranks are comparable since they do not differ by more than 0.2 (Rhule et al, 2009). Overall, the Biofidelity Rank of Dummy A is better than that of Dummy B.

Table 1.
Biofidelity Ranks for Dummies A and B

	Dummy A	Dummy B
External	2.53	2.95
Internal	1.42	1.53
Overall	**1.98**	**2.24**

DISCUSSION

Normalization

The example of force-deflection curves presented in Figure 1 of the Methods section provides an excellent representation of the benefit of effective stiffness normalization.

Phase Optimization

If we assume that time zero in an impact test event is established by initial contact with the PMHS, it is likely that subjects with excessive body fat will have response data that occurs later in time than will the response data from slender subjects with minimal body fat, and vice versa. If these response curves are not phase-optimized the resulting point by point mean curve will have a broad time duration and possibly a lower magnitude. Phase optimizing allows for the mean curve to be more typical of the basic structural response characteristic of the musculoskeletal system. The Phase Optimization method (Donnelly and Moorhouse, 2012) retains all of the phase lag information among all of the PMHS and it is used to establish the average time zero for the mean curve.

Target Building

The development of a statistically-based PMHS target using a point by point mean and standard deviation has been suggested in the past (Maltese et al, 2002; Rhule et al, 2002, 2009). When the magnitude of the response data is very nearly the same at a point in the time history, perhaps at a point where multiple response curves cross, the standard deviation can be very small. This can result in "necking" where the target created by the plus and minus standard deviation is very small. This feature in a plot of the PMHS target does not affect the mathematical calculation of the $\sqrt{R}$ value (or SM); however, this disconcerting feature can be eliminated by plotting the average standard deviation. The average standard deviation is found by summing all the point by point standard deviations for the upper 80% of the mean PMHS response and dividing by the total number of data points included. Again, this does not affect the calculation of the $\sqrt{R}$ value but does provide a better feel for the quality of an overplotted dummy curve.

Biofidelity Assessment

Figure 19 provides another illustration of why minimizing the phase differences between the dummy response and the mean PMHS response is necessary to obtain an accurate assessment of the biofidelity of a dummy response. Because the SM is calculated relative to the upper 80% of the mean

PMHS curve (note the start and end points of the standard deviation curves), the portion of the unshifted dummy curve (dotted blue line) that is assessed occurs after the main dummy response and is not very meaningful. When the phase difference between the dummy response and the mean PMHS response is minimized, the portion of the shifted dummy response (solid blue line) that is assessed is much more appropriate and meaningful. The SM value for the shifted curve (0.59) compared to that of the unshifted curve (1.17) reflects the better fit of the dummy response after minimizing the phase difference, while the P value (1.93) quantifies the biofidelity of the phase response of the dummy.

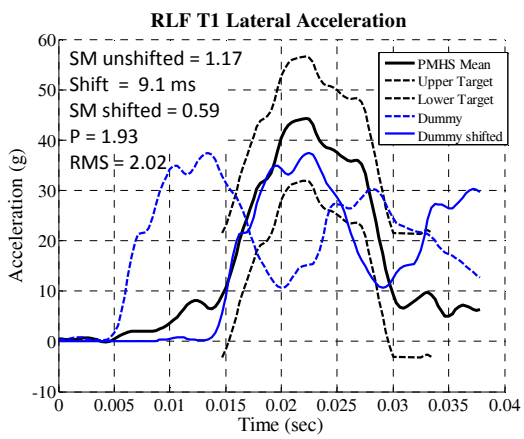

Figure 19. Unshifted and shifted response curves for Dummy A with biofidelity target for RLF T1 Lateral Acceleration

The RMS value for the RLF T1 lateral acceleration for Dummy A is 2.02, which is much different from the 1.17 SM value for the unshifted curve (which represents the $\sqrt{R}$ that would have been calculated in previous versions of the BRS). When the dummy phase response is poor, as it is in this case, the quantitative biofidelity assessment value for the response measurement (RMS) will show a larger difference from its predecessor, $\sqrt{R}$, as compared to when the dummy phase response is good. By individually assessing the biofidelity of dummy phase and shape/magnitude responses, the biofidelity assessment is more meaningful since the SM values (and thus RMS values) are now more appropriately calculated. Furthermore, the additional phase biofidelity information helps to indicate more specifically where improvement to the dummy response is needed.

Figure 20 shows the External Biofidelity assessment schematic for Dummy A using $\sqrt{R}$ values, as would have been done using the 2009 version of the BRS. Notice that the External Biofidelity Rank of 2.83 unshifted is not very different compared to that of the 2.53 for Dummy A using the shifted data of the new methodology (Figure 15). This is because the two methods will produce similar results for well-conditioned responses (i.e, not highly out of phase or very short duration high peak responses), while the new method is able to much more accurately quantify the biofidelity for those dummy responses that exhibit some of these issues. Since this occurrence is relatively rare it is unlikely that previously published biofidelity ranks need to be re-calculated.

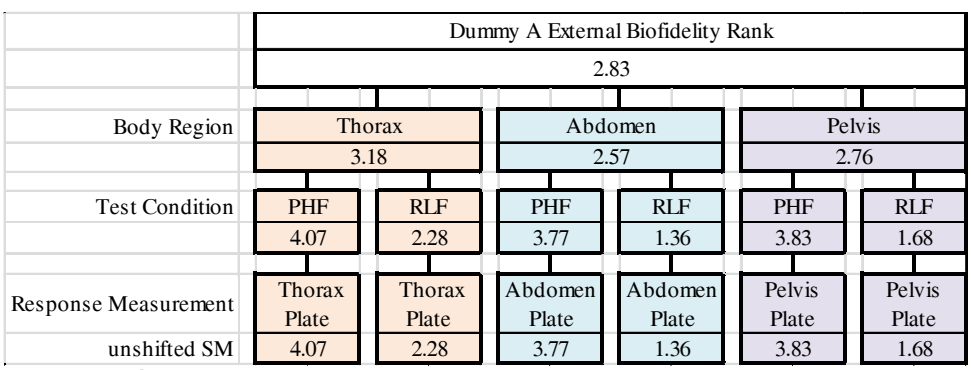

Figure 20. $\sqrt{R}$ values for external biofidelity response measurements of Dummy A (2009 version of BRS), and biofidelity ranks for test condition, body region and external biofidelity levels.

SUMMARY

A set of tools are presented that can be applied to a set of PMHS responses, in sequence, to obtain a biofidelity target. The updated Biofidelity Ranking System is also presented for quantitatively assessing the biofidelity of a dummy as compared to the PMHS targets for phase and for shape and magnitude.

The tools are:

- Normalization for modifying PMHS response data to better represent a 50th percentile male human (or other target population).
- Phase Optimization based on all permutations of the cross-correlation functions and the Lagrange Multiplier method to find the best phase fit simultaneously for all PMHS response curves as well as determine the average PMHS phase shift to locate the mean curve in time.
- Target Building creates a PMHS response target that is statistically based and can be used to quantitatively assess the quality of a dummy response, or multiple dummies' responses.
- The Biofidelity Ranking System (BRS) has been updated to include the Shape and Magnitude Response Comparison Value, SM, the Phase Response Comparison Value, P, and the Channel Biofidelity Value, RMS. These features improve the quantitative assessment of internal and external dummy biofidelity quality.

REFERENCES

Donnelly, B.R., and Moorhouse, K. (2012) Optimized Phasing of PMHS Response Curves for Biofidelity Targets. Proc. IRCOBI Conference 2012.

Eppinger, R. H., Marcus, J. H., and Morgan, R. M. (1989). Development of dummy and injury index for NHTSA's thoracic side impact protection research program. SAE 840885. Society of Automotive Engineers, Warrendale, PA.

Kang, Y., Moorhouse, K., Donnelly, B., Herriott, R., Bolte, J. (2012) Biomechanical Responses of PMHS in Moderate-Speed Rear Impacts and Development of Response Targets for Evaluating the Internal and External Biofidelity of ATDs. Stapp Car Crash Journal 56.

Maltese, M.R., Eppinger, R.H., Rhule, H.H., Donnelly, B., Pintar, F.A. and Yoganandan, N. (2002) Response Corridors of Human Surrogates In Lateral Impacts. Stapp Car Crash Journal 46: 321-351.

Mertz, H. J., (1984). A procedure for normalizing impact response data. SAE 840884. Society of Automotive Engineers, Warrendale, PA.

Moorhouse, K., Donnelly, B., Kang, Y., Bolte, J., Herriott, R. (2012) Evaluation of the Internal and External Biofidelity of Current Rear Impact ATDs to Response Targets Developed from Moderate-Speed Rear Impacts of PMHS. Stapp Car Crash Journal 56.

Moorhouse, K. (2013) An Improved Normalization Methodology for Developing Mean Human Response Curves. 23rd International Technical Conference on the Enhanced Safety of Vehicles, Paper No.13-0192.

Morgan, R.M., Marcus, J.H., and Eppinger, R.H. (1986) Side Impact – The Biofidelity of NHTSA's Proposed ATD and Efficacy of TTI. Proc. 30th Stapp Car Crash Conference, pp. 27-40. Society of Automotive Engineers, Warrendale, PA.

Rhule, H.H., Maltese, M.R., Donnelly, B.R., Eppinger, R.H., Brunner, J.K., and Bolte, J.H.IV. (2002) Development of a New Biofidelity Ranking System for Anthropomorphic Test Devices. Stapp Car Crash Journal 46: 477-512.

Rhule, H., Moorhouse, K., Donnelly, B., Stricklin, J., 2009. Comparison of WORLDSID and ES-2RE biofidelity using updated biofidelity ranking system. 21st International Technical Conference on the Enhanced Safety of Vehicles, Paper No.09-0563.

Viano, D. C., (1989). Biomechanical responses and injuries in blunt lateral impact. SAE 892432. Society of Automotive Engineers, Warrendale, PA.

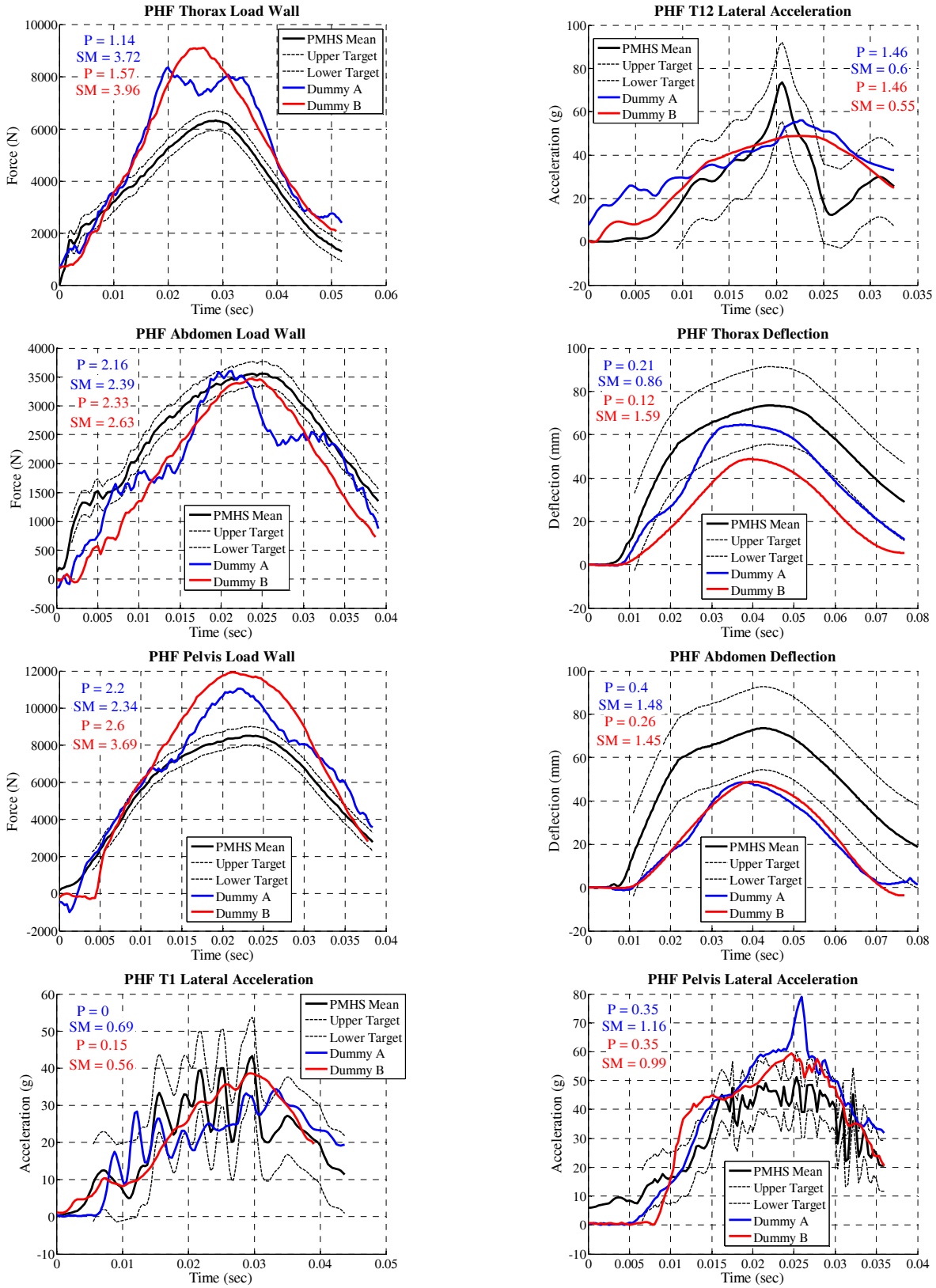

Figure A1. PMHS mean and average standard deviation targets with two side impact dummy responses for Padded High Speed Flat Wall sled tests (Maltese, 2002)

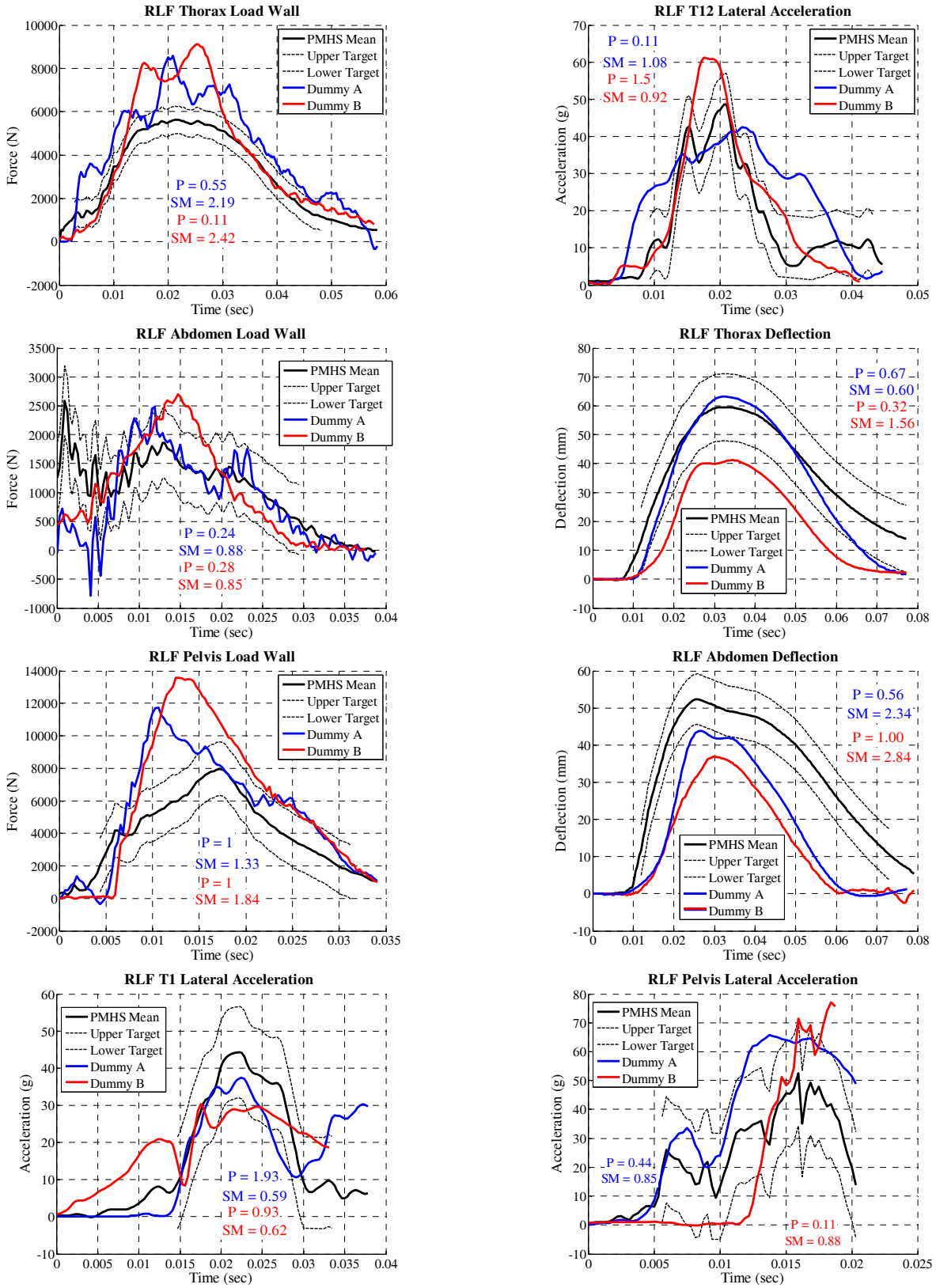

Figure A2. PMHS mean and average standard deviation targets with two side impact dummy responses for Rigid Low Speed Flat Wall sled tests (Maltese, 2002)

BIOFIDELITY OF FORCE RESPONSES OF DIFFERENT TYPES OF HUMAN SURROGATES IN OBLIQUE SIDE IMPACTS

Narayan Yoganandan, Frank A. Pintar, John R. Humm
Medical College of Wisconsin
Milwaukee, WI USA

Rodney W. Rudd, Stephen A. Ridella
US Department of Transportation
NHTSA, Washington, DC

Paper number 13-0179

ABSTRACT

In order to determine the biofidelity responses of anthropomorphic test devices, also called dummies, used in crashworthiness studies and develop injury criteria for trauma assessment devices, studies using post mortem human subjects (PMHS) are often necessary. From the perspective of side impacts, many studies are available on these issues when the applied load vector is pure lateral. Injuries, injury metrics, and injury criteria have been advanced for the current ES-2re device using matched-pair tests. Similar studies are needed for oblique loading as this mode is recognized in modern vehicle environments as an important vector for inducing trauma. Thus, the present study was designed to compare differences in the design of load-walls between different types of pure lateral tests, review literatures to determine the need to conduct oblique side impact sled tests and present a detailed methodology to gather region-specific data (such as force-time curves) which can be used to accurately evaluate the local responses of PMHS and dummies, ES-2re and WorldSID. The consolidated graphs overlaying PMHS and the two dummy responses serve as a first step in the assessment of dummy biofidelity.

INTRODUCTION

Matched-pair sled tests with PMHS and dummies have been used to evaluate the responses of different surrogates under predetermined initial and boundary conditions in a laboratory environment [1-9]. Such tests have also been used to develop dummy-specific injury criteria and advance motor vehicle safety standards around the world. For example, the current United States side impact standards FMVSS No. 214 are based on PMHS tests and matched ES-2re experiments [10, 11].

With regard to the application of the dynamic loading in side impacts, pure lateral loading (corresponding to the clock positions of nine for the driver and three, for the passenger in the United States) has been commonly used as the direction of the loading vector for the evaluation of biomechanics and motor vehicle crashworthiness [2, 5, 8, 12, 13]. Previous studies aimed at determining the biomechanics of nearside impacts consisted of a flat one-unit rigid load-wall attached to the platform of a deceleration sled [13]. These PMHS sled experiments were done in Heidelberg, Germany.

In a series of later studies conducted in the United States, a similar load-wall design (Figure 1) was used by researchers at the Medical College of Wisconsin and elsewhere wherein the dimensions approximated a mid-size sedan [2, 5, 14, 15]. Figure 2 shows the schematic of the PMHS used in these tests with the targeted impact locations in relation to the load-wall, based on the mid-size male anthropometry. A similar segmented load-wall was used by other researchers to determine region-specific responses including dynamic forces applied to the PMHS occupant [12, 16].

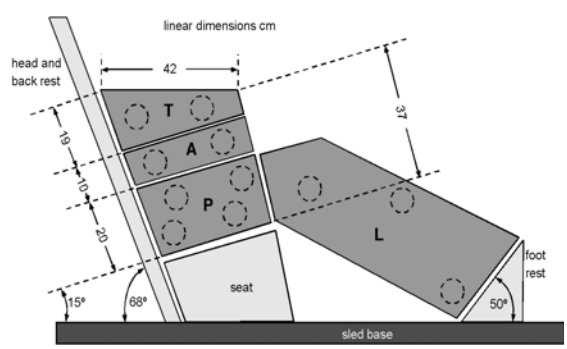

Figure 1: Schematic of the load-wall used to subject human surrogates to pure lateral nearside impact. T, A, P and L respectively represent the load-wall plates for the thorax, abdomen, pelvis and lower leg. The experimental bench seat is also shown.

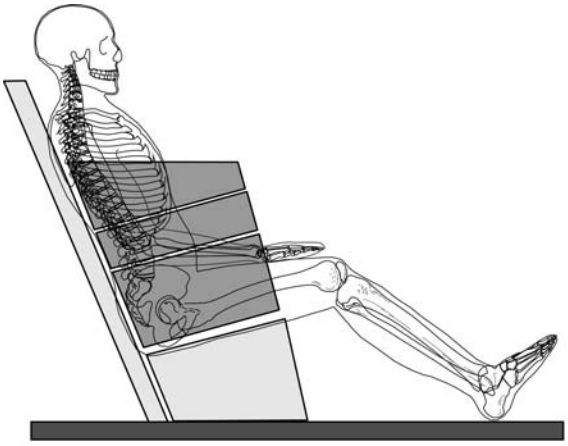

Figure 2: Targeted impact locations from three plates on the PMHS specimen corresponding to the mid-size male anthropometry

Database analyses using the United States National Automotive Sampling System and Crash Injury Research and Engineering Network (NASS and CIREN) have identified the oblique loading as an important vector associated with trauma in real-world side impacts [17]. Because the impact vector is oblique, deflection patterns, occupant kinematics, injuries and injury mechanisms differ from those induced by the pure lateral vector, and the heterogeneous complex three-dimensional anatomy of the human torso also contributes to this effect. Recognition of this oblique vector and quantification of biomechanical data require sled tests with PMHS in simulated environments. The present study is designed to develop a methodology to apply dynamic forces along an oblique vector to both biological and physical models using an anthropometry-specific custom load-wall design and the results are presented from PMHS, ES-2re and WorldSID surrogates to show the feasibility of the experimental design.

METHODS

PMHS specimen preparation: Medical records of an unembalmed PMHS were obtained. The PMHS was screened for HIV, and Hepatitis A, B and C. The surrogate was prepared as follows for conducting sled tests. Anthropomorphic data and pretest x-rays were obtained according to established procedures [5]. All specimens were dressed in tight-fitting leotards and a mask covered the head/face. The prepared surrogates were placed on a custom Teflon-coated bench seat, fixed to the platform of an acceleration sled (Seattle Safety, Seattle, WA, USA). The sled was configured with an impacting load-wall to simulate nearside impacts. The impacting load-wall is described later. The experimental bench seat (not a production one) was 1.3 meter in length. It was reinforced below the seat pan at mid-length. The dimensions of the bench seat used for all sled tests are given (Table 1) and schematically shown in figure 1.

Table 1: Details of the experimental bench seat used in the present study

Description	Value
Width (mm)	1220
Length (mm)	410
Height in the front (mm)	290
Height in the back (mm)	195
Seat back height (mm)	930
Seat bottom angle (deg)	13
Seat back angle (deg)	22

Impacting load-wall: The load-wall used in these studies was scalable and modular. In other words, the design allowed for positioning different surrogates based on individual anthropometry. The load-wall had six plates. Plates were made a priori with different height dimensions (used 12.5 mm increments) to accommodate varying region-specific specimen anthropometry. The first five metal plates consisted of the shoulder, thorax, abdomen, and superior and inferior pelvis (corresponding to the location of the ipsilateral iliac crest and greater trochanter) plates. A schematic of the load-wall showing the five plates is depicted in figure 3.

The positions of the five plates were adjustable in the frontal plane, that is, adjustments could be made along the vertical, superior-inferior and lateral, left-to-right directions to ensure contact of each plate with the intended specific body region. All these five plates were rigidly attached to a vertical fixture and the fixture was securely connected to the platform of the acceleration sled equipment (Figure 3). A gap was allowed between each of the plates to extract region-specific forces during impact.

A separate sixth plate was used to contact/load the lower limb during side impact (Figure 3). It was mounted to a second vertical fixture, also secured rigidly to the platform of the acceleration sled equipment. The two vertical fixtures allowed for independent positioning of the torso-pelvis and lower limb regions of the surrogate. The vertical height and

lateral positioning of the fixtures were adjusted based on the anthropometry of each surrogate.

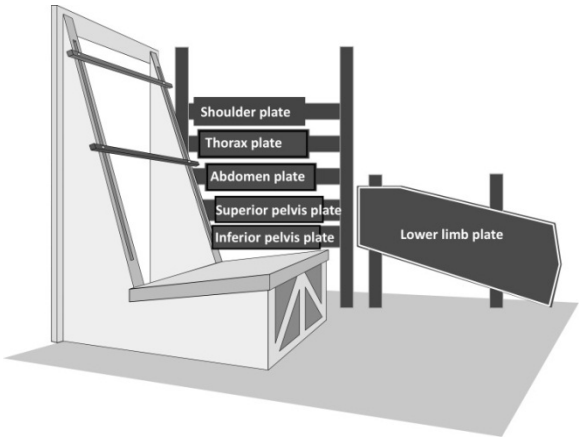

Figure 3: Schematic of the five metal plates (corresponding to the shoulder, thorax, abdomen, superior pelvis and inferior pelvis) attached to the vertical fixture. The lower limb, i.e., sixth plate attached to another vertical fixture is also shown. The reinforced experimental bench seat is shown.

In order to simulate oblique side impact loading, the shoulder, thorax and abdomen plates of the load-wall were oriented at thirty degrees antero-medially with respect to the ipsilateral side of the specimen. Figure 4 shows a schematic of the orientation as viewed from the top.

To ensure simultaneous contact of all torso regions, the individual shoulder, thorax, abdomen and pelvis plates were positioned based on the PMHS specimen anthropometry using the modular and adjustable features of the load-wall design. The shoulder plate was positioned first by moving the upper arm horizontally and rotating antero-medially to the same obliquity as the plate. This ensured contact with the shoulder plate. The resulting position of the shoulder plate was secured to its vertical fixture. The positioning of the shoulder plate is illustrated in figure 5.

Subsequently, the thoracic plate was positioned by moving the plate laterally to contact the thorax at the fourth rib level on the lateral-most aspect of the PMHS specimen and the resulting position of the plate was secured to its vertical fixture. The positioning of the thoracic plate is illustrated in figure 6.

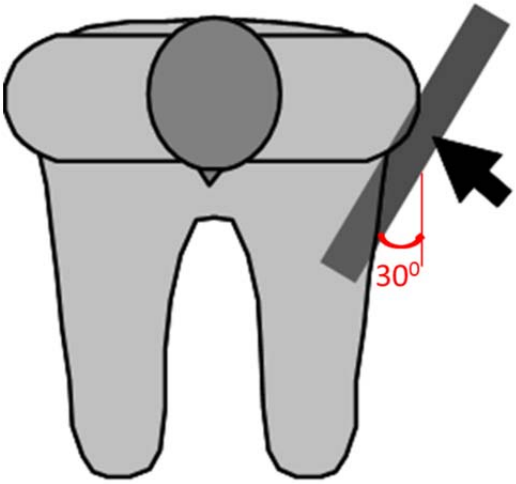

Figure 4: Overhead view showing the alignment of the plates for oblique left side impact.

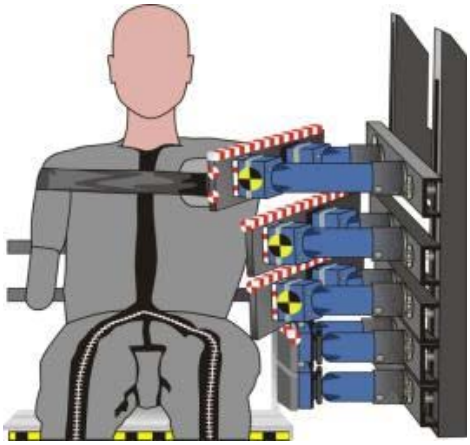

Figure 5: Alignment and positioning of the shoulder load plate with the shoulder.

A similar process was used for the abdomen plate with alignment focusing on the tenth rib of the PMHS specimen. The positioning of the abdomen plate is illustrated in figure 7.

The two pelvic plates were then brought into contact with the lateral protuberances of the iliac crest and greater trochanter regions of the PMHS specimen. The positioning of the pelvis plates is illustrated in figure 8.

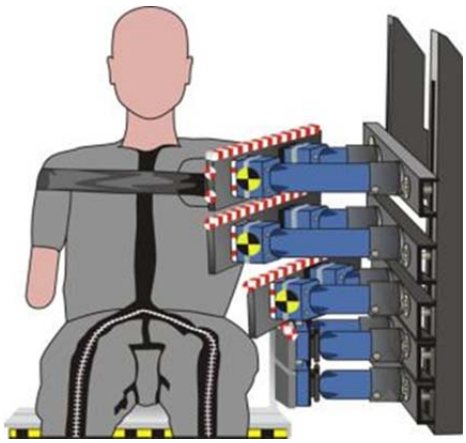

Figure 6: Alignment and positioning of the thorax load plate with the thorax.

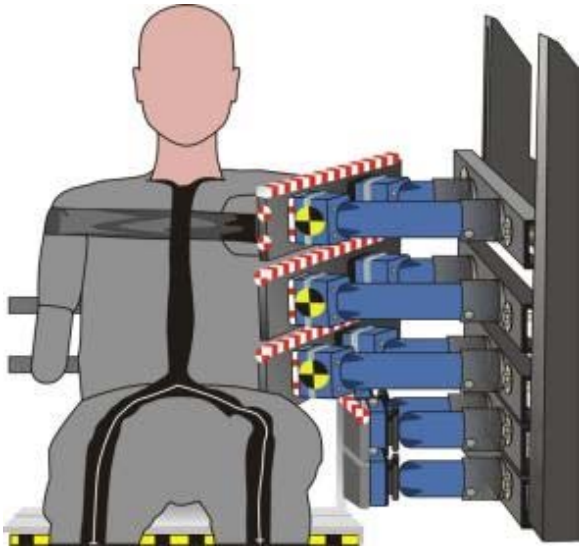

Figure 7: Alignment and positioning of the abdomen load plate with the abdomen

To simulate normal driving position, the left arm was held parallel to the shoulder plate and rotated inferiorly by 45 degrees in the sagittal plane before the start of the experiment.

Anthropomorphic tests device preparation: Two dummies were used in the study to demonstrate the feasibility of the modular scalable load-wall to conduct oblique nearside impact tests with the acceleration sled. The ES-2re dummy was clothed and positioned according to or procedures used in the New Car Assessment Program (NCAP) in the United States.

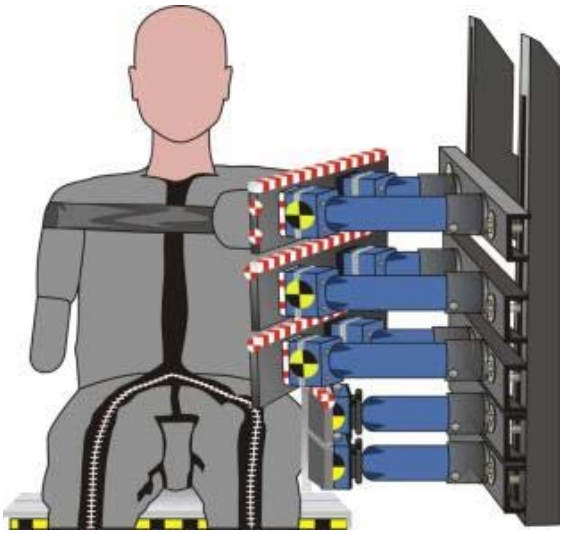

Figure 8: Alignment and positioning of the pelvis load plates with the pelvis regions.

The shoulder plate of the load-wall was positioned by moving the upper arm of the ES-2re dummy horizontally and rotating medially by an angle of 30 degrees to contact the dummy shoulder. The resulting position of the shoulder plate was secured to the vertical fixture. This process was similar to those used in the positioning of the biological surrogate.

The thoracic plate was positioned by moving the thoracic plate laterally to contact the second thoracic rib region of the ES-2re dummy and the resulting position of the plate was fixed as before, again corresponding to methods used for positioning the PMHS. The abdomen plate was also similarly positioned.

Similar to the positioning of the biological surrogate, pelvic plates in the ES2-re dummy were brought into contact with the pelvic region and in addition, the left lower extremity contacted the lower limb plate. The arm was positioned parallel to the plate in the driving posture similar to the PMHS tests and before applying the side impact pulse.

For the positioning of the WorldSID, while all procedures were identical, because of the smaller dimensions of the dummy, only one pelvic plate was used instead of two used in the PMHS and ES-2re tests.

Side impact loading and instrumentation: The following methods are common to all three

surrogates. An acceleration sled was used conduct the tests at a change in velocity of 24 km/h. The sled equipment was instrumented with a uniaxial accelerometer to record the input side impact acceleration pulse from which the change in velocity was computed in the time domain.

The segmented load-wall with the six plates was instrumented with tri-axial load cells. All load cells were located approximately at the mid-height of each plate and one-third distances from the fore and aft edges to obtain generalized force histories corresponding to different body segments.

Biomechanical data: Data were gathered according to the Society of Automotive Engineers specifications [18]. To obtain body region-specific impact force histories, the individual force-time signals from respective load cells were summated for the specific load-wall plate. The biomechanical force data from the biological surrogate were scaled based on the equal velocity, equal mass approach [19]. This methodology has been used in earlier side impact studies [1, 2, 8, 12, 20]. The times of attainment of five percent of the peak force on the pelvis were used as the origin to align force signals from all load-wall plates to ensure consistent extraction of the peak loads on various body regions from all the three surrogates. The maximum forces and the times of attainments of the respective peak amplitudes were obtained for each body region. Plots of the sled acceleration, forces from the shoulder, thorax, abdomen, pelvis and lower limb plates are presented in the results section below for the PMHS, ES-2re and WorldSID surrogates.

RESULTS

Figure 9 shows the sled acceleration applied to the PMHS and the two surrogates. The pulse was uni-modal and was such that the change in velocity was 24 km/h. For the shoulder, the peak forces and times of occurrence for the PMHS and ES-2re were: 0.7 kN occurred at approximately 80.0 ms, and 1.4 kN occurred at approximately 91.7 ms. Forces were low (less than 100 N) for the WorldSID device. These data are shown (Figure 10).

Figure 11 comapres the force-time histories for the thorax for all surrogates. Forces were considerably greater than those encountered by the shoulder. The peak force of 5.8 kN occurred at approximately 76.7 ms for the PMHS, 7.9 kN occurred at approximately 87.5 ms for the ES-2re, and 7.9 kN occurred at approximately 79.3 ms for the WorldSID.

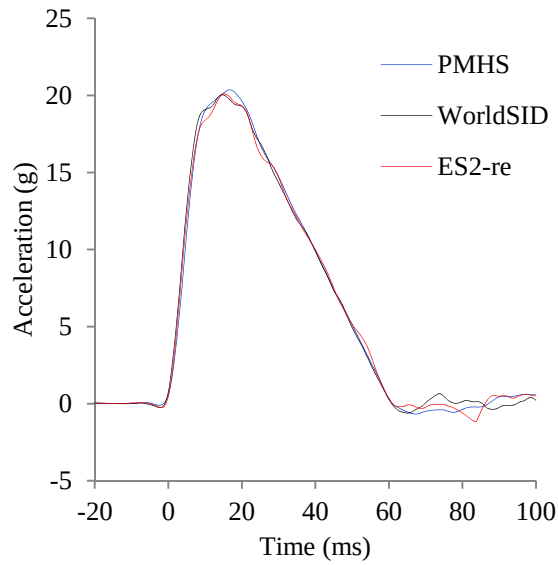

Figure 9: Sled pulse used for all surrogates

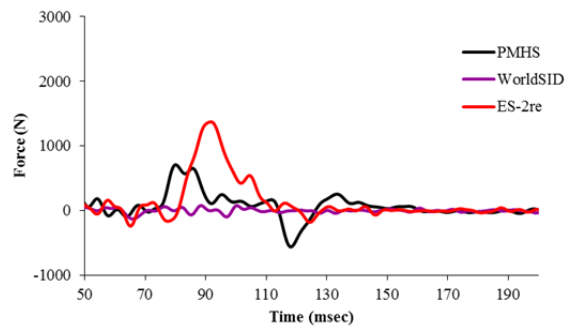

Figure 10: Shoulder force histories.

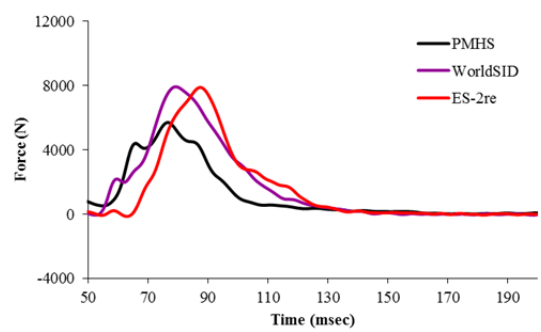

Figure 11: Thorax force histories.

Figure 12 compares the force-time histories for the abdomen for all surrogates. The peak force of 4.4 kN occurred at approximately 75.7 ms for the PMHS, 7.8 kN occurred at approximately 86.9 ms for the ES-2re,

and 3.3 kN occurred at approximately 79.69 ms for the WorldSID.

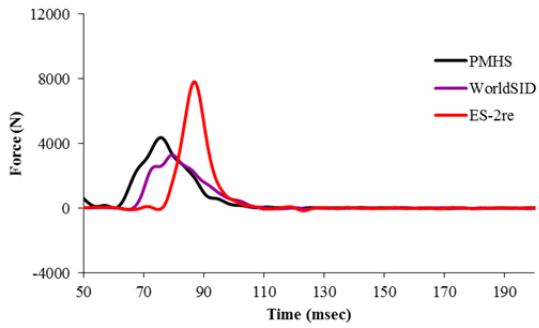

Figure 12: Abdomen force histories.

Figure 13 compares the force-time histories for the pelvis for all surrogates. The peak force of 12.5 kN occurred at approximately 75.1 ms for the PMHS, 18.9 kN occurred at approximately 85.6 ms for the ES-2re, and 12.4 kN occurred at approximately 76.2 ms for the WorldSID.

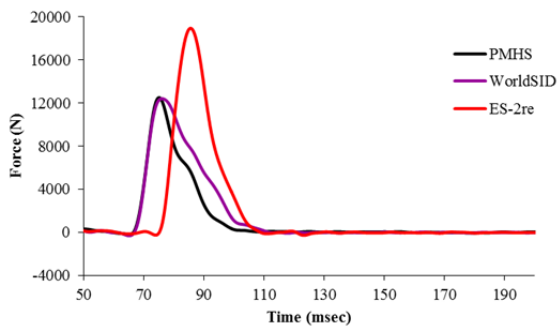

Figure 13: Pelvis force histories.

DISCUSSION

As indicated in the introduction, the objective of the present study was to compare differences in the design of load-walls between different types of pure lateral tests, review literatures to determine the need to conduct oblique side impact sled tests and present a detailed methodology to gather region-specific data (such as force-time curves) which can be used to accurately evaluate the local responses of PMHS and dummies, ES-2re and WorldSID. The consolidated graphs overlaying PMHS and the two dummy responses serve as a first step in the assessment of dummy biofidelity.

This was accomplished by using a scalable modular load-wall capable of isolating forces on the shoulder, thorax, abdomen, superior and inferior pelvis regions, and the ipsilateral lower limb of all surrogates. The load-wall was configured such that it was angled to induce oblique loading antero-medially to the PMHS, WorldSID and ES2-re surrogates, simulating nearside dynamic contact loading to the driver or passenger.

The chosen velocity of 24 km/h has been used in previous studies with pure lateral loading [2, 5, 10, 20]. Thus, it is possible to evaluate the present oblique loading data with the data from the other vector. Extending the present methodology to include additional PMHS tests and repeat dummy tests would render such evaluations possible, and this is considered as future research. As forces are extracted from different body region, with additional tests it should also be possible to evaluate regional biofidelity responses of the two dummies, and to accomplish these goals, methods are available in the literature [21, 22].

The load-wall configuration used in these oblique loading tests included multiple segmented plates to individually contact the shoulder, thorax, abdomen, pelvis and lower limb on the ipsilateral side of each surrogate. Allowing gaps between the torso plates facilitated the isolation of forces in the respective body regions. However, this was not the sole determinant to extract region-specific forces from the three surrogates. This is because the same dimension/geometry, non-anthropometry specific load-wall cannot be used for all surrogates. It is well known that the seating heights of the mid-size male 50th percentile side impact dummies are not identical [6, 23]. Further, the overall seating and region-specific heights of biological surrogates vary. From this perspective, it is imperative to accommodate a scalable and modular load-wall in the experimental design so that the individual body regions can be positioned such that the plate contacts only those respective regions to extract forces. This feature was also included in the present study. Thus, the biomechanical metrics from this study represent the true region-specific information.

The surrogates were placed at a distance from the load-wall such that impact occurred at the end of the acceleration pulse during the region of constant velocity. Due to the nature of the servo sled control mechanism, this zone is relatively large. Thus, timing of the initial impact with the load-wall with the specimen was not critical. Therefore, surrogates may have contacted the load-wall at different times during the region of constant velocity. To accurately compare signals between surrogates, it was necessary to determine the timing of initial impact with the

load-wall. The pelvis plate was chosen for this process because it was parallel to the mid-sagittal plane of the surrogate and consistently demonstrated unimodal response. The close agreement in the times of attainments of peak forces (within 5, 9 and 7 ms for the PMHS, WorldSID and ES-2re) shows that the modular load-wall is effective in delivering region-specific impact loads uniformly in all surrogates.

The alignment of the signals using this method with respect to the close times of attainments of the peak forces in all surrogates show that the modular load-wall is capable of delivering the impact forces within the same time domain, thereby assisting in a better evaluation of dummy biofidelity.

Energy absorbing materials exist in real-world motor vehicle environments. However, no such materials were used in the present study, i.e., the load-wall plates were not covered with padding components. While rigid load-wall tests have been used in sled tests in previous studies, it should be noted to cover the full spectrum of research paralleling those conducted for pure lateral tests, it would be necessary to extend the present series of tests to other initial/boundary conditions. This includes offset (abdomen and pelvis) conditions and probably other angulations to determine the most practically feasible detriment obliquity condition to understand the mechanism of injuries, injury tolerance and injury criteria. It should be possible to conduct such studies based on earlier research used for the development of ES-2re pure lateral injury criteria [1, 10]. Another area of potential application is postero-lateral loading which has been recognized as another oblique loading vector for injuries to organs such as the spleen and kidneys [24]. It should be possible to reorient the angulations of the different plates to induce postero-lateral oblique loading and conduct similar tests with different surrogates to determine injuries, injury mechanisms, regional biomechanical metrics, injury criteria and dummy biofidelity. These are considered as future research and dissemination topics.

CONCLUSIONS

a) The present study compared differences in the design of load-walls between different types of pure lateral tests, reviewed literatures to determine the need to conduct oblique side impact sled tests and presented a detailed methodology to gather region-specific data (such as force-time curves) which can be used to accurately evaluate the local responses of PMHS and dummies, ES-2re and WorldSID.

b) A scalable modular load-wall was developed for conducting oblique side impact studies.

c) The load-wall design included segmentation of forces to the shoulder, thorax, abdomen, superior and inferior pelvis, and ipsilateral lower limb.

d) To demonstrate the feasibility of using the developed methodologies, tests were conducted using the PMHS, a biological surrogate; the ES-2re, the currently federalized dummy for side impact crashworthiness in the United States according to FMVSS No. 214 and NCAP protocols; and the WorldSID, a dummy under development which has different designs for the shoulder, thorax, abdomen and pelvic regions.

e) Force-time histories were compared for each of the various body regions on surrogate-by-surrogate bases by conducting sled tests at a velocity of 24 km/h.

f) Peak forces and the time of occurrences of these metrics for all surrogates and body regions were also presented.

g) It should be possible to extend these studies with additional samples, boundary/initial conditions and velocities similar to those used in pure lateral side impact studies for the derivation of injury criteria/probability-based risk functions and assessment of dummy biofidelity responses on a regional basis.

h) The provided consolidated graphs overlaying PMHS and dummy response serve as a first step in the overall biofidelity goals.

ACKNOWLEDGMNETS

This research study was supported in part by DTNH22-07-H-00173, Department of Neurosurgery at the Medical College of Wisconsin, Milwaukee, WI and VA Medical Research. The assistance of the Neuroscience research staff is acknowledged.

REFERENCES

1. Kuppa, S., F. Eppinger, M. Maltese, R. Naik, N. Yoganandan, et al. *Assessment of thoracic injury criteria for side impact*. in *IRCOBI*. 2000. Montpellier, France.
2. Maltese, M.R., R.H. Eppinger, H.H. Rhule, B.R. Donnelly, F.A. Pintar, et al., *Response corridors of human surrogates in lateral impacts.* Stapp Car Crash J, 2002. 46: p. 321-51.
3. Morgan, R.M., JM and R. Eppinger. *Correlation of side impact dummy/cadaver tests*. in *Stapp Car Crash Conf.* 1981.
4. Morgan, R.M., JM and R. Eppinger. *Side impact - The biofidelity of NHTSA's proposed ATD and efficacy of TTl*. in *Stapp Car Crash Conf.* 1986.
5. Pintar, F.A., N. Yoganandan, M.H. Hines, M.R. Maltese, J. McFadden, et al. *Chestband analysis of human tolerance to side impact*. in *Stapp Car Crash Conf.* 1997. Lake Buena Vista, FL.
6. Pintar, F.A., N. Yoganandan, B.D. Stemper, O. Bostrom, S.W. Rouhana, et al., *Comparison of PMHS, WorldSID, and THOR-NT responses in simulated far side impact.* Stapp Car Crash J, 2007. 51: p. 313-60.
7. Yoganandan, N., R.M. Morgan, R.H. Eppinger, F.A. Pintar, A. Sances, Jr., et al., *Mechanisms of thoracic injury in frontal impact.* J Biomech Eng, 1996. 118(4): p. 595-7.
8. Yoganandan, N., F.A. Pintar, B.D. Stemper, T.A. Gennarelli, and J.A. Weigelt, *Biomechanics of side impact: injury criteria, aging occupants, and airbag technology.* J Biomech, 2007. 40(2): p. 227-43.
9. Yoganandan, N., D. Skrade, F.A. Pintar, J. Reinartz, and A. Sances Jr, *Thoracic deformation contours in frontal impact.* 35th Stapp Car Crash Conf, 1991: p. 47-63.
10. Kuppa, S., R.H. Eppinger, F. McKoy, T. Nguyen, F.A. Pintar, et al., *Development of side impact thoracic injury criteria and their application to the modified ES-2 dummy with rib extensions (ES-2re).* Stapp Car Crash J, 2003. 47: p. 189-210.
11. FMVSS-214, *49 Code of Federal Regulations: 571.214*. 2008, US Government Printing Office: Washington, DC.
12. Cavanaugh, J.M., Y. Zhu, Y. Huang, and A.I. King, *Injury and response of the thorax in side impact cadaveric tests*, in *Biomechanics of Impact Injury and Injury Tolerances of the Thorax-Shoulder Complex*, S.H. Backaitis and W.H. Mertz, Editors. 1994, SAE, Inc.: Warrendale, PA. p. 949-972.
13. Kallieris, D., R. Mattern, G. Schmidt, and R.H. Eppinger. *Quantification of side impact responses and injuries*. in *Stapp Car Crash Conf.* 1981. San Francisco, CA: Society of Automotive Engineers, Inc.
14. Pintar, F.A., N. Yoganandan, A. Sances, and R. Eppinger. *Instrumentation of Human Surrogates for Side Impact*. in *Stapp Car Crash Conference*. 1996. Albuquerque, NM.
15. Yoganandan, N., F.A. Pintar, and T.A. Gennarelli. *Chest injuries and injury mechanisms in oblique lateral impacts*. in *IRCOBI*. 2007. Maastricht, The Netherlands.
16. Cavanaugh, J.M., T.J. Walilko, A. Malhotra, Y. Zhu, and A.I. King. *Biomechanical response and injury tolerance of the thorax in twelve sled side impacts*. in *Proc 34th Stapp Car Crash Conf.* 1990. Orlando, FL.
17. Pintar, F.A., D.J. Maiman, and N. Yoganandan. *Occupant dynamics and injuries in narrow-object side impact*. in *Experimental Safety of Vehicles*. 2007. Lyon, France.
18. *Instrumentation for impact test: Part 1 - electronic Instrumentation-SAE J211/1*. SAE 2003, Society of Automotive Engineers (SAE): Warrendale, PA.
19. Eppinger, R. *Prediction of thoracic injury using measurable experimental parameters*. in *6th International Conference on Experimental Safety Vehicles*. 1976. Washington, DC: NHTSA.
20. Yoganandan, N. and F.A. Pintar, *Deflection, acceleration, and force corridors for small females in side impacts.* Traffic Inj Prev, 2005. 6(4): p. 379-86.
21. Rhule, H.H., M.R. Maltese, B.R. Donnelly, R.H. Eppinger, J.K. Brunner, et al., *Development of a new biofidelity ranking system for anthropomorphic test devices.* Stapp Car Crash J, 2002. 46: p. 477-512.
22. Rhule, H.H., K. Moorhouse, B. Donnelly, and J. Stricklin. *Comparison of WorldSID and ES2-re biofidelity using an updated biofidelity ranking system*. in *Experimental Safety of Vehicles*. 2009. Stuttgart, Germany.
23. Scherer, R., K. Bortenschlager, A. Akiyama, S. Tylko, M. Hartlieb, et al. *WorldSID production dummy biomechanical responses.* in *Experimental Safety of Vehicles*. 2009. Stuttgart, Germany.
24. Hallman, J.J., K.J. Brasel, N. Yoganandan, and F.A. Pintar, *Splenic trauma as an adverse effect of torso-protecting side airbags: biomechanical and case evidence.* Ann Adv Automot Med, 2009. 53: p. 13-24.

INFLUENCE OF PELVIS FLESH ON ABDOMEN DEFLECTIONS IN THE WORLDSID IN SIDE IMPACT SLED TESTS

John R. Humm, Narayan Yoganandan, Frank A. Pintar
Medical College of Wisconsin
Milwaukee, WI USA

Rodney W. Rudd
US Department of Transportation
NHTSA, Washington, DC USA

Paper number 13-0386

ABSTRACT

The ES-2re has limited abilities to output measures such as abdominal deflections which may be used to predict region-specific injuries. The WorldSID is being increasingly used in full-scale crash tests and sled experiments because of its ability to extract biomechanical metrics such as abdominal deflections in lateral impacts. Concerns have been raised by researchers around the world regarding the issue of the pelvis flesh interference in allowing the abdominal rib to deflect in side impacts and underestimate the local deflection/injury. The present study was conducted using a WorldSID 50th percentile male dummy to determine the influence of the flesh in constraining the abdomen rib kinetics.

A standard and modified pelvis was tested on a side impact buck with a 50 mm abdomen offset at 3, 4, and 5 m/s. The jacket, struck side arm, and rib padding were removed. Of specific study focus, deflections from the second abdomen rib are discussed. Increasing velocities produced increasing forces and deflections. Force and deflection responses were uni-modal and repeatable under both seating conditions and both types of pelvises. Peak deflections were not significantly different between the standard and modified dummies in the reclined seat configuration. This was independent of velocity. In the upright configuration, peak abdomen deflections were slightly greater at 3 and 4 m/s, and the trend was reversed at 5 m/s. Only two extreme seat configurations were chosen as a range of dummy pelvis angles in motor vehicles. A comparison with earlier tests was difficult due to numerous differences in test methodologies. These findings indicate that the standard WorldSID pelvis may be used without pelvic flesh-rib interaction inhibiting abdomen kinetics and that modification of the pelvis flesh is not necessary at this time.

INTRODUCTION

Recent changes to the U.S. FMVSS No. 214 regulatory side impact safety standards have incorporated the EuroSID 2re (ES-2re) dummy to assess crashworthiness in motor vehicles [1]. In 2007, the National Highway Traffic Safety Administration (NHTSA) commented that the WorldSID dummy was not ready for regulation and it would continue its evaluation of the WorldSID for future incorporation into Part 572. Future updates to FMVSS No. 214 may consider the WorldSID dummy which was designed to be the next generation side impact dummy for harmonization of worldwide safety standards.

The WorldSID has a shoulder rib, three thorax ribs and two abdominal ribs, all of which can measure individual rib acceleration and deflection [2]. Measurement of abdomen deflection extends the ability of the WorldSID to provide additional biomechanical metrics and injury criteria. The rib design is a double hoop structure made up of an outer plastic band to define the torso geometry and an inner ring which is tuned to produce the region specific response. The outer band is connected posteriorly to the spine box and anteriorly to a flexible plastic sternum. The inner band is connected to the outer band at the most lateral point of the rib. The pelvis consists of a two-piece hard plastic skeleton surrounded by a single molded flesh. The skeleton design was based on the Reynolds' pelvis anatomy data while the exterior dimensions used the Anthropometry for Motor Vehicle Occupants (AMVO) shape.

Depending on the seating condition, part of the anterior portion of the 2nd abdominal rib (lowest rib) rests behind the posterior wall of the anterior pelvis skin. As the angle between the spine and pelvis decreases (flexion), the contact between the rib and pelvis increases. In tests conducted by Transport

Research Labs (TRL) it was discovered that certain seating positions placed the 2nd abdominal rib on top of or in front of the anterior pelvis flesh [3]. The pre-test misalignment of the rib was difficult to detect as the jacket covered the pelvis and torso. One way to minimize rib contact with the pelvis is to remove material from the posterior side of the anterior pelvis to allow more clearance. It is not known how removal of material may change the WorldSID's response and raises the issue of the anterior pelvis's effect on abdomen deflection. The present study was conducted to determine the influence of the flesh in constraining the abdomen rib kinetics.

METHODS

A WorldSID 50th percentile male dummy was placed on Teflon coated bench seat fixed to the top of an acceleration sled (Seattle Safety Systems, Seattle, WA). A uni-axial accelerometer measured sled acceleration. All data were sampled at 20 kHz according to SAE J211 [4]. The seat was positioned so that the occupant slid along the bench and impacted a pure lateral modular load-wall (Figure 1) at the time of maximum sled velocity [2, 5, 6]. The load-wall consisted of four rigid plates that were aligned to isolate loading to the thorax, abdomen, pelvis, and lower extremities. The abdomen plate was offset laterally from the thorax, pelvis, and lower limb plates by 50 mm to induce focal loads to the abdomen ribs. Tri-axial load cells mounted to the back of the rigid plates recorded the force time histories of the thorax, abdomen, and pelvis, while uni-axial load cells were used for the lower extremity plate.

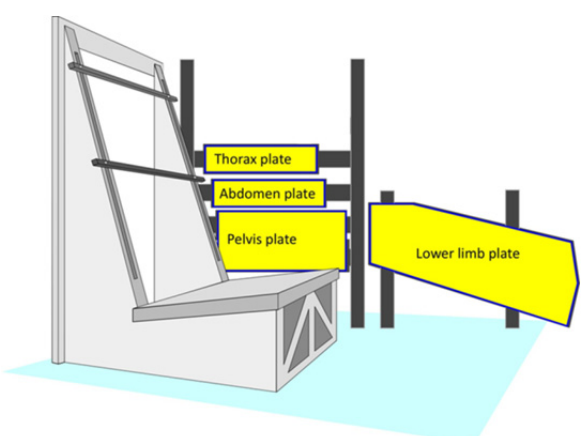

Figure 1: Schematic of the sled test setup showing the segmented load-wall. The bench seat and the lower limb plate are also shown.

The seat and seat back angle were independently adjusted and set to achieve two different pelvis/abdomen rib alignments. The upright seat position had a seat back and seat pan angle of 18 and 13 degrees, respectively (Figure 2) while the reclined seat configuration was 23 and 0 degrees (Figure 3).

The jacket, left shoulder, and left rib pad were removed to better isolate and visualize the abdomen ribs and the interaction with the anterior pelvis. Rib displacement was measured using WorldSID's internal deflection sensor, the InfraRed Telescoping Rod for Assessment of Chest Compression (IRTRACC) [7]. A standard pelvis was used for the first test series. The second series used a modified pelvis in which material was removed from the posterior section of the anterior pelvis skin extending from the left to the right anterior superior iliac spine. The anterior most surface of the pelvis was not altered (Figure 4). The upright configuration placed the 2nd abdominal rib directly in contact with the anterior portion of the standard pelvis while the reclined position had approximately 15 mm of clearance between the rib and posterior surface of the anterior standard pelvis.

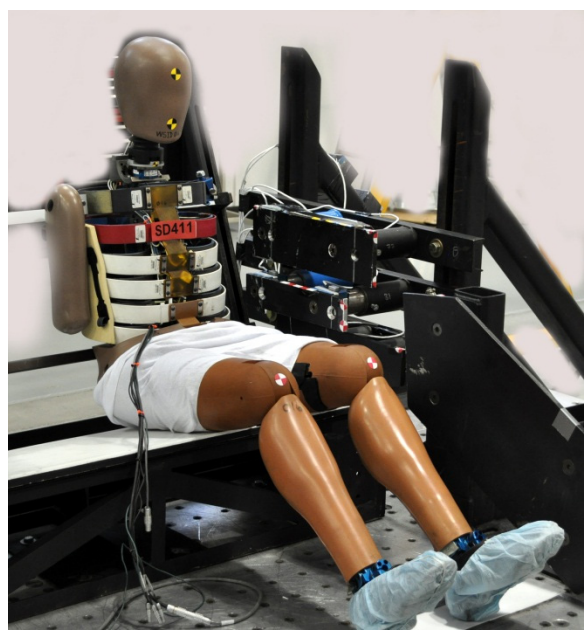

Figure 2: Photograph showing the WorldSID 50th device in the upright seated condition.

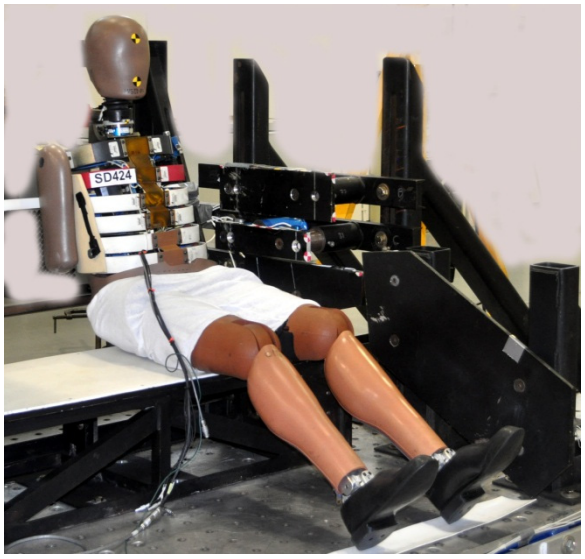

Figure 3: Photograph showing the WorldSID 50th device in the reclined seated position.

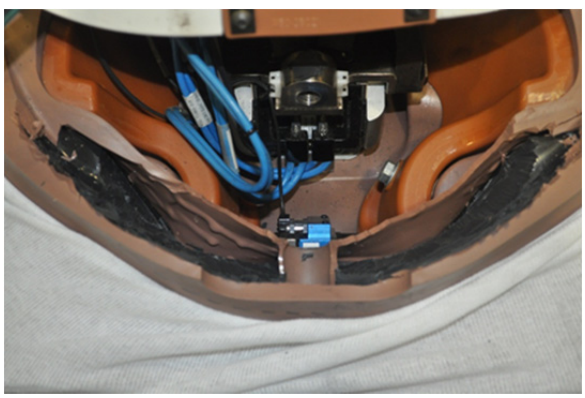

Figure 4: Photograph of the modification to the posterior portion of anterior pelvis flesh

Three repeat tests were run at 3, 4, and 5 m/s in the upright and reclined seating positions with the standard and modified pelvis for a total of 36 tests. Four high speed video cameras recorded the event at 1000 frames/sec from the front and overhead.

RESULTS

Sled accelerations for 3, 4, and 5 m/s are shown (Figure 5). Mean and standard deviations for the three pulses were 2.96 ± 0.07 m/s, 3.99 ± 0.05, and 5.01 ± 0.05. Peak abdominal rib 2 deflections and peak abdomen load-wall forces for all tests are shown (Table 1-Table 4). Average peak deflections and standard deviations for the standard pelvis in the upright position at 3, 4, and 5 m/s were 25.6 ± 0.7 mm, 37.1 ± 0.5 mm, and 53.9 ± 1.2 mm, respectively.

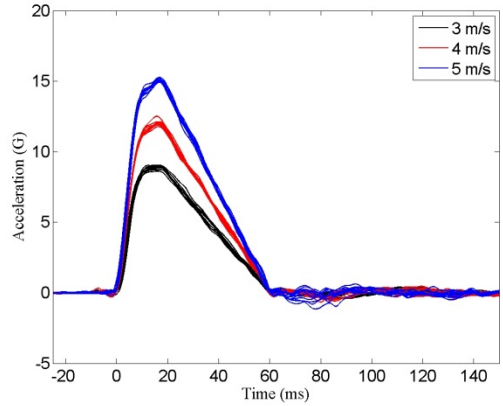

Figure 5: Sled acceleration pulses for the three velocities.

Deflections for the modified pelvis in upright position were 28.4 ± 0.6 mm, 40.1 ± 0.6 mm, and 51.8 ±0.4 mm; standard pelvis in reclined position 31.8 ± 0.4 mm, 44.4 ± 0.9 mm, and 56.6 ± 0.8 mm; and modified pelvis in reclined position 32.1 ± 0.3 mm, 44.8 ± 0.4 mm, and 56.3 ± 0.7 mm, respectively. Average peak deflections and standard deviations are compared (Figures 6-9).

Table 1: Peak rib 2 deflection and peak abdomen force – Standard Upright Tests

Test	Velocity	Pelvis	Seat Condition	Peak Deflection mm	Peak force N
1	3	Standard	Upright	26.0	2394.0
2	3	Standard	Upright	24.9	2312.9
3	3	Standard	Upright	26.0	2268.5
4	4	Standard	Upright	37.5	2848.9
5	4	Standard	Upright	36.5	2717.8
6	4	Standard	Upright	37.4	2778.3
7	5	Standard	Upright	52.5	3394.6
8	5	Standard	Upright	54.2	3280.9
9	5	Standard	Upright	54.9	3292.2

Table 2: Peak rib 2 deflection and peak abdomen force - Modified Upright Tests

Test	Velocity	Pelvis	Seat Condition	Peak Deflection mm	Peak force N
10	3	Modified	Upright	27.7	2211.1
11	3	Modified	Upright	28.7	2187.4
12	3	Modified	Upright	28.6	2191.5
13	4	Modified	Upright	40.7	2743.6
14	4	Modified	Upright	40.2	2799.5
15	4	Modified	Upright	39.4	2848.6
16	5	Modified	Upright	51.8	3336.7
17	5	Modified	Upright	52.2	3461.7
18	5	Modified	Upright	51.4	3169.1

Table 3: Peak rib 2 deflection and peak abdomen force - Standard Reclined Tests

Test ID	Velocity	Pelvis	Seat Condition	Peak Deflection mm	Peak force N
19	3	Standard	Reclined	31.4	2192.6
20	3	Standard	Reclined	32.2	2152.2
21	3	Standard	Reclined	31.8	2119.1
22	4	Standard	Reclined	44.5	2713.4
23	4	Standard	Reclined	43.4	2716.9
24	4	Standard	Reclined	45.3	2711.9
25	5	Standard	Reclined	56.5	3287.6
26	5	Standard	Reclined	55.8	3303.7
27	5	Standard	Reclined	57.4	3258.5

Table 4: Peak rib 2 deflection and peak abdomen force - Modified Reclined Tests

Test ID	Velocity	Pelvis	Seat Condition	Peak Deflection mm	Peak force N
28	3	Modified	Reclined	32.4	2163.4
29	3	Modified	Reclined	31.9	2169.2
30	3	Modified	Reclined	32.0	2165.5
31	4	Modified	Reclined	45.1	2663.2
32	4	Modified	Reclined	45.0	2687.4
33	4	Modified	Reclined	44.4	2655.5
34	5	Modified	Reclined	55.6	3339.1
35	5	Modified	Reclined	56.3	3343.9
36	5	Modified	Reclined	57.0	3386.6

Force-deflection curves are shown (Figures 10-15). Briefly, average peak deflection increased for all configurations with increasing velocity. The reclined seated position had similar values and curve morphologies for average peak displacements and force deflection functions at all velocities for the standard and modified pelvis. In the upright seated condition comparing the standard and modified pelvises, average peak deflections were lower at 3 and 4 m/s and slightly higher at 5 m/s. Force deflection responses were slightly stiffer at the lower velocities and similar at 5 m/s.

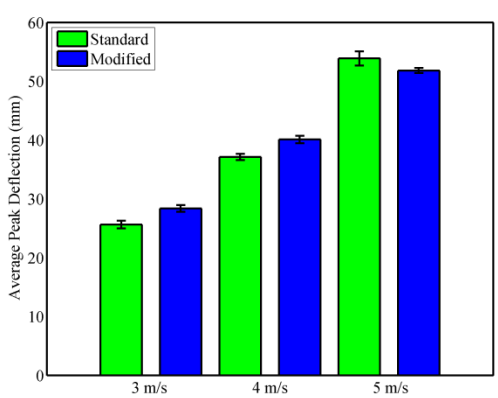

Figure 6: Average peak deflections and standard deviations for the upright seat.

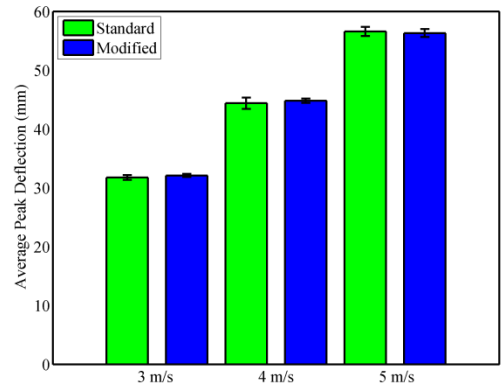

Figure 7: Average peak deflections and standard deviations for the reclined seat.

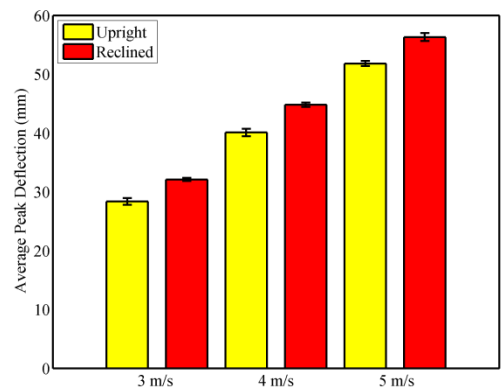

Figure 8: Average peak deflections and standard deviations for the modified pelvis.

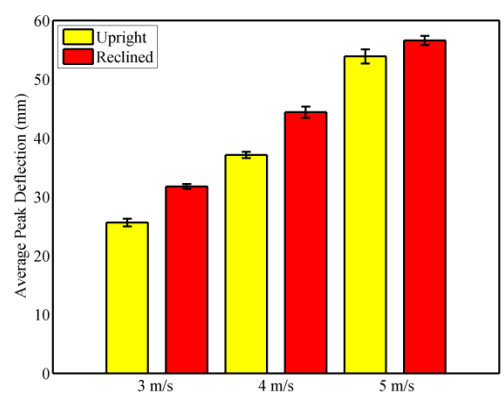

Figure 9: Average peak deflections and standard deviations for the standard pelvis.

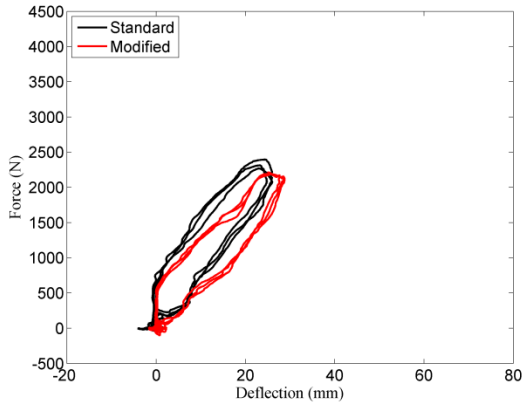

Figure 10: Force-deflection curves at 3 m/s for the upright seat.

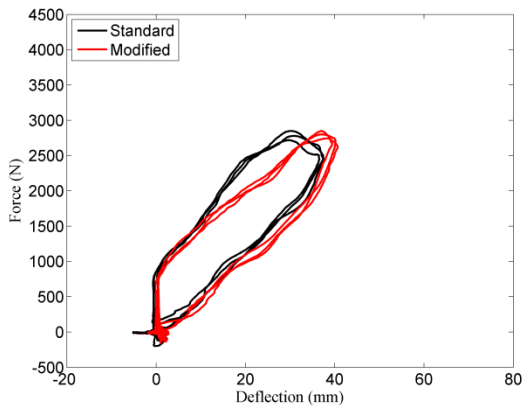

Figure 11: Force-deflection curves at 4 m/s for the upright seat.

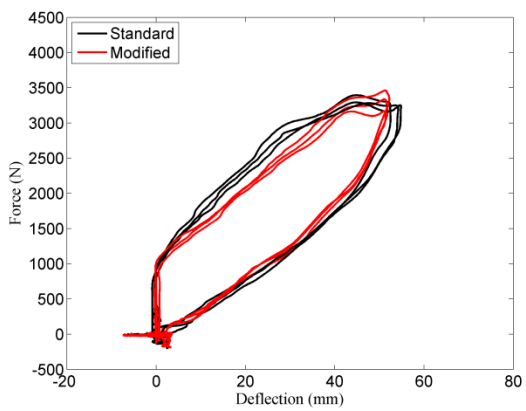

Figure 12: Force-deflection curves at 5 m/s for the upright seat.

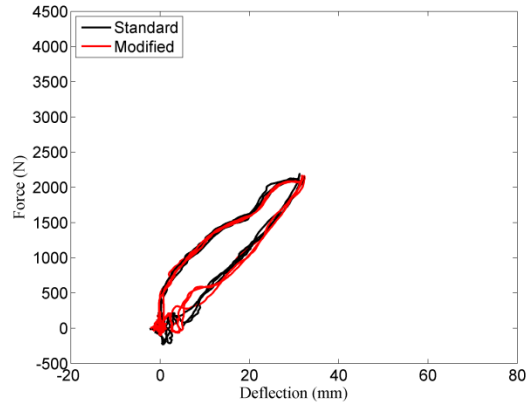

Figure 13: Force-deflection curves at 3 m/s for the reclined seat.

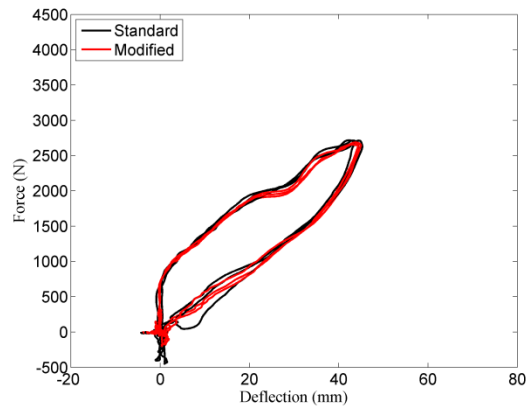

Figure 14: Force-deflection curves at 4 m/s for the reclined seat.

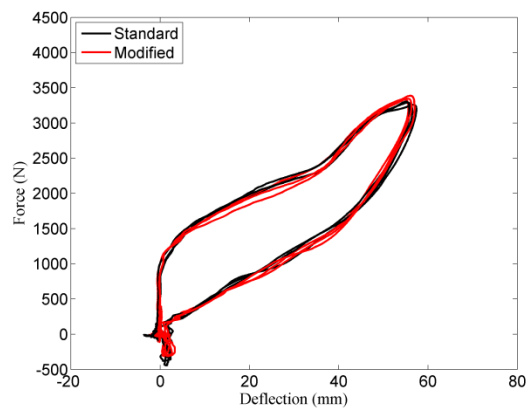

Figure 15: Force-deflection curves at 5 m/s for the reclined seat.

DISCUSSION

A report by TRL discussed tests with the WorldSID 50th device in which it was possible to accidentally position the dummy such that (a) abdomen rib 2 rested on top of the flat upper face of the anterior pelvis flesh or (b) the anterior pelvis flesh was pushed behind/tucked under the lower abdomen rib [3]. The authors of the report further examined this problem using a WorldSID 5th device equipped with a 2d IRTRACC and ran a series of sled tests at 5 m/s with an impacting abdomen plate. The dummy was tested in three conditions:

1. Normal seating position with standard pelvis.
2. Anterior pelvis flesh pushed behind Abdomen rib 2 with standard pelvis.
3. Normal seating position with modified pelvis flesh.

The pelvis was modified using a procedure similar to the current study. Slightly higher rib deflections and less rib rotation were seen with the misaligned rib position compared to the normal seating position. The modified pelvis had a similar trend with more rib rotation and higher deflections than the normally seated standard pelvis. TRL concluded that it is very difficult to force the abdomen rib on top of the pelvis during normal use and proper orientation and position of the rib is easy to verify with a quick visual check. While pelvis modification was probably not needed to prevent rib misalignment, they concluded that the standard pelvis flesh did limit abdomen rib 2 deflections.

Results from the TRL tests are difficult to compare to the current study as the WorldSID 5th device has been shown to have a stiffer rib response than the WorldSID 50th device. For similar force inputs, the overall rib contour shape and deflection may be different between the two dummies. The relative shape of the rib may affect the contact area and location with the posterior wall of the anterior pelvis and the extent to which it influences rib deflection.

TRL also tested the dummy with the arm, rib pad, and jacket, whereas these components were removed in the current study. The rib pad and jacket may have modulated some of the initial deflection of the rib, which could have changed the timing of the interaction with the pelvis flesh.

In addition, TRL used a 2d IRTRACC which incorporates rib rotation to calculate rib deflection. The 1d IRTRACC does not measure rib rotation and tests have shown it to be insensitive to certain loading conditions [8, 9]. Also, the TRL tests used a single plate positioned to impact the abdomen on the load-wall. It is not known how this single plate configuration compares with the offset modular load-wall. In the current study, the thorax and pelvis plates eventually accept the load of the dummy after initial abdomen compression. This load sharing with the other plates limited the overall abdomen rib compression.

Finally, TRL used a single, slightly different, seat configuration where the relative angle between the seat back and seat bottom was 90 degrees. In the current study, the reclined seat configuration relative angle was 113 degrees and the upright was 95 degrees which corresponded to a difference of about 18 degrees between the two seat positions. The seat back and seat bottom angles for the current study were selected as a range of likely seating positions in motor vehicles and probably had more clearance in the reclined position and more interference in the upright position than what are seen in most full scale vehicle crash tests. The TRL tests had 5 more degrees of relative forward lean than the upright seated condition. As shown in Figures 8 and 9, the current study demonstrated significant differences in rib deflections for the standard and modified pelvis based on seating position. Based on this result, there may be enough of a difference in occupant position between the two studies to produce differences in rib deflections.

The reclined seat position showed no statistical difference ($p<0.05$) in peak deflections between the standard and modified pelvis and the force deflection functions were very similar for the two pelvises at all velocities. As the lateral most point of the rib gets pushed inward the plastic sternum rib mount and the anterior portion of the rib gets pushed outward (Figure 16). With the modified pelvis, there is very little or no contact of the rib with the pelvis as it bulges outward. The standard pelvis shows some contact with sternum, but little with the rib. Results of the reclined test suggest that the pelvis does not contain the anterior portion of the rib and has little influence on the rib deflection.

The upright seat position demonstrated statistically ($p<0.05$) greater deflections for the modified pelvis at 3 and 4 m/s and no statistical difference ($p>0.05$) at 5 m/s. The force deflections functions at 3 and 4 m/s showed a stiffer response with the standard pelvis. With the standard pelvis, the entire anterior portion of the rib is placed in contact with the pelvis, while the modified pelvis has slight gap anterio-laterally increasing up to about 10 mm at the sternum. The

standard pelvis may have restricted the outward bulging of the sternum rib mount more than the modified pelvis yielding different rib contour profiles. The 1d IRTRACC single axis of deflection measurement may have been insensitive to the different rib shapes at 5 m/s.

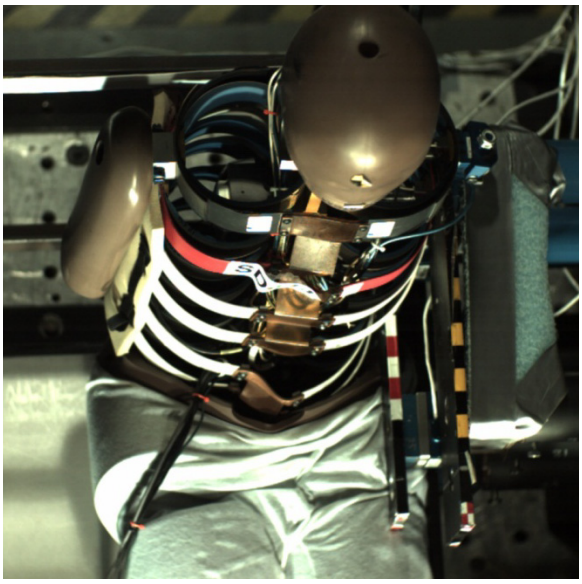

Figure 16: Overhead photograph of WorldSID 50th during impact showing the anterior bulging of the abdomen ribs.

Results of the current investigation suggest that modification to the anterior pelvis flesh may not be the best solution to prevent misalignment of the 2nd abdomen rib. While the pelvis flesh influenced the average peak deflection of the rib at lower velocities in the upright configuration, this effect was insignificant at the highest velocity. Because higher velocities are more representative of real world scenarios wherein the intruding door and side airbag interact with the occupant's torso, the modification of the pelvis may not be necessary. This is further reinforced by the observation that the force deflection curves derived at 5 m/s were very similar for the modified and standard pelvis. Thinning out the pelvis wall may have consequences to regional biofidelity of the pelvis and the overall biofidelity of the dummy. If the pelvis is modified to allow more abdomen deflection, it may reduce deflections in the superior ribs. A more practical solution would be to add a visual/physical check of the abdomen ribs prior to testing. From these perspectives modification of the pelvis should be considered only if rib misalignment becomes an issue in full-scale vehicle crash tests.

ACKNOWLEDGMNETS

This research study was supported in part by DTNH22-07-H-00173, Department of Neurosurgery at the Medical College of Wisconsin, Milwaukee, WI and VA Medical Research. The assistance of the Neuroscience research staff is acknowledged.

REFERENCES

1. FMVSS-214, *Federal Register, Docket No. 88-06*, in *49 CFR; Parts 571, et al. Side Impact Protection*. 1990, US Government Printing Office: Washington, DC. p. 43722-45780.
2. Yoganandan, N., J.R. Humm, F.A. Pintar, and K. Brasel, *Region-specific deflection responses of WorldSID and ES2-re devices in pure lateral and oblique side impacts.* Stapp Car Crash J, 2011. 55: p. 351-78.
3. Carroll, J.A., O. Foodacre, and D. Hynd, *Global Impact Dummies - Assessment Concerning WorldSID in Future Regulatory Applications*. 2012: European Commission DG Enterprise and Industry, Directorate D - Industrial Innovation and Mobility Industries, Transport Research Laboratory.
4. SAE, *Instrumentation for impact test-Part 1-electronic Instrumentation-SAE J211/1*. 1995: Society of Automotive Engineers, Warrendale, PA.
5. Yoganandan, N., J.R. Humm, and F.A. Pintar, *Modular and scalable load-wall sled buck for pure-lateral and oblique side impact tests.* J Biomech, 2012. 45(8): p. 1546-9.
6. Yoganandan, N., J.R. Humm, F.A. Pintar, and D.J. Maiman, *Determination of peak deflections from human surrogates using chestbands in side impact tests.* Med Eng Phys, 2013.
7. Rouhana, S., A. Elhagediab, and J. Chapp. *A high-speed sensor for measuring chest deflection in crash test dummies*. in *16th International Technical Conference on the Enhanced Safety of Vehicles* 1998. Washington, DC.
8. Been, B., K. Waagmeester, C. Tosseille, J.A. Carroll, and D. Hynd. *WorldSID small feamle two-dimensional chest defelction sensors and sensitivity to oblique impacts*. in *Enhanced Safety of Vehicles*. 2009. Stuttgart, Germany.
9. Belcher, T. and M. Terrell. *An Assessment of WorldSID 50th percentile male injury responses to oblique and perpendicular pole side impacts*. in *Enhanced Safety of Vehicles*. 2011. Washington, DC.